

# Micromorphic continuum model: granular materials to designed granular metamaterials

By  
© 2021

Nima Nejadsadeghi  
M.S., Sharif University of Technology, 2016  
B.S., Iran University of Science and Technology, 2013

Submitted to the graduate degree program in Mechanical Engineering and the Graduate Faculty of the University of Kansas in partial fulfillment of the requirements for the degree of Doctor of Philosophy.

---

Chair: Professor Anil Misra

---

Professor Candan Tamerler

---

Associate Professor Reza Barati

---

Associate Professor Mark Ewing

---

Assistant Professor Xianglin Li

---

Research Professor Francois Hild

Date Defended: 6 May 2021

The dissertation committee for Nima Nejadsadeghi certifies that this is the approved version of the following dissertation:

**Micromorphic continuum model: granular materials to designed granular metamaterials**

---

Chair: Professor Anil Misra

Date Approved: 6 May 2021

## Abstract

This work investigates the mechanical response of granular-microstructured solids (natural and synthetic) in static and dynamic problems. Firstly, a non-classical micromorphic theory of degree  $n$  based upon granular micromechanics approach is developed to model the mechanical behavior of granular materials. This model is derived based on Hamilton's principle, and provides variationally consistent boundary conditions. Moreover, less expensive models, namely micromorphic model of degree one, micropolar model, and second gradient model, are derived.

Secondly, the micromorphic model of degree one is specialized to describe one-dimensional granular structures and the effect of different material parameters and higher order inertia on the wave propagation characteristics of such systems is parametrically studied. This model is able to describe dispersion, negative group velocity, and frequency band gaps. Moreover, the proposed model is further extended to investigate the effect of external electric field on tuning the dispersive behavior of dielectric granular materials in quasi-electro-statics. The model shows that an external electric field can potentially create, remove, or change location and width of the stop band in the granular medium. In addition, the micromorphic model of degree one is specialized to describe and analyze the wave propagation characteristics in axially moving materials with granular microstructure by employing an Eulerian frame of reference. The model predicts elastic wave dispersion asymmetries and the emergence and removal of stop bands for non-vanishing axial velocity.

Thirdly, the micromorphic model of degree one is used to study the static behavior of one-dimensional materials with granular microstructure. The model predicts localization of deformation energy in the boundary layers for particular boundary conditions. The model is thereafter utilized to study the free vibration characteristics of one-dimensional granular-

microstructured solids. The model predicts mode shapes similar to those of a classical rod, and natural frequencies different from those of a classical rod. The model also predicts length-scale effects such as stiffening of the material as the size of the structure shrinks.

Finally, a micropolar model is developed to describe one-dimensional chiral granular (meta-) materials in a two-dimensional deformation plane. The proposed model is used to predict the behavior of chiral granular strings in tension. The domain of validity of the proposed model is thereafter investigated through parametric experimentation. To this end, particular chiral granular strings composed of 11 grains with varying geometrical parameters are considered. The granular strings are fabricated using 3D printing technology, and undergo tensile testing. The images taken from the experiment are analyzed using digital image correlation technique. The results are used to investigate the range of applicability of the model to predict the behavior of granular strings by comparing the predicted displacements and rotation fields by the model and the experimental results.



## Acknowledgments

First and foremost, I would like to express my gratitude to my advisor, Dr. Anil Misra, for the opportunity to work with him, and for his invaluable support throughout this research. His guidance helped me in all the time of research and writing of this dissertation. I could not have imagined having a better advisor and mentor for my Ph.D. study.

I would like to thank the rest of my dissertation committee, Dr. Reza Barati, Dr. Mark Ewing, Dr. Francois Hild, Dr. Xianglin Li, and Dr. Candan Tamerler, for their insightful comments and encouragement. In particular, I would like to appreciate Dr. Hild for his support and help on digital image correlation development and analysis. I would also like to thank the research grant CMMI-1727433 from National Science Foundation (NSF) for supporting this research.

My sincere thanks goes to Dr. Luca Placidi and Dr. Maurizio Romeo for their valuable comments on wave propagation characteristics in solids. I also thank my fellow labmates Dr. Michele De Angelo, Dr. Rizacan Sarikaya, and Jacob Hammil for all the discussions and fun we have had in the last few years.

I would like to express my deepest gratitude to my family who have always been supportive of my pursuits. To my parents, for their unparalleled love and support throughout my journey, and to my sister, Azin, for her support.

Finally, I would like to thank my beautiful better half and best friend, Mahboobeh, for her unconditional love and support. This work would have not been possible without her, and hence, is dedicated to her.

## Table of Contents

Abstract .....	iii
Acknowledgments.....	v
Chapter 1: Introduction.....	1
Significance .....	1
Scope of Dissertation .....	3
Chapter 2: Granular Micromechanics Based Micromorphic Model.....	6
Chapter 3: Elastic Wave Propagation Characteristics in Granular Materials .....	8
Chapter 4: On the Statics and Dynamics of Granular-Microstructured Rods with Higher Order Effects .....	11
Chapter 5: Investigating the domain of validity of one-dimensional micropolar chiral granular model through parametric experimentation .....	14
Chapter 6: Conclusions and Recommendations .....	16
Appendix A: Paper P1 .....	19
Appendix B: Paper P2.....	43
Appendix C: Paper P3.....	65
Appendix D: Paper P4 .....	75
Appendix E: Paper P5.....	85
Appendix F: Paper P6.....	97
Appendix G: Paper P7 .....	142

## Chapter 1: Introduction

### Significance

Materials with granular microstructure are characterized as materials composed of many individual grains mediated by interfaces. Generally, granular materials exhibit a wide variety of behaviors. These range from fluid-like behavior at a low concentration of grains, to plastic solid-like behavior in higher concentrations, as in soil, to elastic solid-like behavior in much higher concentrations or in consolidated granular media in which the grains could be bonded together, as in sedimentary rocks. In particular, granular solids span the spectrum from highly consolidated dense solids formed of particulate precursors to confined packings of non-cohesive particles. Many engineering and science disciplines such as material development, transportation and infrastructure systems, pharmaceuticals, drug delivery, and natural processes in geophysics encompass the applications of granular materials, suggesting a necessity to better understand how such materials behave. Moreover, granular-microstructured materials have also been widely used in the context of mechanical metamaterials to obtain desired unusual behavior that natural materials do not exhibit. In both natural and synthetic granular (meta-) materials, the grain-pair interfacial mechanisms play a key role in the macro-scale behavior. These micro-scale mechanisms influence the macro-scale behavior of the granular material and hence, should be taken into account in the description of granular media.

Based on the scale of interest, different approaches can be utilized to model and analyze granular materials. At scales close to the size of grains, such materials can be considered an assembly of many individual grains in contact, where Newtonian mechanics can be applied to solve the  $n$ -body problem with  $n$  being the number of grains. Such an analysis results in an accurate and detailed description of the granular system provided that a complete information regarding the

position, geometry, and material properties of each grain, as well as grain-pair interactions is required. However, such complete information is rarely available for granular materials composed of many grains. As the number of grains within a granular material increases, and especially when the system is viewed at larger scales (for example hundred times greater than the grain size), continuum models remain the most efficient. Continuum models incorporate grain-scale information by considering the mean behavior of grain-pair interaction and translating it into the macro-scale behavior characteristics of the system. Continuum models often require model parameter identifications for the description of the macro-scale phenomena. Nevertheless, given the incomplete information and intractable details about the micro-mechano-morphological aspects of the granular system, continuum models provide good approximation for the collective behavior of grains.

The classical form of continuum mechanics assumes each material point is independent of the others, and interacts with its surrounding by means of mass, moment, energy, and entropy equations. The size of a material point in classical continuum mechanics approaches zero, and rotation of material points is not accounted for. However, in granular media, grain rotation is an integral part of energy transfer, and therefore, classical continuum mechanics may not offer a good model especially in cases where grains within the granular medium undergo significant rotations. Moreover, classical continuum mechanics is only sufficient to characterize the immediate neighborhood (local) effects in the medium, while the description of granular structures requires consideration of not only local effects, but also nonlocal effects. As a result of the complexity of granular medium in both mechanical and morphological effects, a refined continuum model that overcomes the shortcomings of classical continuum mechanics deems necessary.

This dissertation aims to investigate/develop non-classical continuum models of granular materials and granular metamaterials with a goal to transforming how granular systems are analyzed. Overall, two objectives are followed:

1. To develop non-classical continuum models of solids with granular microstructure using granular micromechanics approach. Such models are considered to be able to address the shortcomings of classical continuum models in both statics and dynamics, such as singularities and energy localization in static problems, and wave dispersion and size-effects in dynamic problems.
2. To design and perform experiments for model validation and verification using 3D printing technology.

The ultimate goal of this research is to develop refined, yet tractable, models that describe materials with granular microstructure and account for the micro-mechano-morphological effects of these complex systems. Such models are necessary to analyze natural granular materials and microstructured solids that are largely inaccessible through purely experimental techniques, and help novel (meta-) material development for particular applications.

### **Scope of Dissertation**

In this dissertation, the following research problems are addressed:

1. Develop a continuum model to describe the mechanical behavior of granular materials and granular metamaterials, accounting for the micro-mechano-morphological effects. To this end, in Paper **P1**, a non-classical micromorphic model of degree  $n$  is presented. This model is based upon granular micromechanics approach and accounts for the complex kinematics of granular media. Reduced versions of the proposed model,

- namely a micromorphic model of degree two, a micromorphic model of degree one, a micropolar model, and a second gradient model are also presented.
2. Study the elastic wave propagation characteristics of materials with granular microstructure utilizing the developed micromorphic model predictions. To this end, Paper **P2** investigates the longitudinal wave propagation characteristics of a one-dimensional granular material modeled as an infinite micromorphic medium, as well as the transverse wave propagation characteristics of a one-dimensional granular structure that has a two-dimensional microstructure. This paper studies the different intergranular stiffness effects on the dispersive behavior of granular structures through an extensive parametric study. Paper **P3** develops upon Paper **P2** by investigating the effect of external electric field on modulating the dispersive behavior of dielectric one-dimensional granular materials in electrostatic case. Paper **P4** specializes the analysis in paper **P2** to the problem of axially moving media by considering the effect of axial velocity on the dispersive behavior of one-dimensional granular structures by describing the kinetic energy of the system in an Eulerian frame of reference. Finally, Paper **P5** studies the effect of higher order inertia on the wave propagation characteristics of granular media, and shows how the grain density distribution in a granular system alters its dynamic properties.
  3. Study the static and dynamic behavior of one-dimensional granular structures modeled as a micromorphic model of degree one. Paper **P6** specializes and builds upon Paper **P1** to describe the mechanical behavior of one-dimensional materials with granular microstructure. This paper investigates the effect of different stiffnesses and boundary conditions on the static and dynamic (free vibration) behavior of the granular structures.

4. Develop a continuum model to describe chirality in granular media and validate the model through experimentation. Paper **P7** specializes and builds upon Paper **P1** to develop a chiral granular beam model that incorporates axial, transverse, rotational, and coupling stiffnesses. The developed model is used to predict the response of the granular material to tensile experiment, and is validated through experimentation where granular strings were 3D printed, tested, the full-field displacement field was obtained through digital image correlation technique, and compared with model predictions.

The dissertation is presented in a summary style. Chapters 2-5 introduce the research problems mentioned above, and briefly present the key results of the published papers which constitute the dissertation and are provided in the Appendices. Finally, Chapter 6 presents the conclusions and recommendations.

## Chapter 2: Granular Micromechanics Based Micromorphic Model

Granular materials are ubiquitous in nature and are characterized as composed of distinct grains mediated by interfaces. The intricacy of the mechanics of interfaces between grains results in complex behavior of granular medium in response to an externally applied disturbance. Classical elasticity is unable to predict many aspects of such behavior in both statics and dynamics problems. In particular, classical continuum mechanics assumes that a continuum is composed of material points with their sizes approaching zero, and does not provide nonlocal effects in the medium. Moreover, classical continuum mechanics does not consider rotations as a degree of freedom to the material points, and hence is unable to account for grain rotations in a granular medium, which is an integral part of grain kinematics. Furthermore, classical elasticity does not consider the underlying microstructure of a material, and therefore micro-mechano-morphological effects are not accounted for.

To model materials with granular microstructure, a refined model is required. The model should be able to capture the phenomena that classical elasticity overlooks, and must be based on the complex kinematics of granular systems. While it does not provide exact behavior of each grain within a granular system, the granular micromechanics based micromorphic model presented in Paper **P1** attempts to provide a tractable model of the collective behavior of granular media. The presented continuum model is based on the kinematics of granular structures and accounts for different micro- and macro-scale deformation mechanisms.

To set up the problem, we consider a granular medium of finite size. Each material point in the granular structure, in contrast to classical elasticity, is treated as a micro-volume composed of several grains, interacting with each other through some form of interaction. It is assumed that both the granular structure and the micro-volume are continuous media, and macro- and micro-



scale displacement fields are both continuous up to desired order. Therefore, one can write the displacement of grains within the volume element using a polynomial expansion. The model presented in Paper **P1** is a generalized micromorphic model of degree  $n$  and assumes that the terms in the expansion should be kept up to the order  $n+1$ . Paper **P1** provides a systematic approach to obtain a micromorphic model of degree  $n$  to describe granular structures by recognizing the micro-scale deformation measures pertinent to the assumed kinematic field. The paper thereafter links the micro- and macro-scale kinematic measures and provides the governing equations of motion for describing a granular material using an energy approach. The presented governing equations of motion are coupled partial differential equations and can be employed to investigate static and dynamic behavior of granular systems.

In the remainder of Paper **P1**, reduced models are provided. The reduced models have less degrees of freedom and less material constants to be identified, compared to the micromorphic model of degree  $n$ . A micromorphic model of degree two is achieved if the polynomial expansion is done up to cubic term, and a micromorphic model of degree one is obtained for a polynomial expansion up to quadratic term. Other well-known models are also obtained if constraints are applied to the macro-scale kinematic measures. In particular, as a reduced micromorphic model of degree one, a micropolar model is obtained and presented. Moreover, a second gradient medium is obtained and presented where the deformation energy is not only a function of the first gradient of displacement field, but also the second gradient of displacement field.

### Chapter 3: Elastic Wave Propagation Characteristics in Granular Materials

Materials with granular microstructure show dispersion in elastic wave propagation. In other words, different frequency components of external disturbance propagate with different speeds in granular structures due to their underlying microstructure. In Paper **P2**, Paper **P3**, Paper **P4**, and Paper **P5**, we focus on the elastic wave propagation characteristics of one-dimensional materials with granular microstructure. Studying elastic wave propagation in granular media results in a better realization of how these materials react to external actions, and in general, promotes the understanding of such materials. Granular materials, due to their grain-scale mechano-morphological properties, have an inherent microstructural characteristic length with which the wavelength of excitation at high frequencies becomes comparable. As a result, effects of the micro-mechano-morphology become significant when the material experiences high frequency loads. Therefore, it becomes important to include information about the material's micro-structure in wave propagation studies. Notably, in these cases, the classical wave equation of the form of a hyperbolic partial differential equation becomes complicated as additional terms are introduced to account for the micro-mechano-morphology.

Paper **P2** investigates dispersion in two infinite-length one-dimensional systems, longitudinal wave propagation characteristics in a one-dimensional granular material with one-dimensional microstructure, and transverse wave propagation characteristics on a one-dimensional granular material with two-dimensional microstructure. To this end, the granular micromechanics based micromorphic model of degree one presented in Paper **P1** is employed. The governing equations of motion are fed with plane wave solutions, and dispersive relation relating frequency and wavenumber is obtained. For a one-dimensional classical continuum, the frequency is a linear function of wavenumber, and therefore, wave speed is constant and independent of frequency. For

the one-dimensional granular structures studied, frequency is a nonlinear function of wavenumber, and therefore, each frequency component travels with a different speed. Moreover, in a classical one-dimensional model, there exists only one wave branch, while in the granular structures studied, there exists multiple wave branches, acoustic and optical, where acoustic wave branch starts from zero frequency and zero wavenumber and optical wave branch starts at nonzero frequency for zero wavenumber. The effect of different material parameters on the dispersive behavior of granular structures are investigated. In particular, Results predict the emergence of frequency band gaps (frequency range with no propagation in the medium) and negative group velocities for certain values of the parameters involved.

Paper **P3** studies wave propagation characteristics of a one-dimensional granular structure that is composed of dielectric grains in the presence of an external electric field in electro-statics. In this paper, the electro-elastic coupling is due to bound charge micro-density in granular grains, and micro-strain is linked to electric dipole and quadrupole densities. The dispersive behavior is shown to be affected by the polarizability (dipole effect), intrinsic quadrupole density, and external electric field. Results predict an acoustic and an optical branch in the dispersive curve. Polarizability and external electric field are mainly affecting small wavenumber behavior of the wave branches, while quadrupole density alters the behavior of the material at large wavenumbers. Moreover, creating or removing stop-bands using the external electric field is discussed.

Paper **P4** studies the effect of axial velocity on the dispersive behavior of axially moving materials with granular microstructure. The mechanics of axially moving media is significant due to their broad applications, e.g. aerial tramways, mono-cable ropeways, ski lifts. As technological advancements have made it possible to fabricate microstructured solids, it is important to understand how the wave propagation characteristics of granular structures change due to nonzero

axial velocity. To this end, a one-dimensional granular string model based on the model presented in Paper **P1** is further extended to account for the presence of axial velocity. For this problem, an Eulerian frame of reference is used and the kinetic energy is described using the notion of material derivative to account for the convective terms. In the absence of microstructure, the axially moving material model shows non-dispersive non-symmetric forward and backward waves. In the case of axially moving materials with granular microstructure, the model predicts dispersive non-symmetric waves. In this case, there are two acoustic and two optical wave branches. Axial velocity leads to narrowing and widening in the frequency band gaps in the forward and backward waves, respectively. Negative group velocity is also observed in certain wavenumber ranges.

Paper **P5** considers wave propagation characteristics in a one-dimensional granular medium and investigates the effect of higher order inertia terms. The higher order inertia terms are consequences of the assumed kinematic field and account for correcting the large wavenumber large frequency behavior of granular systems. It is shown that the micro-density distribution can have large effects on the dynamic mechanical response of the granular structures. Moreover, negative group velocity in optical branch can be obtained.

## **Chapter 4: On the Statics and Dynamics of Granular-Microstructured Rods with Higher Order Effects**

Materials with granular microstructure show strong dependence of grain-scale interactions in their macro-scale mechanical behavior in both static and dynamic problems. In Paper P6, the granular micromechanics based micromorphic model of degree one introduced in Paper P1 is utilized to investigate the static and free vibration behavior of one-dimensional materials with granular microstructure. To this end, the kinematic description of the problem is introduced, from which micro-scale deformation mechanisms are identified. Macro-scale deformation mechanisms are linked to their micro-scale counterparts, and constitutive relationships are obtained by assuming a quadratic form of deformation energy density. Hamilton's principle is used to obtain the governing equations of motion for a one-dimensional material with granular microstructure. The governing equations of motion are two coupled partial differential equations. Moreover, the variationally consistent boundary conditions are obtained. The model is used to investigate the static and free vibration behavior of one-dimensional granular-microstructured solids.

In the static case, three possible scenarios for the applied boundary conditions in order to explore the static behavior of the 1D granular rod are considered. In all the scenarios, a conventional displacement-control experimental setup is adopted, differing only in the application of the non-classical boundary conditions. This study promotes the understanding of how non-classical boundary conditions alter the response of the material. The results of this study suggest that for imposing fixed and prescribed macro-scale displacements at left and right ends of the structure, respectively, one observes a classical-like behavior only if at each end, the contact double traction is held to be zero, or the micro-scale kinematic measure is assigned a value equal to the macro-scale displacement gradient (macro-scale strain). For the cases where the macro-scale

displacement gradient and micro-scale kinematic measure have non-equal values on the boundary, localized deformation energy density of finite thickness near that boundary is observed, while the deformation energy density in the rest of the domain of the problem is rather uniform. Second, for fixed macro-scale displacement applied at both boundaries and imposed double traction or micro-scale kinematic measure at one end, we notice both compression and tension (negative and positive macro-scale displacement gradient) induced within the granular structure. Third, the gradients appearing because of the imposed field variables and at both ends only exist close to the outer boundaries of the structure, thereby signifying the existence of boundary layers. Finally, one notices the small change in the macro-scale displacement in response to the alterations in the imposed non-classical boundary conditions. Nevertheless, such small changes have large influence on the energy localization near the boundaries, and such energy localization becomes even more noticeable as the size of the rod shrinks.

In the dynamic case, the free vibration characteristics of the one-dimensional granular rod is studied for different boundary conditions. In particular, for a rod fixed at both ends, the effect of non-classical boundary conditions on the mode shapes and natural frequencies is probed. To this end, the analytical solutions are obtained from the model, and the first three natural frequencies and mode shapes are obtained for different boundary conditions imposed on the system. It is shown that while the mode shapes corresponding to the macro-scale displacement are similar to that of a classical rod, microstructural properties of granular structures affect the value of their natural frequencies. Moreover, as the size of the structure shrinks, the natural frequencies grow, which show the stiffening effect. Finally, it is interesting to note that the higher mode frequencies are not integer multiples of the fundamental mode, which is a departure from the results for classical 1D

elastic rod under the considered boundary conditions, and seems to suggest an apparent internal damping.

The results of Paper **P6** promote the understanding of the complex behavior of granular-microstructured solids, and are useful if experiments are to be devised. The model predicts measurable effects such that experimental approaches/protocols can be designed to detect these effects.

## **Chapter 5: Investigating the domain of validity of one-dimensional micropolar chiral granular model through parametric experimentation**

The significance of chirality lies in its wide range of applications in diverse branches of science, and hence, understanding the mechanisms leading to chirality deems necessary. The literature on lattice chirality offers comprehensive studies on the chiral properties of particular pre-designed microstructural units using novel experimental and numerical schemes. However, to further enhance the understanding on mechanical chirality, a general analysis in determining the effect of different factors contributing to chirality proves essential. Paper **P7** focuses upon chiral granular (meta-) materials and investigates the role of different micro-level deformation mechanisms on the macroscopic chiral behavior of the system by incorporating the coupling between the deformation mechanisms in different axes and rotations. To this end, a granular micromechanics based micropolar model is obtained through Hamilton's principle to describe chirality in a one-dimensional chiral granular string in a two-dimensional deformation plane. The model is shown to reduce to Timoshenko beam model if particular inter-granular mechanisms vanish. Moreover, predictions of the behavior of chiral granular strings in tension is parametrically investigated.

To investigate the domain of validity of the proposed model through experimentation, a particular chiral granular string composed of 11 grains is considered. Each grain is interacting with its neighboring grain through some form of mechanism that induces chirality. The granular string is varied in two geometrical parameters describing the interaction between the two grains, hence providing parametric spaces with respect to the considered geometrical parameters. The granular strings are fabricated using a Formlabs Form 3 3D printer in Durable resin, and undergo tensile experiment in an ElectroForce 3200, TA Instruments, uniaxial testing machine. The surface of



granular strings is sprayed in black to obtain a speckle pattern. A DSLR camera is used to obtain images from the experiment, which were thereafter analyzed using Digital Image Correlation (DIC) technique in three different scales. The DIC results are used to investigate the range of applicability of the model to predict the behavior of granular strings by comparing the predicted displacements and rotation fields by the model and the experimental results.

## Chapter 6: Conclusions and Recommendations

The granular micromechanics based models developed and analyzed in this research expand upon a classical continuum by incorporating additional degrees of freedom and different micro- and macro-scale deformation mechanisms. The proposed models were shown to predict phenomena in static and dynamic problems that classical elasticity is unable to, and can describe the observed behavior of granular-microstructured materials. In particular, the micromorphic model of degree one was shown to describe the dispersive behavior of granular materials. The model predicted the emergence of stop bands due to the specific material parameters, the effect of the external electric field, and the effect of the axial velocity. The model was also used to study the static behavior of granular rods. It was shown that the nature of the boundary conditions imposed on the system can have significant effect on the energy localization, especially in the boundary layers. It was also shown that the material parameters can affect the width of the boundary layers. The micromorphic model of degree one was further used to study the free vibration behavior of granular rods in different boundary conditions, where it was observed that the natural frequencies of the system are affected by the microstructural properties of the rod, and are different from those predicted by classical elasticity. The stiffening of the material was also predicted as the size of the structure shrinks. Finally, in an attempt to describe chirality in granular media, a one-dimensional chiral granular string in a two-dimensional deformation plane was described as a micropolar model, where the effect of material parameters on the response of the granular string in tension was studied. Moreover, digital image correlation technique was used to experimentally investigate the domain of validity of the model by comparing the theory predictions and experimental results.

The models and the analyses presented in this work can be used to describe natural granular materials as well as granular metamaterials. In fact, the predictive models discussed in this research can be adopted to help identify and link the observed macro-scale behavior to the underlying micro-scale grain pair interaction mechanisms. As a result, the proposed models can help design granular metamaterials that exhibit particular static and/or dynamic behavior to be used in engineering applications.

During the course of addressing the objectives of this dissertation, several future investigation topics can be identified. Below, the research recommendations are discussed.

1. In Chapter 3 of this research, the wave propagation characteristics of one-dimensional granular-microstructured solids were predicted using a micromorphic model of degree one. It is interesting to further explore the dispersive behavior of higher dimensional granular materials using the proposed model. Moreover, experiments should be devised to validate the model's predictions.
2. In Chapter 4, the static and dynamic behavior of the one-dimensional granular microstructured solids were studied. It is recommended that the analysis is expanded to investigate the static and dynamic behavior of higher-dimensional structures, and to devise experiments to validate the model's predictions.
3. In chapter 5, the micropolar model to describe chirality in one-dimensional granular metamaterials was developed and examined using experimentation on granular strings and digital image correlation technique to obtain full-field deformation. It is suggested that nonlinearity in the grain-pair interactions are included in the mathematical model and the effect of nonlinearities is compared to the results

obtained in the current research, especially in large applied strains. Moreover, higher dimensional models to predict chirality accompanied by validation through experiments can be of great value.

4. Finally, the physical interpretation of higher order boundary conditions is still not fully understood. More research in this avenue is highly suggested as it also paves the way to experimentally identification of material parameters in the proposed models.

## Appendix A: Paper P1

### Title:

Extended granular micromechanics approach: a micromorphic theory of degree  $n$

### Authors:

Nima Nejadi Sadeghi

Anil Misra

### Journal:

Mathematics and Mechanics of Solids

### Permission from journal:



Extended granular micromechanics approach: a micromorphic theory of degree  $n$

Author: Nima Nejadi Sadeghi, Anil Misra

Publication: Mathematics and Mechanics of Solids

Publisher: SAGE Publications

Date: 02/01/2020

Copyright © 2020, © SAGE Publications

**Gratis Reuse**

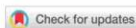
If you are a SAGE journal author requesting permission to reuse material from your journal article, please note you may be able to reuse your content without requiring permission from SAGE. Please review SAGE's author re-use and archiving policies at <https://us.sagepub.com/en-us/nam/journal-author-archiving-policies-and-re-use> for more information.

If your request does not fall within SAGE's reuse guidelines, please proceed with submitting your request by selecting one of the other reuse categories that describes your use. Please note, a fee may be charged for reuse of content requiring permission. Please submit a ticket through the SAGE Permissions Portal if you have questions.

BACK
CLOSE WINDOW

### Credit authorship statement:

N.N. and A.M. conceived the idea. N.N. performed calculations and theory development. N.N. and A.M. contributed to the discussion of all aspects of this work. N.N. and A.M. wrote and edited the manuscript.



Article

**MMS**

# Extended granular micromechanics approach: a micromorphic theory of degree $n$

Mathematics and Mechanics of Solids  
2020, Vol. 25(2) 407–429  
© The Author(s) 2019  
Article reuse guidelines:  
sagepub.com/journals-permissions  
DOI: 10.1177/1081286519879479  
journals.sagepub.com/home/mms

**Nima NejadSadeghi**

Mechanical Engineering Department, University of Kansas, 1530 W 15<sup>th</sup> Street, Learned Hall, Lawrence, Kansas, USA

**Anil Misra**

Civil, Environmental and Architectural Engineering Department, University of Kansas, 1530 W 15<sup>th</sup> Street, Learned Hall, Lawrence, Kansas, USA

Received 19 August 2019; accepted 5 September 2019

**Abstract**

For many problems in science and engineering, it is necessary to describe the collective behavior of a very large number of grains. Complexity inherent in granular materials, whether due to the variability of grain interactions or grain-scale morphological factors, requires modeling approaches that are both representative and tractable. In these cases, continuum modeling remains the most feasible approach; however, for such models to be representative, they must properly account for the granular nature of the material. The granular micromechanics approach has been shown to offer a way forward for linking the grain-scale behavior to the collective behavior of millions and billions of grains while keeping within the continuum framework. In this paper, an extended granular micromechanics approach is developed that leads to a micromorphic theory of degree  $n$ . This extended form aims at capturing the detailed grain-scale kinematics in disordered (mechanically or morphologically) granular media. To this end, additional continuum kinematic measures are introduced and related to the grain-pair relative motions. The need for enriched descriptions is justified through experimental measurements as well as results from simulations using discrete models. Stresses conjugate to the kinematic measures are then defined and related, through equivalence of deformation energy density, to forces conjugate to the measures of grain-pair relative motions. The kinetic energy density description for a continuum material point is also correspondingly enriched, and a variational approach is used to derive the governing equations of motion. By specifying a particular choice for degree  $n$ , abridged models of degrees 2 and 1 are derived, which are shown to further simplify to micro-polar or Cosserat-type and second-gradient models of granular materials.

**Keywords**

Granular materials, micromechanics, micromorphic continuum, microstructured solids, higher-order theories

**1. Introduction**

Granular solids may be characterized as composed of distinct grains mediated by interfaces. The complexity and variety of the interfaces that could be cohesive or non-cohesive, the irregularities of grain

**Corresponding author:**

Anil Misra, Civil, Environmental and Architectural Engineering Department, University of Kansas, 1530 W 15th Street, Learned Hall, Lawrence, KS 66045-7609, USA.  
Email: amisra@ku.edu

shapes, the disordered granular structure, and the presence of voids are some of the factors that make the behavior of granular solids particularly challenging to describe [1, 2]. More generally, granular materials exhibit a wide variety of behaviors. These range from fluid-like behavior at a low concentration of grains, to plastic solid-like behavior in higher concentrations, as in soil, to elastic solid-like behavior in much higher concentrations or in consolidated granular media in which the grains could be bonded together, as in sedimentary rocks (see, for example [3,4]). The focus of this paper is upon granular solids, which have high concentrations of grains and may be described as solids with granular microstructure that can be either naturally occurring or man-made, for example, granular metamaterials. The underlying feature of these solids is the profound effect of grain interactions, which, in some granular material systems, are associated with the concentration of deformations in the close neighborhood of the grain boundaries or grain contacts. In all cases of granular materials, the collective behavior of millions of grains comprising the granular material system is inextricably connected to the grain-pair interactions and granular structures. Based upon the scale of interest, different approaches may be utilized to model granular systems. At scales close to the size of grains, such materials can be considered an assembly of discrete particles in contact and hence the D'Alembertian (Newtonian) mechanics can be applied leading to discrete models [5], such as the distinct (discrete) element method (DEM). Using discrete models, the mechanical state of granular materials can be described in detail given the knowledge of the position, geometry, and the material properties of each grain and grain-pair interaction [6–10]. New advancements in computational approaches (including various multi-scaling approaches [11–13]) have been integrated into discrete models in recent years to reduce the steep computational cost. These advancements have permitted the analysis of models with an increasing number of grains. Nevertheless, there are persistent challenges associated with the specification of accurate information about each grain and its neighborhood geometrical properties, as well as the mechanical behavior between every interacting grain-pair.

For a large number of grains inside the granular medium, especially when viewed at larger scales (e.g. hundred times greater than grain size), continuum models remain the most efficient. The continuum description of granular material behavior provides a systematic approach through which the macroscopic behavior of granular material can be predicted with considerably less computational effort while explicitly considering the effects of grain interactions (see [14–21] for a subset of early efforts in this direction and [22] for a brief historical review). These continuum models incorporate grain-scale information by, typically, considering mean behaviors of grain-pair interactions in different directions. Clearly, the continuum models do not track the trajectories of all particles and, consequently, do not accurately resolve every grain motion or satisfy grain-scale minimization of deformation energy. These models rely upon certain approximations as well as the need for model parameter identifications for accurate description of the macro-scale phenomena. Nevertheless, they provide good approximations for the collective behavior of grain behavior given incomplete information and intractable details about the microstructure and the micromechanical parameters. This paper further expounds the granular micromechanics approach (GMA) [1,2,23] for the development of continuum models of granular materials.

In classical continuum mechanics, the assumed constitutive behavior permits one to study each material point independent of the others, interacting only by means of mass, momentum, energy, and entropy equations. In the standard form of continuum mechanics, the material point is declared with its size approaching zero, which is sufficient to characterize the immediate neighborhood (local effects) [24]. In such a theory, grain rotations, an integral part of energy transfer in granular systems [2], are not accounted for. In granular media, the collective behavior of granular materials at the continuum scale depends upon the micro-mechano-morphology of grains and grain-pair interactions. Because of the complexity of the granular medium in both mechanical and morphological aspects, a refined description of the material behavior in continuum models is needed for modeling many observed phenomena that classical continuum mechanics is unable to predict, for example, elastic wave dispersion in a granular medium [2,23,25–27]. This is especially true if the characteristic wavelength is below the resolution of the standard continuum mechanics model [24,28]. Indeed, a key shortcoming of the classical continuum theory is its inability to describe the effects of complex kinematics and energy distribution within the material point. In this aspect, it is particularly useful to note the work of the Cosserat brothers [29] with regards to rotational degrees of freedom.



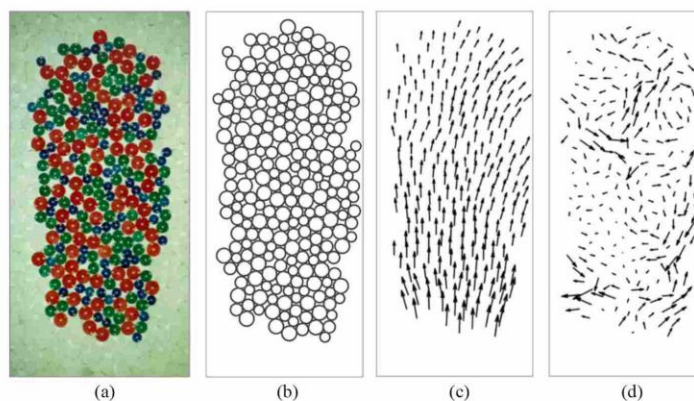


**Figure 1.** Experimental results for a randomly packed granular material: (a) original picture taken from the initial configuration of the structure; (b) digitized picture of the granular structure; (c) total displacement field where vectors represent grain centroid displacements; (d) the fluctuation in the displacement field from the mean behavior.

In the sequel, we first elucidate the complex kinematics in granular media with the aid of experimental measurements and discrete models. Subsequently, we describe the general framework for the continuum model and present an extended GMA that leads to an  $n$ th degree micromorphic continuum model. Abridged versions of the derived model for the case of micromorphic models of degrees 2 and 1 are then presented. The degree 1 model is further elaborated to extract micro-polar and second-gradient continuum descriptions. In all these derivations and discussions, the kinematical approximations, the identifications of grain motions with continuum kinematic measures, and the micro-macro identification of deformation energies have a central role. The aim of this work is to achieve a clear interpretation of the continuum kinematic measures in terms of the grain motions.

## 2. Grain-scale kinematics of granular structures

A promising approach to model the behavior of granular materials is utilizing the variational methods to derive the governing equations of a system based upon a postulated action functional, provided that the correct kinematics are known [30–33]. To fix our ideas regarding the need for refined relationships between continuum and grain-scale kinematics, we utilize examples drawn from experiments on grain packing as well as simulations using discrete models. Figure 1 shows the results from experiments performed on a set of granular discs lying on a horizontal plane, thus manifesting a two-dimensional (2D) granular structure. The excerpted granular structure shown in Figure 1(a) is composed of a 240-grain (disc) cluster of three different grain sizes. This grain cluster is embedded within a larger grain assembly such that it is far from the applied boundary conditions that are designed to mimic the biaxial confined shear test (for more details see [34]). It is notable that in the studied system in Figure 1, there is a randomness of grains in terms of geometry and grain-pair interactions, as no two grains (even those with the same size) have the same surface properties. Figure 1(b) shows the digitized granular assembly under study obtained from the computer-analyzed pictures taken from the experiment, and Figure 1(c) displays the displacement field inside the assembly from the initial to the current configuration. Each vector represents the displacement of a grain centroid as the assembly experiences quasi-static loading. The loading is such that infinitesimal deformation assumption holds. The displacement field can be decomposed into a mean displacement part (coming from the applied macroscopic boundary displacements) and a fluctuation part (the difference between the total displacement vectors and the mean displacement vectors). Figure 1(d) shows the fluctuation in the displacements of grains. One can notice the complexity of such a field induced by the randomness in the granular system studied. Note that the scales in Figures 1(c) and (d) are different and have been adjusted for better visualization. The fluctuation vectors observed have



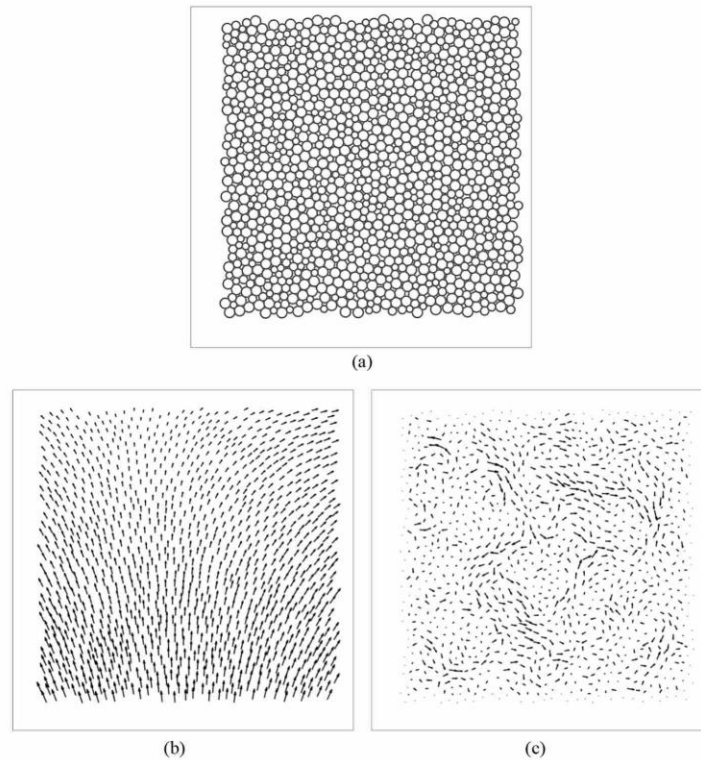


**Figure 2.** Discrete simulation results for a randomly packed granular material with equal grain-pair interactions in all grains: (a) initial configuration of the granular structure; (b) total displacement field where vectors represent grain centroid displacements; (c) the fluctuation in the displacement field from the mean behavior.

maximum  $x$  and  $y$  components that are, respectively,  $\sim 53\%$  and  $\sim 18\%$  of the maximum  $x$  and  $y$  components of the total displacements.

Clearly, in the experimentally observed system both the morphology and grain-pair mechanical properties are disordered. We now consider the case that isolates the effect of morphology disorder (which has been shown to have a strong effect on wave attenuation in granular media [35]). In this example, we use discrete simulation to model a randomly packed granular structure with 1152 grains (see [36] for the detailed formulation of discrete simulation). The granular structure is composed of three grains sizes (52% small, 26% intermediate, and 22% large), as shown in Figure 2(a). We assume that in this elastic process no contact between two grains is lost or initiated. Further, we assume elastic grain-pair interactions with a quadratic form of energy. Even for the case of nonlinear grain-pair interactions, such an assumption is reasonable for small deformations at states close to the structural equilibrium. Figure 2(b) gives the displacement field obtained by applying boundary conditions that mimic the deformation of the 240-grain cluster in the first example. Further, Figure 2(c) displays the fluctuation in the displacement field for each grain, where they have maximum  $x$  and  $y$  components that are, respectively,  $\sim 6\%$  and  $\sim 3\%$  of the maximum  $x$  and  $y$  components of the total displacements. In these calculations, the grain-pair stiffnesses were assumed to be such that they satisfy the ratios  $K_s/K_n = 0.5$ ,  $G/K_n = 1$ , where  $K_n$ ,  $K_s$ , and  $G$  are the normal stiffness, tangential (shear) stiffness, and rotational stiffness of the grains, respectively. It is notable that the fluctuations will become larger if there is a larger contrast in the grain

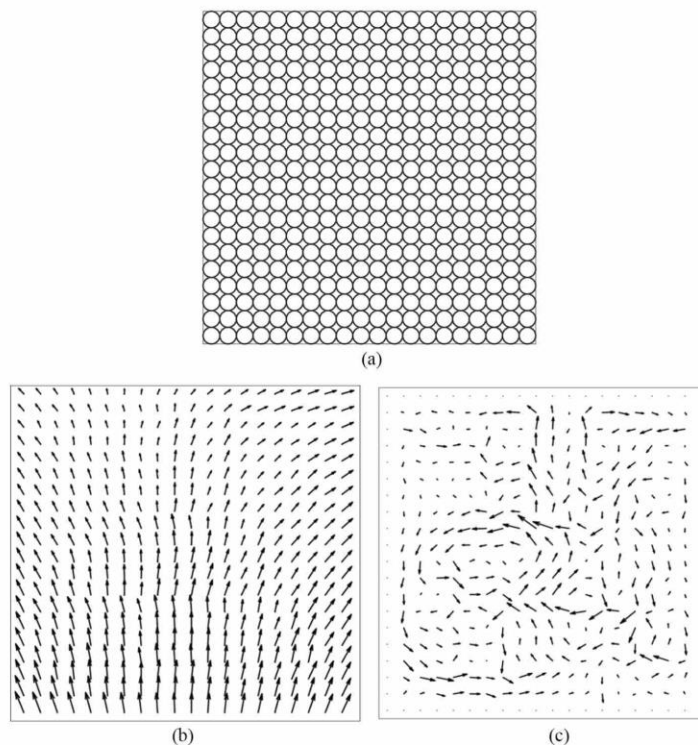


**Figure 3.** Discrete simulation results for a regularly packed granular material with random grain-pair interactions: (a) initial configuration of the granular structure; (b) total displacement field where vectors represent grain centroid displacements; (c) the fluctuation in the displacement field from the mean behavior.

stiffnesses, or in the size of the grains, or if the packing has more randomness in terms of coordination number (the number of contacts for each grain). It is clear from these calculations that the geometrical disorder leads to displacement fluctuations even in dense elastic granular structures.

Similar fluctuations can be found in geometrically ordered granular structures, provided the grain-pair interactions have some disorder. It is worth remarking that the bulk of the literature dealing with granular media has focused upon materials with disordered morphology (see, among others, [4,35,37]), with only a few studies related to ordered structures (see, for example, [14,16,38,39]). However, it is reasonable to conceive of an ordered granular material with natural (or artificially made) disorder in grain-pair interactions. In the third example provided here, we use discrete simulation to model an ordered granular structure with 400 grains with equal sizes (see Figure 3(a)). In this case, we randomly assign the values of stiffness parameters to grain-pairs, such that in a normalized sense with respect to the minimum value for the stiffness  $K_n$ , the assigned values of grain-pair stiffnesses are as follows:  $1 \leq K_n \leq 1000$ ,  $0.1 \leq K_s \leq 10$ , and  $1 \leq G \leq 10$ . The total displacement field is shown in Figure 3(b), along with the displacement fluctuations in Figure 3(c), under the same boundary conditions as in the previous example. The fluctuation vectors observed have maximum  $x$  and  $y$  components that are, respectively,  $\sim 37\%$  and  $\sim 16\%$  of the maximum  $x$  and  $y$  components of the total displacements. Indeed, larger variations in grain-pair stiffnesses will result in even larger fluctuations and, hence, a morphologically ordered granular structure with disordered grain interaction can have complex kinematics fields.

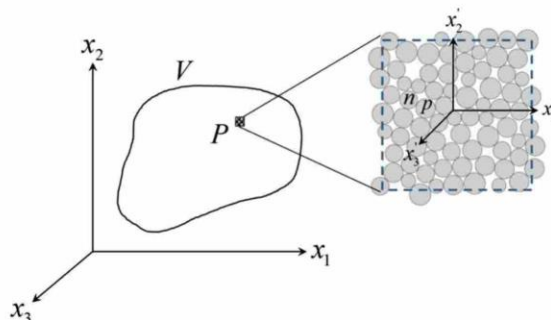


**Figure 4.** Schematic of the continuum material point,  $P$ , and its granular microstructure magnified for visualization, where the  $x'$  coordinate system is attached to its barycenter.

Such fluctuations (as shown in the three aforementioned examples) in the displacement field are neglected in the classical Cauchy continuum model. To capture the behavior of granular systems, a refined theory with enhanced kinematics is necessary. Of course, the extent of accuracy we seek and the capability of the theory to describe different phenomena influence the complexity of the theory and a compromise should be made based on the aim of the study. In this regard, the GMA [23], a micromechanics-based continuum model for granular solids, develops the continuum description of granular solids in a statistical sense by considering the mean behavior of grain-pair interactions. Indeed, the statistical framework implemented in the GMA leads to the loss of ability to track all the particles and mechanisms occurring at the scale of the microstructure (grain scale). Nevertheless, as complete information in the grain-scale is usually not available for granular structures with a large number of grains, such statistical approximations are reasonably justified, and an incomplete solution, such as the mean behavior, based on incomplete data, is sufficient [22]. The GMA treats each material point as a micromorphic medium to allow relative displacement and rotations of the granular microstructure embedded in each material point. Such a method proves fruitful in describing natural granular materials with random packing, or in designing granular metamaterials with known micro-mechano-morphology in their microstructure for particular applications, such as granular structures showing tunable frequency band gaps [2,23,25,26]. For a brief discussion on using the GMA in the design of granular metamaterials, see [26].

### 3. Continuum framework for granular micromechanics

From a macroscopic viewpoint, we consider a body formed of granular material to be a continuum of volume  $V$  bounded by the surface  $S$  (see Figure 4 for a 2D representation). We further consider that this body can be constructed by stacking a finite volume of the material (a collection of particles with different sizes and shapes), termed here as the representative volume element (RVE), and refer to it as a continuum material point, which in the macroscopic scale is geometrically represented by point  $P$ . The RVE plays the role of a unit cell defined in the context of metamaterials (e.g. see [40]). In a granular material with a broad range of grain shapes, sizes, and types of interaction, the integral range discussed in [41–44] will be very large and may even be indeterminate. The implication is that the RVE size should be very large compared to the grain size, such that the significance of relative fluctuations from the average values could be smaller. Indeed, for a true randomly packed granular material, such a RVE is more of a statistical sample of the whole material under study and the stacking of the RVE does not really make up the whole structure. However, as large-scale effects are mainly controlled by the average behavior in the microstructure, assuming such a RVE is valid (see, among others, the recent studies on determination of the RVE for heterogeneous materials in [45–48]). We associate with the material point  $P$  the properties of density, volume, and mass, represented by  $\rho$ ,  $dV = V'$ , and  $dm = \rho V'$ , respectively, where  $V'$  is the volume of the RVE. Denoting by  $\mathbf{X}$ , the position vector of point  $P$  at initial configuration measured from a

fixed Euclidean rectangular coordinate system (which will be called the macro-scale coordinate system in what follows), and taking the time reference to coincide with the initial configuration of the medium ( $t_0 = 0$ ), we can write, for the position vector  $\mathbf{x}$  of the material point  $P$  at time  $t \geq t_0$

$$\mathbf{x} = \chi(X, t), \quad X = \chi(X, t = 0), \quad (1)$$

or in component format

$$x_i = \chi_i(X_j, t), \quad X_i = \chi_i(X_j, t = 0), \quad i, j = 1, 2, 3, \quad (2)$$

where the placement function relating the positions in the initial and the current configurations in the macro-scale coordinate system is given the symbol  $\chi$ . Therefore, the macro-scale displacement vector  $\mathbf{u}$  attributed to point  $P$  is defined as

$$\mathbf{u} = \mathbf{x} - \mathbf{X}, \quad (3)$$

or in component form

$$u_i = x_i - X_i. \quad (4)$$

Microscopically, and as mentioned before, point  $P$  is itself a collection of grains and, hence, can be regarded as a continuum, called a micro-continuum [49]. Each grain centroid inside point  $P$  assumes the position vector  $\mathbf{x}'$  at time  $t$  with respect to a second rectangular micro-scale coordinate system  $x'_i$ . The coordinate system  $x'_i$  is attached to the center of mass (COM) of material point  $P$ , parallel to the macro-scale coordinate system  $x_i$ , and moving with the macro-scale displacement  $\mathbf{u}$ . The micro-scale coordinate system  $x'_i$  is able to distinguish different grains inside material point  $P$  (see Figure 4). Therefore, the position vector of the centroid of a grain  $p$  is written as

$$\mathbf{x}' = \chi'(X, X', t), \quad X' = \chi'(X, X', t = 0), \quad (5)$$

where  $X'$  is the position vector of grain  $p$  in the initial configuration, and the placement function relating the positions in the initial and the current configurations in the micro-scale coordinate system has been given the symbol  $\chi'$ . Equation (5) in component form reads

$$x'_i = \chi'_i(X_j, X'_j, t), \quad X'_i = \chi'_i(X_j, X'_j, t = 0), \quad i, j = 1, 2, 3. \quad (6)$$

We attribute the micro-scale displacement vector  $\mathbf{u}'$  to the grain centroids in the RVE according to the definition

$$\mathbf{u}' = \mathbf{x}' - \mathbf{X}', \quad (7)$$

or in component form

$$u'_i = x'_i - X'_i. \quad (8)$$

Although the micro-scale displacement in Equation (7) (and Equation (8)) is a function of the macro-scale position vector  $\mathbf{X}$ , it lies in the vector space spanned by the micro-scale coordinate system bases only. In other words, it does not capture macro-scale displacements. The absolute values of the both macro- and micro-scale displacement gradients have been assumed to be small when compared to unity, which in mathematical notation reads

$$\left| \frac{\partial u_i}{\partial X_j} \right| \ll 1, \quad \left| \frac{\partial u'_i}{\partial X'_j} \right| \ll 1. \quad (9)$$

As a result, we consider infinitesimal deformation in granular media in both macro- and micro-scales. Consequently, with regards to Equation (9), we write

$$\frac{\partial u_i}{\partial X_j} \approx \frac{\partial u_i}{\partial x_j}, \quad \frac{\partial u'_i}{\partial X'_j} \approx \frac{\partial u'_i}{\partial x'_j}, \quad (10)$$

and

$$u_i = u_i(x_j, t), \quad u'_i = u'_i(x_j, x'_j, t). \quad (11)$$

Equation (11) is the most general form for the assumed physics in infinitesimal deformation. Equation (11) was introduced in [49–51] for materials with microstructure. In this paper, we assume that  $\mathbf{u}$  and  $\mathbf{u}'$  are continuous and differentiable functions of  $x_i$  and  $x'_i$  up to the desired order. These assumptions suggest that the discrete nature of grains is modeled as a continuum. For an accurate description of the displacement of individual grains within the RVE, the displacement field, by nature, is complex.

#### 4. Extended/generalized granular micromechanics: micromorphic theory of degree $n$

Motivated by the examples considered in Section 2, we write for the micro-scale vector  $\mathbf{u}'$ , using a polynomial expansion up to  $(n+1)$ th order with respect to  $\mathbf{x}'$  about the COM of the RVE

$$u'_i = \psi_{ij_1}(x_m, t)x'_{j_1} + \psi_{ij_1j_2}(x_m, t)x'_{j_1}x'_{j_2} + \dots + \psi_{ij_1j_2 \dots j_{n+1}}(x_m, t)x'_{j_1}x'_{j_2} \dots x'_{j_{n+1}}, \quad (12)$$

where  $\psi_{ij_1}$ ,  $\psi_{ij_1j_2}$ ,  $\dots$ ,  $\psi_{ij_1j_2 \dots j_{n+1}}$  are the second, third,  $\dots$ ,  $(n+2)$ th rank micro-deformation tensors only functions of  $\mathbf{x}$  and  $t$ . In expansion Equation (12), the term of the 0th order vanishes as a consequence of the fact that the micro-scale coordinate system is attached to the COM of the RVE. Henceforward, the indices in the subscript take values of 1, 2, and 3 corresponding to the three coordinate axes, and the summation convention over repeated indices (in the subscript) is implied unless noted otherwise. Note that the same letters with different numerical subscripts represent different indices (for example,  $j_1$  and  $j_2$  in the expression  $\psi_{ij_1j_2}$ ). Without loss of generality and similar to [49], we assume that tensors  $\psi_{ij_1 \dots j_m}$ ,  $m = 2, 3, \dots, n+1$  are symmetric with respect to indices  $j_1, j_2, \dots, j_m$  (for example, these could be chosen as derivatives in a Taylor series expansion). Equation (12) imposes a deformation field inside the RVE and, hence, reduces a problem that has a very large number of degrees of freedom (depending upon the number of grains) to a problem with a reduced number of degrees of freedom (depending upon the order of expansion), in this case a micromorphic model of degree  $n$ . An immediate consequence of such reduction is a decrease in computational cost needed to solve a problem. The suitability of such simplification should be evaluated by the ability of the proposed continuum model in describing desired phenomena in granular materials. Based on Equation (12), for a micromorphic medium of degree  $n$ , the total displacement vector for the grains inside the RVE can be written as

$$\phi_i = u_i + u'_i = \bar{\phi}_i + \psi_{ij_1}x'_{j_1} + \psi_{ij_1j_2}x'_{j_1}x'_{j_2} + \dots + \psi_{ij_1j_2 \dots j_{n+1}}x'_{j_1}x'_{j_2} \dots x'_{j_{n+1}}, \quad (13)$$

where  $\bar{\phi}_i = u_i$ , which is used so that the notation is in harmony with earlier publications [2, 23, 25, 26]. For the neighboring grains  $n$  and  $p$  in the RVE corresponding to the material point  $P$ , the total displacements are written as

$$\phi_i^p = \bar{\phi}_i + \psi_{ij_1}l_{j_1}^p + \psi_{ij_1j_2}l_{j_1}^p l_{j_2}^p + \dots + \psi_{ij_1j_2 \dots j_{n+1}}l_{j_1}^p l_{j_2}^p \dots l_{j_{n+1}}^p, \quad (14)$$

$$\phi_i^n = \bar{\phi}_i + \psi_{ij_1}l_{j_1}^n + \psi_{ij_1j_2}l_{j_1}^n l_{j_2}^n + \dots + \psi_{ij_1j_2 \dots j_{n+1}}l_{j_1}^n l_{j_2}^n \dots l_{j_{n+1}}^n, \quad (15)$$

where  $l_m^u$ ,  $m = 1, 2, \dots, n+1$  represents the  $j_m$ th component of the vector joining the origin of the micro-scale coordinate system (COM of the RVE) to the  $u$ th grain. The relative displacement of the two neighboring grains  $n$  and  $p$  is, therefore

$$\delta_i^{np} = \phi_i^p - \phi_i^n = \psi_{ij_1}J_{j_1}^{np} + \psi_{ij_1j_2}J_{j_1j_2}^{np} + \dots + \psi_{ij_1j_2 \dots j_{n+1}}J_{j_1j_2 \dots j_{n+1}}^{np}, \quad (16)$$

In Equation (16), we define the geometry moment measures of  $J_{j_1j_2 \dots j_k}^{np} = J_{j_1j_2 \dots j_k}^p - J_{j_1j_2 \dots j_k}^n$ , where  $J_{j_1j_2 \dots j_k}^\beta = l_{j_1}^\beta l_{j_2}^\beta \dots l_{j_k}^\beta$  and  $J_{j_1}^\beta = l_{j_1}^\beta$  for the grain labeled  $\beta$ .

Inspired by [49,50], we introduce the following relative deformation tensors

$$\gamma_{ij_1} = \bar{\phi}_{i,j_1} - \psi_{ij_1}, \quad \gamma_{ij_1j_2} = \psi_{ij_1,j_2} - \psi_{ij_1j_2}, \quad \dots, \quad \gamma_{ij_1j_2 \dots j_{n+1}} = \psi_{ij_1j_2 \dots j_n, j_{n+1}} - \psi_{ij_1j_2 \dots j_{n+1}}, \quad (17)$$

where hereafter a comma in the subscript denotes differentiation with respect to the spatial coordinates. In Equation (17), the considered differentiation is with respect to the macro-scale spatial coordinates that define the macro-scale gradients of the micro-deformation tensors. For a micromorphic theory of degree  $n$ , it is assumed that the  $(n+2)$ th rank relative deformation tensor  $\gamma_{ij_1j_2 \dots j_{n+1}}$  is zero, such that  $\psi_{ij_1j_2 \dots j_{n+1}} = \psi_{ij_1j_2 \dots j_n, j_{n+1}}$ . Such an assumption alters the independent nature of the micro-deformation tensor  $\psi_{ij_1j_2 \dots j_{n+1}}$  to the dependent macro-scale gradient measure  $\psi_{ij_1j_2 \dots j_n, j_{n+1}}$  (similar to when one simplifies the kinematic measures to go from a Timoshenko beam model to an Euler beam model by relating the rotational degree of freedom in a Timoshenko beam model to the gradient of vertical deflection). Using Equations (16) and (17), we can therefore write, for the relative displacement of two neighboring grains  $n$  and  $p$ , the following

$$\begin{aligned} \delta_i^{np} = \phi_i^p - \phi_i^n = & (\bar{\phi}_{i,j_1} - \gamma_{ij_1}) J_{j_1}^{np} + (\psi_{ij_1,j_2} - \gamma_{ij_1j_2}) J_{j_1j_2}^{np} + \dots \\ & + (\psi_{ij_1j_2 \dots j_{n-1}, j_n} - \gamma_{ij_1j_2 \dots j_n}) J_{j_1j_2 \dots j_n}^{np} + \psi_{ij_1j_2 \dots j_n, j_{n+1}} J_{j_1j_2 \dots j_{n+1}}^{np}, \end{aligned} \quad (18)$$

Equation (18) can be written as

$$\delta_i^{np} = \delta_i^M - \delta_i^{m_1} + \delta_i^{g_1} - \dots - \delta_i^{m_n} + \delta_i^{g_n}, \quad (19)$$

where the relative displacement of a grain-pair has been decomposed into the following micro-scale kinematic measures

$$\delta_i^M = \bar{\phi}_{i,j_1} J_{j_1}^{np}, \quad \delta_i^{m_k} = \gamma_{ij_1j_2 \dots j_k} J_{j_1j_2 \dots j_k}^{np}, \quad \delta_i^{g_k} = \psi_{ij_1j_2 \dots j_k, j_{k+1}} J_{j_1j_2 \dots j_{k+1}}^{np}, \quad k = 1, 2, \dots, n. \quad (20)$$

The micro-scale kinematic measures introduced in Equation (20) are functions of both the assumed displacement field and geometry moment measures. It is noteworthy that these micro-scale kinematic measures, in a sense, define the multi-body interactions that can capture the influence of far neighbors (successively farther neighbors) on the behavior of a grain-pair.

The macro-rotation in the macro-scale coordinate system,  $\bar{\kappa}_i$ , is defined as

$$\bar{\kappa} = \frac{1}{2} \nabla \times \mathbf{u}, \quad (21)$$

or in component form

$$\bar{\kappa}_i = \frac{1}{2} e_{lki} u_{k,l} = \frac{1}{2} e_{lki} \bar{\phi}_{k,l}. \quad (22)$$

The micro-rotation in the micro-scale coordinate system,  $\hat{\kappa}$ , is

$$\hat{\kappa} = \frac{1}{2} \nabla \times \mathbf{u}', \quad (23)$$

or in component form

$$\hat{\kappa}_i = \frac{1}{2} e_{lki} u'_{k,l} = \frac{1}{2} e_{lki} \phi_{k,l}, \quad (24)$$

where the differentiation is with respect to the micro-scale coordinates  $\mathbf{x}'$ . We note that the two neighboring grains  $n$  and  $p$  experience the same macro-rotation  $\bar{\kappa}$ . Therefore, the relative rotation of grains  $n$  and  $p$  is only due to the micro-rotation in the micro-scale coordinate system,  $\hat{\kappa}$ , which based on the assumption for the displacement field in Equation (12), is continuous. It is noteworthy that the macro- and micro-rotations defined above do not consider grain spin, as in [2]. In the formulation presented in



this paper, the effect of grain spin has been neglected with the aim of keeping the development focused upon the generalization of one key aspect of granular material kinematics. Indeed, grain spins can be significant in some cases, as has been pointed in our previous papers [1,2], and a complete theory of granular materials should not ignore the effect of grain spins. The micro-rotation related to the micro-scale displacement can be written using Equation (13) as

$$\widehat{\kappa}_i = \frac{1}{2} (e_{lki}\psi_{kl} + 2e_{lki}\psi_{klj_1}x'_{j_1} + \cdots + (n+1)e_{lki}\psi_{klj_1j_2\cdots j_n}x'_{j_1}x'_{j_2}\cdots x'_{j_n}). \quad (25)$$

Thus, for grains  $n$  and  $p$

$$\widehat{\kappa}_i^p = \frac{1}{2} (e_{lki}\psi_{kl} + 2e_{lki}\psi_{klj_1}J_{j_1}^p + \cdots + (n+1)e_{lki}\psi_{klj_1j_2\cdots j_n}J_{j_1j_2\cdots j_n}^p), \quad (26)$$

$$\widehat{\kappa}_i^n = \frac{1}{2} (e_{lki}\psi_{kl} + 2e_{lki}\psi_{klj_1}J_{j_1}^n + \cdots + (n+1)e_{lki}\psi_{klj_1j_2\cdots j_n}J_{j_1j_2\cdots j_n}^n). \quad (27)$$

Therefore, the relative rotation of two neighboring grains  $n$  and  $p$ ,  $\theta_i^{np}$ , can be written in terms of the introduced parameters in Equation (17) as

$$\begin{aligned} \theta_i^{np} &= \widehat{\kappa}_i^p - \widehat{\kappa}_i^n = \frac{1}{2} (2e_{lki}\psi_{klj_1}J_{j_1}^{np} + \cdots + (n+1)e_{lki}\psi_{klj_1j_2\cdots j_n}J_{j_1j_2\cdots j_n}^{np}) \\ &= e_{lki}(\psi_{klj_1} - \gamma_{klj_1})J_{j_1}^{np} + \cdots + \frac{n}{2} e_{lki}(\psi_{klj_1j_2\cdots j_{n-2}j_{n-1}} - \gamma_{klj_1j_2\cdots j_{n-2}j_{n-1}})J_{j_1j_2\cdots j_{n-1}}^{np} \\ &\quad + \left(\frac{n+1}{2}\right) e_{lki}\psi_{klj_1j_2\cdots j_{n-1}j_n}J_{j_1j_2\cdots j_n}^{np}. \end{aligned} \quad (28)$$

In Equation (28), the relative rotation of two neighboring grains  $n$  and  $p$  is decomposed as

$$\theta_i^{np} = \theta_i^{g_1} - \theta_i^{m_1} + \cdots + \theta_i^{g_{n-1}} - \theta_i^{m_{n-1}} + \theta_i^{g_n}, \quad (29)$$

where we have defined the micro-scale kinematic measures

$$\begin{aligned} \theta_i^{g_m} &= \left(\frac{m+1}{2}\right) e_{lki}\psi_{klj_1j_2\cdots j_{m-1}j_m}J_{j_1j_2\cdots j_m}^{np}, \quad m = 1, 2, \dots, n \\ \theta_i^{m_m} &= \left(\frac{m+1}{2}\right) e_{lki}\gamma_{klj_1j_2\cdots j_m}J_{j_1j_2\cdots j_m}^{np}, \quad m = 1, 2, \dots, n-1. \end{aligned} \quad (30)$$

Similar to the micro-scale kinematic measures in Equation (20), the measures introduced in Equation (30) are also dependent on the assumed displacement field and geometry moment measures.

To obtain the equation of motion based on Hamilton's principle using the variational approach, we require expressions for the deformation energy, kinetic energy, and the energy introduced to the system by external actions. To this end we consider the macro-scale deformation energy density to be a function of the macro-scale continuum kinematic measures as  $W = W(\phi_{(i,j)}, \gamma_{j_1}, \dots, \gamma_{ij_1j_2\cdots j_n}, \psi_{ij_1j_2}, \dots, \psi_{ij_1j_2\cdots j_n, j_{n+1}})$ . The proposed approach is therefore a first-gradient model where the quantities  $\psi_{ij_1j_2\cdots j_m}; m = 1, \dots, n$  are considered as internal variables. We note in this regard that it would be interesting to explore the relationship of degree  $n$  micromorphic model envisaged here with the case of the  $n$ th gradient model discussed in [52,53], particularly with respect to the interpretation of the micro-deformation tensors. In a later section, we will describe the conditions in which a second-gradient medium can be deduced from a micromorphic model of degree 1. We remark that an elegant interpretation of the kinematics of the second- and higher gradient media has been presented in [54] and the possibility of  $n$ th gradient continuum theory has been discussed by Piola in seminal works on continuum mechanics [55,56].

The macro-scale stress components can be defined as conjugates to the continuum kinematic measures as follows

$$\begin{aligned}
\tau_{ij} &= \frac{\partial W}{\partial \bar{\phi}_{(i,j)}} \\
\sigma_{ij_1 \dots j_m} &= \frac{\partial W}{\partial \gamma_{ij_1 \dots j_m}}, \quad m = 1, 2, \dots, n \\
\mu_{ij_1 j_2 \dots j_m} &= \frac{\partial W}{\partial \psi_{ij_1 j_2 \dots j_{m-1}, j_m}}, \quad m = 2, 3, \dots, n+1.
\end{aligned} \tag{31}$$

The kinetic energy density (kinetic energy per unit macro-volume)  $T$  for the problem at hand is assumed to be quadratic in form and is expressed as

$$T = \frac{1}{V'} \int_{V'} \frac{1}{2} \rho' \dot{\phi}_i \dot{\phi}_i dV', \tag{32}$$

where  $\rho'$  is the micro-scale mass density per unit macro-volume and over-dots indicate differentiation with respect to time. In general,  $\rho'$  can be non-uniform inside the RVE, such that it is a function of micro-scale coordinate system  $\mathbf{x}'$ . Substituting from Equation (13) into Equation (32) and utilizing König's theorem [57] yields

$$T = \frac{1}{2} \rho \dot{\phi}_i \dot{\phi}_i + \frac{1}{2} \sum_{p=1}^{n+1} \sum_{m=1}^{n+1} \dot{\psi}_{ik_1 \dots k_p} \dot{\psi}_{ij_1 \dots j_m} \rho_{j_1 \dots j_m k_1 \dots k_p}, \tag{33}$$

where we have defined the following inertia measures

$$\rho = \frac{1}{V'} \int_{V'} \rho' dV', \quad \rho_{j_1 \dots j_m} = \frac{1}{V'} \int_{V'} \rho' x'_{j_1} \dots x'_{j_m} dV'. \tag{34}$$

It is noted here for Equation (33), and henceforward, that summation convention is not applied when the equation is in compact form using summation notation  $\Sigma$ , but when expanded, summation convention applies. Note that  $\rho_{j_1}$  in Equation (34) vanishes since the origin of the micro-scale coordinate system coincides with the COM of the RVE. The inertia measures in Equation (34) can be considered gyration tensors of higher orders in the continuum limit. The kinetic energy density in Equation (33) is an extension of those in earlier publications for the GMA based on micromorphic theory of degree 1 found in [23,25,26]. The added terms in the description of the kinetic energy and the introduced inertia measures affect the dynamic behavior of the granular material. Such an effect will be studied in future publications.

The Hamilton principle requires the action functional (Lagrangian) to be minimum. Such a requirement necessitates that the variation of the action functional is zero, and is expressed as

$$\delta \int_{t_0}^{t_1} (\tilde{T} - \tilde{W} + \tilde{W}_{ext}) dt = 0, \tag{35}$$

where the terms  $\tilde{T}$ ,  $\tilde{W}$ , and  $\tilde{W}_{ext}$  are defined in the following.  $\tilde{T} = \int_V T dV$  is the total kinetic energy, defined as the integral of the kinetic energy density over the whole domain. The variational of the kinetic energy functional is written, after integration by parts and assuming the values of  $\bar{\phi}_j, \psi_{ij_1 \dots j_m}$ ,  $m = 1, \dots, n+1$  to be known at  $t = t_0, t_1$ , as

$$\delta \int_{t_0}^{t_1} \tilde{T} dt = - \int_{t_0}^{t_1} \int_V \rho \ddot{\phi}_i \delta \bar{\phi}_i dV dt - \sum_{p=1}^{n+1} \sum_{m=1}^{n+1} \int_{t_0}^{t_1} \int_V \rho_{j_1 \dots j_m k_1 \dots k_p} \ddot{\psi}_{ik_1 \dots k_p} \delta \psi_{ij_1 \dots j_m} dV dt. \tag{36}$$

In Equation (35),  $\tilde{W} = \int_V W dV$  is the total macro-scale deformation energy, defined as the integral of the deformation energy density over the whole domain. Hence, the variational of the macro-scale deformation energy functional, using Equation (31) and applying Gauss's divergence theorem, is obtained as



$$\begin{aligned}
\delta \int_{t_0}^{t_1} \bar{W} dt &= - \int_{t_0}^{t_1} \int_V (\tau_{ij} + \sigma_{ij})_{,j} \delta \bar{\phi}_i dV dt - \sum_{m=2}^n \int_{t_0}^{t_1} \int_V (\sigma_{ij_1 \dots j_m} + \mu_{ij_1 \dots j_m})_{,j_m} \delta \psi_{ij_1 \dots j_{m-1}} dV dt \\
&- \sum_{m=1}^n \int_{t_0}^{t_1} \int_V \sigma_{ij_1 \dots j_m} \delta \psi_{ij_1 \dots j_m} dV dt - \int_{t_0}^{t_1} \int_V (\mu_{ij_1 \dots j_{n+1}})_{,j_{n+1}} \delta \psi_{ij_1 \dots j_n} dV dt + \int_{t_0}^{t_1} \int_S (\tau_{ij} + \sigma_{ij}) n_j \delta \bar{\phi}_i dS dt \quad (37) \\
&+ \sum_{m=2}^n \int_{t_0}^{t_1} \int_V (\sigma_{ij_1 \dots j_m} + \mu_{ij_1 \dots j_m}) n_{j_m} \delta \psi_{ij_1 \dots j_{m-1}} dS dt + \int_{t_0}^{t_1} \int_V \mu_{ij_1 \dots j_{n+1}} n_{j_{n+1}} \delta \psi_{ij_1 \dots j_n} dS dt.
\end{aligned}$$

In Equation (35),  $\bar{W}_{ext} = \int_V W_{ext} dV$  is the total external energy and its form is motivated by the expression for  $\bar{W}$ , consisting of non-contact volumic (body) forces,  $f_i$ , double forces,  $\Phi_{ij}$ , and other higher order forces  $\Phi_{ij_1 \dots j_m}$ ,  $m=2, \dots, n$  acting on the granular material, and contact traction,  $t_i$ , contact double traction,  $T_{ij}$ , and other higher order contact tractions  $T_{ij_1 \dots j_m}$ ,  $m=2, \dots, n$  defined as surface forces, double forces, etc. per unit area. Consistent with Equation (37), the following form is considered for the variational of the external work

$$\begin{aligned}
\delta \int_{t_0}^{t_1} \bar{W}_{ext} dt &= \int_{t_0}^{t_1} \int_V f_i \delta \bar{\phi}_i dV dt + \sum_{m=1}^n \int_{t_0}^{t_1} \int_V \Phi_{ij_1 \dots j_m} \delta \psi_{ij_1 \dots j_m} dV dt \quad (38) \\
&+ \int_{t_0}^{t_1} \int_S t_i \delta \bar{\phi}_i dS dt + \sum_{m=1}^n \int_{t_0}^{t_1} \int_S T_{ij_1 \dots j_m} \delta \psi_{ij_1 \dots j_m} dS dt.
\end{aligned}$$

Hamilton principle in Equation (35), using Equations (36)–(38), results in  $\frac{3}{2}(3^{n+1} - 1)$  balance equations in three dimensions and  $2(2^{n+1} - 1)$  balance equations in two dimensions. These balance equations are

$$(\tau_{ij} + \sigma_{ij})_{,j} + f_i = \rho \ddot{\phi}_i, \quad (39a)$$

$$\begin{aligned}
\sigma_{ij_1 \dots j_m} + (\sigma_{ij_1 \dots j_{m+1}} + \mu_{ij_1 \dots j_{m+1}})_{,j_{m+1}} + \Phi_{ij_1 \dots j_m} &= \sum_{p=1}^n \rho_{j_1 \dots j_m k_1 \dots k_p} \ddot{\psi}_{ik_1 \dots k_p} + \rho_{j_1 \dots j_m k_1 \dots k_{n+1}} \ddot{\psi}_{ik_1 \dots k_n, k_{n+1}}, \quad (39b) \\
m &= 1, \dots, n-1
\end{aligned}$$

$$\begin{aligned}
\sigma_{ij_1 \dots j_n} + \mu_{ij_1 \dots j_{n+1}, j_{n+1}} + \Phi_{ij_1 \dots j_n} &= \sum_{p=1}^n \rho_{j_1 \dots j_n k_1 \dots k_p} \ddot{\psi}_{ik_1 \dots k_p} - \sum_{p=1}^{n-1} \rho_{j_1 \dots j_{n+1} k_1 \dots k_p} \ddot{\psi}_{ik_1 \dots k_p, j_{n+1}} \quad (39c) \\
&- \rho_{j_1 \dots j_{n+1} k_1 \dots k_{n+1}} \ddot{\psi}_{ik_1 \dots k_n, k_{n+1}, j_{n+1}}.
\end{aligned}$$

The natural boundary conditions are

$$(\tau_{ij} + \sigma_{ij}) n_j = t_i, \quad (40a)$$

$$(\sigma_{ij_1 \dots j_{m+1}} + \mu_{ij_1 \dots j_{m+1}}) n_{j_{m+1}} = T_{ij_1 \dots j_m}, \quad m=1, \dots, n-1, \quad (40b)$$

$$\left( \sum_{p=1}^n \rho_{j_1 \dots j_{n+1} k_1 \dots k_p} \ddot{\psi}_{ik_1 \dots k_p} + \rho_{j_1 \dots j_{n+1} k_1 \dots k_{n+1}} \ddot{\psi}_{ik_1 \dots k_n, k_{n+1}} + \mu_{ij_1 \dots j_{n+1}} \right) n_{j_{n+1}} = T_{ij_1 \dots j_n}. \quad (40c)$$

The macro-scale stress measures can be related to the micro-scale force and moment measures by equating the macro-scale and the micro-scale deformation energy densities. The micro-scale deformation energy density (per macro-volume) is assumed to be a function of the micro-scale kinematic measures introduced in Equations (20) and (30), written as

$$W = \frac{1}{V'} \sum_{\alpha} W^{\alpha} (\delta_i^{\alpha M}, \delta_i^{\alpha m_1}, \dots, \delta_i^{\alpha m_n}, \delta_i^{\alpha g_1}, \dots, \delta_i^{\alpha g_n}, \theta_i^{\alpha m_1}, \dots, \theta_i^{\alpha m_{n-1}}, \theta_i^{\alpha g_1}, \dots, \theta_i^{\alpha g_n}), \quad (41)$$

where  $\alpha$  shows the  $\alpha$ th grain-pair and the summation is over all grain-pairs inside the RVE. The energy introduced in Equation (41) must be invariant to rigid body rotations and translations. Therefore, we only take the symmetric part of the micro-scale kinematic measure  $\delta_i^{\alpha M}$  in the energy expression in Equation (41). Further, the micro-scale forces and moments conjugate to the micro-scale kinematic measures are defined as follows

$$\begin{aligned}
 \frac{\partial W^\alpha}{\partial \delta_i^{\alpha M}} &= f_i^{\alpha M} \\
 \frac{\partial W^\alpha}{\partial \delta_i^{\alpha m_k}} &= f_i^{\alpha m_k}, \quad k = 1, 2, \dots, n \\
 \frac{\partial W^\alpha}{\partial \delta_i^{\alpha g_k}} &= f_i^{\alpha g_k}, \quad k = 1, 2, \dots, n \\
 \frac{\partial W^\alpha}{\partial \theta_i^{\alpha m_k}} &= m_i^{\alpha m_k}, \quad k = 1, 2, \dots, n-1 \\
 \frac{\partial W^\alpha}{\partial \theta_i^{\alpha g_k}} &= m_i^{\alpha g_k}, \quad k = 1, 2, \dots, n.
 \end{aligned} \tag{42}$$

The grain-pair force/moment measures denoted by superscript  $m_k$  and  $g_k$  are particularly interesting, since these capture the non-local effects of successively farther neighbors on the grain-pair formed of nearest neighbors. Substituting Equation (41) into Equation (31), applying the chain rule of differentiation, and making use of Equations (20), (30), and (42) will lead to expressions for macro-scale stress measures in terms of micro-scale forces, moments, and geometry moment measures. Subsequently, defining a local coordinate system for each interacting grain pair, decomposing intergranular force, moment, displacement, and rotation vectors in their normal and tangential components, and assuming a particular form for  $W^\alpha$ , the macro-scale constitutive relationships in the global coordinate system can be derived as functions of the macro-scale kinematic measures. Finally, substituting the derived constitutive equations in Equations (39) and (40) gives the governing equations of motion and boundary conditions in terms of macro-scale kinematic measures. This approach has been taken in previous works (for example, for linear isotropic elasticity in [23]), and will be pursued for more general cases in the future.

## 5. Granular micromechanics: abridged micromorphic theories

The GMA-based micromorphic theory of degree  $n$  may be needed for accurate description in some cases. In many cases, however, a lower order theory could suffice to capture the key phenomena. It is also notable that a theory of degree  $n$  could be (a) computationally expensive, since the number of coupled equations increases in a nonlinear fashion when  $n$  increases, and (b) intricate to interpret because of the existence of the higher order inertia and stress measures for a large  $n$ . As stated before, a consideration of the value of  $n$  must be made according to that needed for accurate description of the material behavior or, conversely, for understanding how a complex material system could be realized. Here we briefly present the simpler cases of micromorphic theories of degrees 2 and lower. It is particularly interesting to consider the case of degree 1 and its simplifications to micro-polar and second-gradient media.

### 5.1. GMA-based micromorphic theory of degree 2

By retaining the terms up to the cubic order ( $n = 3$ ) in the polynomial expansion in Equation (12), the GMA-based micromorphic theory of degree 2 is obtained. The total displacement of the grains in Equation (13), therefore, simplifies to

$$\phi_i = u_i + u'_i = \bar{\phi}_i + \psi_{ij}x'_j + \psi_{ijk}x'_jx'_k + \psi_{ijkl}x'_jx'_kx'_l. \tag{43}$$

The relative deformation parameters here are  $\gamma_{ij}$ ,  $\gamma_{ijk}$ , and  $\gamma_{ijkl}$  where we assume  $\gamma_{ijkl} = 0$ . Such an assumption leads to  $\psi_{ijkl} = \psi_{ijk,l}$  and permits the description of the nonlinear micro-displacement field up to order three. Thus, the relative displacement of two neighboring grains  $n$  and  $p$  is written as

$$\delta_i^{np} = \delta_i^p - \delta_i^n = \delta_i^M - \delta_i^{m_1} + \delta_i^{g_1} - \delta_i^{m_2} + \delta_i^{g_2}, \quad (44)$$

where we have defined the micro-scale kinematic measures

$$\begin{aligned} \delta_i^M &= \bar{\phi}_{i,j} J_j^{np} \\ \delta_i^{m_1} &= \gamma_{ij} J_j^{np}, \quad \delta_i^{m_2} = \gamma_{ijk} J_{jk}^{np} \\ \delta_i^{g_1} &= \psi_{ij,k} J_{jk}^{np}, \quad \delta_i^{g_2} = \psi_{ijk,l} J_{jkl}^{np}. \end{aligned} \quad (45)$$

The relative rotation between the neighboring grains  $n$  and  $p$  is written as

$$\theta_i^{np} = \bar{\kappa}_i^p - \bar{\kappa}_i^n = \theta_i^{g_1} - \theta_i^{m_1} + \theta_i^{g_2}, \quad (46)$$

where we defined the micro-scale kinematic measures

$$\begin{aligned} \theta_i^{g_1} &= e_{lki} \psi_{kl,j} J_j^{np}, \quad \theta_i^{g_2} = \frac{3}{2} e_{lki} \psi_{klj,p} J_{jp}^{np} \\ \theta_i^{m_1} &= e_{lki} \gamma_{klj} J_j^{np}. \end{aligned} \quad (47)$$

Following the case of the GMA based on the micromorphic theory of degree  $n$ , the macro-scale deformation energy density for the present case is of the form  $W = W(\bar{\phi}_{(i,j)}, \gamma_{ij}, \gamma_{ijk}, \psi_{ij,k}, \psi_{ijk,l})$ , and the macro-scale stress components defined as conjugates to the continuum kinematic measures are

$$\tau_{ij} = \frac{\partial W}{\partial \bar{\phi}_{(i,j)}}, \quad \sigma_{ij} = \frac{\partial W}{\partial \gamma_{ij}}, \quad \sigma_{ijk} = \frac{\partial W}{\partial \gamma_{ijk}}, \quad \mu_{ijk} = \frac{\partial W}{\partial \psi_{ij,k}}, \quad \mu_{ijkl} = \frac{\partial W}{\partial \psi_{ijk,l}}. \quad (48)$$

The micro-scale deformation energy density in this case can be written as

$$W = \frac{1}{V'} \sum_{\alpha} W^{\alpha}(\delta_i^{\alpha M}, \delta_i^{\alpha m_1}, \delta_i^{\alpha m_2}, \delta_i^{\alpha g_1}, \delta_i^{\alpha g_2}, \theta_i^{\alpha m_1}, \theta_i^{\alpha g_1}, \theta_i^{\alpha g_2}). \quad (49)$$

The energy must be invariant to rigid body rotations and translations. Therefore, we only take the symmetric part of  $\bar{\phi}_{i,j}$  in the micro-scale kinematic measure  $\delta_i^{\alpha M}$  in Equation (49). The micro-scale force and moment components conjugate to the micro-scale kinematic measures are defined as follows

$$\begin{aligned} \frac{\partial W^{\alpha}}{\partial \delta_i^{\alpha M}} &= f_i^{\alpha M} \\ \frac{\partial W^{\alpha}}{\partial \delta_i^{\alpha m_k}} &= f_i^{\alpha m_k}, \quad \frac{\partial W^{\alpha}}{\partial \delta_i^{\alpha g_k}} = f_i^{\alpha g_k}, \quad k = 1, 2 \\ \frac{\partial W^{\alpha}}{\partial \theta_i^{\alpha m_1}} &= m_i^{\alpha m_1}, \quad \frac{\partial W^{\alpha}}{\partial \theta_i^{\alpha g_k}} = m_i^{\alpha g_k}, \quad k = 1, 2. \end{aligned} \quad (50)$$

Using Hamilton's principle, the integral form of the governing equations for this case is found as

$$\begin{aligned}
& \int_{t_0}^{t_1} \int_V [(\tau_{ij} + \sigma_{ij})_{,j} + f_i - \rho \ddot{\phi}_i] \delta \bar{\phi}_i dV + \int_{t_0}^{t_1} \int_V \left[ \sigma_{ij} + (\sigma_{ijk} + \mu_{ijk})_{,k} + \Phi_{ij} - \rho_{jk} \ddot{\psi}_{ik} - \rho_{jkl} \ddot{\psi}_{ikl} - \rho_{jklm} \ddot{\psi}_{ikl,m} \right] \delta \psi_{ij} dV \\
& + \int_{t_0}^{t_1} \int_V \left[ \sigma_{ijk} + \mu_{ijkl,l} + \Phi_{ijk} - \rho_{jkl} \ddot{\psi}_{il} - \rho_{jklm} \ddot{\psi}_{ilm} + \rho_{jklm} \ddot{\psi}_{im,l} + \rho_{jklmnp} \ddot{\psi}_{imn,pl} \right] \delta \psi_{ijk} dV \\
& + \int_{t_0}^{t_1} \int_S [t_i - (\tau_{ij} + \sigma_{ij}) n_j] \delta \bar{\phi}_i dS + \int_{t_0}^{t_1} \int_S [T_{ij} - (\sigma_{ijk} + \mu_{ijk}) n_k] \delta \psi_{ij} dS \\
& + \int_{t_0}^{t_1} \int_S [T_{ijk} - (\rho_{jklm} \ddot{\psi}_{im} + \rho_{jklmn} \ddot{\psi}_{imn} + \rho_{jklmnp} \ddot{\psi}_{imn,p} + \mu_{ijkl}) n_l] \delta \psi_{ijk} dS = 0.
\end{aligned} \tag{51}$$

Thus, the governing equations of motion for a GMA based on micromorphic theory of degree 2 are written as

$$\begin{aligned}
& (\tau_{ij} + \sigma_{ij})_{,j} + f_i = \rho \ddot{\phi}_i \\
& \sigma_{ij} + (\sigma_{ijk} + \mu_{ijk})_{,k} + \Phi_{ij} = \rho_{jk} \ddot{\psi}_{ik} + \rho_{jkl} \ddot{\psi}_{ikl} + \rho_{jklm} \ddot{\psi}_{ikl,m} \\
& \sigma_{ijk} + \mu_{ijkl,l} + \Phi_{ijk} = \rho_{jkl} \ddot{\psi}_{il} + \rho_{jklm} \ddot{\psi}_{ilm} - \rho_{jklm} \ddot{\psi}_{im,l} - \rho_{jklmnp} \ddot{\psi}_{imn,pl}.
\end{aligned} \tag{52}$$

The natural boundary conditions in this case are

$$\begin{aligned}
& (\tau_{ij} + \sigma_{ij}) n_j = t_i \\
& (\sigma_{ijk} + \mu_{ijk}) n_k = T_{ij} \\
& (\rho_{jklm} \ddot{\psi}_{im} + \rho_{jklmn} \ddot{\psi}_{imn} + \rho_{jklmnp} \ddot{\psi}_{imn,p} + \mu_{ijkl}) n_l = T_{ijk}.
\end{aligned} \tag{53}$$

According to Equation (52), the GMA based on the micromorphic theory of degree 2 involves 39 equations in three dimensions and 14 equations in two dimensions.

## 5.2. GMA-based micromorphic theory of degree 1

If we keep up to the quadratic term in the polynomial expansion ( $n = 2$ ) in Equation (12), we obtain the GMA based on the micromorphic theory of degree 1. The total displacement of the grains in Equation (13), therefore, simplifies to

$$\phi_i = u_i + u'_i = \bar{\phi}_i + \psi_{ij} x'_j + \psi_{ijk} x'_j x'_k. \tag{54}$$

The relative deformation parameters here are  $\gamma_{ij}$  and  $\gamma_{ijk}$ , where we assume  $\gamma_{ijk} = 0$ . Such an assumption reads  $\psi_{ijk} = \psi_{ij,k}$  and permits the description of a nonlinear micro-displacement field up to order two. Thus, the relative displacement of two neighboring grains  $n$  and  $p$  is written as

$$\delta_i^{np} = \delta_i^p - \delta_i^n = \delta_i^M - \delta_i^m + \delta_i^g, \tag{55}$$

where we defined the micro-scale kinematic measures

$$\delta_i^M = \bar{\phi}_{i,j} J_j^{np}, \quad \delta_i^m = \gamma_{ij} J_j^{np}, \quad \delta_i^g = \psi_{ij,k} J_{jk}^{np}. \tag{56}$$

The relative rotation between the neighboring grains  $n$  and  $p$  is written as

$$\theta_i^{np} = \bar{\kappa}_i^p - \bar{\kappa}_i^n = \theta_i^g, \quad (57)$$

where we defined the micro-scale kinematic measure

$$\theta_i^g = e_{lki} \psi_{kl,j} J_j^{np}. \quad (58)$$

For the micromorphic theory of degree 1, the macro-scale deformation energy density is of the form  $W = W(\bar{\phi}_{(i,j)}, \gamma_{ij}, \psi_{ij,k})$ , and the macro-scale stress components defined as conjugates to the continuum kinematic measures are

$$\tau_{ij} = \frac{\partial W}{\partial \bar{\phi}_{(i,j)}}, \quad \sigma_{ij} = \frac{\partial W}{\partial \gamma_{ij}}, \quad \mu_{ijk} = \frac{\partial W}{\partial \psi_{ij,k}}. \quad (59)$$

The micro-scale deformation energy density is written as

$$W = \frac{1}{V_l} \sum_{\alpha} W^{\alpha}(\delta_i^{\alpha M}, \delta_i^{\alpha m}, \delta_i^{\alpha g}, \theta_i^{\alpha g}). \quad (60)$$

Consequently, the micro-scale force and moment components conjugate to the micro-scale kinematic measures are defined as follows

$$\frac{\partial W^{\alpha}}{\partial \delta_i^{\alpha M}} = f_i^{\alpha M}, \quad \frac{\partial W^{\alpha}}{\partial \delta_i^{\alpha m}} = f_i^{\alpha m}, \quad \frac{\partial W^{\alpha}}{\partial \delta_i^{\alpha g}} = f_i^{\alpha g}, \quad \frac{\partial W^{\alpha}}{\partial \theta_i^{\alpha g}} = m_i^{\alpha g}. \quad (61)$$

Using Hamilton's principle, the integral form of the governing equations is found as

$$\begin{aligned} & \int_{t_0}^{t_1} \int_V \left[ (\tau_{ij} + \sigma_{ij})_{,j} + f_i - \rho \ddot{\bar{\phi}}_i \right] \delta \bar{\phi}_i dV + \int_{t_0}^{t_1} \int_V \left[ \sigma_{ij} + \mu_{ijk,k} + \Phi_{ij} - \rho_{jk} \ddot{\psi}_{ik} + \rho_{jklm} \ddot{\psi}_{il,mk} \right] \delta \psi_{ij} dV \\ & + \int_{t_0}^{t_1} \int_S \left[ t_i - (\tau_{ij} + \sigma_{ij}) n_j \right] \delta \bar{\phi}_i dS + \int_{t_0}^{t_1} \int_S \left[ T_{ij} - (\rho_{jkl} \ddot{\psi}_{il} + \rho_{jklm} \ddot{\psi}_{il,m} + \mu_{ijk}) n_k \right] \delta \psi_{ij} dS. \end{aligned} \quad (62)$$

Thus, the following equations of motion for the case of a GMA based on the micromorphic theory of degree 1 are obtained

$$\begin{aligned} (\tau_{ij} + \sigma_{ij})_{,j} + f_i &= \rho \ddot{\bar{\phi}}_i \\ \sigma_{ij} + \mu_{ijk,k} + \Phi_{ij} &= \rho_{jk} \ddot{\psi}_{ik} - \rho_{jklm} \ddot{\psi}_{il,mk}. \end{aligned} \quad (63)$$

The natural boundary conditions also take the form

$$\begin{aligned} (\tau_{ij} + \sigma_{ij}) n_j &= t_i \\ (\rho_{jkl} \ddot{\psi}_{il} + \rho_{jklm} \ddot{\psi}_{il,m} + \mu_{ijk}) n_k &= T_{ij}. \end{aligned} \quad (64)$$

Based on Equation (63), for a GMA based on the micromorphic theory of degree 1, the number of the governing equations of motion are 12 in three dimensions (or six in two dimensions), which indeed is less computationally demanding compared to the GMA based on the micromorphic theory of degree 2. It is notable that the derived governing equations include additional inertial terms not considered in our previous works [23,25,26]. The analyses of wave propagation and vibration behavior of granular media are expected to be further enriched by these additional terms. Such analyses will be pursued in the future

5.2.1. *GMA-based micro-polar or Cosserat medium.* By assuming that only the skew-symmetric part of the micro-scale deformation measure  $\psi_{ij}$  exists, the micromorphic theory of degree 1 can be reduced further to a micro-polar type model. Denoting the skew-symmetric part of a tensor by square brackets around its indices, we can write the grain's total displacement as

$$\phi_i = u_i + u'_i = \bar{\phi}_i + \psi_{[ij]}x'_j + \psi_{ijk}x'_jx'_k. \quad (65)$$

In such a case one can proceed further by defining two forms of relative deformation measures. In the first form, one writes for the relative deformation measures

$$\gamma_{ij} = \bar{\phi}_{i,j} - \psi_{[ij]}, \quad \gamma_{ijk} = \psi_{[ij],k} - \psi_{ijk}. \quad (66)$$

Applying the condition  $\gamma_{ijk} = 0$  and explicitly decomposing the macro-scale displacement gradient into a symmetric part,  $\bar{\phi}_{(i,j)}$ , and a skew-symmetric part,  $\bar{\phi}_{[i,j]}$ , we write

$$\gamma_{ij} = \bar{\phi}_{(i,j)} + \bar{\phi}_{[i,j]} - \psi_{[ij]}, \quad \psi_{ijk} = \psi_{[ij],k} = \psi_{[ik],j}. \quad (67)$$

In such a case, the relative displacement of two neighboring grains  $n$  and  $p$  reads

$$\delta_i^{np} = \delta_i^p - \delta_i^n = \delta_i^M - \delta_i^m + \delta_i^g, \quad (68)$$

where the definitions for the micro-scale kinematic measures are

$$\delta_i^M = \bar{\phi}_{(i,j)}J_j^{np}, \quad \delta_i^m = \gamma_{[ij]}J_j^{np}, \quad \delta_i^g = \psi_{[ij],k}J_{jk}^{np}, \quad (69)$$

and we have assured the micro-scale kinematic measure  $\delta_i^M$  must remain invariant with respect to rigid body rotation and translation. The relative rotation between the neighboring grains  $n$  and  $p$  follows that of Equation (57), with the new definition for the micro-scale kinematic measure as

$$\theta_i^g = e_{lki}\psi_{[kl],j}J_j^{np}. \quad (70)$$

Alternatively, one can assume a second form for the relative deformation measures as

$$\gamma_{ij} = \bar{\phi}_{[i,j]} - \psi_{[ij]}, \quad \gamma_{ijk} = \psi_{[ij],k} - \psi_{ijk}, \quad (71)$$

where it is clear that  $\gamma_{ij} = \gamma_{[ij]}$  and imposing the condition  $\gamma_{ijk} = 0$  results in  $\psi_{ijk} = \psi_{[ij],k} = \psi_{[ik],j}$ , similar to the first form. The relative displacement of two neighboring grains in this case is written as

$$\delta_i^{np} = \delta_i^p - \delta_i^n = \delta_i^M - \delta_i^m + \delta_i^g, \quad (72)$$

where the micro-scale kinematic measures have now the definitions

$$\delta_i^M = \bar{\phi}_{(i,j)}J_j^{np}, \quad \delta_i^m = \gamma_{[ij]}J_j^{np}, \quad \delta_i^g = \psi_{[ij],k}J_{jk}^{np}. \quad (73)$$

The relative rotation between the neighboring grains  $n$  and  $p$  remains the same as that in Equation (70). In both forms defined here, the macro-scale deformation energy density is formally written as  $W = W(\bar{\phi}_{(i,j)}, \gamma_{ij}, \psi_{[ij],k})$ . The micro-scale deformation energy density is written as  $W = \frac{1}{V^*} \sum_{\alpha} W^{\alpha}(\delta_i^{\alpha M}, \delta_i^{\alpha m}, \delta_i^{\alpha g}, \theta_i^{\alpha g})$ . Now, considering a quadratic form for the macro- and micro-scale deformation energy densities for the first form naturally results in a coupling between the extensional and rotational degrees of freedom. The coupling stems from the definition of  $\gamma_{ij}$  in the first form, where both the symmetric and skew-symmetric parts of the macro-scale displacement gradient are present. Such a representation can lead to a first-gradient model that describes chiral behavior in granular media. The result of such a model is different from that in a classical micro-polar or Cosserat medium in which rotation is, typically, not coupled to the extension [49]. The classical micro-polar or Cosserat medium is obtained by using the second form defined for the relative deformations. Considering a quadratic form for the macro- and micro-scale deformation energy densities excludes the mixed term

present in the first form. In this second representation, the coupling between the rotational and extensional degrees of freedom must be explicitly specified for obtaining a model that can describe chiral behavior in granular media. However, when we introduce the coupling terms, one must ensure that the chosen coupling constants are such that the deformation energy remains positive definite. Further, it is notable that the balance equations formally remain the same as that in Equation (63) with the note that the stress measures in the second part of Equation (63) are skew-symmetric, as follows,  $\sigma_{[ij]}$  and  $\mu_{[ijk]}$ .

**5.2.2. GMA-based second-gradient medium.** For the case of where the second rank relative deformation also vanishes, a second-gradient description of granular media can be obtained from a micromorphic theory of degree 1. Thus, we will have

$$\gamma_{ij} = \bar{\phi}_{i,j} - \psi_{ij} = 0 \rightarrow \psi_{ij} = \bar{\phi}_{i,j}, \gamma_{ijk} = \psi_{ij,k} - \psi_{ijk} = 0 \rightarrow \psi_{ijk} = \psi_{ij,k} = \bar{\phi}_{i,jk}. \quad (74)$$

The total displacement of each grain in this case is written as

$$\phi_i = u_i + u'_i = \bar{\phi}_i + \bar{\phi}_{i,j}x'_j + \bar{\phi}_{i,jk}x'_jx'_k. \quad (75)$$

The relative displacement and rotation of two neighboring grains  $n$  and  $p$  can be written as

$$\delta_i^{np} = \delta_i^p - \delta_i^n = \delta_i^M + \delta_i^g, \theta_i^{np} = \hat{\kappa}_i^p - \hat{\kappa}_i^n = \theta_i^g, \quad (76)$$

where the micro-scale kinematic measures can be defined in two forms. One can define (first form)

$$\delta_i^M = \bar{\phi}_{(i,j)}J_j^{np}, \quad \delta_i^g = \bar{\phi}_{i,jk}J_{jk}^{np}, \quad \theta_i^g = e_{lki}\bar{\phi}_{k,l}J_l^{np}, \quad (77)$$

or (second form)

$$\delta_i^M = \bar{\phi}_{(i,j)}J_j^{np}, \quad \delta_i^g = \bar{\phi}_{(i,j)k}J_{jk}^{np}, \quad \theta_i^g = e_{lki}\bar{\phi}_{(k,l)}J_l^{np} = 0. \quad (78)$$

In the first form, the micro-scale kinematic measures  $\delta_i^g$  and  $\theta_i^g$  are defined with respect to the tensor  $\bar{\phi}_{i,j}$ , while in the second form, such kinematic measures are defined only involving the symmetric tensor,  $\bar{\phi}_{(i,j)}$ . A consequence of the second form is the vanishing of the relative rotation term, meaning that the relative rotation of two neighboring grains in contact does not store energy. While for the first form it is natural to consider  $W = W(\bar{\phi}_{(i,j)}, \bar{\phi}_{i,jk})$  and  $W = \frac{1}{V^*} \sum_{\alpha} W^{\alpha}(\delta_i^{\alpha M}, \delta_i^{\alpha g}, \theta_i^{\alpha g})$  for the macro- and micro-scale deformation energy densities, respectively, the second form suggests considering  $W = W(\bar{\phi}_{(i,j)}, \bar{\phi}_{(i,j)k})$  and  $W = \frac{1}{V^*} \sum_{\alpha} W^{\alpha}(\delta_i^{\alpha M}, \delta_i^{\alpha g})$ . We continue with the more general case. In this case, the stress measures are defined as

$$\tau_{ij} = \frac{\partial W}{\partial \bar{\phi}_{(i,j)}}, \quad \mu_{ijk} = \frac{\partial W}{\partial \bar{\phi}_{i,jk}}, \quad (79)$$

and the force and moment measures in the micro-scale are defined as

$$\frac{\partial W^{\alpha}}{\partial \delta_i^{\alpha M}} = f_i^{\alpha M}, \quad \frac{\partial W^{\alpha}}{\partial \delta_i^{\alpha g}} = f_i^{\alpha g}, \quad \frac{\partial W^{\alpha}}{\partial \theta_i^{\alpha g}} = m_i^{\alpha g}. \quad (80)$$

The variationals of kinetic energy, macro-scale deformation energy, and external energy are written as

$$\begin{aligned}
\delta \int_{t_0}^{t_1} \bar{T} dt &= - \int_{t_0}^{t_1} \int_V \rho \ddot{\bar{\phi}}_i \delta \bar{\phi}_i dV dt - \int_{t_0}^{t_1} \int_S \rho_{jk} \ddot{\bar{\phi}}_{i,k} n_j \delta \bar{\phi}_i dS dt + \int_{t_0}^{t_1} \int_V \rho_{jk} \ddot{\bar{\phi}}_{i,kj} \delta \bar{\phi}_i dV dt \\
&- \int_{t_0}^{t_1} \int_S \rho_{jkl} \ddot{\bar{\phi}}_{i,kl} n_j \delta \bar{\phi}_i dS dt + \int_{t_0}^{t_1} \int_V \rho_{jkl} \ddot{\bar{\phi}}_{i,klj} \delta \bar{\phi}_i dV dt + \int_{t_0}^{t_1} \int_S \rho_{jkl} \ddot{\bar{\phi}}_{i,jl} n_k \delta \bar{\phi}_i dS dt - \int_{t_0}^{t_1} \int_V \rho_{jkl} \ddot{\bar{\phi}}_{i,jlk} \delta \bar{\phi}_i dV dt \\
&+ \int_{t_0}^{t_1} \int_S \rho_{jklm} \ddot{\bar{\phi}}_{i,lmk} n_j \delta \bar{\phi}_i dS dt - \int_{t_0}^{t_1} \int_V \rho_{jklm} \ddot{\bar{\phi}}_{i,lmkj} \delta \bar{\phi}_i dV dt \\
&- \int_{t_0}^{t_1} \int_S \rho_{jkl} \ddot{\bar{\phi}}_{i,j} n_l n_k n_p \delta \bar{\phi}_{i,p} dS dt + \int_{t_0}^{t_1} \int_S \operatorname{div}_s (\rho_{jkl} \ddot{\bar{\phi}}_{i,j} n_l) \delta \bar{\phi}_i dS dt - \int_{t_0}^{t_1} \int_L \rho_{jkl} \ddot{\bar{\phi}}_{i,j} n_l v_k \delta \bar{\phi}_i dL dt \\
&- \int_{t_0}^{t_1} \int_S \rho_{jklm} \ddot{\bar{\phi}}_{i,lm} n_k n_j n_p \delta \bar{\phi}_{i,p} dS dt + \int_{t_0}^{t_1} \int_S \operatorname{div}_s (\rho_{jklm} \ddot{\bar{\phi}}_{i,lm} n_k) \delta \bar{\phi}_i dS dt - \int_{t_0}^{t_1} \int_L \rho_{jklm} \ddot{\bar{\phi}}_{i,lm} v_j \delta \bar{\phi}_i dL dt,
\end{aligned} \tag{81}$$

$$\begin{aligned}
\delta \int_{t_0}^{t_1} \bar{W} dt &= \int_{t_0}^{t_1} \int_S \tau_{ij} n_j \delta \bar{\phi}_i dS dt - \int_{t_0}^{t_1} \int_V \tau_{ij,j} \delta \bar{\phi}_i dV dt + \int_{t_0}^{t_1} \int_S \mu_{ijk} n_k n_j n_p \delta \bar{\phi}_{i,p} dS dt \\
&- \int_{t_0}^{t_1} \int_S \operatorname{div}_s (\mu_{ijk} n_k) \delta \bar{\phi}_i dS dt + \int_{t_0}^{t_1} \int_L \mu_{ijk} n_k v_j \delta \bar{\phi}_i dL dt - \int_{t_0}^{t_1} \int_S \mu_{ijk,k} n_j \delta \bar{\phi}_i dS dt + \int_{t_0}^{t_1} \int_V \mu_{ijk,kj} \delta \bar{\phi}_i dV dt,
\end{aligned} \tag{82}$$

$$\delta \int_{t_0}^{t_1} \bar{W}_{ext} dt = \int_{t_0}^{t_1} \int_V f_i \delta \bar{\phi}_i dV dt + \int_{t_0}^{t_1} \int_S t_i \delta \bar{\phi}_i dS dt + \int_{t_0}^{t_1} \int_S h_i \delta \bar{\phi}_{i,p} n_p dS dt + \int_{t_0}^{t_1} \int_L q_i \delta \bar{\phi}_i dL dt, \tag{83}$$

where we have used the concept of surface divergence theorem [53].  $\operatorname{div}_s$  is the surface divergence operator in Equations (81) and (82), and the subscript,  $s$ , pertaining to surface operators does not follow tensor summation notation.  $L$  is the edge formed at the common border of two regular parts of the surface  $S$ , whose normal vectors pointing outward are  $n_i^+$  and  $n_i^-$ , and whose tangents (outward normal at the edge) are  $v_i^+$  and  $v_i^-$ , respectively. The derivation of Equations (81) and (82) follows the treatment of surface integrals in [58]. In Equation (83),  $f_i$  is the body force density,  $t_i$  is the surface contact traction that expends work on surface virtual displacements,  $h_i$  is the surface contact double traction that expends work on the normal derivative of the surface virtual displacements, and  $q_i$  is the edge contact force per unit length that expends work on edge virtual displacements. Substituting the indicial form of the terms containing surface divergence using [59], Hamilton's principle results in the following governing equations of motion and boundary conditions

$$\left( \tau_{ij} - \mu_{ijk,k} \right)_{,j} + f_i = \rho \ddot{\bar{\phi}}_i - \rho_{jk} \ddot{\bar{\phi}}_{i,kj} + \rho_{jklm} \ddot{\bar{\phi}}_{i,lmkj} \tag{84}$$

$$\begin{aligned}
\tau_{ij} n_j - \mu_{ijk,k} n_j - \left( \mu_{ijp} n_p \right)_{,j} + \left( \mu_{ikp} n_p n_k n_j \right)_{,j} + \rho_{jk} \ddot{\bar{\phi}}_{i,k} n_j + \rho_{jkl} \ddot{\bar{\phi}}_{i,kl} n_j - \rho_{jkl} \ddot{\bar{\phi}}_{i,jl} n_k \\
- \rho_{jklm} \ddot{\bar{\phi}}_{i,lmk} n_j - \left( \rho_{mjl} \ddot{\bar{\phi}}_{i,m} n_l \right)_{,j} + \left( \rho_{mkl} \ddot{\bar{\phi}}_{i,m} n_l n_k n_j \right)_{,j} - \left( \rho_{jplm} \ddot{\bar{\phi}}_{i,lm} n_p \right)_{,j} + \left( \rho_{kplm} \ddot{\bar{\phi}}_{i,lm} n_p n_k n_j \right)_{,j} = t_i,
\end{aligned} \tag{85}$$

$$\mu_{ijk} n_k n_j + \rho_{jkl} \ddot{\bar{\phi}}_{i,j} n_l n_k + \rho_{jklm} \ddot{\bar{\phi}}_{i,lm} n_k n_j = h_i \tag{86}$$

$$\mu_{ijk} n_k^+ v_j^+ - \mu_{ijk} n_k^- v_j^- + \rho_{jkl} \ddot{\bar{\phi}}_{i,j} n_l^+ v_k^+ - \rho_{jkl} \ddot{\bar{\phi}}_{i,j} n_l^- v_k^- + \rho_{jklm} \ddot{\bar{\phi}}_{i,lm} n_k^+ v_j^+ - \rho_{jklm} \ddot{\bar{\phi}}_{i,lm} n_k^- v_j^- = q_i. \tag{87}$$

We remark that the second-gradient theory has played an important role in the development of pantographic metamaterials, as shown in [40, 54, 60–64]. It has been shown that second-gradient theories are



necessary for describing patterns formations in sheets containing internal transition zones of finite thicknesses [65] and modeling out-of-plane deformations in sheets [66], as well as for damage and fracture modeling in complex microstructured materials [58, 67–69].

## 6. Conclusions

The main outcome of the presented work is the micromorphic model of degree  $n$ , derived in Section 3, that is applicable for describing the collective behavior of granular solids within a continuum framework. The need for such an enriched model is motivated through experimental observations of grain-scale kinematics in deformed confined granular assemblies of discs, and supported by the results of simulations based upon discrete models of granular systems. These experiments and simulations give ample evidence of the complex kinematic fields that can arise from disorder of either the granular structure or the grain-scale interactions. Indeed, simulation results for regularly ordered discs in a square arrangement interacting through quadratic grain-pair potentials of random strength show significant displacement fluctuations from the mean behavior. To describe the effect of these complex grain-scale motions, additional continuum kinematical measures represented as tensorial quantities up to order  $n$  are needed, as introduced in this work. The deformation energy density and kinetic energy density for the continuum material point (or RVE) are then defined in terms of these continuum kinematic measures and their grain-scale counterparts, and a variational approach is utilized to derive the equations of motion. The general model of degree  $n$  can be particularized by specifying the value for  $n$ , depending upon the material variability and the desired accuracy. In many cases, lower order theories may suffice to capture the key phenomena with tractable analytical and computational effort. To demonstrate the model complexity, we have given the expressions for models of degrees 2 and 1. We have shown that further simplification by ignoring certain kinematical terms can lead to second-gradient and micro-polar/Cosserat-type models. In this regard, it will be interesting to examine the relationship of the micromorphic model of degree  $n$  and the  $n$ th gradient model discussed in [52, 53].

For an assumed degree for the micromorphic theory, stresses conjugate to the continuum kinematic measures can be defined and related, through the equivalence of deformation energy density, to forces conjugate to the measures of grain-pair relative motions and the geometry moment measures. These stress–force–geometry moment relationships are useful for revealing the form of constitutive relationships of granular continua in terms of strains and conjugated stress measures [2, 23]. Further, an identification procedure to find macroscopic stiffness tensors can translate the information from the discrete model of granular material to the continuum model [36, 70].

Based on the materials presented in this paper, we here raise some questions: what is the physical meaning of geometry moment measures for a grain-pair in contact? How can one interpret the inertia measures for an assumed RVE, for example, how does the inertia measure look for a rectangular RVE composed of grains with equal micro-density in a regularly packed granular structure, or for the same RVE with non-uniform micro-density? How does increasing  $n$  change the behavior of the granular material predicted by the GMA, for instance, how does its dispersive behavior change? Such queries are of great importance and their answers complement the proposed approach. Utilizing the GMA in practical problems will elaborate on the concepts presented here and respond to the questions raised, and will be pursued in future publications.

## Funding

The author(s) disclosed receipt of the following financial support for the research, authorship, and/or publication of this article: This work was supported in part by the United States National Science Foundation (grant CMMI-1727433).

## References

- [1] Misra, A, and Pooorolhjouy, P. Grain- and macro-scale kinematics for granular micromechanics based small deformation micromorphic continuum model. *Mech Res Commun* 2017; 81: 1–6.
- [2] Pooorolhjouy, P, and Misra, A. Granular micromechanics based continuum model for grain rotations and grain rotation waves. *J Mech Phys Solid* 2019; 129: 244–260.

- [3] Digby, PJ. The effective elastic moduli of porous granular rocks. *J Appl Mech* 1981; 48: 803-808.
- [4] Walton, K. Wave propagation within random packings of spheres. *Geophys J Int* 1988; 92: 89-97.
- [5] Misra, A, Placidi, L, and Turco, E. Variational methods for discrete models of granular materials. In: Altenbach, H, and Ochsner, A (eds) *Encyclopedia of continuum mechanics*. Berlin: Springer, 2018.
- [6] Bagi, K. Stress and strain in granular assemblies. *Mech Mater* 1996; 22: 165-177.
- [7] Cundall, PA, and Strack, ODL. Discrete numerical-model for granular assemblies. *Geotechnique* 1979; 29: 47-65.
- [8] Kuhn, MR. *Granular geomechanics*. London: Elsevier, 2017.
- [9] Radjai, F, and Dubois, F. *Discrete-element modeling of granular materials*. London: Wiley-Iste, 2011.
- [10] Turco, E, dell'Isola, F, and Misra, A. A nonlinear Lagrangian particle model for grains assemblies including grain relative rotations. *Int J Numer Anal Meth Geomech* 2019; 43: 1051-1079.
- [11] Andrade, JE, et al., Multiscale modeling and characterization of granular matter: from grain kinematics to continuum mechanics. *J Mech Phys Solid* 2011; 59: 237-250.
- [12] Guo, N, and Zhao, J. A coupled FEM/DEM approach for hierarchical multiscale modelling of granular media. *Int J Numer Meth Eng* 2014; 99: 789-818.
- [13] Zhao, J, and Shan, T. Coupled CFD-DEM simulation of fluid-particle interaction in geomechanics. *Powder Technol* 2013; 239: 248-258.
- [14] Chang, CS, and Misra, A. Theoretical and experimental-study of regular packings of granules. *J Eng Mech ASCE* 1989; 115: 704-720.
- [15] Chang, CS, and Misra, A. Packing structure and mechanical-properties of granulates. *J Eng Mech ASCE* 1990; 116: 1077-1093.
- [16] Duffy, J, and Mindlin, RD. Stress-strain relations and vibrations of a granular medium. *J Appl Mech* 1957; 24: 585-593.
- [17] Jenkins, J, et al. Fluctuations and the effective moduli of an isotropic, random aggregate of identical, frictionless spheres. *J Mech Phys Solid* 2005; 53: 197-225.
- [18] Jenkins, JT. Volume change in small strain axisymmetric deformations of a granular material. In: Satake, M, and Jenkins, JT (eds) *Micromechanics of granular materials*. Amsterdam: Elsevier Science Publishers, 1988, 245-252.
- [19] Jenkins, JT. Inelastic Behavior of Random Arrays of Identical Spheres. In: Fleck, NA and Cocks, ACF (eds) IUTAM Symposium on Mechanics of Granular and Porous Materials. *Solid Mechanics and its Applications*. Dordrecht: Springer, 1997.
- [20] Kruyt, N, and Rothenburg, L. Kinematic and static assumptions for homogenization in micromechanics of granular materials. *Mech Mater* 2004; 36: 1157-1173.
- [21] Walton, K. The effective elastic moduli of a random packing of spheres. *J Mech Phys Solid* 1987; 35: 213-226.
- [22] Misra, A, Placidi, L, and Turco, E. Variational methods for continuum models of granular materials. In: Altenbach, H, and Ochsner, A (eds) *Encyclopedia of continuum mechanics*. Berlin: Springer GmbH, 2019.
- [23] Misra, A, and Poorsolhjouy, P. Granular micromechanics based micromorphic model predicts frequency band gaps. *Continuum Mech Thermodynam* 2016; 28: 215-234.
- [24] Abali, BE, Müller, WH, and dell'Isola, F. Theory and computation of higher gradient elasticity theories based on action principles. *Arch Appl Mech* 2017; 87: 1495-1510.
- [25] Nejadsadeghi, N, et al. Frequency band gaps in dielectric granular metamaterials modulated by electric field. *Mech Res Commun* 2019; 95: 96-103.
- [26] Misra, A, and Nejadsadeghi, N. Longitudinal and transverse elastic waves in 1D granular materials modeled as micromorphic continua. *Wave Motion* 2019; 90: 175-195.
- [27] Nejadsadeghi, N, and Misra, A. Axially moving materials with granular microstructure. *Int J Mech Sci* 2019; 161-162: 105042.
- [28] Jirásek, M. Nonlocal theories in continuum mechanics. *Acta Polytechnica* 2004; 44: 16-34.
- [29] Cosserat, E, and Cosserat, F. *Theory of deformable bodies*. Paris: Scientific Library A. Hermann and Sons, 1909.
- [30] Placidi, L, et al. Variational methods in continuum damage and fracture mechanics. In: Altenbach, H, and Ochsner, A (eds) *Encyclopedia of continuum mechanics*. Berlin: Springer, 2017.
- [31] Eugster, SR, and dell'Isola, F. Exegesis of the Introduction and Sect. I from "Fundamentals of the Mechanics of Continua"\*\*\* by Hellinger, E. *ZAMM J Appl Math Mech/Zeitschrift für Angewandte Mathematik und Mechanik* 2017; 97: 477-506.
- [32] Eugster, SR, and dell'Isola, F. Exegesis of Sect. III. B from "Fundamentals of the Mechanics of Continua" by Hellinger, E.. *ZAMM J Appl Math Mech/Zeitschrift für Angewandte Mathematik und Mechanik* 2018; 98: 69-105.
- [33] Eugster, SR, and Dell'Isola, F. Exegesis of Sect. II and III. A from "Fundamentals of the Mechanics of Continua" by Hellinger, E.. *ZAMM J Appl Math Mech/Zeitschrift für Angewandte Mathematik und Mechanik* 2018; 98: 31-68.
- [34] Misra, A, and Jiang, H. Measured kinematic fields in the biaxial shear of granular materials. *Comput Geotechn* 1997; 20: 267-285.
- [35] Shukla, A, Sadd, MH, and Mei, H. Experimental and computational modeling of wave propagation in granular materials. *Exp Mech* 1990; 30: 377-381.

- [36] Misra, A, and Poorsolhjoui, P. Elastic behavior of 2D grain packing modeled as micromorphic media based on granular micromechanics. *J Eng Mech* 2016; 143: C4016005.
- [37] Mühlhaus, HB, and Oka, F. Dispersion and wave propagation in discrete and continuous models for granular materials. *Int J Solid Struct* 1996; 33: 2841–2858.
- [38] Deresiewicz, H. Stress-Strain relations for a simple model of a granular medium. *J Appl Mech* 1958; 25: 402–406.
- [39] Misra, A, and Poorsolhjoui, P. Micro-macro scale instability in 2D regular granular assemblies. *Continuum Mech Thermodynam* 2013; 27: 63-82.
- [40] NejadSadeghi, N, et al. Parametric experimentation on pantographic unit cells reveals local extremum configuration. *Exp Mech* 2019; 59: 927–939.
- [41] Kanit, T, et al. Determination of the size of the representative volume element for random composites: statistical and numerical approach. *Int J Solid Struct* 2003; 40: 3647–3679.
- [42] Matheron, G. *The theory of regionalized variables and its applications*. Vol. 5. Paris: Ecole nationale supérieure des mines de Paris, 1971.
- [43] Matheron, G. *Random sets and integral geometry*. New York: John Wiley Sons, 1975.
- [44] Matheron, G. *Estimating and choosing*. Berlin: Springer, 1989.
- [45] Stroeven, M, Askes, H, and Sluys, LJ. Numerical determination of representative volumes for granular materials. *Comput Meth Appl Mech Eng* 2004; 193: 3221–3238.
- [46] Wellmann, C, Lillie, C, and Wriggers, P. Homogenization of granular material modeled by a three-dimensional discrete element method. *Comput Geotechn* 2008; 35: 394–405.
- [47] Bargmann, S, et al. Generation of 3D representative volume elements for heterogeneous materials: a review. *Progr Mater Sci* 2018; 96: 322–384.
- [48] Gitman, IM, Askes, H, and Sluys, LJ. Representative volume: existence and size determination. *Eng Fract Mech* 2007; 74: 2518–2534.
- [49] Germain, P. Method of virtual power in continuum mechanics. 2. Microstructure. *Siam J Appl Math* 1973; 25: 556–575.
- [50] Mindlin, RD. Micro-structure in linear elasticity. *Arch Ration Mech Anal* 1964; 16: 51-78.
- [51] Eringen, A. *Microcontinuum field theories I: foundations and solids*. New York: Springer, 1999.
- [52] dell’Isola, F, Seppecher, P, and Della Corte, A. The postulations à la D’Alembert and à la Cauchy for higher gradient continuum theories are equivalent: a review of existing results. *Proc R Soc A* 2015; 471: 20150415.
- [53] dell’Isola, F, Seppecher, P, and Madeo, A. How contact interactions may depend on the shape of Cauchy cuts in Nth gradient continua: approach “à la D’Alembert”. *Zeitschrift für angewandte Mathematik und Physik* 2012; 63: 1119–1141.
- [54] Seppecher, P, Alibert, J-J, and dell’Isola, F. Linear elastic trusses leading to continua with exotic mechanical interactions. *J Phys Conf Ser* 2011; 319: 012018.
- [55] dell’Isola, F, Andreaus, U, and Placidi, L. At the origins and in the vanguard of peri-dynamics, non-local and higher gradient continuum mechanics. An underestimated and still topical contribution of Gabrio Piola. *Mech Math Solid* 2015; 20: 887-928.
- [56] dell’Isola, F, et al. *The complete works of Gabrio Piola: volume I commented English translation - English and Italian edition*. Berlin: Springer Publishing Company, Incorporated, 2014, 813.
- [57] Essén, H. Average angular velocity. *Eur J Phys* 1993; 14: 201.
- [58] Yang, Y, and Misra, A. Micromechanics based second gradient continuum theory for shear band modeling in cohesive granular materials following damage elasticity. *Int J Solid Struct* 2012; 49: 2500–2514.
- [59] Gray, WG, et al. *Mathematical tools for changing scale in the analysis of physical systems*. New York: CRC Press, 1993.
- [60] Dell’Isola, F, et al. Pantographic metamaterials: an example of mathematically driven design and of its technological challenges. *Continuum Mech Thermodynam* 2018; 31: 851-884.
- [61] Misra, A, et al. Pantographic metamaterials show atypical Poynting effect reversal. *Mech Res Commun* 2018; 89: 6–10.
- [62] dell’Isola, F, et al. Advances in pantographic structures: design, manufacturing, models, experiments and image analyses. *Continuum Mech Thermodynam* 2019; 31: 1231–1282.
- [63] Turco, E., et al. King post truss as a motif for internal structure of (meta) material with controlled elastic properties. *R Soc Open Sci* 2017; 4: 171153.
- [64] Turco, E., et al. Enhanced Piola–Hencky discrete models for pantographic sheets with pivots without deformation energy: numerics and experiments. *Int J Solid Struct* 2018; 147: 94–109.
- [65] Giorgio, I, et al. Pattern formation in the three-dimensional deformations of fibered sheets. *Mech Res Commun* 2015; 69: 164–171.
- [66] Giorgio, I, Rizzi, N, and Turco, E. Continuum modelling of pantographic sheets for out-of-plane bifurcation and vibrational analysis. *Proc R Soc A Math Phys Eng Sci* 2017; 473: 20170636.
- [67] Placidi, L, and Barchiesi, E. Energy approach to brittle fracture in strain-gradient modelling. *Proc R Soc A* 2018; 474: 20170878.
- [68] Placidi, L, Barchiesi, E, and Misra, A. A strain gradient variational approach to damage: a comparison with damage gradient models and numerical results. *Math Mech Complex Syst* 2018; 6: 77–100.

- 
- [69] Placidi, L., Misra, A., and Barchiesi, E. Two-dimensional strain gradient damage modeling: a variational approach. *Zeitschrift für angewandte Mathematik und Physik* 2018; 69: 56.
- [70] Misra, A., and Poorsolhjoui, P. Identification of higher-order elastic constants for grain assemblies based upon granular micromechanics. *Math Mech Complex Syst* 2015; 3: 285–308.

## Appendix B: Paper P2

**Title:**

Longitudinal and transverse elastic waves in 1D granular materials modeled as micromorphic continua

**Authors:**


Anil Misra

Nima NejadiSadeghi

**Journal:**

Wave Motion

**Permission from journal:**



Longitudinal and transverse elastic waves in 1D granular materials modeled as micromorphic continua  
Author: Anil Misra, Nima NejadiSadeghi  
Publication: Wave Motion  
Publisher: Elsevier  
Date: August 2019  
© 2019 Elsevier B.V. All rights reserved.

---

**Journal Author Rights**

Please note that, as the author of this Elsevier article, you retain the right to include it in a thesis or dissertation, provided it is not published commercially. Permission is not required, but please ensure that you reference the journal as the original source. For more information on this and on your other retained rights, please visit: <https://www.elsevier.com/about/our-business/policies/copyright#Author-rights>

**Credit authorship statement:**

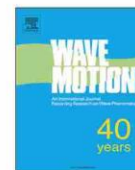
A.M. conceived the idea. N.N. performed the analysis. N.N. and A.M. contributed to the discussion of all aspects of this work. N.N. and A.M. wrote and edited the manuscript.



Contents lists available at ScienceDirect

## Wave Motion

journal homepage: [www.elsevier.com/locate/wamot](http://www.elsevier.com/locate/wamot)



# Longitudinal and transverse elastic waves in 1D granular materials modeled as micromorphic continua

Anil Misra <sup>a,\*</sup>, Nima Nejadi Sadeghi <sup>b</sup>

<sup>a</sup> Civil, Environmental and Architectural Engineering Department, University of Kansas, 1530 W. 15th Street, Learned Hall, Lawrence, KS 66045-7609, United States

<sup>b</sup> Mechanical Engineering Department, University of Kansas, 1530 W. 15th Street, Learned Hall, Lawrence, KS 66045-7609, United States



### HIGHLIGHTS

- Longitudinal and transverse wave dispersion in granular material is investigated.
- Granular micromechanics model with enriched kinematic description is utilized.
- Wave dispersion is connected to the underlying physics of grain-pair interactions.
- Emergence of frequency band gaps and negative group velocities is predicted.

### ARTICLE INFO

#### Article history:

Received 6 August 2018  
 Received in revised form 26 February 2019  
 Accepted 14 May 2019  
 Available online 21 May 2019

#### Keywords:

Micromorphic continuum  
 Dispersion  
 Micro-structure  
 Frequency band gaps  
 Metamaterials  
 Granular micromechanics

### ABSTRACT

In this paper, the granular micromechanics approach proposed by Misra and Poursolhjouy (2016) is used to study the dispersive behavior of granular materials in response to elastic deformation waves. This study is motivated by the typical lack of connection between the mathematical models, the parameters involved, and the physics of granular materials. Therefore, extensive parametric studies are carried out in order to understand how each intergranular stiffness coefficient contributes to the dispersive behavior of the material. Two cases of one dimensional wave propagation problems have been investigated. Case 1 focuses upon longitudinal wave propagation in a one dimensional continuum, while case 2 considers transverse wave propagation in a one dimensional continuum that has a two-dimensional micro-structure. Results predict the emergence of frequency band gaps and negative group velocities for certain values of the parameters involved. Such phenomena can be produced by starting from the micro-structure and producing materials for which the inter-granular stiffness parameters are the ones the granular micromechanics approach predict. This, however, is not a one to one mapping, and therefore, sets of solutions to achieve a particular behavior might exist. Therefore, granular micromechanics provides a systematic material design process, eliminating ad-hoc processes and potentially leading to large data libraries.

© 2019 Elsevier B.V. All rights reserved.

## 1. Introduction

Many engineering and science disciplines such as material development, transportation and infrastructure systems [1, 2], pharmaceuticals, drug delivery, and natural processes in geophysics encompass the applications of granular materials,

\* Corresponding author.

E-mail address: [amisra@ku.edu](mailto:amisra@ku.edu) (A. Misra).



suggesting a necessity to better understand how such materials behave. Studying elastic wave propagation in granular media results in a better realization of how these materials react to external actions, and in general, promotes the understanding of such materials. Granular materials, due to their grain-scale mechano-morphological properties, have an inherent microstructural characteristic length with which the wavelength of excitation at high frequencies becomes comparable [3]. As a result, effects of the micro-mechano-morphology become significant when the material experiences high frequency loads. Therefore, it becomes important to include information about the material's micro-structure in wave propagation studies [4]. Notably, in these cases, the classical wave equation of the form of a hyperbolic partial differential equation becomes complicated as additional terms are introduced to account for the micro-mechano-morphology. A previous study on dielectric granular materials revealed the potential tenability of the range, and location of frequency bandgaps in the presence of external electric field using straightforward examples [5], but did not analyze thoroughly the material parameters' effects on the dispersive behavior of granular media. Such analysis is pursued in the present paper.

Herein, the granular micromechanics approach proposed in [6] to develop a micromorphic model is used to study the dispersive behavior of the granular materials in response to the elastic deformation waves. In granular micromechanics approach, the material representative volume element (RVE) is modeled as a collection of grains which are interacting with each other through different inter-granular mechanisms. This approach treats the problem in a statistical sense by considering mean behavior of grain-pairs [7]. The proposed approach to developing continuum models provides the framework to describe the average behavior of many types of granular materials. The approach taken is clearly different from that proposed in the literature by combining masses, linear springs, rotational springs, beams etc. (see for example [8–10]). Indeed, the ansatz to this approach can be traced to the work of Piola [11] and Hellinger [12]. Moreover, the necessity of extended continua including higher gradients of displacements as envisaged by Piola has been exemplified in the recent works of wave propagation [13–15].

In the continuum description based upon granular micromechanics approach, the material point is modeled as a granular volume element composed of distinct grains, and grain-pair interactions are elementary units of the material's microscopic behavior. The resulting continuum model is similar to the micro-structure elasticity model of [16] and micromorphic media [3,4,18,19], typically, the considered physics has a weak relation to materials with granular micro-structure. To this extent, the current work is motivated by the lack of connection between the mathematical models, the parameters involved, and the physics of granular materials. Here we explore this connection through a theoretical approach, since the complexities of measuring parameters in experiments are typically unsurmountable and experimental approaches fail to provide a comprehensive analysis of the behavior of the materials with micro-structures. The paper is organized as follows.

An overview of the theory is presented in Section 2, where the kinematics of the model and the variational approach to derive the governing equations of motion are introduced. To avoid complexities, and to be better able to interpret the role of the micro-structure in the dispersive behavior of the granular materials, we limit our studies to two cases of one dimensional wave propagation. We perform extensive parametric studies to emphasize the effect of micro- and macro-scale parameters on the dispersive behavior of the material. Case 1 focuses upon the longitudinal wave propagation in a one dimensional continuum with granular micro-structure which is described in Section 3. Case 2 considers the transverse wave propagation in a one dimensional continuum that has a two-dimensional granular micro-structure as described in Section 4. Section 5 is devoted to the micro-mechanical implication of the analyses presented in Sections 3 and 4, where a connection between the observed behavior and the grain-pair interactions is made. Furthermore, a discussion on the potential applicability of the theory used here in the design and fabrication of granular metamaterials with specific material properties for particular purposes is made. Finally, the summary and conclusion of the present work is embraced in Section 6, where the possibility for future research is also proposed.

## 2. Micromorphic model based upon granular micromechanics

The granular micromechanics proceeds from an identification of the grain-scale motions in terms of the continuum measures and the volume average of grain-pair interaction energies with the macro-scale deformation energy density. In the current format of granular micromechanics [20], two grain-scale kinematic measures are defined, one for determining relative displacements and the other for relative rotations. It is remarkable that the considered grain-scale kinematic measures represent the combined effect of the grain centroid displacement, spin and size, and do not follow the decomposition adopted in some previous attempts of micro-macro identifications [21–23]. These grain-scale motions are identified with six set of continuum kinematic measures that include the macro-scale displacement/rotation gradients, micro-scale displacement/rotations gradients identified with displacement/rotation fluctuations within a material point, and macro-gradient of the micro-scale displacement/rotation gradients. The deformation energy density of a material point is then expressed in terms of the kinematic measures at the two scales and the inter-granular force measures as well as the continuum stress are defined as conjugates of the kinematic measures. Subsequently, the relationships are derived between stress and inter-granular forces that include stretch/compression, tangential, bending and torsional actions as well as for further derivation of the constitutive relations, variational principle, and balance equations for non-classical micromorphic model whose parameters can be identified in terms of the grain-scale properties [6,24,25]. In what follows, we briefly state the mathematical model and derive the equations of motion. The reader is referred to [6,20] for more detailed description.

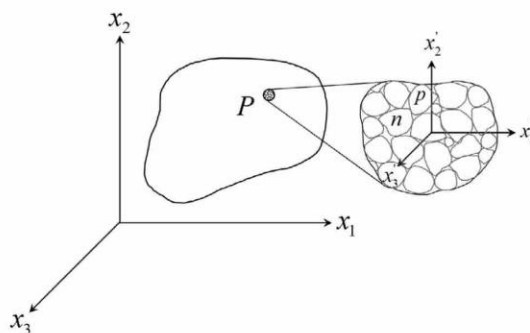


**Fig. 1.** Schematic of the continuum material point,  $P$ , and its granular micro-structure magnified for better visualization, where the  $x'$  coordinate system is attached to its barycenter.

To develop a continuum model, each material point is considered a representative volume element (RVE), as shown in Fig. 1. Consider the coordinate system  $x$  to be relevant to the global (macro-scale) model, and attach a local or micro-scale coordinate system  $x'$  to the material point  $P$  or the barycenter of the RVE with its axes parallel to the global coordinate system axes  $x$ . The micro-scale coordinate system is defined such that it is able to distinguish different grains inside the material point. The displacement of the grains are then not only a function of the coordinates of the material point  $P$ , but also of the micro-scale coordinates of the grain within the material point, i.e.,

$$\phi_i = \phi_i(x, x', t), \quad (1)$$

where  $\phi_i$  is the displacement of grain centroids. Now consider the displacement,  $\phi_i^p$ , of the centroid of grain,  $p$ , contained within the continuum material point, where the displacement is defined in [6]. Utilizing the Taylor's expansion, this displacement can be related to the displacement,  $\phi_i^n$ , of the centroid of neighboring grain,  $n$ , such that the difference will be the relative displacement,  $\delta_i^{np}$ , of the two grains, which is given as follows, where we have included only the first and second order terms in the Taylor series expansion

$$\delta_i^{np} = \phi_i^p - \phi_i^n = \phi_{i,j}^n l_j + \frac{1}{2} \phi_{i,jk}^n l_j l_k. \quad (2)$$

In Eq. (2),  $l_j$  is the vector joining the centroids of  $n$  and  $p$ , and the tensor product  $l_j l_k (=J_{jk})$  is a geometry moment tensor. The differentiation in Eq. (2) is with respect to  $x'$ . In the rest of the paper, a comma in the subscript represents differentiation with respect to the position, and dots on the parameters express differentiation with respect to time. Also note that the summation convention over repeated indices (in the subscript) is implied unless noted otherwise. Following a similar analysis, the relative rotations of two interacting grains,  $n$  and  $p$ , denoted by  $\theta_i$  is found as [6]

$$\theta_i^{np} = e_{jki} \phi_{k,jp} l_p, \quad (3)$$

where  $e_{ijk}$  is permutation symbol and the differentiation is with respect to  $x'$ . We introduce the decomposition of the displacement gradient field as [6,20,26]

$$\psi_{ij} = \phi_{i,j} = \bar{\phi}_{i,j} - \gamma_{ij}, \quad (4)$$

where  $\psi_{ij}$  is the displacement gradient in the RVE,  $\bar{\phi}_{i,j}$  is the macro-scale displacement gradient which is a constant in a material point, and  $\gamma_{ij}$  is the relative deformation due to the fluctuations of the micro-displacement of the grains inside the RVE. This suggests that the micro-deformation  $\psi_{ji}$  is taken to be homogenous in the RVE but can be non-homogenous in the macro-medium. The relative displacement of grains  $p$  and  $n$  can then be decomposed as

$$\delta_i^{np} = \bar{\phi}_{i,j} l_j - \gamma_{ij} l_j + \frac{1}{2} \phi_{i,jk} l_j l_k = \delta_i^M - \delta_i^m + \delta_i^g, \quad (5)$$

where

$$\delta_i^M = \bar{\phi}_{i,j} l_j, \quad \delta_i^m = \gamma_{ij} l_j, \quad \delta_i^g = \frac{1}{2} \phi_{i,jk} l_j l_k. \quad (6)$$

With regards to Eq. (6),  $\delta_i^M$  is due to the average displacement gradient,  $\bar{\phi}_{i,j}$ ,  $\delta_i^m$  is due to the gradients of the fluctuation in grain displacement,  $\gamma_{ij}$ , and  $\delta_i^g$  is due to the second gradient term,  $\phi_{i,jk}$ , which is same as the gradient of the relative deformation,  $\gamma_{ij,k}$ .



Macro-scale deformation energy density  $W$  of the granular continua can be defined as a function of the continuum kinematic measures as

$$W = W(\bar{\phi}_{(i,j)}, \gamma_{ij}, \phi_{i,jk}), \tag{7}$$

where  $\bar{\phi}_{(i,j)}$  is the symmetric part of the macro-scale displacement gradient. Macro-scale stress components conjugate to these kinematic measures are obtained as

$$\tau_{ij} = \frac{\partial W}{\partial \bar{\phi}_{(i,j)}} = \frac{\partial W}{\partial \varepsilon_{ij}}, \quad \sigma_{ij} = \frac{\partial W}{\partial \gamma_{ij}}, \quad \mu_{ijk} = \frac{\partial W}{\partial \gamma_{ij,k}}, \tag{8}$$

where  $\tau_{ij}$ ,  $\sigma_{ij}$ , and  $\mu_{ijk}$  are Cauchy stress, relative stress, and double stress, respectively. Macro-scale deformation energy density can be expressed in terms of micro-scale deformation defined for the  $\alpha$ th interacting pair as  $W^\alpha(\delta_i^{\alpha M}, \delta_i^{\alpha m}, \delta_i^{\alpha g}, \theta_i^{\alpha u})$ , such that

$$W = \frac{1}{V'} \sum_{\alpha} W^\alpha(\delta_i^{\alpha M}, \delta_i^{\alpha m}, \delta_i^{\alpha g}, \theta_i^{\alpha u}). \tag{9}$$

In Eq. (9)  $V'$  is the volume of the assumed RVE. The intergranular force and moment conjugates are introduced, using Eq. (9), as

$$\frac{\partial W}{\partial \delta_i^{\alpha \zeta}} = f_i^{\alpha \zeta}; \quad \zeta = M, m, g, \quad \frac{\partial W}{\partial \theta_i^{\alpha u}} = m_i^{\alpha u}. \tag{10}$$

Substituting Eq. (9) in Eq. (8), and using Eqs. (6) and (10), it follows that [6]

$$\tau_{ij} = \frac{1}{V'} \sum_{\alpha} f_i^{\alpha M} J_j^{\alpha}, \quad \sigma_{ij} = \frac{1}{V'} \sum_{\alpha} f_i^{\alpha m} J_j^{\alpha}, \quad \mu_{ijk} = \frac{1}{V'} \left( \sum_{\alpha} f_i^{\alpha g} J_{jk}^{\alpha} + \sum_{\alpha} m_i^{\alpha u} e_{jil} l_k^{\alpha} \right). \tag{11}$$

Therefore, the macro-scale stress measures are defined in terms of the inter-granular forces, branch vector, and the geometry moment tensor.

Defining a local coordinate system for each interacting grain pair, decomposing intergranular force, moment, displacement, and rotation vectors in their normal and tangential components, and assuming a quadratic form of  $W^\alpha$  for linear isotropic elasticity case, the macro-scale constitutive relationships in the global coordinate system are derived [6] as

$$\tau_{ij} = C_{ijkl}^M \varepsilon_{kl}, \quad \sigma_{ij} = C_{ijkl}^m \gamma_{kl}, \quad \mu_{ijk} = (A_{ijklmn}^g + A_{ijklmn}^u) \phi_{l,mn}, \tag{12}$$

where  $C_{ijkl}^M$  and  $C_{ijkl}^m$  are fourth rank tensors, and  $A_{ijklmn}^g$  and  $A_{ijklmn}^u$  are sixth rank tensors, defined as (Refer to [6] for more details)

$$C_{ijkl}^M = \frac{1}{V'} \sum_{\alpha} K_{ik}^M l_j^{\alpha} l_l^{\alpha}, \quad C_{ijkl}^m = \frac{1}{V'} \sum_{\alpha} K_{ik}^m l_j^{\alpha} l_l^{\alpha}, \tag{13}$$

$$A_{ijklmn}^g = \frac{1}{V'} \sum_{\alpha} K_{ij}^g J_{mnl}^{\alpha} J_{jk}^{\alpha}, \quad A_{ijklmn}^u = \frac{1}{V'} \sum_{\alpha} C_{pq}^u e_{mlq} e_{jip} l_k^{\alpha} l_n^{\alpha}.$$

We note here that for many granular systems (including those formed by grain-packings for which Hertz Law has been used widely [27]), grain-pair interactions are nonlinear and include dissipation. Nevertheless, understanding linear elastic behavior has practical significance for small amplitude vibrations, for which a quadratic form of  $W^\alpha$  can be assumed. In addition, linear elastic behavior provides a point of departure for exploring more complex phenomena introduced by nonlinearity and dissipation. In Eq. (13), the four different inter-granular stiffness measures are defined as  $K_q^p$  and  $G_q^u$ , where  $K$  and  $G$  denote the stretch and rotational stiffnesses, respectively,  $p = M, m$  and  $q = n, w$ . Further in Eq. (13), superscript  $M$  denotes macro-stiffness,  $m$  denotes the micro-stiffness,  $g$  denotes the second gradient stiffness, and  $u$  denotes the rotation terms, respectively, introduced for each term of the decomposed relative displacement and rotation; and the subscripts  $n$  and  $w$  refer to the normal and tangential grain-pair interaction directions.

We now briefly outline the derivation of the balance equations and equations of motion for a material with granular micro-structure using a variational approach. To this end, we can write for the variation of the internal potential energy, using Eqs. (4) and (8)

$$\delta W = \tau_{ij} \delta \varepsilon_{ij} + \sigma_{ij} \delta \gamma_{ij} + \mu_{ijk} \delta \phi_{i,jk} = \tau_{ij} \delta \bar{\phi}_{(i,j)} + \sigma_{ij} (\delta \bar{\phi}_{(i,j)} - \delta \phi_{i,j}) + \mu_{ijk} \delta \phi_{i,jk}. \tag{14}$$

Using Leibniz differentiation rule, we can write Eq. (14) in the form

$$\delta W = [(\tau_{ij} + \sigma_{ij}) \delta \bar{\phi}_i]_j - (\tau_{ij} + \sigma_{ij})_j \delta \bar{\phi}_i - \sigma_{ij} \delta \psi_{ij} + (\mu_{ijk} \delta \psi_{ij})_{,k} - \mu_{ijk,k} \delta \psi_{ij}. \tag{15}$$

The variational of the macro-scale deformation energy functional can be obtained using Gauss's divergence theorem of integration and Eq. (15) as

$$\delta \tilde{W} = - \int_V (\tau_{ij} + \sigma_{ij})_{,j} \delta \bar{\phi}_i dV - \int_V (\mu_{ijk,k} + \sigma_{ij}) \delta \psi_{ij} dV + \int_S (\tau_{ij} + \sigma_{ij}) n_j \delta \bar{\phi}_i dS + \int_S \mu_{ijk} n_k \delta \psi_{ij} dS. \tag{16}$$

We also define the variational of the external work as

$$\delta \bar{W}_{ext} = \int_V f_i \delta \bar{\phi}_i dV + \int_V \Phi_{ij} \delta \psi_{ij} dV + \int_S t_i \delta \bar{\phi}_i dS + \int_S T_{ij} \delta \psi_{ij} dS, \quad (17)$$

where  $f_i$  is the non-contact volumic (body) force per unit volume,  $t_i$  is the contact traction defined as a surface force per unit area,  $\Phi_{ij}$  is the non-contact volumic (body) double force per unit volume, and  $T_{ij}$  is the contact double traction defined as double force per unit area.

The kinetic energy density (kinetic energy per unit macro-volume)  $T$  is defined as

$$T = \frac{1}{V'} \int_{V'} \frac{1}{2} \rho' \dot{\phi}_i \dot{\phi}_i dV', \quad (18)$$

where  $\rho'$  is the micro-scale mass density per unit macro-volume. For a constant  $\rho'$  in the RVE and the continuum, we have, for the macro-scale mass density per unit macro-volume,

$$\rho = \frac{1}{V'} \int_{V'} \rho' dV' = \frac{\rho'}{V'} \int_{V'} dV' = \rho'. \quad (19)$$

Therefore, the densities in micro- and macro-scales become identical. Note that for graded materials with spatially varying densities, one can take  $\rho'$  to be non-uniform. This assumption leads to additional terms in the final form of the kinetic energy derived in this paper, and will be pursued in future publications. Eq. (18), after substituting for  $\phi_i$ , using Eq. (19), and neglecting higher order inertia terms, can be written as

$$T = \frac{1}{2} \rho \dot{\phi}_i \dot{\phi}_i + \frac{1}{2} \rho d_{jk} \dot{\psi}_{ij} \dot{\psi}_{ik}, \quad (20)$$

which is similar to [28], and where  $d_{jk}$  is defined as follows

$$d_{jk} = \frac{1}{V'} \int_{V'} x'_j x'_k dV'. \quad (21)$$

In the rest of the paper, we assume the RVE to be cubic with edges  $2d$  parallel to the axes  $x'$ . In such a case, Eq. (21) simplifies to

$$d_{jk} = \frac{1}{3} d^2 \delta_{jk}, \quad (22)$$

where  $\delta_{jk}$  is the Kronecker delta. From Eq. (22) it is clear that  $d_{jk}$  is a diagonal matrix with equal diagonal terms. The total kinetic energy is the integral of the kinetic energy density over the whole domain, and is written as

$$\tilde{T} = \int_V T dV. \quad (23)$$

Using Eqs. (20) and (23), the variational of the kinetic energy functional is written, after integration by parts and assuming the values of  $\phi_j$  and  $\psi_{ij}$  to be known at  $t = t_0, t_1$ , as

$$\delta \int_{t_0}^{t_1} \tilde{T} dt = - \int_{t_0}^{t_1} \int_V \rho \ddot{\phi}_i \delta \bar{\phi}_i dV dt - \int_{t_0}^{t_1} \int_V \frac{1}{3} \rho d^2 \ddot{\psi}_{ij} \delta \psi_{ij} dV dt. \quad (24)$$

Hamilton principle requires the action functional to be minimum, and is expressed as

$$\delta \int_{t_0}^{t_1} (\tilde{T} - \bar{W} + \bar{W}_{ext}) dt = 0. \quad (25)$$

Substituting Eqs. (16), (17), and (24) in Eq. (25) results in the balance equations and the boundary conditions. The balance equations are

$$\begin{aligned} (\tau_{ij} + \sigma_{ij})_j + f_i &= \rho \ddot{\phi}_i, \\ \mu_{ijk,k} + \sigma_{ij} + \Phi_{ij} &= \frac{1}{3} \rho d^2 \ddot{\psi}_{ij}, \end{aligned} \quad (26)$$

and the two natural boundary conditions given in terms of the stress measures are

$$(\tau_{ij} + \sigma_{ij}) n_j = t_i, \quad \mu_{ijk} n_k = T_{ij}. \quad (27)$$

Finally, equations of motion can be derived, by substituting the constitutive equations, Eq. (12), in the balance equations, Eq. (26). Assuming volumic (body) forces and volumic double forces to be absent, the equations of motion are described as

$$\begin{aligned} (C_{ijkl}^M + C_{ijkl}^m) \bar{\phi}_{k,lj} - C_{ijkl}^m \psi_{kl,j} &= \rho \ddot{\phi}_i, \\ (A_{ijklmn}^g + A_{ijklmn}^u) \psi_{lm,nk} + C_{ijkl}^m \bar{\phi}_{k,l} - C_{ijkl}^m \psi_{kl} &= \frac{1}{3} \rho d^2 \ddot{\psi}_{ij}. \end{aligned} \quad (28)$$

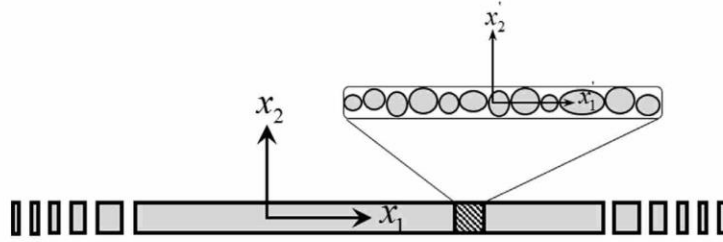


**Fig. 2.** Schematic of a 1D continuum in  $x_1$  direction with granular micro-structure in  $x_2$  direction. A material point in the macro-scale coordinate system is itself a collection of grains that can differ in micro-density, micro-morphology and micro-mechanical properties.

### 3. Longitudinal wave propagation in a 1D isotropic continuum with granular micro-structure

#### 3.1. Mathematical formulation

In what follows, we consider the longitudinal (P) wave propagation in an isotropic one dimensional infinite continuum in macro- and micro-scale along the  $x_1$  axis. A schematic of the general problem has been shown in Fig. 2. Note again that a 1D homogenous isotropic continuum can be, in general, non-homogenous in the RVE (micro-scale). This inhomogeneity may come from the mass density distribution, or the variation of grain pair interaction in the medium. The former is depicted in Fig. 2, while the latter is rather difficult to visualize. As the underlying assumption for deriving Eq. (31) is having a constant  $\rho'$ , our focus in this section is inhomogeneity in grain-pair interactions. In this case, the twelve equations of motion Eq. (28) reduce to the following two equations

$$\begin{aligned} (P + Q) \bar{\phi}_{1,11} - Q \psi_{11,1} &= \rho \ddot{\bar{\phi}}_1, \\ R \psi_{11,11} + Q \bar{\phi}_{1,1} - Q \psi_{11} &= I \ddot{\psi}_{11}, \end{aligned} \quad (29)$$

where the symbols  $P$ ,  $Q$ ,  $R$ , and  $I$  have been used for brevity, to represent the macro-scale modulus  $C_{1111}^M$ , the micro-scale modulus  $C_{1111}^m$ , the second-gradient modulus  $A_{111111}^g$ , and micro-inertia  $\frac{1}{3}\rho d^2$ , respectively. Solutions of the Eq. (29) are of the form

$$\bar{\phi}_1 = \bar{\phi}_1(x_1, t), \quad \psi_{11} = \psi_{11}(x_1, t), \quad (30)$$

in which the kinematic measures  $\bar{\phi}_1$  and  $\psi_{11}$  are only functions of time and  $x_1$ . Following Mindlin [16] and specializing the solutions in Eq. (30) to harmonic plane waves, we will have the following form for the solution of Eq. (29)

$$\bar{\phi}_1 = \text{Re}(A_1 i e^{i(kx_1 - \omega t)}), \quad \psi_{11} = \text{Re}(B_{11} e^{i(kx_1 - \omega t)}), \quad (31)$$

where  $k$  is the wave number,  $\omega$  is the angular frequency (to which we refer for the rest of the paper as frequency),  $A_1 i$  and  $B_{11}$  are the amplitudes of the macro displacement and micro displacement gradient, respectively, and  $i^2 = -1$ . Note that the amplitudes  $A_i$  and  $B$  can take complex values.

Substituting Eq. (31) into Eq. (29), the set of equations can be rewritten in the following matrix form

$$\begin{bmatrix} c_0^2 k^2 & c_A^2 k \\ k & p^2 c_1^2 k^2 + 1 \end{bmatrix} \begin{bmatrix} A_1 \\ B_{11} \end{bmatrix} = \omega^2 \begin{bmatrix} A_1 \\ B_{11} \end{bmatrix}, \quad (32)$$

where, following [4], we have introduced the velocities,  $c_0$ ,  $c_1$ , and  $c_A$ , and characteristic time,  $p$  as follows

$$c_0^2 = \frac{P + Q}{\rho}, \quad c_1^2 = \frac{R}{I}, \quad c_A^2 = \frac{Q}{\rho}, \quad p^2 = \frac{I}{Q}. \quad (33)$$

Eq. (32) is an eigenvalue problem with the eigenvalue  $\omega^2$  and the eigenvector comprising the amplitudes of the propagating macro-displacement waves and micro-displacement gradient waves, respectively. The relationship between the components  $A_1$  and  $B_{11}$  is given, using Eq. (32), as

$$B_{11} = A_1 \left( \frac{\omega^2 - c_0^2 k^2}{c_A^2 k} \right). \quad (34)$$

Solving for the eigenvalues  $\omega^2$ , Eq. (32) yields the secular equation

$$\omega^2 = (c_0^2 - c_A^2) k^2 + p^2 (\omega^2 - c_0^2 k^2) (\omega^2 - c_1^2 k^2). \quad (35)$$



Eq. (35) is the dispersion relation for the problem under study. A similar form of dispersion relation can be found, for example in [4,29]. It is noteworthy that the parameters introduced in this paper can be identified with those in [4,29] as follows:  $\hat{\alpha} = (P + Q)$ ,  $\hat{B} = -\hat{A} = Q$ ,  $\hat{C} = R$ . What is noteworthy in the present paper is the connection of these parameters with the micro-measures (such as micro-stiffnesses and grain sizes) relevant for elastic granular systems. This connection between the continuum models and micro-measures presents a new paradigm for exploring the micro-mechanical antecedents of phenomena predicted by Eq. (35), which are described in further in Section 5. In very low frequency/wavenumber ranges, higher order terms of frequency and wave number in Eq. (35) can be neglected and the waves propagate, expectedly, with the macro-scale velocity  $\sqrt{c_0^2 - c_A^2}$ , related only to the macro-scale moduli and density as  $\frac{p}{\rho}$ . Although it appears that the effect of micro-structure is seemingly lost in the first part of the right hand side of Eq. (35), however it is to be noted that the grain-scale effects are reflected in the macro-scale moduli and density (as seen from Eqs. (13) and (19)). Furthermore, microstructural effects become increasingly prominent for larger frequencies and wavenumbers through the terms  $c_0$  and  $c_1$  in the second part of the right hand side of Eq. (35). Clearly, Eq. (35) shows that for very small frequencies and wavenumbers, fluctuation in grain-pair stiffnesses in the RVE has negligible effect and wave propagation is controlled by the macro-scale properties, while in larger frequencies and wavenumbers, the effect of fluctuation in grain-pair stiffnesses on the velocity of propagating waves become increasingly significant through the micro-moduli, second-gradient moduli and micro-inertia whose antecedents are further discussed in Section 5.

Introducing the dimensionless wave number and frequency

$$\xi = pc_0k, \quad \eta = p\omega, \quad (36)$$

and dimensionless velocities

$$\gamma_A = \frac{c_A}{c_0} = \sqrt{\frac{Q}{P+Q}}, \quad \gamma_1 = \frac{c_1}{c_0} = \sqrt{\frac{R}{P+Q}} \sqrt{\frac{\rho}{I}}. \quad (37)$$

Eq. (35) can be recast in the form

$$\eta^2 = (1 - \gamma_A^2) \xi^2 + (\eta^2 - \xi^2) (\eta^2 - \gamma_1^2 \xi^2). \quad (38)$$

We also introduce the parameter  $B'_{11}$  as

$$B'_{11} = pc_0B_{11}. \quad (39)$$

Now, using Eqs. (34), (36), (37), and (39), we can write

$$B'_{11} = \frac{\eta^2 - \xi^2}{\gamma_A^2 \xi} A_1. \quad (40)$$

By introducing the dimensionless parameter  $\beta$  defined as the ratio of  $B'_{11}$  to  $A_1$ , we can rewrite Eq. (40) as

$$\beta = \frac{\eta^2 - \xi^2}{\gamma_A^2 \xi}. \quad (41)$$

The phase and group velocities can be obtained as follows

$$v_p = \frac{\omega}{k}, \quad v_g = \frac{d\omega}{dk}, \quad (42)$$

where  $v_p$  is the phase velocity, and  $v_g$  is the group velocity. Introducing the dimensionless phase and group velocities, respectively, as

$$v_p = \frac{v_p}{c_0}, \quad v_g = \frac{v_g}{c_0}, \quad (43)$$

and using Eqs. (36) and (42), we can write Eq. (43) in the form

$$v_p = \frac{\eta}{\xi}, \quad v_g = \frac{d\eta}{d\xi}. \quad (44)$$

Also, the mechanical energy transfer ratios associated with the micro-scale and macro-scale degrees of freedom can be obtained, using Eqs. (31), (33), and (41) and considering the time average of the mechanical energy density over a time

period as

$$\begin{aligned} \frac{E_{\text{micro}}}{E_{\text{total}}} &= \frac{\frac{1}{2T} \int_t^{t+T} (I\dot{\psi}_{11}^2 + Q\psi_{11}^2 + R\psi_{11,1}^2) dt}{\frac{1}{2T} \int_t^{t+T} \left( I\dot{\psi}_{11}^2 + Q\psi_{11}^2 + R\psi_{11,1}^2 + \rho\dot{\phi}_1^2 + P\bar{\phi}_{1,1}^2 \right) dt} \\ &= \frac{\beta^2 (\gamma_A^2 \eta^2 + \gamma_A^2 + \gamma_A^2 \gamma_1^2 \xi^2)}{\beta^2 (\gamma_A^2 \eta^2 + \gamma_A^2 + \gamma_A^2 \gamma_1^2 \xi^2) + \eta^2 + \xi^2 - \gamma_A^2 \xi^2}, \\ \frac{E_{\text{macro}}}{E_{\text{total}}} &= 1 - \frac{E_{\text{micro}}}{E_{\text{total}}} = \frac{\eta^2 + \xi^2 - \gamma_A^2 \xi^2}{\beta^2 (\gamma_A^2 \eta^2 + \gamma_A^2 + \gamma_A^2 \gamma_1^2 \xi^2) + \eta^2 + \xi^2 - \gamma_A^2 \xi^2}. \end{aligned} \quad (45)$$

### 3.2. Results

From the first of Eq. (37), it is clear that dimensionless velocity  $\gamma_A$  has lower bound limit of 0 and upper bound limit of 1. Very small values of  $\gamma_A$  represent materials in which the micro-stiffness is negligible compared to their macro-stiffness, and values close to the upper bound level have large micro-stiffness compared to their macro-stiffness. A value of  $\gamma_A = 0.71$  corresponds to approximately equal macro- and micro-stiffness of the material. On the other hand,  $\gamma_1$  has lower bound of 0 and an upper bound that can theoretically tend to infinity. For a particular ratio of macro-density to micro-inertia, larger  $\gamma_1$  implies a growing dominance of second gradient behavior. Figs. 3, 4, 5, and 6 show the dispersion curves, phase velocities, group velocities, and the energy transfer ratios of the micro-scale degree of freedom to the total energy transferred for different values of  $\gamma_A$  and  $\gamma_1$ . We observe in the case where second gradient terms are small (Figs. 3 and 5), increasing  $\gamma_A$  and decreasing  $\gamma_1$  leads to emergence of frequency band gaps. For  $\gamma_1$  larger than a certain limiting value the stopband vanishes. The reason for the vanishing of band gaps can be understood by examining the group velocity plots in Fig. 5. We note that the dimensionless group velocity of the optical and acoustic branches have the values of 0 and  $\sqrt{1 - \gamma_A^2}$  (corresponding to group velocities of 0 and  $\sqrt{c_0^2 - c_A^2}$ ) at small wavenumbers and asymptotic values of 1 and  $\gamma_1$  (corresponding to group velocities of  $c_0$  and  $c_1$ ), respectively. Therefore, a large value for the group velocity of the acoustic branch in both its small and large wavenumber ranges is the cause for vanishing band gaps. Complete band gaps emerge when the asymptote of the acoustic branch at large wavenumbers is a horizontal line. However, band gaps over a wide range of wavenumbers exist even for non-vanishing small values of  $\gamma_1$ . The starting point of the dimensionless frequency range in which the band gap appears varies, but is always between 0 and 1, while the end point of the dimensionless frequency is fixed at 1, corresponding to the frequency  $\omega = \sqrt{\frac{Q}{I}}$ , which is a function of the micro-scale properties. Also as  $\gamma_A$  increases and  $\gamma_1$  decreases, size of the band gap grows. Dimensionless phase velocity for the optical branch starts at infinity and reaches the value of 1 (phase velocity of  $c_0$ ) for large wavenumbers regardless of the value of  $\gamma_1$  (phase velocity of  $c_1$ ). The acoustic branch has an initial dimensionless phase velocity of  $\sqrt{1 - \gamma_A^2}$  (phase velocity of  $\sqrt{c_0^2 - c_A^2}$ ) and therefore, depends solely on the macro-scale stiffness of the material, while the asymptotic value reaches  $\gamma_1$  (phase velocity of  $c_1$ ). Therefore, based on the values of the parameters  $\gamma_A$  and  $\gamma_1$  we may have decreasing or increasing phase and group velocities of the acoustic branch depending on the values of  $\gamma_A$  and  $\gamma_1$ .

In materials with very large second gradient properties ( $\gamma_1 > 1$ ), as seen in Figs. 4 and 6, the acoustic branch at small wavenumbers starts with the dimensionless phase and group velocities of  $\sqrt{1 - \gamma_A^2}$  (corresponding to phase and group velocities  $\sqrt{c_0^2 - c_A^2}$ ), which is similar to the previous case. However, in this case, the terms containing higher orders of  $\xi$  and  $\gamma_1$  in the dispersion relation become dominant as we evaluate their limit at high wavenumbers. Hence, the asymptotic slope of the dispersion curve for the optical branch becomes  $\gamma_1$  (corresponding to the asymptote  $\omega = c_1 k$ ), and that of the acoustic branch becomes 1 (the asymptote  $\omega = c_0 k$  with asymptotic phase and group velocity of  $c_0$ ). This means for the cases where  $\gamma_1 > 1$ , the asymptotes of the two branches switch. Therefore, it is not possible to have stopbands.

We further observe that the energy transfer in 1D granular continuum during wave transmission occurs via two mechanisms, one governed by the macro-, and the other by the micro-scale degrees of freedom of the material. According to Fig. 3, in the acoustic branch at small wave numbers, energy transfer is affected mainly by the macro-scale degree of freedom, while for larger wave numbers, micro-scale degree of freedom plays the main part in energy transfer. This obviously shows the hierarchical nature of the wave propagation in micro-structured media. Large values of  $\gamma_1$  result in smoother shift from macro to micro-scale degree of freedom mechanism. In the case of optical wave, at small wavenumbers, the energy transfer is purely governed by the micro-scale degree of freedom. The model predicts transition of energy transfer mechanism from micro- to macro-scale, but it is well understood that for such large wavenumbers, the characteristic length of the excitation can be smaller than the characteristic length of the micro-structure, and hence, the proposed continuum mechanics theory may not be applicable. Note that when both  $\gamma_A$  and  $\gamma_1$  take very small values (e.g., in Fig. 3 for  $\gamma_A = 0.03$  and  $\gamma_1 = 0.0002$ ), we reach the classical wave propagation through the medium, and the energy transfer is almost completely due to the macro-scale degree of freedom.

Similar to the case where second gradient terms are small, for the case of large second gradient terms, energy transfer for small wavenumbers in the optical and acoustic waves are governed mainly by means of micro and macro-scale degrees



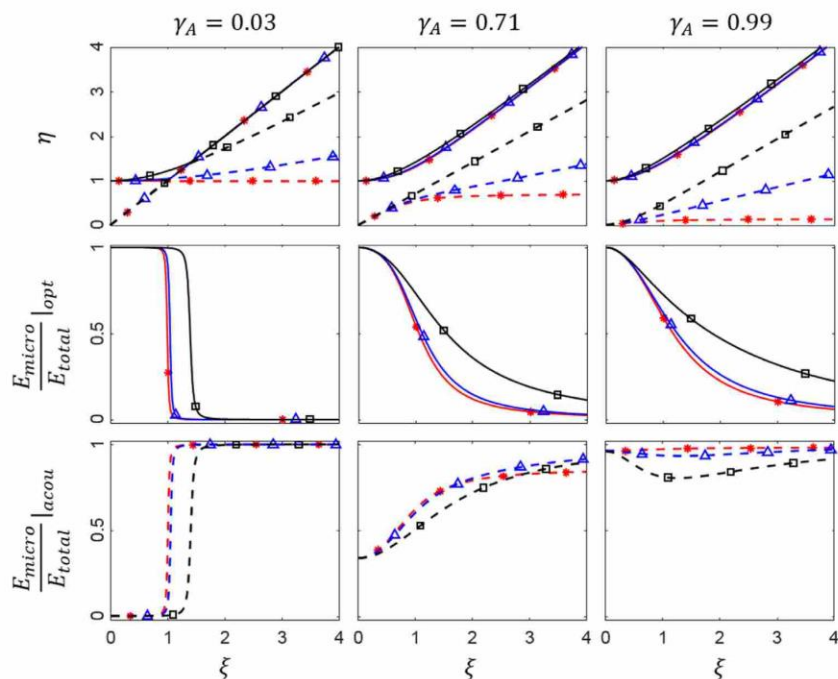


**Fig. 3.** Dispersion curves, and ratio of energy transferred by micro-scale degree of freedom to the total energy for optical and acoustic branches, for different values of  $\gamma_A$  and  $\gamma_1$ , where solid lines and dashed lines represent optical branches and acoustic branches respectively, and lines with  $\star$ ,  $\Delta$ , and  $\square$  represent  $\gamma_1 = 0.0002$ ,  $\gamma_1 = 0.3$ , and  $\gamma_1 = 0.7$ , respectively.

of freedom, respectively. As shown in Fig. 6, for a material with dominant second gradient terms, this behavior continues for higher wavenumbers as well, which is in contrast to the case of small second gradient terms, where the energy transfer at the micro-scale tends to disappear and be replaced by macro-scale mechanisms or vice versa. This decoupling effect in transferring energy in the optical and acoustic branches becomes more significant for smaller values of  $\gamma_A$  and larger values of  $\gamma_1$ .

### 3.3. Special cases

For a purely second gradient material, following [30], we begin from the internal potential energy expression and assume  $\psi_{ij} = \phi_{i,j}$ , followed by the variational approach to obtain the governing equations of motion. Solving for the wave propagation, thereafter, leads to a dispersion curve in which only one acoustic wave exists. At small wavenumbers, the wave has group velocity of  $\sqrt{1 - \gamma_A^2}$ , and at large wavenumbers, it follows the asymptote  $\eta = \gamma_1 \xi$ . Therefore, band gaps do not exist in second gradient materials. It is noteworthy to mention that one cannot reduce Eq. (29) to obtain a second gradient material model. Reducing Eq. (29) to obtain the equations of motion for a second gradient material by assuming  $\psi_{11} = \phi_{1,1}$  leads to a dispersion relation for which solving the equation gives rise to two acoustic waves.

To retrieve the classical wave dispersion relation, we assume  $\gamma_A = 0$  and  $\gamma_1 = 0$  in Eq. (38). The result is

$$\eta = \xi, \quad (46)$$

which is the non-dispersive relation between the frequency and wavenumber in their dimensionless form. For this case, there is only one acoustic wave and frequency bandgaps are not possible.

## 4. Transverse wave propagation in a one dimensional isotropic continuum with a two dimensional granular micro-structure

### 4.1. Mathematical formulation

We now turn our focus on the propagation of a transverse wave in a one dimensional isotropic continuum lying along  $x_2$  axis, with a two dimensional micro-structure in  $x_1$  and  $x_2$  directions. A schematic of the general problem is depicted in

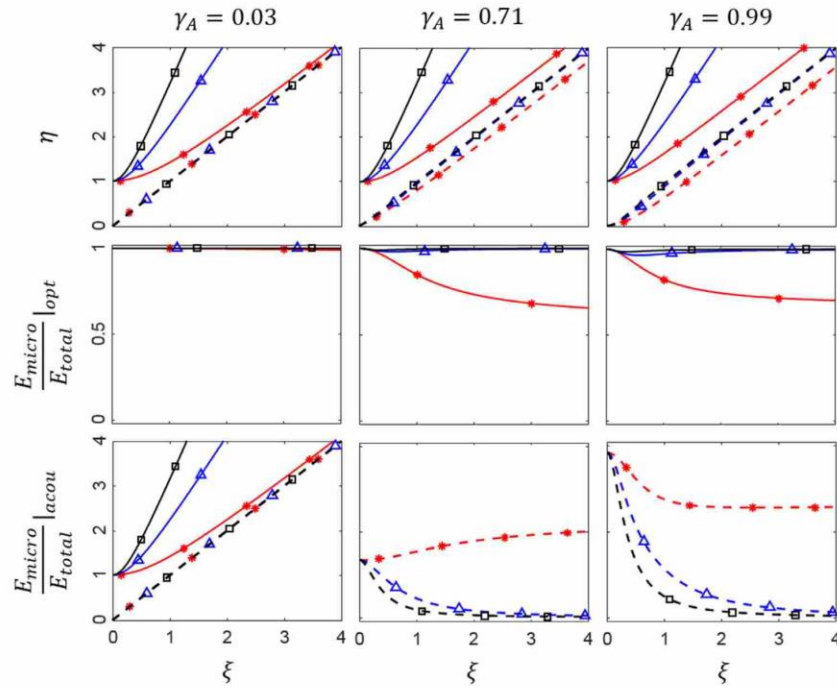


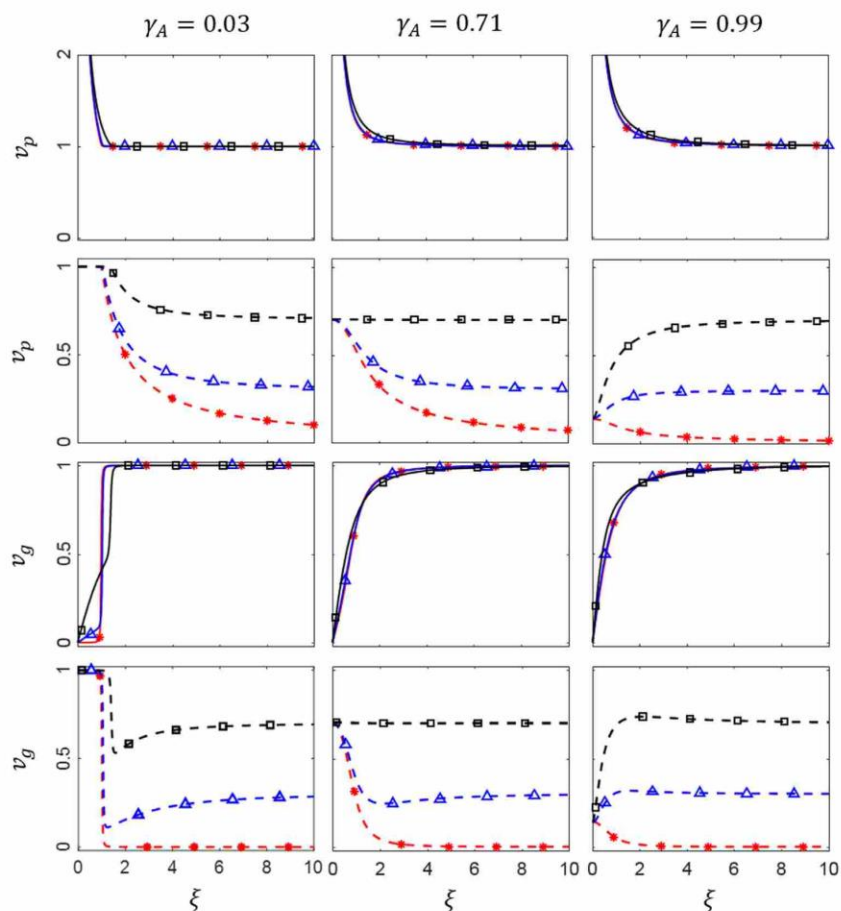
Fig. 4. Dispersion curves, and ratio of energy transferred by micro-scale degree of freedom to the total energy for optical and acoustic branches, for different values of  $\gamma_A$  and  $\gamma_1$ , where solid lines and dashed lines represent optical branches and acoustic branches respectively, and lines with  $*$ ,  $\Delta$ , and  $\square$  represent  $\gamma_1 = 1$ ,  $\gamma_1 = 2$ , and  $\gamma_1 = 3$ , respectively.

Fig. 7. Note again that a 1D homogenous isotropic continuum can be, in general, non-homogenous in the RVE (micro-scale). This inhomogeneity may come from the mass density distribution, or the variation of grain pair interaction in the medium. The former is depicted in Fig. 7, while the latter is rather difficult to picturize. As the underlying assumption for deriving Eq. (31) is having a constant  $\rho'$ , our focus in this section is inhomogeneity in grain-pair interactions. We therefore assume that the nonzero kinematic measures are  $\bar{\phi}_1, \psi_{11}, \psi_{22}, \psi_{12}, \psi_{21}$  which are functions of  $x_2$  and  $t$  only. The displacement equations Eq. (28), after omitting the terms with zero coefficients for an isotropic granular material using [6], reduces to the following,

$$\begin{aligned}
 (\hat{P} + \hat{Q}) \bar{\phi}_{1,22} - \hat{Q} \psi_{12,2} - \hat{F} \psi_{21,2} &= \rho \ddot{\bar{\phi}}_1, \\
 (\hat{T} + \hat{U}) \psi_{12,22} + (\hat{S} - \hat{U}) \psi_{21,22} + \hat{Q} \bar{\phi}_{1,2} - \hat{Q} \psi_{12} - \hat{F} \psi_{21} &= I \ddot{\psi}_{12}, \\
 (\hat{S} - \hat{U}) \psi_{12,22} + (\hat{R} + \hat{U}) \psi_{21,22} + \hat{F} \bar{\phi}_{1,2} - \hat{F} \psi_{12} - \hat{Q} \psi_{21} &= I \ddot{\psi}_{21}, \\
 \hat{V} \psi_{11,22} + \hat{S} \psi_{22,22} - \hat{W} \psi_{11} - \hat{Z} \psi_{22} &= I \ddot{\psi}_{11}, \\
 \hat{S} \psi_{11,22} + \hat{N} \psi_{22,22} - \hat{Z} \psi_{11} - \hat{W} \psi_{22} &= I \ddot{\psi}_{11},
 \end{aligned} \tag{47}$$

where we have used the symbols  $\hat{P} = C_{1212}^m, \hat{Q} = C_{1212}^m = C_{2121}^m, \hat{F} = C_{1221}^m = C_{2112}^m, \hat{W} = C_{1111}^m = C_{2222}^m, \hat{Z} = C_{1122}^m = C_{2211}^m, \hat{S} = A_{122212}^g = A_{212122}^g = A_{112222}^g = A_{222112}^g, \hat{R} = A_{212212}^g, \hat{T} = A_{122122}^g, \hat{V} = A_{112112}^g, \hat{N} = A_{222222}^g, \hat{U} = A_{122122}^u = A_{212122}^u = -A_{122212}^u = -A_{212122}^u$ , and  $I = \frac{1}{3} \rho' d^2$  for brevity.

Eq. (47) entails two uncoupled systems of equations, the first consisting of degrees of freedom  $\bar{\phi}_1, \psi_{12}, \psi_{21}$ , and the second encompassing  $\psi_{11}$  and  $\psi_{22}$ . Each system needs to be separately evaluated. Transverse displacement in macro-scale, therefore, induces only the shear terms in the micro-scale. Interestingly, and in contrast to the behavior at the macro-scale, a perturbation imposed in  $x_2$  direction on the micro-scale leads to not only a dilatational wave in  $x_2$  direction, but also a longitudinal shear wave in the  $x_2$  direction. We note, though, that the focus of the discussion hereafter will be devoted to only the first system of three coupled equations in Eq. (47).



**Fig. 5.** Phase velocities  $v_p$ , and group velocities  $v_g$ , for optical and acoustic branches, for different values of  $\gamma_A$  and  $\gamma_1$ , where solid lines and dashed lines represent optical branches and acoustic branches respectively, and lines with  $*$ ,  $\Delta$ , and  $\square$  represent  $\gamma_1 = 0.0002$ ,  $\gamma_1 = 0.3$ , and  $\gamma_1 = 0.7$ , respectively.

In this paper, we take all the coefficients in the first three equations in Eq. (47) to be positive. This is equivalent to assuming that the micro-scale stiffnesses introduced in [6] in normal direction are greater than their tangential counterparts. Relaxing such an assumption will result in three different systems of equations, each differing with the others only in the sign of the coefficients  $\hat{S}$  and  $\hat{F}$ , however the form of the results remains the same. By assuming solutions of the form

$$\bar{\phi}_1 = \bar{\phi}_1(x_2, t), \quad \psi_{12} = \psi_{12}(x_2, t), \quad \psi_{21} = \psi_{21}(x_2, t), \quad (48)$$

and specializing the solutions in Eq. (48) to plane waves, following [16], we will have

$$\bar{\phi}_1 = \text{Re} \left( \hat{A}_1 e^{i(kx_2 - \omega t)} \right), \quad \psi_{12} = \text{Re} \left( \hat{B}_{12} e^{i(kx_2 - \omega t)} \right), \quad \psi_{21} = \text{Re} \left( \hat{B}_{21} e^{i(kx_2 - \omega t)} \right), \quad (49)$$

where  $k$  is the wave number,  $\omega$  is the angular frequency, and  $\hat{A}_1$ ,  $\hat{B}_{12}$ , and  $\hat{B}_{21}$  are the amplitudes of the macro-displacement and two micro-displacement gradients, respectively. Similar to Section 3, we use the term “frequency” for  $\omega$  hereafter.



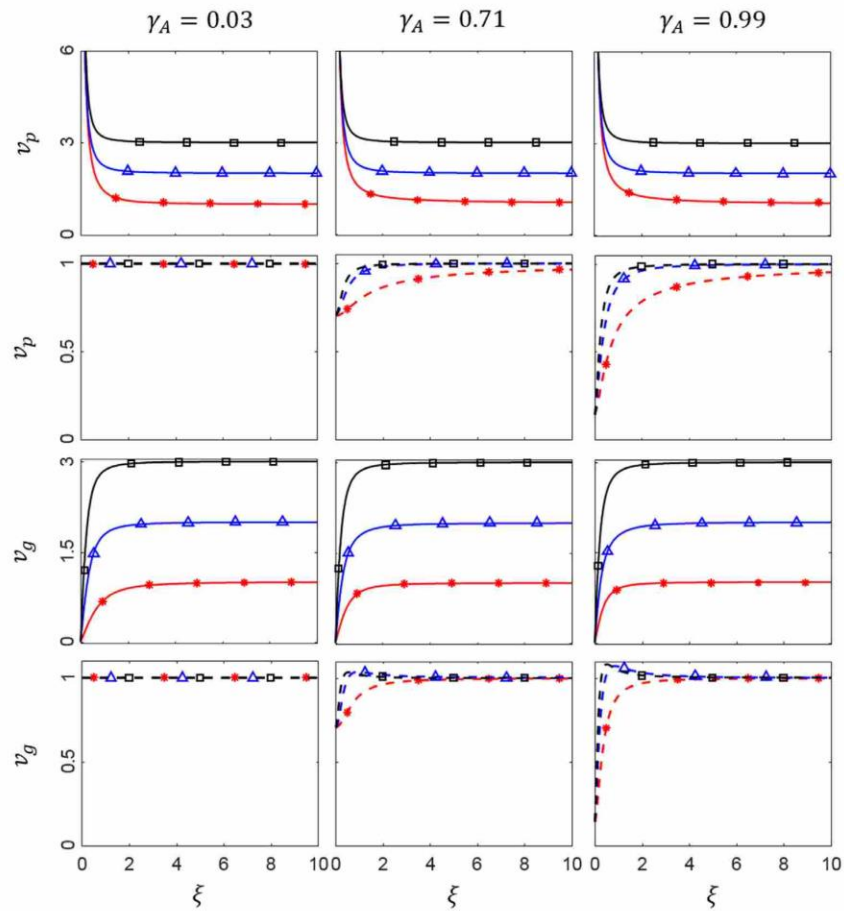


Fig. 6. Phase velocities  $v_p$ , and group velocities  $v_g$ , for optical and acoustic branches, for different values of  $\gamma_A$  and  $\gamma_1$ , where solid lines and dashed lines represent optical branches and acoustic branches respectively, and lines with  $*$ ,  $\Delta$ , and  $\square$  represent  $\gamma_1 = 1$ ,  $\gamma_1 = 2$ , and  $\gamma_1 = 3$ , respectively.

Substituting Eq. (49) in the first three equations in Eq. (47) leads to the following matrix form of the governing equations

$$\begin{bmatrix} \hat{c}_0^2 k^2 & \hat{c}_A^2 k & \hat{c}_B^2 k \\ k & \hat{p}_1^2 (\hat{c}_1^2 + \hat{c}_4^2) k^2 + 1 & \hat{p}_2^2 (\hat{c}_2^2 - \hat{c}_4^2) k^2 + 1 \\ \hat{p}_1^2 & \hat{p}_1^2 & \hat{p}_2^2 \\ k & \hat{p}_2^2 (\hat{c}_2^2 - \hat{c}_4^2) k^2 + 1 & \hat{p}_1^2 (\hat{c}_3^2 + \hat{c}_4^2) k^2 + 1 \\ \hat{p}_2^2 & \hat{p}_2^2 & \hat{p}_1^2 \end{bmatrix} \begin{bmatrix} \hat{A}_1 \\ \hat{B}_{12} \\ \hat{B}_{21} \end{bmatrix} = \omega^2 \begin{bmatrix} \hat{A}_1 \\ \hat{B}_{12} \\ \hat{B}_{21} \end{bmatrix}, \quad (50)$$

where we have defined the velocities  $\hat{c}_0$ ,  $\hat{c}_A$ , and  $\hat{c}_B$ , related to the macro- and micro-stiffnesses, velocities,  $\hat{c}_1$ ,  $\hat{c}_2$ ,  $\hat{c}_3$ , and  $\hat{c}_4$ , related to the second gradient stiffnesses, and characteristic times  $\hat{p}_1$  and  $\hat{p}_2$  as

$$\hat{c}_0^2 = \frac{\hat{P} + \hat{Q}}{\rho}, \quad \hat{c}_A^2 = \frac{\hat{Q}}{\rho}, \quad \hat{c}_B^2 = \frac{\hat{F}}{\rho}, \quad (51)$$

$$\hat{c}_1^2 = \frac{\hat{T}}{I}, \quad \hat{c}_2^2 = \frac{\hat{S}}{I}, \quad \hat{c}_3^2 = \frac{\hat{R}}{I}, \quad \hat{c}_4^2 = \frac{\hat{U}}{I}, \quad (52)$$

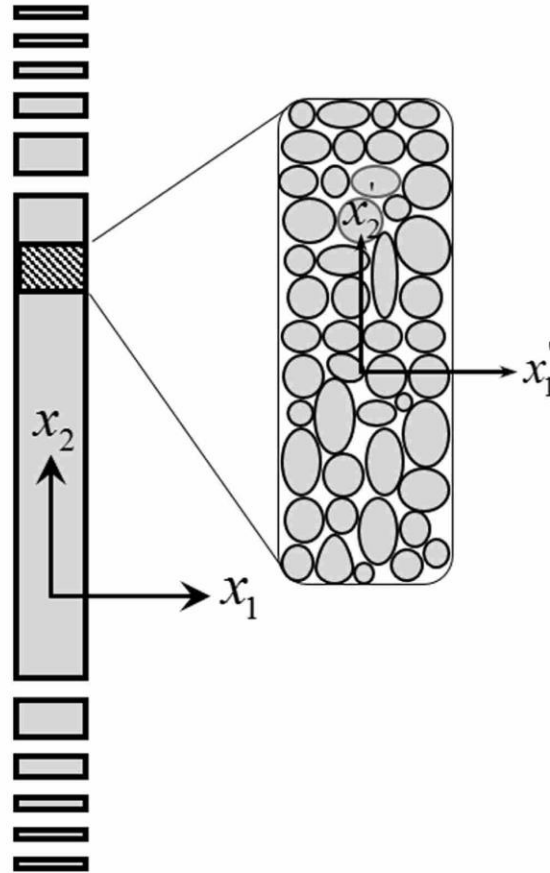


**Fig. 7.** Schematic of a 1D continuum in  $x_2$  direction with granular micro-structure in both  $x_1'$  and  $x_2'$  directions. A material point in the macro-scale coordinate system is itself a collection of grains that can differ in micro-density, micro-morphology and micro-mechanical properties.

$$\hat{p}_1^2 = \frac{I}{\hat{Q}}, \quad \hat{p}_2^2 = \frac{I}{\hat{F}}. \quad (53)$$

Eq. (50) is an eigenvalue problem with the eigenvalue  $\omega^2$  and the eigenvector comprising the amplitudes of the propagating macro-displacement waves and two micro displacement gradient waves as its entries, respectively. It is beneficial to introduce the dimensionless parameter

$$\chi^2 = \frac{\hat{c}_B^2}{\hat{c}_A^2} = \frac{\hat{p}_1^2}{\hat{p}_2^2} = \frac{\hat{F}}{\hat{Q}}, \quad (54)$$

which is the ratio of the material parameters  $\hat{F}$  and  $\hat{Q}$ . In order to have an at least semi positive definite energy expression, we must have  $\chi \leq 1$ .

We also introduce the dimensionless velocities as follows

$$\hat{\gamma}_A^2 = \frac{\hat{c}_A^2}{\hat{c}_0^2}, \quad \hat{\gamma}_1^2 = \frac{\hat{c}_1^2}{\hat{c}_0^2}, \quad \hat{\gamma}_2^2 = \frac{\hat{c}_2^2}{\hat{c}_0^2}, \quad \hat{\gamma}_3^2 = \frac{\hat{c}_3^2}{\hat{c}_0^2}, \quad \hat{\gamma}_4^2 = \frac{\hat{c}_4^2}{\hat{c}_0^2}. \quad (55)$$

Using Eqs. (54), (55), and dimensionless wavenumber and frequency

$$\hat{\xi} = \hat{p}_2 \hat{c}_0 k, \quad \hat{\eta} = \hat{p}_2 \omega, \quad (56)$$

we can write the characteristic equation of Eq. (50) as follows

$$\begin{aligned} \hat{\eta}^2 &= \hat{\xi}^2 \left( 1 - \hat{\gamma}_A^2 \left( 1 - \chi^4 \left( 1 + 2\hat{\xi}^2 (\hat{\gamma}_2^2 - \hat{\gamma}_4^2) \right) \right) \right) \\ &- \chi^4 \left( \hat{\eta}^2 - \hat{\xi}^2 \right) \left( \hat{\eta}^2 - (\hat{\gamma}_1^2 + \hat{\gamma}_4^2) \hat{\xi}^2 \right) \left( \hat{\eta}^2 - (\hat{\gamma}_3^2 + \hat{\gamma}_4^2) \hat{\xi}^2 \right) \\ &+ \chi^2 \left( \hat{\eta}^2 - \hat{\xi}^2 \right) \left( \hat{\eta}^2 - (\hat{\gamma}_3^2 + \hat{\gamma}_4^2) \hat{\xi}^2 \right) + \chi^2 \left( \hat{\eta}^2 - \hat{\xi}^2 \right) \left( \hat{\eta}^2 - (\hat{\gamma}_1^2 + \hat{\gamma}_4^2) \hat{\xi}^2 \right) \\ &+ \chi^4 \left( \hat{\eta}^2 - \hat{\xi}^2 \right) \left( (\hat{\gamma}_2^2 - \hat{\gamma}_4^2) \hat{\xi}^2 + 1 \right)^2 + \chi^6 \hat{\gamma}_A^2 \hat{\xi}^2 \left( \hat{\eta}^2 - (\hat{\gamma}_1^2 + \hat{\gamma}_4^2) \hat{\xi}^2 \right) \\ &+ \chi^2 \hat{\gamma}_A^2 \hat{\xi}^2 \left( \hat{\eta}^2 - (\hat{\gamma}_3^2 + \hat{\gamma}_4^2) \hat{\xi}^2 \right). \end{aligned} \quad (57)$$

Eq. (57) is the general dispersion relation for the considered problem. Concurrent or hierarchical micro-structures result in rather similar dispersion relations and have been studied in [3]. Although the form of the dispersion relation has similarities in terms of the order of the equation, the physics here addresses shear wave in a 1D granular medium with a 2D micro-structure. We note that for the case of  $\psi_{21} = 0$ , the matrix in Eq. (50) reduces to a two by two matrix and leads to the physics of the transverse wave propagation in a one dimensional continuum with one dimensional micro-structure, which is similar in form to the previous problem of longitudinal wave propagation in a one dimensional continuum.

It is useful to include the relation between the parameters  $\hat{T}$ ,  $\hat{S}$ , and  $\hat{R}$ , since all three, for an isotropic granular material, are linear functions of  $K_n^g$  and  $K_w^g$ , according to [6]. Solving for  $\hat{R}$ , and using Eqs. (52) and (55) yields:

$$\hat{\gamma}_3^2 = \frac{1}{3} \hat{\gamma}_1^2 + \frac{2}{3} \hat{\gamma}_2^2. \quad (58)$$

Similar to the approach taken in Section 3, we introduce the parameters

$$\hat{B}'_{12} = \hat{p}_2 \hat{c}_0 \hat{B}_{12}, \quad \hat{B}'_{21} = \hat{p}_2 \hat{c}_0 \hat{B}_{21}, \quad (59)$$

and the dimensionless parameters

$$\hat{\beta}_{12} = \frac{\hat{B}'_{12}}{\hat{A}_1}, \quad \hat{\beta}_{21} = \frac{\hat{B}'_{21}}{\hat{A}_1}. \quad (60)$$

Then, using rows 1 and 2 of the matrix in Eqs. (50), (59), and (60), we can write

$$\begin{aligned} \hat{\beta}_{12} &= \frac{\left( \hat{\xi}^2 (\hat{\gamma}_2^2 - \hat{\gamma}_4^2) + 1 \right) \left( \hat{\eta}^2 - \hat{\xi}^2 \right) + \hat{\xi}^2 \hat{\gamma}_A^2}{\chi^2 \hat{\gamma}_A^2 \hat{\xi} \hat{\eta}^2 + \hat{\gamma}_A^2 \hat{\xi}^3 (\hat{\gamma}_2^2 - \hat{\gamma}_4^2 - \chi^2 (\hat{\gamma}_1^2 + \hat{\gamma}_4^2))}, \\ \hat{\beta}_{21} &= \frac{\left( \chi^2 \hat{\eta}^2 - \chi^2 \hat{\xi}^2 (\hat{\gamma}_1^2 + \hat{\gamma}_4^2) - 1 \right) \left( \hat{\eta}^2 - \hat{\xi}^2 \right) - \hat{\gamma}_A^2 \hat{\xi}^2}{\chi^4 \hat{\gamma}_A^2 \hat{\xi} \hat{\eta}^2 + \chi^2 \hat{\gamma}_A^2 \hat{\xi}^3 (\hat{\gamma}_2^2 - \hat{\gamma}_4^2 - \chi^2 (\hat{\gamma}_1^2 + \hat{\gamma}_4^2))}. \end{aligned} \quad (61)$$

The energy transfer ratio due to the micro- and macro-scale degrees-of-freedom,  $\psi_{12}$ ,  $\psi_{21}$ , and  $\phi_1$ , to the total energy, similar to the approach taken in Section 3, can be found, respectively, as

$$\begin{aligned} \frac{E_{\psi_{12}}}{E_{total}} &= \frac{\chi^2 \hat{\gamma}_A^2 \hat{\eta}^2 \hat{\beta}_{12}^2 + \hat{\gamma}_A^2 (1 + \chi^2) \hat{\beta}_{12}^2 + \chi^2 \hat{\gamma}_A^2 (\hat{\gamma}_1^2 + \hat{\gamma}_2^2 + 2\hat{\gamma}_4^2) \hat{\xi}^2 \hat{\beta}_{12}^2}{\hat{\gamma}_A^2 (\chi^2 \hat{\eta}^2 + 1 + \chi^2) (\hat{\beta}_{12}^2 + \hat{\beta}_{21}^2) + \chi^2 \hat{\gamma}_A^2 (\hat{\gamma}_1^2 + \hat{\gamma}_2^2 + 2\hat{\gamma}_4^2) \hat{\xi}^2 \hat{\beta}_{12}^2 + \chi^2 \hat{\gamma}_A^2 (\frac{1}{3} \hat{\gamma}_1^2 + \frac{5}{3} \hat{\gamma}_2^2 + 2\hat{\gamma}_4^2) \hat{\xi}^2 \hat{\beta}_{21}^2 + \hat{\eta}^2 + \hat{\xi}^2 (1 - \hat{\gamma}_A^2)}, \\ \frac{E_{\psi_{21}}}{E_{total}} &= \frac{\chi^2 \hat{\gamma}_A^2 \hat{\eta}^2 \hat{\beta}_{21}^2 + \hat{\gamma}_A^2 (1 + \chi^2) \hat{\beta}_{21}^2 + \chi^2 \hat{\gamma}_A^2 (\frac{1}{3} \hat{\gamma}_1^2 + \frac{5}{3} \hat{\gamma}_2^2 + 2\hat{\gamma}_4^2) \hat{\xi}^2 \hat{\beta}_{21}^2}{\hat{\gamma}_A^2 (\chi^2 \hat{\eta}^2 + 1 + \chi^2) (\hat{\beta}_{12}^2 + \hat{\beta}_{21}^2) + \chi^2 \hat{\gamma}_A^2 (\hat{\gamma}_1^2 + \hat{\gamma}_2^2 + 2\hat{\gamma}_4^2) \hat{\xi}^2 \hat{\beta}_{12}^2 + \chi^2 \hat{\gamma}_A^2 (\frac{1}{3} \hat{\gamma}_1^2 + \frac{5}{3} \hat{\gamma}_2^2 + 2\hat{\gamma}_4^2) \hat{\xi}^2 \hat{\beta}_{21}^2 + \hat{\eta}^2 + \hat{\xi}^2 (1 - \hat{\gamma}_A^2)}, \\ \frac{E_{macro}}{E_{total}} &= \frac{\hat{\eta}^2 + \hat{\xi}^2 (1 - \hat{\gamma}_A^2)}{\hat{\gamma}_A^2 (\chi^2 \hat{\eta}^2 + 1 + \chi^2) (\hat{\beta}_{12}^2 + \hat{\beta}_{21}^2) + \chi^2 \hat{\gamma}_A^2 (\hat{\gamma}_1^2 + \hat{\gamma}_2^2 + 2\hat{\gamma}_4^2) \hat{\xi}^2 \hat{\beta}_{12}^2 + \chi^2 \hat{\gamma}_A^2 (\frac{1}{3} \hat{\gamma}_1^2 + \frac{5}{3} \hat{\gamma}_2^2 + 2\hat{\gamma}_4^2) \hat{\xi}^2 \hat{\beta}_{21}^2 + \hat{\eta}^2 + \hat{\xi}^2 (1 - \hat{\gamma}_A^2)}. \end{aligned} \quad (62)$$

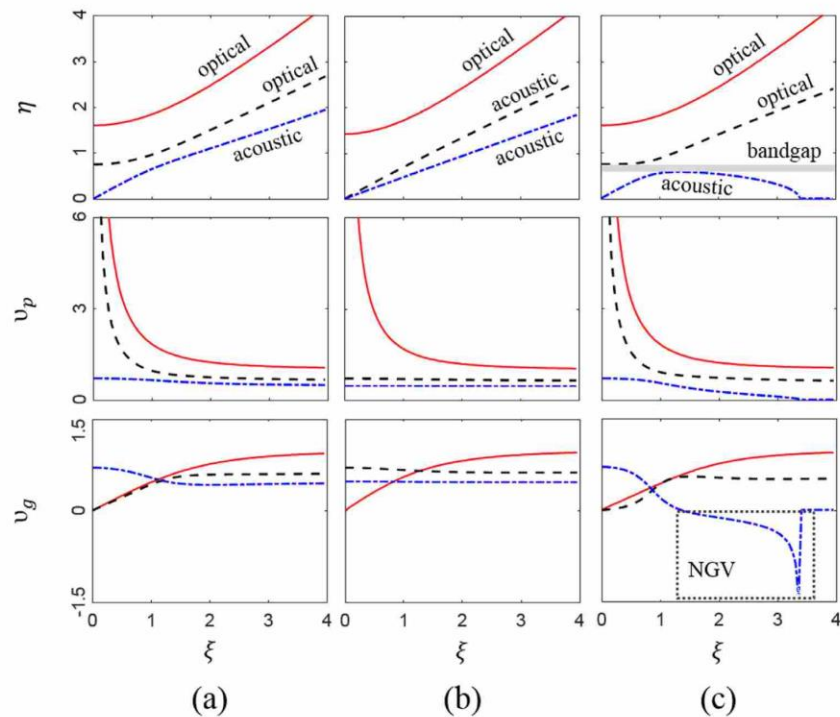


**Fig. 8.** Dispersion curves, phase velocities  $v_p$ , and group velocities  $v_g$  for the optical branch, the third branch, and the acoustic branch, respectively, where solid line represents an optical branch, dash-dotted line represents an acoustic branch, and dashed line is either acoustic or optical (third branch). (a) A material with properties of  $\hat{\gamma}_A = 0.71$ ,  $\hat{\gamma}_1 = 0.5$ ,  $\hat{\gamma}_2 = 0.3$ ,  $\hat{\gamma}_4 = 0.1$ , and  $\chi = 0.8$ ; (b) A material with properties of  $\hat{\gamma}_A = 0.71$ ,  $\hat{\gamma}_1 = 0.5$ ,  $\hat{\gamma}_2 = 0.3$ ,  $\hat{\gamma}_4 = 0.1$ , and  $\chi = 1$ ; (c) A material with properties of  $\hat{\gamma}_A = 0.71$ ,  $\hat{\gamma}_1 = 0.2$ ,  $\hat{\gamma}_2 = 0.4$ ,  $\hat{\gamma}_4 = 0.1$ , and  $\chi = 0.8$ .

#### 4.2. Results

Similar to Section 3, it is easy to verify that  $\hat{\gamma}_A$  has lower bound limit of 0 and upper bound limit of 1. Very small values of  $\hat{\gamma}_A$  represent materials in which the micro-stiffness in the corresponding direction is negligible compared to their macro-stiffness, and values close to the upper bound level have large micro-stiffness compared to their macro-stiffness. A value of  $\hat{\gamma}_A = 0.71$  corresponds to approximately equal macro- and micro-stiffness of the material.  $\chi$  represents the ratio of the micro-scale stiffness in the two directions considered here, and takes values zero to one. On the other hand,  $\hat{\gamma}_1$ ,  $\hat{\gamma}_2$ ,  $\hat{\gamma}_3$ , and  $\hat{\gamma}_4$  have lower bound of 0, with an upper bound that theoretically can tend to infinity. For a particular ratio of macro-density to micro-inertia, larger  $\hat{\gamma}_i$ ,  $i = 1, 2, 3, 4$  implies a growing dominance of second gradient behavior. Fig. 8 illustrates the dispersion curves, phase, and group velocities for different values of  $\gamma_A$ ,  $\gamma_1$ ,  $\gamma_2$ ,  $\gamma_4$ , and  $\chi$ , and Fig. 9 shows the energy transfer ratio for the active degrees of freedom here to the total energy transferred by the particular branch under study for the same parameters used in Fig. 8.

Solving the dispersion relation Eq. (57) for the dimensionless frequency,  $\hat{\eta}$ , generally results in three wave branches in the dispersion curve, one acoustic branch, one optical branch, and a third branch. The third branch is an optical branch when  $\chi < 1$  (Fig. 8(a) and (c)) and becomes an acoustic wave when  $\chi = 1$  (Fig. 8(b)). The dimensionless frequencies at which the wave branches start, for the acoustic, optical, and the third branch are  $\hat{\eta} = 0$ ,  $\hat{\eta} = \frac{\sqrt{1+\chi^2}}{\chi}$ , and  $\hat{\eta} = \frac{\sqrt{1-\chi^2}}{\chi}$ , respectively.

At small wavenumbers, the acoustic wave has dimensionless group velocity of  $\sqrt{1 - \hat{\gamma}_A^2}$  (corresponding to the group velocity of  $\sqrt{\hat{c}_0^2 - \hat{c}_A^2}$ ), while the optical wave has dimensionless group velocity of 0. The third branch has 0 and a value of  $\frac{\sqrt{2\hat{\gamma}_1^2 - 4\hat{\gamma}_2^2 + 2\hat{\gamma}_3^2 + 4\hat{\gamma}_4^2}}{2}$  as its dimensionless group velocity at the small wavenumbers when  $\chi < 1$  and  $\chi = 1$ , respectively. Moreover, the asymptotes of the dispersion curves for the acoustic wave, optical wave, and the third wave at large



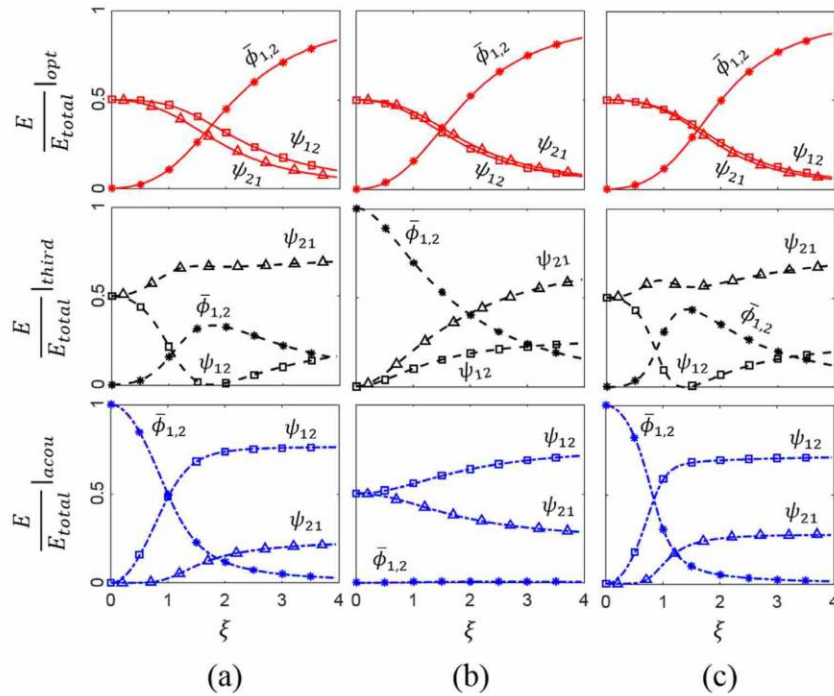


**Fig. 9.** Ratio of energy transferred by macro- and micro-scale degrees of freedom to the total energy for the optical branch, the third branch, and the acoustic branch, respectively, where solid line represents an optical branch, dash-dotted line represents an acoustic branch, and dashed line is either acoustic or optical (third branch). Lines with  $*$ ,  $\wedge$ , and  $\square$  represent energy transferred by macro-scale degree of freedom  $\bar{\phi}_{1,2}$ , and micro-scale degrees of freedom  $\psi_{21}$  and  $\psi_{12}$ , respectively. (a) A material with properties of  $\hat{\gamma}_\lambda = 0.71$ ,  $\hat{\gamma}_1 = 0.5$ ,  $\hat{\gamma}_2 = 0.3$ ,  $\hat{\gamma}_4 = 0.1$ , and  $\chi = 0.8$ ; (b) A material with properties of  $\hat{\gamma}_\lambda = 0.71$ ,  $\hat{\gamma}_1 = 0.5$ ,  $\hat{\gamma}_2 = 0.3$ ,  $\hat{\gamma}_4 = 0.1$ , and  $\chi = 1$ ; (c) A material with properties of  $\hat{\gamma}_\lambda = 0.71$ ,  $\hat{\gamma}_1 = 0.2$ ,  $\hat{\gamma}_2 = 0.4$ ,  $\hat{\gamma}_4 = 0.1$ , and  $\chi = 0.8$ .

wavenumbers are

$$\begin{aligned} \hat{\eta} &= \frac{1}{2} \sqrt{2(\hat{\gamma}_1^2 + \hat{\gamma}_3^2 + 2\hat{\gamma}_4^2) - 2\sqrt{(\hat{\gamma}_1^2 - \hat{\gamma}_3^2)^2 + 4(\hat{\gamma}_2^2 - \hat{\gamma}_4^2)^2} \xi}; \\ \hat{\eta} &= \hat{\xi}; \\ \hat{\eta} &= \frac{1}{2} \sqrt{2(\hat{\gamma}_1^2 + \hat{\gamma}_3^2 + 2\hat{\gamma}_4^2) + 2\sqrt{(\hat{\gamma}_1^2 - \hat{\gamma}_3^2)^2 + 4(\hat{\gamma}_2^2 - \hat{\gamma}_4^2)^2} \xi}. \end{aligned} \quad (63)$$

Frequency band gaps may appear when the starting point of the optical branches are large dimensionless frequencies, and when group velocities of the acoustic branches at small and large wavenumbers are of small values. There also cases (e.g. Fig. 8(c)) that the real part of the frequency solution of the acoustic branch reduces to zero after a certain wavenumber for a special combination of the material parameters. In this case, there is a region for which the sign of the group velocity for the acoustic branch becomes negative and the peak of the pulse propagates backwards, but the energy flow is always forward [31]. Interestingly, negative group velocity (NGV) occurs for those cases in which the asymptotic dimensionless frequency solution for the acoustic branch given in Eq. (63) takes imaginary values or

$$\hat{\gamma}_1^4 + 2\hat{\gamma}_1^2\hat{\gamma}_2^2 + 4\hat{\gamma}_1^2\hat{\gamma}_4^2 - 3\hat{\gamma}_2^4 + 8\hat{\gamma}_2^2\hat{\gamma}_4^2 < 0, \quad (64)$$

which for the solutions shown in Fig. 8(c) for the noted material parameters corresponds to dimensionless wavenumber  $\sim 1.5$ . Inequality in Eq. (64), can be further expressed in terms of grain-pair second gradient stiffnesses introduced in [6] as follows

$$4(3K_n^g + 4K_w^g)(C_n^u + 4C_w^u) + 3K_w^g(4K_n^g + 3K_w^g) < 0. \quad (65)$$

which indicates that the condition for NGV occurrence coincides with the requirement for some negative grain-pair second gradient stiffnesses. Grain-pair mechanism which would lead to such conditions are conceivable for granular systems in

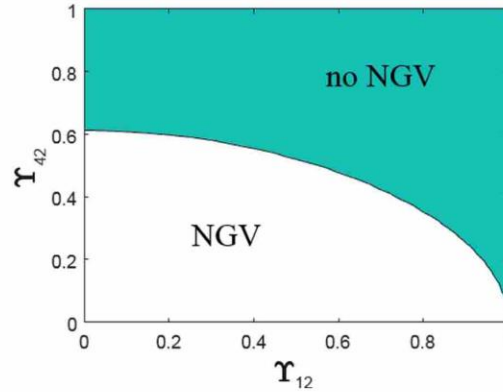


**Fig. 10.** White indicates the sets of parameters for which negative group velocity (NGV) occurs in the acoustic branch, while green color indicates the sets of parameters for which there is no NGV.

which the first gradient approximation overestimates the grain-pair deformation energy, such as those in which grain-pair can have large relative shear displacement with low deformation energy caused by small resistance to relative rotations. In addition, it is noteworthy that the overall positive definiteness of energy for the RVE admits the possibility of negative grain-pair second gradient stiffnesses. Such a possibility is surely tantalizing and needs to be further explored with the viewpoint of realizing such granular systems. Further, the inequality in Eq. (64) can be recast, by assuming  $\hat{\gamma}_2 \neq 0$  and introducing the ratios  $\Upsilon_{12} = \frac{\hat{\gamma}_1}{\hat{\gamma}_2}$ , and  $\Upsilon_{42} = \frac{\hat{\gamma}_4}{\hat{\gamma}_2}$ , in the form

$$(\Upsilon_{12}^2 + 4\Upsilon_{42}^2)(\Upsilon_{12}^2 + 2) - 3 < 0, \quad (66)$$

such that, NGV occurs when Eq. (66) is satisfied. Fig. 10 shows the set of parameters  $\Upsilon_{12}$  and  $\Upsilon_{42}$ , for which the NGV arises. In this figure, white region indicates the sets of parameters for which NGV occurs, and the green color indicates the sets of parameters for which there is no NGV in the acoustic branch. It is noteworthy that NGVs for deformation waves in solids have also been predicted for longitudinal waves in materials with multi-scale micro-structures whose material properties satisfy certain conditions [32]. Finally, we remark that at higher wavenumbers (beyond dimensionless wavenumber  $\sim 3.4$  in Fig. 8(c)), the frequency solution for the acoustic branch becomes purely imaginary and positive indicating instability.

According to Fig. 9, the energy transferred by the optical wave branch (solid line) is mainly due to micro-scale degrees of freedom at small wavenumbers, and as the wavenumber increases the role of the macro-scale degree of freedom becomes apparent. In the cases where there is only one acoustic branch, the acoustic branch (dashed line) transfers energy by a mechanism largely due to the macro-scale degree of freedom for small wavenumbers, and as the wavenumber increases, the role that the micro-scale degrees of freedom play becomes dominant. A difference between the proportions of energy each microstructural degree of freedom transfers pertains to the value of the parameter  $\chi$  as it plays the role of a weighting factor for the terms involved in Eq. (54). In the case when  $\chi = 1$  in Fig. 9(b), the acoustic branch reveals a different behavior. In this case, energy is transferred completely by the micro-scale degrees of freedom and the macro-scale degree of freedom plays no role. When  $\chi < 1$  (Fig. 9(a) and (c)), the third branch transfers energy mostly due to the micro-scale degrees of freedom in the ranges where wavenumber is small. This follows by an increase in macro-scale degree of freedom share of energy transfer, and eventually at large wavenumbers, the micro-scale degrees of freedom take over as the degree of freedom  $\psi_{21}$  becomes dominant. In the case of  $\chi = 1$ , the third branch acts as an acoustic branch and the energy transfer mechanism for such branch follows the behavior of acoustic branch in the case of  $\chi < 1$ , except for the large wavenumber behavior in which the degree of freedom  $\psi_{21}$  plays the dominant part.

#### 4.3. Special cases

To model a material with negligible second gradient terms, Eq. (57) reduces to

$$\hat{\eta}^2 = \hat{\xi}^2 (1 - \hat{\gamma}_A^2 (1 - \chi^4)) + \chi^2 (\hat{\eta}^2 - \hat{\xi}^2) (\chi^2 - \chi^2 \hat{\eta}^4 + 2\hat{\eta}^2) + \hat{\gamma}_A^2 \hat{\xi}^2 \hat{\eta}^2 \chi^2 (1 + \chi^4). \quad (67)$$

The parameter  $\chi$  defined in Eq. (54) relates the two material constants  $\hat{F}$  and  $\hat{Q}$  which themselves are functions of  $K_n^m$  and  $K_w^m$  using [6]. Therefore,  $\chi$  can be rewritten as

$$\chi = 1 - \frac{5K_w^m}{K_n^m + 4K_w^m}. \quad (68)$$

Taking into consideration the assumption made earlier in this section,  $K_n^m \geq K_w^m$ , it is seen that  $\chi$  reaches the value 0 when  $K_w^m = K_n^m$  and takes the value 1 only when  $K_w^m = 0$ . In the case of  $K_w^m \neq 0$ , Eq. (67) can be further simplified, by assuming that  $\chi^4$  is negligible, to give

$$\hat{\eta}^2 = \hat{\xi}^2 (1 - \hat{\gamma}_A^2) + 2\hat{\eta}^2 \chi^2 (\hat{\eta}^2 - \hat{\xi}^2) + \hat{\gamma}_A^2 \hat{\xi}^2 \hat{\eta}^2 \chi^2. \quad (69)$$

Eq. (69) has two solutions where one of the solutions is a wave propagating with negligible value for its dimensionless group velocity. Therefore, neglecting the mentioned solution, we can reduce the dispersion relation Eq. (69) to

$$\hat{\eta}^2 = \hat{\xi}^2 (1 - \hat{\gamma}_A^2), \quad (70)$$

which is a non-dispersive acoustic wave with constant phase and group velocity of  $\sqrt{\hat{c}_0^2 - \hat{c}_A^2}$ .

In the case where  $K_w^m = 0$ , Eq. (67) reduces to

$$\hat{\eta}^2 = \hat{\xi}^2 + (\hat{\eta}^2 - \hat{\xi}^2) (1 - \hat{\eta}^4 + 2\hat{\eta}^2) + 2\hat{\gamma}_A^2 \hat{\xi}^2 \hat{\eta}^2, \quad (71)$$

which gives rise to one standing (evanescent) wave, one acoustic wave that reaches zero group velocity as wavenumber increases, and one optical wave with an asymptote of  $\hat{\eta} = \hat{\xi}$ .

For the case in which the second gradient terms are large,  $\hat{\gamma}_A$  is negligible, and  $\chi = 1$ , one must start from Eq. (47) and let  $\hat{Q} = \hat{F} = 0$ . Solution includes three wave branches of

$$\begin{aligned} \omega &= \hat{c}_0 k, \\ \omega &= \frac{1}{2} \sqrt{2(\hat{c}_1^2 + \hat{c}_3^2 + 2\hat{c}_4^2) + 2\sqrt{((\hat{c}_1^2 - \hat{c}_3^2)^2 + 4(\hat{c}_2^2 - \hat{c}_4^2)^2)}} k, \\ \omega &= \frac{1}{2} \sqrt{2(\hat{c}_1^2 + \hat{c}_3^2 + 2\hat{c}_4^2) - 2\sqrt{((\hat{c}_1^2 - \hat{c}_3^2)^2 + 4(\hat{c}_2^2 - \hat{c}_4^2)^2)}} k. \end{aligned} \quad (72)$$

According to Eq. (72), the first solution is a classical wave with the constant velocity  $\hat{c}_0$  depending on the macro-scale properties which propagates as an acoustic wave. Second and third solutions are also acoustic waves having constant velocities with the third branch only existing when the expression under the square root is positive, which is simplified to

$$\hat{c}_4^4 + 2\hat{c}_1^2 \hat{c}_2^2 + 4\hat{c}_1^2 \hat{c}_4^2 - 3\hat{c}_2^4 + 8\hat{c}_2^2 \hat{c}_4^2 > 0. \quad (73)$$

Due to its physical nature,  $\hat{c}_4$  is usually negligible compared to the other two parameters involved. Therefore, Eq. (73) reduces to  $\hat{c}_1 > \hat{c}_2$ . As a result, for the cases where  $\hat{c}_2$  is comparatively higher than  $\hat{c}_1$ , an evanescent wave is expected as the third solution of the dispersion equation. Starting from Eq. (57) to obtain the solutions for the dispersive behavior, however, leads to a set of three solutions for which one of the solutions is an optical wave.

For a purely second gradient material, as discussed in Section 3, the form of deformation energy must be appropriately specified and the governing equation must be derived applying the variational approach. In this case, only one acoustic wave will exist for the considered problem, whose dispersion relation will be similar to that given in [30].

Finally, assuming that  $\hat{\gamma}_i$ ,  $i = A, 1, 2, 3, 4$  are negligible and  $\chi = 1$ , Eq. (57) reduces to the dispersion relation for the classical wave equation which has a non-dispersive solution similar to Eq. (46).

## 5. Micromechanical implications to metamaterial design

To illustrate the effects of the inter-granular stiffness coefficients on the behavior of the systems studied, we proceed as follows. We assume, as in Sections 3 and 4, that the normal components of the inter-granular stiffness are larger than their corresponding tangential values and they are both nonnegative.

In Section 3 of this paper, we discussed the different behavior the system might exhibit based on the values the dimensionless velocities  $\gamma_A$  and  $\gamma_1$  take. We have shown that  $\gamma_A$  is bounded between zero and one, whilst  $\gamma_1$  can take any nonnegative value. Using Eq. (37), and substituting for the material parameters computed in [6] we can write

$$\gamma_A = \sqrt{\frac{K_n^m (3 + 2\Omega^m)}{K_n^m (3 + 2\Omega^m) + K_n^M (3 + 2\Omega^M)}}, \quad \gamma_1 = \sqrt{\frac{3\rho l^2}{7I}} \sqrt{\frac{K_n^g (5 + 2\Omega^g)}{K_n^m (3 + 2\Omega^m) + K_n^M (3 + 2\Omega^M)}}, \quad (74)$$

where we have introduced ratios of tangential to normal stiffness coefficients as

$$\Omega^M = \frac{K_w^M}{K_n^M}, \quad \Omega^m = \frac{K_w^m}{K_n^m}, \quad \Omega^g = \frac{K_w^g}{K_n^g}. \quad (75)$$

The same approach can also be taken for the dimensionless velocities in Section 4. It is straightforward to see that a specific value of  $\gamma_A$  can be retained if the ratio  $\frac{K_n^M (3 + 2\Omega^M)}{K_n^m (3 + 2\Omega^m)}$  remains constant. For instance, taking the values of  $\Omega^M$  and  $\Omega^m$



to remain constant,  $\gamma_A$  retains its value provided the ratio  $K_n^M/K_n^m$  is constant (such as for the two sets of  $K_n^M = 2, K_n^m = 1$ , and  $K_n^M = 4, K_n^m = 2$ ). The implication is that by changing the micro-stiffness coefficients in certain predefined manner, similar macro-scale phenomena may be achieved. However, these two sets will generate two different values for  $\gamma_1$ , which means that while one part of the phenomena can be preserved, another associated may not.

Furthermore, Eq. (74) proposes that for a given ratio of macro- and micro-inertia, the parameters

$$\gamma_A = \gamma_A(K_n^m, K_n^M, \Omega^m, \Omega^M), \quad \gamma_1 = \gamma_1(K_n^g, K_n^m, K_n^M, \Omega^g, \Omega^m, \Omega^M), \quad (76)$$

are purely functions of stiffnesses associated to the introduced kinematic quantities. It is worthwhile to consider effects arise mainly from elasticity rather than inertia considering that the grain-pair interactions can vary strongly while the grain density, granular structure and RVE size remain virtually similar. Now, according to what has been discussed in Section 3, emergence of bandgaps with a certain location and width is dependent on a certain combinations of the parameters  $\gamma_1$  and  $\gamma_A$ . Therefore, to design a structure with a desired bandgap location and width, a multi-objective optimization problem must be posed. The problem becomes more intricate as we increase the dimension of the physics involved and add to the desired properties for the design.

An advantage of the proposed continuum model is the availability of the explicit form of the functions, thereby promising a complete domain to search for possible solutions (see similar approach exemplified for pantographic material systems in [33]). Such theory based approaches are in contrast to certain efforts that proceed by postulating *a priori* certain predetermined sets of micro-structures [8,10] or propose to combine micro-elements [34,35] to achieve an objective that is circumscribed within a known domain of behaviors without the aid of theories that can predict possibilities beyond those that are already known. The optimization problem may be solved using metaheuristic algorithms, such as Genetic Algorithm. There is always possible to have many different combinations of grain-pair stiffnesses yielding the same result, since the expressions for the dimensionless velocities are not one-to-one functions. This means that there is more than one solution to the problem being solved. This is equivalent to stating that many physically different structures can demonstrate similar behavior when excited, and hence, be typified in the same category, and be manufactured based on the existing manufacturing processes and resources. The knowledge obtained from such analyses is particularly useful in the design and fabrication of metamaterials with specific material properties for particular purposes, e.g. to be used as wave attenuators or nanoscale energy harvesting devices, as recent studies on granular crystals have shown [33,36–39]. The granular micromechanics based continuum model, therefore, suggests, and predicts, that controlling or varying the inter-granular stiffness coefficients and micro-structure results in a material for which the behavior it manifests when undergoing different loading conditions can be tuned, thus providing us with a practical mechanism to make materials with unusual desired behavior. Linking microstructural properties of the material to its macroscopic behavior promises optimizing large scale structures in terms of their stiffness to weight ratios and desired directional properties, which seems infeasible using current approaches such as discrete element methods, namely due to their substantial computational cost. Since the dimensionless speeds are responsible for the way the material behaves when subjected to external actions, and since intergranular stiffness coefficients are the building elements that the dimensionless speeds are functions of, starting from the micro-scale and proceed with a tailored micro-structure with desired stiffness coefficients using novel technological advancements will lead to a material whose behavior is predicted, yet complex and unprecedented, as for instance the predicted granular materials displaying negative group velocities or frequency band gaps.

## 6. Summary and conclusions

In the present paper, two cases of wave propagation in linear elastic granular continua were studied. Case 1 investigated a longitudinal wave propagating in a one dimensional infinite continuum, while case 2 studied a transverse wave propagating in a one dimensional continuum that has a two dimensional micro-structure. The results obtained are expected to provide a baseline and point of departure for more complex problems that could involve nonlinearities and dissipation. For each case, the effect of parameters involved in the dispersion equations was investigated. For case 1, there are two waves emerging in the dispersion curve, optical and acoustic branches. Results show that the wave speed for both the branches is dictated by the macro- and micro-scale properties for the small and large wavenumbers, respectively. The study on energy transfer mechanism reveals a shift between macro- and micro-scale degrees of freedom for the two branches as the wavenumber increases. Large values of second gradient terms prevent this shift, and therefore, lead to the case where the energy in optical wave is mainly transferred by the micro-scale degree of freedom, and macro-scale degree of freedom leads the energy transfer in the acoustic wave. For case 2, dispersive behavior of the material gives rise to three wave branches, one acoustic, one optical, and the third branch being acoustic or optical depending on the value of the parameter  $\chi$ . As discussed in the paper, the model proposed in [6] reflects, in a sufficient way, the effect of micro-measures (such as micro-stiffnesses, grain sizes and granular structure) on the macro-scale motion, accounting for frequency band gaps and negative group velocities. The results discussed in this paper show that the connection between the micro-measures and the continuum model can pave a way for exploring the micro-mechanical antecedents of phenomena observed at macro-scales. The granular micromechanics can thus provide the theoretical underpinning and an efficient paradigm for designing granular metamaterials with desired dispersive behavior that may be needed for particular applications. In absence of such a theory, the possibilities of many predicted behavior would remain concealed and undiscovered. Clearly, a more expansive model accounting for the electro-magneto-elasticity of the



granular materials [5,40,41], or dissipation and damage mechanisms [42,43] that also takes rotation (spin) of the grains as extra degrees of freedom will reveal more complex features of the granular materials, and hence, will be pursued in following research. Given that experimental procedures for wave propagation in complex granular materials are not easily devised, numerical simulations with discrete models could be potentially utilized to verify the results presented here. The future work will also consider such discrete models with full dynamic identification procedure between the discrete and continuum models.

### Acknowledgment

This research is supported in part by the United States National Science Foundation grant CMMI -1727433.

### References

- [1] M. Bazzaz, M.K. Darabi, D.N. Little, N. Garg, A straightforward procedure to characterize nonlinear viscoelastic response of asphalt concrete at high temperatures, *Transp. Res. Rec.* 2672 (28) (2018) 481–492.
- [2] A. Misra, V. Singh, M.K. Darabi, Asphalt pavement rutting simulated using granular micromechanics-based rate-dependent damage-plasticity model, *Int. J. Pavement Eng.* (2017) 1–14.
- [3] A. Berezovski, J. Engelbrecht, A. Salupere, K. Tamm, T. Peets, M. Berezovski, Dispersive waves in microstructured solids, *Int. J. Solids Struct.* 50 (11) (2013) 1981–1990.
- [4] J. Engelbrecht, A. Berezovski, F. Pastrone, M. Braun, Waves in microstructured materials and dispersion, *Philos. Mag.* 85 (33–35) (2005) 4127–4141.
- [5] N. Nejadi Sadeghi, L. Placidi, M. Romeo, A. Misra, Frequency band gaps in dielectric granular metamaterials modulated by electric field, *Mech. Res. Commun.* 95 (2019) 96–103.
- [6] A. Misra, P. Poorsolhjouy, Granular micromechanics based micromorphic model predicts frequency band gaps, *Contin. Mech. Thermodyn.* 28 (1–2) (2016) 215–234.
- [7] A. Misra, L. Placidi, E. Turco, Variational Methods for Continuum Models of Granular Materials, 2019, pp. 1–11.
- [8] J. Li, S. Li, Generating ultra wide low-frequency gap for transverse wave isolation via inertial amplification effects, *Phys. Lett. A* 382 (5) (2018) 241–247.
- [9] A. Colombi, R.V. Craster, D. Colquitt, Y. Achaoui, S. Guenneau, P. Roux, et al., Elastic wave control beyond band-gaps: Shaping the flow of waves in plates and half-spaces with subwavelength resonant rods, *Front. Mech. Eng.* 3 (10) (2017).
- [10] X. An, H. Fan, C. Zhang, Elastic wave and vibration bandgaps in two-dimensional acoustic metamaterials with resonators and disorders, *Wave Motion* 80 (2018) 69–81.
- [11] F. dell'Isola, G. Maier, U. Perego, U. Andreaus, R. Esposito, S. Forest, *The Complete Works of Gabrio Piola: Volume I: Commented English Translation-English and Italian Edition*, Springer International Publishing, 2014, p. 813.
- [12] S.R. Eugster, F. dell'Isola, Eugster SR dell'isola f exegesis of the introduction and sect. i from fundamentals of the mechanics of continua\*\* by e. hellinger, *ZAMM-J. Appl. Math. Mech./Z. Angew. Math. Mech.* 97 (4) (2017) 477–506.
- [13] G. Rosi, N. Auffray, Anisotropic and dispersive wave propagation within strain-gradient framework, *Wave Motion* 63 (2016) 120–134.
- [14] G. Rosi, L. Placidi, N. Auffray, On the validity range of strain-gradient elasticity: a mixed static-dynamic identification procedure, *Eur. J. Mech.-A/Solids* 69 (2018) 179–191.
- [15] L. Placidi, G. Rosi, I. Giorgio, A. Madeo, Reflection and transmission of plane waves at surfaces carrying material properties and embedded in second-gradient materials, *Math. Mech. Solids* 19 (5) (2014) 555–578.
- [16] R.D. Mindlin, Micro-structure in linear elasticity, *Arch. Ration. Mech. Anal.* 16 (1) (1964) 51–78.
- [17] A.C. Eringen, *Microcontinuum Field Theories: Foundations and Solids*, Springer New York, 1999.
- [18] J. Engelbrecht, A. Berezovski, Reflections on mathematical models of deformation waves in elastic microstructured solids, *Math. Mech. Complex Syst.* 3 (1) (2015) 43–82.
- [19] F. Pastrone, J. Engelbrecht (Eds.), *Waves and complexity of microstructured solids*, in: 2012 Proceedings of the International Conference Days on Diffraction; 2012 May 28 2012-June 1, 2012.
- [20] A. Misra, P. Poorsolhjouy, Grain- and macro-scale kinematics for granular micromechanics based small deformation micromorphic continuum model, *Mech. Res. Commun.* 81 (2017) 1–6.
- [21] A.S.J. Suiker, R. de Borst, C.S. Chang, Micro-mechanical modelling of granular material. part 1: Derivation of a second-gradient micro-polar constitutive theory, *Acta Mech.* 149 (1–4) (2001) 161–180.
- [22] A.S.J. Suiker, R. de Borst, C.S. Chang, Micro-mechanical modelling of granular material. part 2: Plane wave propagation in infinite media, *Acta Mech.* 149 (1–4) (2001) 181–200.
- [23] A. Merkel, S. Luding, Enhanced micropolar model for wave propagation in ordered granular materials, *Int. J. Solids Struct.* 106 (2017) 91–105.
- [24] A. Misra, P. Poorsolhjouy, Identification of higher-order elastic constants for grain assemblies based upon granular micromechanics, *Mathematics and Mechanics of Complex Systems.* 3 (3) (2015) 285–308.
- [25] A. Misra, P. Poorsolhjouy, Elastic behavior of 2D grain packing modeled as micromorphic media based on granular micromechanics, *J. Eng. Mech.* 143 (1) (2016) C4016005.
- [26] R. Mindlin, Micro-structure in linear elasticity, *Arch. Ration. Mech. Anal.* 16 (1) (1964) 51–78.
- [27] A. Misra, L. Placidi, E. Turco, Variational methods for discrete models of granular materials, in: H. Altenbach, A. Ochsner (Eds.), *Encyclopedia of Continuum Mechanics*, Springer Verlag, 2018.
- [28] P. Germain, Method of virtual power in continuum mechanics.2. Microstructure, *SIAM J. Appl. Math.* 25 (3) (1973) 556–575.
- [29] T. Peets, Internal scales and dispersive properties of microstructured materials, *Math. Comput. Simul.* 127 (2016) 220–228.
- [30] A. Madeo, P. Neff, I.-D. Chiba, L. Placidi, G. Rosi, Wave propagation in relaxed micromorphic continua: modeling metamaterials with frequency band-gaps, *Contin. Mech. Thermodyn.* (2013) 1–20.
- [31] T. Peets, D. Kartofelev, K. Tamm, J. Engelbrecht, Waves in microstructured solids and negative group velocity, *EPL* 103 (1) (2013) 16001.
- [32] K. Tamm, T. Peets, J. Engelbrecht, D. Kartofelev, Negative group velocity in solids, *Wave Motion* 71 (2017) 127–138.
- [33] F. dell'Isola, P. Seppächer, J.J. Alibert, T. Lekszycki, R. Grygoruk, M. Pawlikowski, et al., Pantographic metamaterials: an example of mathematically driven design and of its technological challenges, *Contin. Mech. Thermodyn.* (2018) 1–34.
- [34] K.H. Matlack, M. Serra-Garcia, A. Palermo, S.D. Huber, C. Daraio, Designing perturbative metamaterials from discrete models, *Nat. Mater.* 17 (4) (2018) 323.
- [35] O.R. Bilal, R. Süssstrunk, C. Daraio, S.D. Huber, Intrinsically polar elastic metamaterials, *Adv. Mater.* 29 (26) (2017) 1700540.

- [36] R. Kumar Pal, R.F. Waymel, P.H. Geubelle, J. Lambros, Tunable wave propagation in granular crystals by altering lattice network topology, *J. Eng. Mater. Technol.* 139 (1) (2016) 011005–011007.
- [37] R.K. Pal, P.H. Geubelle, Wave tailoring by precompression in confined granular systems, *Phys. Rev. E* 90 (4) (2014) 042204.
- [38] J. Xu, B. Zheng, Stress wave propagation in two-dimensional buckyball lattice, *Sci. Rep.* 6 (2016) 37692.
- [39] A. Merkel, V. Tournat, V. Gusev, Experimental evidence of rotational elastic waves in granular phononic crystals, *Phys. Rev. Lett.* 107 (22) (2011).
- [40] M. Romeo, Electroelastic waves in dielectrics modeled as polarizable continua, *Wave Motion* 60 (2016) 121–134.
- [41] M. Romeo, Microcontinuum approach to electromagneto-elasticity in granular materials, *Mech. Res. Commun.* 91 (2018) 33–38.
- [42] A. Misra, V. Singh, Thermomechanics-based nonlinear rate-dependent coupled damage-plasticity granular micromechanics model, *Contin. Mech. Thermodyn.* 27 (4–5) (2014) 787–817.
- [43] L. Placidi, A. Misra, E. Barchiesi, Two-dimensional strain gradient damage modeling: a variational approach, *Z. Angew. Math. Phys.* 69 (3) (2018) 56.

## Appendix C: Paper P3

**Title:**

Frequency band gaps in dielectric granular metamaterials modulated by electric field

**Authors:**

Nima Nejadi Sadeghi

Luca Placidi

Maurizio Romeo

Anil Misra

**Journal:**

Mechanics Research Communications

**Permission from journal:**

Frequency band gaps in dielectric granular metamaterials modulated by electric field

Author: Nima Nejadi Sadeghi, Luca Placidi, Maurizio Romeo, Anil Misra

Publication: Mechanics Research Communications

Publisher: Elsevier

Date: January 2019

© 2019 Elsevier Ltd. All rights reserved.

**Journal Author Rights**

Please note that, as the author of this Elsevier article, you retain the right to include it in a thesis or dissertation, provided it is not published commercially. Permission is not required, but please ensure that you reference the journal as the original source. For more information on this and on your other retained rights, please visit: <https://www.elsevier.com/about/our-business/policies/copyright#Author-rights>


BACK

CLOSE WINDOW


**Credit authorship statement:**

A.M. conceived the idea. N.N. performed the analysis. All authors contributed to the discussion of all aspects of this work. N.N. wrote the manuscript. All authors edited the manuscript.

**Approval from other authors of the publication:**

 Mon 3/29/2021 8:41 AM  
Placidi, Luca <luca.placidi@uninettunouniversity.net>  
Re: Putting our MRC paper in my dissertation

To: Nejadsadeghi, Nima

 You replied to this message on 3/29/2021 8:41 AM.  
[Click here to download pictures.](#) To help protect your privacy, Outlook prevented automatic download of some pictures in this message.


---

Yes, of course.


I acknowledge your contribution to the MRC paper "Frequency band gaps in dielectric granular metamaterials modulated by electric field" and I agree that you use it in your PhD dissertation.

Best regards,

Luca

 Mon 3/29/2021 9:03 AM  
Maurizio Romeo <maurizio.romeo@unige.it>  
RE: Putting MRC paper in my dissertation

To: Nejadsadeghi, Nima

 You replied to this message on 3/29/2021 9:04 AM.

---

Dear Nima,  
I acknowledge your significant contribution to our paper "Frequency band gaps in dielectric granular metamaterials modulated by electric field" published in "Mechanics Research Communications". I fully agree that you use it in your PhD dissertation.  
Sincerely  
Maurizio





Contents lists available at ScienceDirect

## Mechanics Research Communications

journal homepage: [www.elsevier.com/locate/mechrescom](http://www.elsevier.com/locate/mechrescom)

## Frequency band gaps in dielectric granular metamaterials modulated by electric field

Nima Nejadi Sadeghi<sup>a</sup>, Luca Placidi<sup>b,c</sup>, Maurizio Romeo<sup>d</sup>, Anil Misra<sup>e,\*</sup>

<sup>a</sup> Mechanical Engineering Department, University of Kansas, 1530 W. 15th Street, Learned Hall, Lawrence, KS 66045-7609, United States

<sup>b</sup> International Telematic University Uninettuno, Rome, Italy

<sup>c</sup> International Research Center on Mathematics and Mechanics of Complex System, Università degli Studi dell' Aquila, Italy

<sup>d</sup> DIMA, Università degli Studi di Genova, Genoa, Italy

<sup>e</sup> Civil, Environmental and Architectural Engineering Department, University of Kansas, 1530 W. 15th Street, Learned Hall, Lawrence, KS 66045-7609, United States



### ARTICLE INFO

#### Article history:

Received 26 October 2018

Revised 19 November 2018

Accepted 25 January 2019

Available online 27 January 2019

#### Keywords:

Granular micromechanics

Micromorphic continua

Electro-elasticity

Tunable metamaterial

Frequency band gaps

Wave dispersion

### ABSTRACT

Wave propagation in granular materials is known to be dispersive. Micromorphic continuum model based upon granular micromechanics (Misra, A. and P. Poorsolhjouy, Continuum Mech. Thermodyn, 2016, 28(1-2): p. 215-234.) has the ability to describe this dispersion behavior. In this paper we show that the dispersive behavior can be modulated by using electric field when the grains have dielectric properties. To this end, we apply the recently enhanced model that incorporates electro-elastic coupling by connecting microstrain to electric dipole and quadrupole densities due to bound charges in dielectric grains (Romeo, M., Mech. Res. Commun., 2018, 91: p. 33-38.). We particularly investigate the effect of induced polarization that arises due to an imposed electric field. Two cases of dielectric one dimensional infinite rods with the same micromorphic properties have been studied, where case 1 and 2 are in null and nonzero external electric fields, respectively. Parametric studies are performed to understand the contribution of the polarizability (dipole effect), intrinsic quadrupole density, and external electric field on the dispersive behavior of granular media. Results predict an acoustic and an optical branch in the dispersive curve. Polarizability and external electric field are mainly affecting small wavenumber behavior of the wave branches, while quadrupole density alters the behavior of the material at large wavenumbers. A possibility of altering the optical branch to an acoustic branch is also observed, for which instability or attenuation occurs depending upon the direction of the imposed electric field with respect to the wave propagation direction. We find that the location and the width of the frequency band gaps can be altered using external electric field. The possibility of creating or removing frequency band gaps is also shown to exist. The extended theory accounting for electro-elasticity can therefore be utilized as a tool to analyze existing granular media, or to design granular metamaterials, as it systematizes the design process and eliminates ad-hoc manners leading to large data libraries.

© 2019 Elsevier Ltd. All rights reserved.

### 1. Introduction

Granular solids are ubiquitous and impact diverse areas of engineering and science such as material development, transportation and infrastructure systems [3,4], pharmaceuticals and drug delivery, and natural processes in geophysics, with applications including, but not limited to wave attenuation and energy harvesting devices, as recent studies on granular crystals have shown [5–8]. The granular micromechanics based micromorphic continuum model introduced in [1] has the ability to describe and predict

natural or synthetic granular materials (metamaterials) behavior and can be used as a tool to design and analyze granular materials. The proposed continuum model also provides the freedom to describe the average behavior of many micro-structures that are being currently proposed by combining masses, linear springs, rotational springs, beams, etc. (see for example [9–11]). Extending this model to account for electro-elasticity coupling seems essential because of the numerous potential engineering applications which include sensors, actuators, acoustic metamaterials, and ultra-sound imagers [12–14]. This extended theory is not only beneficial to give a comprehensive description of the involved physics resulting in a particular effect, but also crucial as a tool for developing new materials with desired behavior. To describe electro-elasticity effects in granular materials and gran-

\* Corresponding author.

E-mail address: [amisra@ku.edu](mailto:amisra@ku.edu) (A. Misra).

ular metamaterials it is necessary to take into account the coupling of the mechanical deformation and electric charge displacements in the material's internal (micro-) structure [2,15,16]. A micromorphic theory of electro-magnetic non-conducting (dielectric) materials has recently been published [2], having cast a consistent continuum description of polarization and magnetization. In this paper, the granular micromechanics based micromorphic continuum model [1] equipped with the electro-elasticity coupling effect developed for non-conducting materials introduced in [2] is used to study the dispersive behavior of the granular materials in response to the elastic deformation waves subjected to a constant electric field in a quasi-electro-static case. Using this theory, the classical linear hyperbolic partial differential wave equation becomes intricate because of the additional terms introduced to account for the micro-mechano-morphology and electro-elasticity coupling. An understanding of the effects of the electro-elasticity coupling on the behavior of granular materials proves indispensable for both describing the behavior of existing natural granular materials, and designing metamaterials with desired objectives.

The paper is organized as follows. An overview of the theory is presented in Section 2, where the kinematics of the model and the variational approach to derive the governing equations of motion are introduced. To avoid complexities, and to be better able to interpret the effects of the electro-elasticity in the dispersive behavior of the granular materials, we limit our studies to two cases of longitudinal wave propagation in one dimensional infinite rods. Section 3 describes the analysis for two cases with equal microstructural properties. Cases 1 and 2 are in null and nonzero external electric fields, respectively. We perform extensive studies to emphasize the effect of micro- and macro-scale parameters on the dispersive behavior of the material. Section 4 is devoted to the summary of the work done in this paper, along with a discussion on the potential applicability of the theory used here in the design and fabrication of metamaterials with specific material properties for particular purposes.

## 2. Micromorphic model based upon granular micromechanics

The granular micromechanics proceeds from an identification of the grain-scale motions in terms of the continuum measures and the volume average of grain-pair interaction energies with the macro-scale deformation energy density, in an approach reminiscent of developments in continuum modeling presented by Piola [17]. In the current format of granular micromechanics [18], two grain-scale kinematic measures are defined, one for determining relative displacements and the other for relative rotations. It is remarkable that the considered grain-scale kinematic measures represent the combined effect of the grain centroid displacement, spin and size, and do not follow the decomposition adopted in some previous attempts of micro-macro identifications [19,20]. These grain-scale motions are identified with six set of continuum kinematic measures that include the macro-scale displacement/rotation gradients, micro-scale displacement/rotations gradients identified with displacement/rotation fluctuations within a material point, and macro-gradient of the micro-scale displacement/rotation gradients. The deformation energy density of a material point is then expressed in terms of the kinematic measures at the two scales and the inter-granular force measures as well as the continuum stress are defined as conjugates of the kinematic measures. Subsequently, the relationships are derived between stress and inter-granular forces that include stretch/compression, tangential, bending and torsional actions as well as for further derivation of the constitutive relations, variational principle, and balance equations for non-classical micromorphic model whose parameters can be identified in terms of the grain-scale properties [1,21,22].

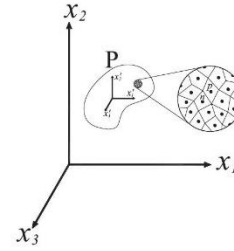


Fig. 1. Schematic of continuum material point, P, with its granular microstructure and the coordinate systems  $x$  and  $x'$  (from [18]).

To develop a continuum description, each material point is considered a volume element (VE), as shown in Fig. 1. Let the coordinate system,  $x$ , be considered in the global (macro-scale) model, and attach a local or micro-scale coordinate system,  $x'$ , to the material point P or the barycenter of the VE with its axes parallel to the global coordinate system axes. The micro-scale coordinate system is defined such that it is able to distinguish different grains inside the material point. The displacement of the grains are then not only a function of the coordinates of the material point P, but also of the micro-scale coordinates of the grain within the material point, i.e.,

$$\phi_i = \phi_i(x, x') \quad (1)$$

where  $\phi_i$  is the displacement of grain centroids. Now consider the displacement,  $\phi_i^p$ , of the centroid of grain, p, contained within the continuum material point, where the displacement is defined in [1]. Utilizing the Taylor's expansion, this displacement can be related to the displacement,  $\phi_i^n$ , of the centroid of neighboring grain, n, such that the difference will be the relative displacement,  $\delta_i^{np}$ , of the two grains, which is given as follows, where we have included the first and second order terms in the Taylor series expansion,

$$\delta_i^{np} = \phi_i^p - \phi_i^n = \phi_{i,j}^n l_j + \frac{1}{2} \phi_{i,jk}^n l_j l_k + \dots \quad (2)$$

where  $l_j$  is the vector joining the centroids of n and p. Following a similar analysis, the relative rotations of two interacting grains, n and p, denoted by  $\theta_i$  is found as [1]

$$\theta_i^{np} = e_{ijk} \phi_{k,jp} l_p \quad (3)$$

where  $e_{ijk}$  is permutation symbol. Note that the summation convention over repeated indices (in the subscript) is implied unless noted otherwise.

By introducing the decomposition of the displacement gradient field into an average field,  $\bar{\phi}_{i,j}$ , and a fluctuation field,  $\gamma_{ij}$ , as [1,23]

$$\psi_{ij} = \phi_{i,j} = \bar{\phi}_{i,j} - \gamma_{ij} \quad (4)$$

the relative displacement of grains p and n can be decomposed as

$$\delta_i^{np} = \bar{\phi}_{i,j} l_j - \gamma_{ij} l_j + \frac{1}{2} \phi_{i,jk}^n l_j l_k + \dots = \delta_i^M - \delta_i^m + \delta_i^g \quad (5)$$

Conjugate to each gradient term in Eqs. (2) and (4), stress measures may be defined. Similarly force/moment measures conjugate to each grain-scale relative displacement/rotation term in Eqs. (2) and (4) may be introduced (see [1]). Furthermore, for linear elasticity, the micro-scale deformation energy is formulated as quadratic functions of the grain-pair kinematic measures introduced in Eqs. (2) and (4), which requires introduction of four different inter-granular stiffness measures defined as  $k_{ij}^p$ ;  $G_{ij}^g$  where K and G denote the stretch and rotational stiffnesses, respectively,  $p = M, m$  and  $g; q = n, w$ ; M denotes macro-stiffness; m denotes the



micro-stiffness;  $g$  denotes the second gradient stiffness;  $u$  denotes the rotation; and the subscripts  $n$  and  $w$  refer to the normal and tangential grain-pair interaction directions. The macro-scale constitutive moduli tensors,  $\mathbf{C}^M$ ,  $\mathbf{C}^m$ ,  $\mathbf{A}^g$ , and  $\mathbf{A}^u$  are then obtained in terms of these inter-granular stiffness measures.

To account for the electro-elasticity coupling effect, bound charge micro-density  $\sigma'(x, x')$  representing the bound charges in dielectric grains, is introduced. The charge density  $\sigma$ , which is a volume average of the charge micro-density, is zero for dielectric materials, but this does not prevent the existence of nonzero electric dipole density  $p$  and quadrupole density  $Q$ , defined as functions of micro-deformation [2]. Polarization as a function of dipole and quadrupole densities is introduced, and subsequently, electric displacement can be defined in the usual manner [2]. The energy density coming from the electric field can be accounted for using a micro-density Lorentz force. To this end, the mean dipole density of a VE of granular media is estimated in the form  $p_i = \alpha E_i^{(0)}$  [24] where  $E_i^{(0)}$  is the constant electric field vector and  $\alpha$  is the equivalent polarizability constant related to the number of grains in the VE and the grains intrinsic dipole, while the quadrupole density is estimated in terms of quadrupole intrinsic to the dielectric grains in an analogy to the microinertia [2]. Thus formulated electric energy density with added terms to account for the electro-elasticity coupling in terms of polarization is then used, and subsequently, the principle of stationary action can be applied to find the governing equations of motions. For an electrostatic case, the governing equations then take the form:

$$(C_{ijkl}^M + C_{ijkl}^m) \bar{\phi}_{k,lj} - C_{ijkl}^m \psi_{kl,j} - \alpha E_k^{(0)} \varphi_{,ik} - \frac{1}{2} \bar{Q}_{jk} \varphi_{,ikj} = \rho \ddot{\phi}_i \quad (6a)$$

$$(A_{jklmn}^g + A_{jklmn}^u) \psi_{lm,ni} + C_{jklm}^m \bar{\phi}_{l,m} - C_{jklm}^m \psi_{lm} + \alpha E_j^{(0)} (E_k^{(0)} - \varphi_{,k}) + \alpha E_i^{(0)} E_k^{(0)} \psi_{ji} - \bar{Q}_{ji} \varphi_{,kl} = I \ddot{\psi}_{jk} \quad (6b)$$

$$-\varphi_{,ii} + \alpha E_i^{(0)} \psi_{ii,i} - \bar{Q}_m \psi_{ii,m} = 0 \quad (6c)$$

where the noncontact mechanical volumic forces and double forces are assumed to be absent,  $\rho$  and  $I$  are the overall density and micro-inertia [1], respectively, of the granular medium,  $\bar{Q}$  is the mean quadrupole density in the representative volume element, and  $\phi$  is the scalar electric potential [2]. This term arises from separation of the electric field in the present quasi-electrostatic case as  $\mathbf{E} = \mathbf{E}^{(0)} - \nabla \phi$  where is the fixed applied field and the scalar potential is responsible for the dynamic contribution. The micro-inertia depends on the representative volume element (RVE). The micro-volume can consist of one or more grains, depending on the assumed RVE. In practice, an RVE is a collection of grains that can be stacked to develop the whole structure. Therefore, the RVE size depends on the granular fabric tensor, and intergranular interaction mechanism. If the granular structure is homogenous in both fabric tensor (geometrical aspect) and grain-pair interactions, the RVE can be assumed to have only one grain (for example a 2D hexagonal structure with no defects and with equal grain-pair interaction in every direction, such as [25]). However, taking an RVE with only one grain could result in loss of additional degrees of freedom introduced in the micromorphic theory, and the theory simplifies to the classical continuum mechanics theory. The governing equations (Eq. 6) have been derived using an energy approach where the virtual work of electrical body forces derived from the Lorentz force in the micromorphic description of polarization have been included in a micromorphic continua obtained from granular micromechanics based homogenization framework. Eqs. (6a) and (6b) are displacement equations of motion derived in [1] with terms accounting for the electro-elasticity coupling, and Eq. (6c) represents the Gauss's law. The Ampere's law in the quasi-static case decouples from the governing equations Eq. 6.

### 3. Longitudinal wave propagation in a one dimensional granular rod

#### 3.1. Mathematical formulation

In what follows, we consider the longitudinal (P) wave propagation along  $x_1$  axis in an isotropic one dimensional infinite rod formed of dielectric grains. In this case, the solutions of Eq. 6 are of the form

$$\bar{\phi}_1 = \bar{\phi}_1(x_1, t), \quad \psi_{11} = \psi_{11}(x_1, t), \quad \varphi_{11} = \varphi_{11}(x_1, t) \quad (7)$$

and the governing equations in Eq. 6 reduce to

$$(P + Q) \bar{\phi}_{1,11} - Q \psi_{11,1} - \alpha E_1^{(0)} \varphi_{,11} - \frac{1}{2} \bar{Q}_{11} \varphi_{,111} = \rho \ddot{\phi}_1 \quad (8a)$$

$$R \psi_{11,11} + Q \bar{\phi}_{1,1} - Q \psi_{11} + \alpha E_1^{(0)} E_1^{(0)} - \alpha E_1^{(0)} \varphi_{,1} + \alpha E_1^{(0)} E_1^{(0)} \psi_{11} - \bar{Q}_{11} \varphi_{,11} = I \ddot{\psi}_{11} \quad (8b)$$

$$-\varphi_{,11} + \alpha E_1^{(0)} \psi_{11,1} - \bar{Q}_{11} \psi_{11,11} = 0 \quad (8c)$$

where the symbols of  $P$ ,  $Q$ , and  $R$ , following [26], have been used for brevity, and have the values of  $C_{1111}^M$ ,  $C_{1111}^m$ , and  $A_{111111}^g$ , respectively, and  $\bar{Q}_{11}$  is the mean quadrupole density in the representative volume element.

The solution for the system of partial differential equations in Eq. 8 consists of two parts – the general and the particular, satisfying the homogenous and the non-homogenous forms of Eq. 8, respectively. The homogenous solution is formed of the plane wave functions. The particular solution depends upon the term,  $\alpha E_1^{(0)} E_1^{(0)}$ , a body force induced by the electric field independent of  $\bar{\phi}_1$  and  $\psi_{11}$ , and does not contribute to the eigen solutions. Therefore, we focus only upon the general solution of Eq. 8. Specializing the solutions in Eq. 8 to plane waves [23], and only considering progressing waves, and accounting for the coupling between electric potential and mechanical deformation for a coherent plane-wave problem, we will have the following oscillatory form for the solutions of Eq. 8

$$\bar{\phi}_1 = \text{Re}(A_1 i e^{i(kx_1 - \omega t)}), \quad \psi_{11} = \text{Re}(B_{11} e^{i(kx_1 - \omega t)}), \quad \varphi = \text{Re}(C e^{i(kx_1 - \omega t)}) \quad (9)$$

where  $k$  is the wavenumber,  $\omega$  is the frequency,  $iA_1$  and  $B_{11}$  are the amplitudes of the macro-displacement and micro-displacement gradient, respectively, and  $C$  is the amplitude of the potential function. Substituting for  $\phi$  from Eq. (9) in Eq. (8c) gives

$$C = \left( -\bar{Q} - i \frac{\alpha E_1^{(0)}}{k} \right) B_{11} \quad (10)$$

Using Eqs. (9) and (10), we can rewrite Eqs. (8a) and (8b) in the following matrix form

$$\begin{bmatrix} c_0^2 k^2 & \frac{d^2}{2} k^3 - i \frac{\alpha c_3}{2} k^2 + (c_A^2 + \alpha^2 c_3^2) k \\ \frac{k}{p^2} & (c_1^2 + c_2^2) k^2 + \frac{1}{p^2} + \frac{\alpha^2 c_3^2}{c_3^2 p^2} - \frac{\alpha c_3^2}{c_3^2 p^2} \end{bmatrix} \begin{bmatrix} A_1 \\ B_{11} \end{bmatrix} = \omega^2 \begin{bmatrix} A_1 \\ B_{11} \end{bmatrix} \quad (11)$$

where, following [26], we have introduced the velocities  $c_0$ ,  $c_1$ , and  $c_A$ , characteristic time,  $p$ , written as

$$c_0^2 = \frac{P+Q}{\rho}, \quad c_1^2 = \frac{R}{I}, \quad c_A^2 = \frac{Q}{\rho}, \quad p^2 = \frac{I}{Q} \quad (12)$$

as well as a new velocities  $c_2$  and  $c_3$  and the parameter  $d$  as

$$c_2^2 = \frac{\bar{Q}^2}{I}, \quad c_3 = \frac{E_1^{(0)}}{\sqrt{\rho}}, \quad d^2 = \frac{\bar{Q}^2}{\rho} = p^2 c_2^2 c_A^2 \quad (13)$$

We remark that  $c_3$  has the dimension of velocity due to the use of Heaviside-Lorentz units, and has been introduced so as to inherit the sign of the applied electric field. Further, it is noteworthy

that parameter  $d$  is not independent, and interestingly takes the dimension of kinematic viscosity (length squared per time). From Eq. (11), utilizing the parameters defined in Eqs. (12) and (13), we get the following secular equation in terms of the eigenvalues  $\omega^2$ ,

$$\omega^2 = (c_0^2 - c_A^2 - \alpha^2 c_3^2)k^2 + p^2(\omega^2 - c_0^2 k^2) \left( \omega^2 - (c_1^2 + c_2^2)k^2 - \frac{(\alpha^2 - \alpha)c_3^2}{c_A^2 p^2} \right) - \frac{d^2}{2} k^4 + i \frac{\alpha c_3 d}{2} k^3 \quad (14)$$

Eq. 14 is the dispersion equation for a one dimensional infinite rod formed of dielectric grains, such that it is endowed with dipole and quadrupole densities in an electrostatic condition with constant external electric field. In the absence of external electric field, the dispersion is a function of quadrupole density. Such observation arises from the assumption made in this work that the dipole density is directly related to, while the quadrupole density is independent of the external electric field [2]. The corresponding eigenvectors from Eq. (11) comprise the amplitudes of the propagating macro-displacement waves and micro-displacement gradient waves (modes of vibration), respectively. The relationship between the eigenvector components  $A_1$  and  $B_{11}$  are given as

$$B_{11} = A_1 \left( \frac{\omega^2 - c_0^2 k^2}{(c_A^2 + \alpha^2 c_3^2)k - i \frac{\alpha c_3 d}{2} k^2 + \frac{d^2}{2} k^3} \right) \quad (15)$$

for a physically admissible eigenvalue  $\omega^2$  which ensures the existence of non-null fields.

Similar to the approach taken in [26], we introduce the dimensionless wavenumber and frequency

$$\xi = pc_0 k \quad (16a)$$

$$\eta = p\omega \quad (16b)$$

We also define dimensionless velocities and a dimensionless term corresponding to the parameter  $d$  as follows

$$\begin{aligned} \gamma_A &= \frac{c_A}{c_0} = \sqrt{\frac{Q}{P+Q}}, \quad \gamma_1 = \frac{c_1}{c_0} = \sqrt{\frac{R}{P+Q}} \sqrt{\frac{\rho}{I}} \\ \gamma_2 &= \frac{c_2}{c_0} = \frac{\tilde{Q}}{\sqrt{P+Q}} \sqrt{\frac{\rho}{I}}, \quad \gamma_3 = \frac{c_3}{c_0} = \frac{E_1^{(0)}}{\sqrt{P+Q}} \\ \mu &= \frac{d}{pc_0^2} = \frac{\tilde{Q}\sqrt{Q}}{P+Q} \sqrt{\frac{\rho}{I}} = \gamma_A \gamma_2 \end{aligned} \quad (17)$$

Using Eqs. 16 and (17), Eq. 14 can be recast in the form

$$\eta^2 = (1 - \gamma_A^2 - \alpha^2 \gamma_3^2)\xi^2 + (\eta^2 - \xi^2) \left( \eta^2 - (\gamma_1^2 + \gamma_2^2)\xi^2 - \frac{(\alpha^2 - \alpha)\gamma_3^2}{\gamma_A^2} \right) - \frac{\mu^2}{2} \xi^4 + i \frac{\alpha \gamma_3 \mu}{2} \xi^3 \quad (18)$$

Eq. (18) is the dimensionless form of the dispersion relation in Eq. 14. We introduce the parameter

$$B'_{11} = pc_0 B_{11} \quad (19)$$

and the dimensionless parameter

$$\beta = \frac{B'_{11}}{A_1} \quad (20)$$

Now Eq. (15) can be written, using Eqs. 16, (17), (19), and (20), as

$$\beta = \frac{\eta^2 - \xi^2}{(\gamma_A^2 + \alpha^2 \gamma_3^2)\xi - i \frac{\alpha \gamma_3 \mu}{2} \xi^2 + \frac{\mu^2}{2} \xi^3} \quad (21)$$

Further, the phase and group velocities can be obtained as follows

$$v_p = \frac{\omega}{k}, \quad v_g = \frac{d\omega}{dk} \quad (22)$$

where  $v_p$  is the phase velocity, and  $v_g$  is the group velocity. Using Eq. 16, the dimensionless form of the phase and group velocities can be written, respectively, as

$$v_p = \frac{\eta}{\xi}, \quad v_g = \frac{d\eta}{d\xi} \quad (23)$$

Further, the mechanical energy transfer ratios associated with the micro- and macro-scale degrees of freedom can be obtained, using Eqs. (9), (12), (13), and (21) and considering the time average of the mechanical energy density over a time period

$$\begin{aligned} \frac{E_{micro}}{E_{total}} &= \frac{\frac{1}{2T} \int_t^{t+T} (I\dot{\psi}_{11}^2 + Q\psi_{11}^2 + R\psi_{11,1}^2) dt}{\frac{1}{2T} \int_t^{t+T} (I\dot{\psi}_{11}^2 + Q\psi_{11}^2 + R\psi_{11,1}^2 + \rho\dot{\phi}_1^2 + P\dot{\phi}_{1,1}^2) dt} \\ &= \frac{\beta^2 (\gamma_A^2 \eta^2 + \gamma_A^2 + \gamma_A^2 \gamma_1^2 \xi^2)}{\beta^2 (\gamma_A^2 \eta^2 + \gamma_A^2 + \gamma_A^2 \gamma_1^2 \xi^2) + \eta^2 + \xi^2 - \gamma_A^2 \xi^2} \end{aligned} \quad (24a)$$

$$\frac{E_{macro}}{E_{total}} = 1 - \frac{E_{micro}}{E_{total}} = \frac{\eta^2 + \xi^2 - \gamma_A^2 \xi^2}{\beta^2 (\gamma_A^2 \eta^2 + \gamma_A^2 + \gamma_A^2 \gamma_1^2 \xi^2) + \eta^2 + \xi^2 - \gamma_A^2 \xi^2} \quad (24b)$$

### 3.2. Results

From Eq. (17), it is clear that  $\gamma_A$  has lower bound limit of 0 and upper bound limit of 1. Very small values of  $\gamma_A$  represent materials in which the micro-stiffness is negligible compared to their macro-stiffness, and values close to the upper bound level have large micro-stiffness compared to their macro-stiffness. A value of  $\gamma_A = 0.71$  corresponds to approximately equal macro- and micro-stiffness of the material. On the other hand  $\gamma_1, \gamma_2$ , and  $\mu$  have lower bound of 0 and an upper bound that can theoretically tend to infinity.  $\gamma_3$  can be any negative or positive value, depending on the sign of the external electric field. For a particular ratio of macro-density to micro-density, larger  $\gamma_1$  implies a growing dominance of second gradient behavior, while large values of  $\gamma_2$  and  $\mu$  imply significant quadrupole effect. Large value for the magnitude of  $\gamma_3$  imply large external electric field, and large  $\alpha$  suggest large polarizability.

To illustrate the effect of the electro-elasticity we study 2 cases with equal micromorphic properties. Case 1 is in a null external electric field, while case 2 is under the effect of a nonzero external electric field. The particular values used for the involved parameters have been chosen to be of the same order of material properties used in [1,2], except that the electric field and polarizability have been chosen larger in order to facilitate visual comparison. For both cases, the parameters chosen are  $\gamma_A = 7.1 \times 10^{-1}$ ,  $\gamma_1 = 5 \times 10^{-3}$ ,  $\gamma_2 = 7.6 \times 10^{-4}$ , and  $\alpha = 1.0 \times 10^{-2}$ , except that for case 1,  $\gamma_3 = 0$  and for case 2,  $\gamma_3 = 3.9$ . The dispersion curves for both cases 1 and 2 are plotted in Fig. 2. Fig. 2 implies that the optical branch for case 1 starts at the dimensionless frequency 1, while optical branch for the case 2 starts at a value less than unity. This value can be obtained by introducing  $\xi = 0$  in Eq. (18), which gives, for the optical branch,

$$\eta = \sqrt{1 + (\alpha)(\alpha - 1) \frac{\gamma_3^2}{\gamma_A^2}} \quad (25)$$

Eq. (25) corresponds to the frequency  $\omega = \sqrt{\frac{c_A^2 + (\alpha)(\alpha - 1)c_3^2}{p^2 c_A^2}}$ . Therefore, the starting dimensionless frequency for the optical



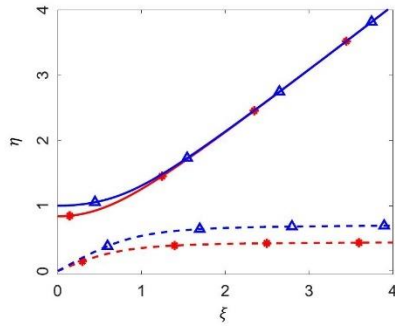


**Fig. 2.** Dispersion curve for cases 1 and 2. Case 1 is depicted by blue lines (marked with triangles), and case 2 by red lines (marked with asterisks). Solid lines and dashed lines represent optical and acoustic branches, respectively. (For interpretation of the references to colour in this figure legend, the reader is referred to the web version of this article.)

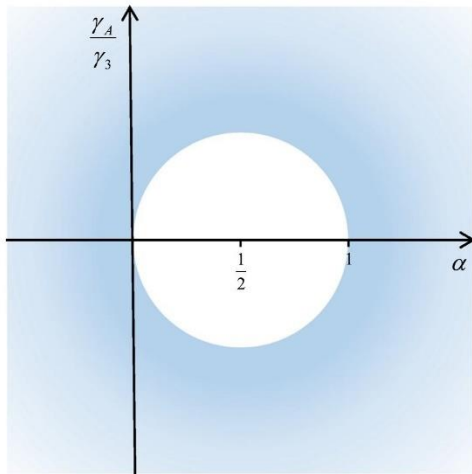


**Fig. 3.** Instability criterion for a positive external electrical field, where any point inside the circle leads to instability.

branch is only related to the external electric field and the polarizability, with quadrupole density having no effect [27] (considering mechanical micromorphic properties to be fixed). Clearly, the starting point of the optical wave is dimensionless frequency of 1 when either  $\alpha$  or  $\gamma_3$  vanishes, and can be less or greater than 1 based on whether the value for  $\alpha$  is less or greater than unity. However, usual values of  $\alpha$  are orders of magnitude smaller than unity. Theoretically, there is a possibility that the expression under the square root in Eq. (25) becomes negative, hence resulting in an imaginary dimensionless frequency with zero real part. The condition for such a possibility is as follows:

$$\left(\alpha - \frac{1}{2}\right)^2 + \left(\frac{\gamma_A}{\gamma_3}\right)^2 < \frac{1}{4} \tag{26}$$

which simply is the area inside a circle with center of  $(\frac{1}{2}, 0)$  and the radius of  $\frac{1}{2}$  in a coordinate system with a horizontal axis  $\alpha$  and a vertical axis  $\frac{\gamma_A}{\gamma_3}$  (See Fig. 3). In cases where the external electric field is positive (the directions of external electric field and propa-

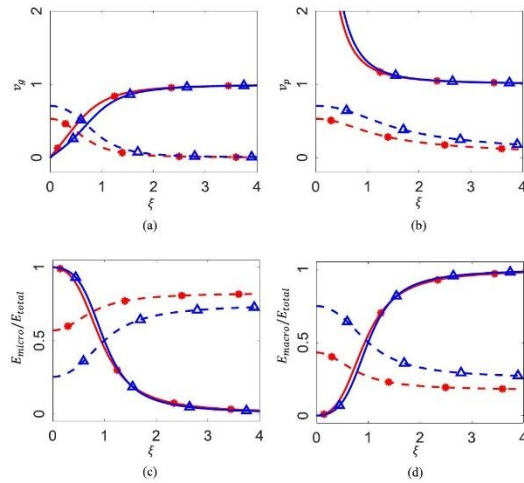


**Fig. 4.** (a) Dimensionless group velocity for cases 1 and 2. (b) Dimensionless phase velocities for cases 1 and 2. (c) Energy transfer ratio associated with the micro-scale degree of freedom to the total energy transferred by the wave, for cases 1 and 2. (d) Energy transfer ratio associated with the macro-scale degree of freedom to the total energy transferred by the wave, for cases 1 and 2. Case 1 is depicted by blue lines (marked with triangles), and case 2 by red lines (marked with asterisks). Solid lines and dashed lines represent optical and acoustic branches, respectively. (For interpretation of the references to colour in this figure legend, the reader is referred to the web version of this article.)

gating wave are the same) and Eq. (26) is satisfied, the imaginary part of the frequency takes positive values, suggesting instability. If the external electric field is negative, attenuation occurs.

Dimensionless group velocities of the optical branches at small wavenumbers in both cases are zero, therefore, electro-elasticity coupling has no effect on the group velocity of the optical branch at small wavenumbers (See Fig. 4a). However, the acoustic branches in cases 1 and 2 have different group velocities at small wavenumbers. Keeping only lower order terms of dimensionless frequency and wavenumber in Eq. (18) results in the dimensionless group velocity of  $\sqrt{1 - \gamma_A^2 \left(\frac{\alpha^2 \gamma_3^2 + \gamma_A^2}{\alpha^2 \gamma_3^2 + \gamma_A^2 - \alpha \gamma_3^2}\right)}$  (corresponding to the group velocity of  $\sqrt{c_0^2 - c_A^2 \left(\frac{\alpha^2 c_3^2 + c_A^2}{\alpha^2 c_3^2 + c_A^2 - \alpha c_3}\right)}$ ). This value, keeping the mechanical properties constant (as is for the cases 1 and 2), is a function of only the electric field and polarizability. For vanishing values of the external electric field, case 1 and 2 behave equally at small wavenumbers for the acoustic branch. Quadrupole density, on the other hand, plays no noticeable role in the group velocity of the acoustic branch at small wavenumbers.

The asymptotes of both the optical and the acoustic branches may be found by keeping only higher order terms of the dimensionless frequency and wavenumber in Eq. (18), which, after solving for the dimensionless frequency, gives

$$\eta = \frac{\sqrt{2}}{2} \sqrt{\gamma_1^2 + \gamma_2^2 + 1 \pm \sqrt{(\gamma_1^2 + \gamma_2^2 - 1)^2 + 2\mu^2 \xi}} \tag{26}$$

or  $\omega = \frac{\sqrt{2}}{2p} \sqrt{\frac{c_1^2 + c_2^2}{c_0^2} + 1 \pm \sqrt{\left(\frac{c_1^2 + c_2^2}{c_0^2} - 1\right)^2 + 2 \frac{d^2}{p^2 c_0^2} k}$ . Obviously, asymptotes are functions of quadrupole density, but polarizability and the external electric field are not appearing in their expression. The coefficients of  $\xi$  in Eq. (26) show the dimensionless group and phase

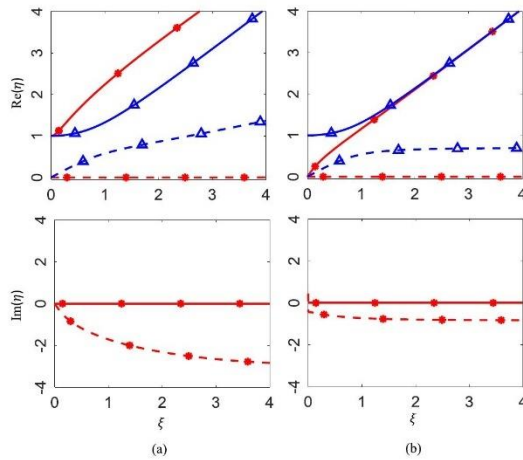


**Fig. 5.** Real and imaginary parts of the dimensionless frequency in the dispersion relation for both optical and acoustic branches where solid and dashed lines represent optical and acoustic branches, respectively. Lines marked with triangle (blue lines) show cases without external electric field and lines marked with asterisk (red line) show the effect of external electric field in electro-elasticity coupling (a) emergence of frequency band gap. Material parameters chosen are  $\gamma_A=0.71$ ,  $\gamma_1=0.3$ ,  $\gamma_2=0.00076$ ,  $\gamma_3=-3.9$ ,  $\alpha=1.01$ , where for the case with zero external electric field the parameter  $\gamma_3$  is zero (b) removing frequency band gap. Material Parameters chosen are  $\gamma_A=0.71$ ,  $\gamma_1=0.005$ ,  $\gamma_2=0.00076$ ,  $\gamma_3=-7.8$ ,  $\alpha=0.01$ , where for the case with zero external electric field the parameter  $\gamma_3$  is zero. (For interpretation of the references to colour in this figure legend, the reader is referred to the web version of this article.)

velocities for both cases 1 and 2 at large wavenumbers, as depicted in Fig. 4a and b. For the case where  $\gamma_2$  (and  $\mu$ ) are negligible, Eq. (26) simplifies to

$$\eta = \xi, \quad \eta = \gamma_1 \xi \quad (27)$$

(corresponding to asymptotes  $\omega=c_0k$  and  $\omega=c_1k$ ), which are the asymptotes for a granular material similar to cases 1 and 2, but without dipole and quadrupole densities (only elasticity).

According to Fig. 4c and d, at small wavenumbers, in both cases 1 and 2, micro-scale degree of freedom is the dominant term playing role for energy transfer in the optical branch, while at large wavenumbers, the macro-scale degree of freedom becomes dominant. For the acoustic branch, micro- and macro-scale degrees of freedom carry almost equal energy at small wavenumbers and the micro-scale's portion increases for larger wavenumbers. External electric field increases micro-scale degree of freedom's energy transfer. This shift, however, is not significant for the two cases studied.

A consequence of electro-elasticity coupling effect can be clearly seen in Fig. 2 where the band gap appears to change size and location as a function of external electric field. It is possible, theoretically, to make band gap emerge for a micro-structure that does not exhibit band gap, by using particular value of external electric field (without changing the microstructure and/or dipole and quadrupole densities). The inverse is also true; band gaps can be removed from the dispersion behavior of a granular medium by choosing appropriate value for external electric field. These two cases have been shown in Fig. 5, where only changing external electric field creates (Fig. 5a) or removes (Fig. 5b) frequency band gaps. Such behavior suggests micro-structures that can be tuned based on the desired response and application. If the directions of external electric field and propagating wave are the same, one

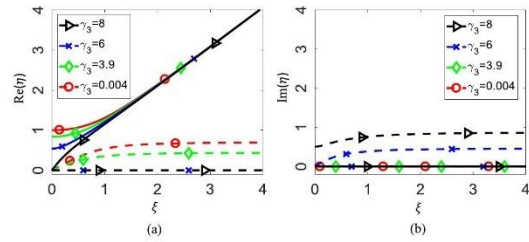


**Fig. 6.** Dispersion curve for four different cases of external electric field (that is proportional to  $\gamma_3$ ) where (a) shows the real part of the frequency and (b) shows the imaginary part of the frequency in the dispersion curve. Solid and dashed lines represent optical and acoustic branches, respectively. The parameters used are equal to case 2 except for  $\gamma_3$  which is taken to be variable.

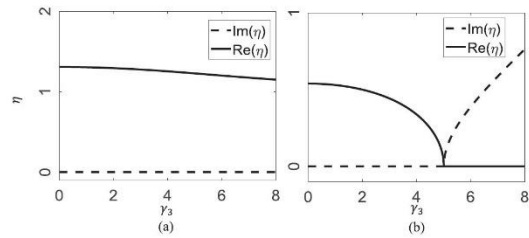


**Fig. 7.** Real and imaginary parts of the dimensionless frequency at dimensionless wavenumber 1 as a function of  $\gamma_3$  for (a) the optical branch and (b) the acoustic branch. The parameters used are equal to case 2 except for  $\gamma_3$  which is taken to be variable.

must pay heed to the rise of instability introduced by the large electric field value. Considering a stable material with specified polarizability and quadrupole density, effect of the positive external electric field on the emergence of instability is illustrated in Fig. 6. The material constants used in the four cases of Fig. 6 are similar to the case 2 of Figs. 2 and 4, except for the dimensionless parameter  $\gamma_3$  related to the external electric field. Four different positive values of the parameter  $\gamma_3$  have been considered and the real and imaginary parts of the dimensionless frequency in the dispersion curve have been plotted, respectively, in Fig. 6a and b. Clearly, increasing positive external electric field shifts the band gap to smaller frequencies and decreases the dimensionless frequency at which the optical branch starts. Also, as discussed before, a large value of positive external electric field causes the optical wave to become an acoustic wave (depicted in Fig. 6 for the cases  $\gamma_3=6$  and  $\gamma_3=8$ ). Such a transition leads to complex frequencies of acoustic wave branch, which have negligible or zero real parts and large values of positive imaginary parts, implying instability caused by the positive external electric field. The instability pertains to the growing of amplitude of the acoustic wave branch with time. Numerical studies suggest a critical point where the instability arises. Fig. 7 shows the real and imaginary parts of the dimensionless frequency at dimensionless wavenumber 1 as a function of  $\gamma_3$  for the optical and acoustic branches (shown in Fig. 7a and b, respectively). The parameters used are the same as that used in case 2 except for the parameter  $\gamma_3$  which is taken to be a variable here. According to Fig. 7a, the optical branch has a zero imaginary part of the dimensionless frequency and the real part of the dimensionless frequency reduces as the positive external electric field increases. The acoustic wave shown in Fig. 7b illustrates a critical point  $\gamma_3=5.01$ . The real part of the acoustic branch decreases with an increase in the external electric field intensity until it reaches



zero at the critical point, and remains zero afterwards. The imaginary part of the dimensionless frequency starts from zero until it reaches the critical point, and obtains positive values for  $\gamma_3$  beyond the critical point. Clearly, any value taken for  $\gamma_3$  greater than the critical point results in the emergence of instability. Each set of material parameters results in a different critical point, and must be accounted for when designing or analyzing the granular media or metamaterials. Since finding possible microstructures for the required desired behavior of the granular medium/metamaterial usually needs optimization algorithms, an inequality constraint to prevent instability can be imposed on the solutions by having the square of the expression of the dimensionless frequency as a function of  $\gamma_3$  for the acoustic branch be nonnegative. As mentioned before, for the case where the directions of external electric field and propagating wave are opposite (negative external electric field), there is no instability. In this case, the imaginary part of the frequency in the acoustic branch becomes negative, suggesting attenuation.

#### 4. Summary and conclusion

In the present paper, we have investigated the electro-elasticity coupling effect in the dispersive behavior of a one dimensional infinite medium composed of dielectric grains placed in a constant electric field. The results were compared with a similar granular medium with zero external electric field. Based on the discussion in Section 3, polarizability and electric field affect the dispersion curve at small wavenumbers, while quadrupole density is responsible for a change in asymptotes of the two branches at large wavenumbers. Therefore, frequency band gaps may emerge by the electro-elasticity coupling, and by the same token, may be removed from a dispersion curve already exhibiting band gaps. The optical wave may also be altered to behave as an acoustic wave. However, a constraint on the value of the external electric field must be insured to prevent instabilities (refer to Fig. 3). The studied problem consider a rod formed of dielectric grains which has no rigid body motion. This assumption yields symmetry in forward and backward waves propagating in the medium. Therefore, we only studied the forward wave propagation. It has been shown that for a moving medium the dispersion becomes asymmetric, leading to different dispersive behavior in the forward and backward propagating waves [28,29]. Such asymmetry for granular structures will be investigated in future works.

Based on the results and discussion presented in the paper, certain combination of the material constants can lead to a particular class of behavior that is suitable for a purpose of interest. This combination is not unique, and there might be many combinations yielding the same result, thus suggesting a not one-to-one relation between the material constants and the behavior. An advantage of the proposed continuum model is the availability of the explicit form of the functions, thereby promising a complete domain of constants to search for possible solutions (see similar approach exemplified for pantographic material systems in [30]). Such theory-based approaches are in contrast to certain efforts that proceed by postulating *a priori* certain predetermined sets of microstructures [9,11] or propose to combine micro-elements [31,32] to achieve an objective that is circumscribed within a known domain of behaviors without the aid of theories that can predict possibilities beyond those that are already known. The granular micromechanics model extended to account for the electro-elasticity coupling can thus provide an efficient paradigm for analyzing natural granular materials, or designing tunable metamaterials with desired dispersive behavior that may be needed for particular applications.

#### Acknowledgements

This research is supported in part by the United States National Science Foundation grant CMMI – 1727433.

#### Supplementary materials

Supplementary material associated with this article can be found, in the online version, at doi:10.1016/j.mechrescom.2019.01.006.

#### References

- [1] A. Misra, P. Poorsolhjouy, Granular micromechanics based micromorphic model predicts frequency band gaps, *Continuum Mech. Thermodyn.* 28 (1–2) (2016) 215–234.
- [2] M. Romeo, Microcontinuum approach to electromagneto-elasticity in granular materials, *Mech. Res. Commun.* 91 (2018) 33–38.
- [3] M. Bazzaz, et al., A straightforward procedure to characterize nonlinear viscoelastic response of asphalt concrete at high temperatures, *Transportation Research Record, Transp. Res. Rec.* 0(0): p. 0361198118782033.
- [4] A. Misra, V. Singh, M.K. Darabi, Asphalt pavement rutting simulated using granular micromechanics-based rate-dependent damage-plasticity model, *Int. J. Pavement Eng.* (2017) 1–14.
- [5] R. Kumar Pal, et al., Tunable wave propagation in granular crystals by altering lattice network topology, *J. Eng. Mater. Technol.* 139 (1) (2016) 011005-011005-7.
- [6] R.K. Pal, P.H. Geubelle, Wave tailoring by precompression in confined granular systems, *Phys. Rev. E, Stat. Nonlin. Soft. Matter Phys.* 90 (4) (2014) 042204.
- [7] J. Xu, B. Zheng, Stress wave propagation in two-dimensional buckyball lattice, *Sci. Rep.* 6 (2016) 37692.
- [8] A. Merkel, V. Tournat, V. Gusev, Experimental evidence of rotational elastic waves in granular phononic crystals, *Phys. Rev. Lett.* 107 (22) (2011).
- [9] J. Li, S. Li, Generating ultra wide low-frequency gap for transverse wave isolation via inertial amplification effects, *Phys. Lett. A* 382 (5) (2018) 241–247.
- [10] A. Colombi, et al., Elastic wave control beyond band-gaps: shaping the flow of waves in plates and half-spaces with subwavelength resonant rods, *Front. Mech. Eng.* 3 (10) (2017).
- [11] X. An, H. Fan, C. Zhang, Elastic wave and vibration bandgaps in two-dimensional acoustic metamaterials with resonators and disorders, *Wave Motion* 80 (2018) 69–81.
- [12] S.A. Cummer, J. Christensen, A. Alù, Controlling sound with acoustic metamaterials, *Nature Rev. Mat.* 1 (2016) 16001.
- [13] Z. Chen, et al., Metamaterials-based enhanced energy harvesting: a review, *Physica B* 438 (2014) 1–8.
- [14] M. Carrara, et al., Metamaterial-inspired structures and concepts for elastoacoustic wave energy harvesting, *Smart Mater. Struct.* 22 (6) (2013) 065004.
- [15] M. Romeo, A variational formulation for electroelasticity of microcontinua, *Math. Mech. Solids* 20 (10) (2015) 1234–1250.
- [16] M. Romeo, Micromorphic continuum model for electromagnetoelastic solids, *Zeitschrift für angewandte Mathematik und Physik* 62 (3) (2011) 513–527.
- [17] F. dell'Isola, et al., in: *The Complete Works of Gabrio Piola: Volume I Commented English Translation - English and Italian Edition*, Springer Publishing Company, 2014, p. 813. Incorporated.
- [18] A. Misra, P. Poorsolhjouy, Grain- and macro-scale kinematics for granular micromechanics based small deformation micromorphic continuum model, *Mech. Res. Commun.* 81 (2017) 1–6.
- [19] A.S.J. Suiker, R. de Borst, C.S. Chang, Micro-mechanical modelling of granular material. Part 1: derivation of a second-gradient micro-polar constitutive theory, *Acta Mech.* 149 (1–4) (2001) 161–180.
- [20] A.S.J. Suiker, R. de Borst, C.S. Chang, Micro-mechanical modelling of granular material. Part 2: plane wave propagation in infinite media, *Acta Mech.* 149 (1–4) (2001) 181–200.
- [21] A. Misra, P. Poorsolhjouy, Identification of higher-order elastic constants for grain assemblies based upon granular micromechanics, *Math. Mech. Comp. Syst.* 3 (3) (2015) 285–308.
- [22] A. Misra, P. Poorsolhjouy, Elastic behavior of 2D grain packing modeled as micromorphic media based on granular micromechanics, *J. Eng. Mech.* 143 (1) (2016) C4016005.
- [23] R.D. Mindlin, Micro-structure in linear elasticity, *Arch. Ration. Mech. Anal.* 16 (1) (1964) 51–78.
- [24] G.A. Maugin, *Continuum Mechanics of Electromagnetic Solids*, 33, Elsevier, 1988.
- [25] C.S. Chang, A. Misra, Theoretical and experimental study of regular packings of granules, *J. Eng. Mech.-Asce* 115 (4) (1989) 704–720.
- [26] J. Engelbrecht, et al., Waves in microstructured materials and dispersion, *Philos. Mag.* 85 (33–35) (2005) 4127–4141.
- [27] M. Romeo, Acoustic waves in micropolar elastic ferroelectrics, *Mech. Res. Commun.* 63 (2015) 33–38.
- [28] M.A. Attarzadeh, M. Nough, Non-reciprocal elastic wave propagation in 2D phononic membranes with spatiotemporally varying material properties, *J. Sound Vib.* 422 (2018) 264–277.

- [29] M.A. Attarzadeh, M. Nouh, Elastic wave propagation in moving phononic crystals and correlations with stationary spatiotemporally modulated systems, *AIP Adv.* 8 (10) (2018) 105302.
- [30] F. dell'Isola, et al., Pantographic metamaterials: an example of mathematically driven design and of its technological challenges, *Continuum Mech. Thermodyn.* (2018) 1–34.
- [31] K.H. Matlack, et al., Designing perturbative metamaterials from discrete models, *Nat. Mater.* 17 (4) (2018) 323–328.
- [32] O.R. Bilal, et al., Intrinsically polar elastic metamaterials, *Adv. Mater.* 29 (26) (2017).

## Appendix D: Paper P4

### Title:

Axially moving materials with granular microstructure

### Authors:


Nima Nejadi Sadeghi

Anil Misra

### Journal:

International Journal of Mechanical Sciences

### Permission from journal:



Axially moving materials with granular microstructure  
Author: Nima Nejadi Sadeghi, Anil Misra  
Publication: International Journal of Mechanical Sciences  
Publisher: Elsevier  
Date: October 2019  
© 2019 Elsevier Ltd. All rights reserved.

---

**Journal Author Rights**

Please note that, as the author of this Elsevier article, you retain the right to include it in a thesis or dissertation, provided it is not published commercially. Permission is not required, but please ensure that you reference the journal as the original source. For more information on this and on your other retained rights, please visit: <https://www.elsevier.com/about/our-business/policies/copyright#Author-rights>

[BACK](#) [CLOSE WINDOW](#)

### Credit authorship statement:

A.M. and N.N. conceived the idea. N.N. developed the model and performed analysis. All authors contributed to the discussion of all aspects of this work. N.N. wrote the manuscript. All authors edited the manuscript.





Contents lists available at ScienceDirect

## International Journal of Mechanical Sciences

journal homepage: [www.elsevier.com/locate/ijmecsci](http://www.elsevier.com/locate/ijmecsci)

## Axially moving materials with granular microstructure

Nima Nejadi Sadeghi<sup>a</sup>, Anil Misra<sup>b,\*</sup><sup>a</sup> Mechanical Engineering Department, University of Kansas, 1530 W 15th Street, Learned Hall, Lawrence, KS 66047-7609, United States<sup>b</sup> Civil, Environmental and Architectural Engineering Department, University of Kansas, 1530 W 15th Street, Learned Hall, Lawrence, KS 66045-7609, United States

## ARTICLE INFO

## Keywords:

Axially moving media  
 Granular microstructure  
 Dispersion relation  
 Frequency band gaps  
 Granular metamaterials

## ABSTRACT

The mechanics of axially moving media is significant because of their broad engineering applications. In many engineering applications, it is beneficial to understand the dynamical material response from a microstructural viewpoint. Here we focus upon wave propagation in axially moving materials with granular microstructure. To this end, the granular micromechanics approach is utilized since the resulting continuum model is known to predict wave dispersion. To consider axially moving materials, this approach is enhanced to account for the axial velocity using an Eulerian description of the system accounting for convective terms in the material derivatives and utilizing variational approach. The dispersive behavior of axially moving 1D materials are then derived and compared with the dispersive behavior of non-moving materials. In the absence of microstructure, the axially moving material model simplifies to published literature and shows non-dispersive non-symmetric forward and backward waves. In the case of axially moving materials with granular microstructure, the model predicts dispersive non-symmetric waves. In this case, there are two acoustic and two optical wave branches. Axial velocity leads to narrowing and widening in the frequency band gaps in the forward and backward waves, respectively. Negative group velocity is also observed in certain wavenumber ranges. Clearly, the stopbands created by the axial velocity and the non-symmetric dispersive behavior studied here should be considered in engineering designs for vibration control when the axially moving material possesses granular microstructure. The results presented here can also be used to help obtain parameters needed for axially moving granular metamaterials to be designed for particular applications.

## 1. Introduction

Due to their engineering importance, axially moving materials have been investigated in a number of previous studies. The interest in these problems have remained high (see for example the review in [1]), with an increasing attention being expended to cases in which the materials possess certain heterogeneities or microstructures (see recent works [2,3]), or undergo complex deformation modes [4,5]. The recent studies on axially moving materials include, but are not limited to, vibration, wave propagation, control and stability analysis of axially moving rods [6,7], cables, belts and strings [1,4,8–17], beams [1,4,5,13–15,18–20], membranes [21], plates [1,3,22], rotating rings [4], and periodic media [2,17]. Interesting application of moving media is found in recently developed 2D graphene sheets [23–25] in which the vibration characteristics [26,27] and stability have been determined to be affected by the axial velocity [28]. Other examples of the applications of axially moving media are aerial tramways, mono-cable ropeways, ski lifts, magnetic and paper tapes, band saw blades, and power transmission chains and belts. These media are considered gyroscopic continua, involving translating and rotating materials [16]. In problems involving such media,

a stationary control volume that the material flows through is taken as the domain of study. Although the moving material is typically a solid, moving materials are closely related to flowing fluids than to structural mechanics [29]. For problems involving axially moving materials an Eulerian frame of reference is needed to formulate the problem.

As a large number of materials have granular microstructures, and as technological advancements in additive manufacturing pave the way for production of (granular) metamaterials with desired microstructures for special engineering applications, a need to study the response of moving media with embedded microstructure is warranted. The existence of the microstructural characteristic length comparable to the wavelength of excitation at large frequencies [30] necessitates the inclusion of micro-mechano-morphological aspects of the microstructure in the mathematical models describing moving media's behavior. Note that "large frequencies" do not necessarily mean frequencies in the order of, e.g., Megahertz, as much as microstructure should not always be inferred as microscopic scale. In fact, the largeness of the frequency is conceived with regards to the material and geometrical properties of the system of interest. In cases where microstructure exists, the classical wave equation for elastic materials in the form of a hyperbolic partial

\* Corresponding author.

E-mail address: [amisra@ku.edu](mailto:amisra@ku.edu) (A. Misra).<https://doi.org/10.1016/j.ijmecsci.2019.105042>

Received 29 March 2019; Received in revised form 11 July 2019; Accepted 22 July 2019

Available online 23 July 2019

0020-7403/© 2019 Elsevier Ltd. All rights reserved.

differential equation needs extra terms contributing to the effects of the micro-mechano-morphology and inertia of the axially moving medium. The microstructural effect of granular materials on their dispersive behavior is known to be responsible for the emergence of frequency band gaps, as has been shown, along with the external electric field effect on the tunability of such band gaps, in [31–33].

Unlike the experiments performed on axially moving media in the literature (see, for example, [8–11,18,19]), the involvedness of evaluating parameters in experiments related to materials with granular microstructure is typically intractable and experimental approaches have difficulty in providing an exhaustive examination of the behavior of the materials incorporating granular microstructure. Therefore, as the first step to understanding the dynamic behavior of axially moving granular materials, a theoretical approach has been adopted and realized through longitudinal elastic wave propagation analysis in an axially moving 1D granular continuum in the present paper. With respect to the theoretical modeling of 1D vibrations accounting for higher-order strain-gradient elasticity, we note the recent works focusing on the exact analytical and asymptotic solutions of boundary-value problems of rods [34,35]. Considering a 1D problem simplifies the mathematics involved, yet makes it possible to qualitatively describe the phenomenon. Doing so, the granular micromechanics approach described in [33,36] is utilized to investigate the dispersive behavior of axially moving media with granular microstructure. In this method, a collection of grains interacting via different grain-pair mechanisms is modeled as the material representative volume element (RVE), where considering the mean behavior of grain pairs results in the treatment of the problem in statistical sense [37]. Such method is well suited for continuum description of random granular media. An understanding of the effects of the axial velocity and material properties of the moving material with granular microstructure on its dispersive behavior will be beneficial for designing new (meta)materials with desired vibration mitigation objectives as well as indispensable for understanding the stability behavior of existing natural materials with granular microstructure.

The rest of the paper is ordered as follows. An outline of the granular micromechanics theory is delivered in Section 2, where we present the kinematics involved in the model and the variational approach utilized to obtain the governing equations of motion. Section 3 is devoted to the study of the dispersive behavior of an axially moving 1D continuum experiencing longitudinal elastic deformation waves. Studying a 1D continuum model is to avoid complexities, and yet be able to interpret the effects of the axial velocity. In Section 4, simpler forms of the problem reducing to published literature are provided, and analyzed first. Thereafter, the general problem involving axially moving 1D continuum with granular microstructure is investigated in terms of wave propagation characteristics. Finally, Section 5 summarizes the paper and provides concluding remarks.

## 2. Mathematical model for axially moving materials with granular microstructure

Granular micromechanics approach describes the continuum measures based upon the micro-mechanics of grain-scale motions. Therefore, the collective behavior of grain-pair interactions is related to the macro-scale continuum description of the material. Such a relationship identifies the volume average of the interaction energies in the scale of individual grains with the macro-scale deformation energy density. In what follows, the continuum modeling framework of granular micromechanics approach is briefly presented. The reader is referred to the reference [33] for more detailed derivations.

Each material point in the continuum model is considered to be a representative volume element (RVE), as shown in Fig. 1. Now Let  $\mathbf{x}$  be the global or macro-scale coordinate system for the continuum. Further, let  $\mathbf{x}'$  be the local or micro-scale coordinate system, parallel to the macro-scale coordinate system  $\mathbf{x}$  and attached to the center of mass of the material point  $P$ . Such micro-scale coordinate system can distin-

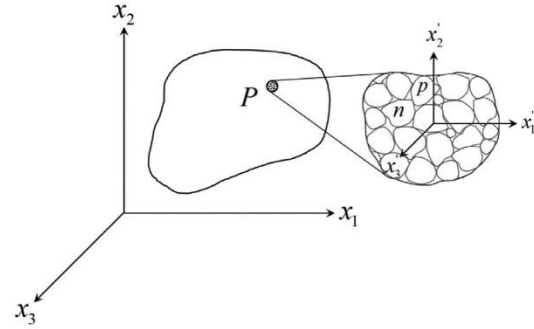


Fig. 1. Schematic of the continuum material point,  $P$ , and its granular microstructure magnified for better visualization, where the  $\mathbf{x}'$  coordinate system is attached to its barycenter.

guish the grains inside the RVE. The displacement of the centroids of the grains are, therefore, described as

$$\phi_i = \phi_i(\mathbf{x}_j, \mathbf{x}'_j, t), \quad (1)$$

where  $\phi_i$  denotes the displacement of grain centroids. Now consider the displacement of the grain  $p$  centroid, denoted by  $\phi_i^p$ , as defined in [33]. The grain  $p$  resides in the continuum material point (the RVE). Consider the neighboring grain  $n$  of grain  $p$ . One can write the displacement of the centroid of grain  $n$ ,  $\phi_i^n$ , using Taylor series expansion about the displacement of grain  $p$  centroid. Keeping up to the quadratic term in the expansion, and denoting the difference between  $\phi_i^p$  and  $\phi_i^n$  as  $\delta_i^{np}$ , results in

$$\delta_i^{np} = \phi_i^p - \phi_i^n = \phi_{i,j}^p l_j + \frac{1}{2} \phi_{i,jk}^p l_j l_k. \quad (2)$$

In Eq. (2),  $l_j$  is the vector joining the centroids of  $n$  and  $p$ , and the tensor product  $l_j l_k$  ( $=J_{jk}$ ) is a geometry moment tensor. The differentiation in Eq. (2) is with respect to the micro-scale coordinate system. Henceforward, differentiation with respect to the spatial coordinate systems is denoted by a comma in the subscript, and over-dots on the parameters express differentiation with respect to time. Moreover, repeated indices in the subscript follow the summation convention unless noted otherwise. The relative rotation of two neighboring grains,  $n$  and  $p$ , denoted by  $\theta_i^n$  is found similarly as [33]

$$\theta_i^n = e_{jki} \phi_{k,jp} l_p, \quad (3)$$

where  $e_{ijk}$  is the permutation symbol. In Eq. (3), the differentiation is with respect to the micro-scale coordinate system. The decomposition of the displacement gradient field can be introduced as [33,36,38]

$$\psi_{ij} = \phi_{i,j} = \bar{\phi}_{i,j} - \gamma_{ij}, \quad (4)$$

where  $\psi_{ij}$  is the micro-scale displacement gradient within the RVE,  $\bar{\phi}_{i,j}$  is the macro-scale displacement gradient and is constant in a material point, and  $\gamma_{ij}$  is the relative deformation due to the fluctuations of the micro-displacement of the grains inside the RVE. Note that the micro-scale deformation measure  $\psi_{ij}$  is homogenous within the material point and is only a function of the macro-scale coordinate system. Using Eq. (4), the relative displacement of grains  $p$  and  $n$  is written as

$$\delta_i^{np} = \bar{\phi}_{i,j} l_j - \gamma_{ij} l_j + \frac{1}{2} \phi_{i,jk} l_j l_k = \delta_i^M - \delta_i^m + \delta_i^e, \quad (5)$$

where

$$\delta_i^M = \bar{\phi}_{i,j} l_j, \quad \delta_i^m = \gamma_{ij} l_j, \quad \delta_i^e = \frac{1}{2} \phi_{i,jk} l_j l_k. \quad (6)$$

In Eq. (6),  $\delta_i^M$  is related to the macro-scale (average) displacement gradient,  $\bar{\phi}_{i,j}$ ,  $\delta_i^m$  is related to the gradients of the fluctuation in grain



displacement,  $\tau_{ij}$ , and  $\delta_i^{\beta}$  is due to the second gradient term,  $\phi_{i,j,k}$ , which is same as the gradient of the relative deformation,  $\gamma_{i,j,k}$ .

Macro-scale deformation energy density,  $W$ , of the granular medium is considered to be a function of the macro-scale kinematic measures, and reads

$$W = W(\bar{\phi}_{(i,j)}, \gamma_{ij}, \phi_{i,j,k}). \quad (7)$$

where  $\bar{\phi}_{(i,j)}$  is the symmetric part of the macro-scale displacement gradient. Conjugates to the macro-scale kinematic measures, are the macro-scale stress components written as

$$\tau_{ij} = \frac{\partial W}{\partial \bar{\phi}_{(i,j)}} = \frac{\partial W}{\partial \epsilon_{ij}}, \quad \sigma_{ij} = \frac{\partial W}{\partial \gamma_{ij}}, \quad \mu_{ijk} = \frac{\partial W}{\partial \gamma_{i,j,k}}, \quad (8)$$

where  $\tau_{ij}$ ,  $\sigma_{ij}$ , and  $\mu_{ijk}$  are Cauchy stress, relative stress, and double stress, respectively. Macro-scale deformation energy density can also be written in terms of micro-scale deformation energy density. Micro-scale deformation energy for the  $\alpha^{\text{th}}$  interacting pair can be defined as  $W^{\alpha}(\delta_i^{\alpha\text{M}}, \delta_i^{\alpha\text{m}}, \delta_i^{\alpha\text{g}}, \theta_i^{\alpha\text{m}})$ . Therefore, the overall energy density of the RVE is given as

$$W = \frac{1}{V'} \sum_{\alpha} W^{\alpha}(\delta_i^{\alpha\text{M}}, \delta_i^{\alpha\text{m}}, \delta_i^{\alpha\text{g}}, \theta_i^{\alpha\text{m}}). \quad (9)$$

In Eq. (9),  $V'$  is the volume of the RVE. The intergranular forces,  $f_i^{\alpha\text{M}}$ ,  $f_i^{\alpha\text{m}}$ ,  $f_i^{\alpha\text{g}}$ , and moment,  $m_i^{\alpha\text{m}}$ , conjugates to the kinematic measures in Eq. (9) are introduced as

$$\frac{\partial W}{\partial \delta_i^{\alpha\text{M}}} = f_i^{\alpha\text{M}}, \quad \zeta = \text{M, m, g}, \quad \frac{\partial W}{\partial \theta_i^{\alpha\text{m}}} = m_i^{\alpha\text{m}}. \quad (10)$$

Substituting Eq. (9) into Eq. (8), and utilizing Eqs. (6) and (10), results in the equations relating macro-scale stress measures to the grain-pair forces and moments, branch vectors and geometry moment tensors as follows [33]

$$\begin{aligned} \tau_{ij} &= \frac{1}{V'} \sum_{\alpha} f_i^{\alpha\text{M}} J_j^{\alpha}, \\ \sigma_{ij} &= \frac{1}{V'} \sum_{\alpha} f_i^{\alpha\text{m}} J_j^{\alpha}, \\ \mu_{ijk} &= \frac{1}{V'} \left( \sum_{\alpha} f_i^{\alpha\text{g}} J_{jk}^{\alpha} + \sum_{\alpha} m_i^{\alpha\text{m}} e_{jil} I_k^{\alpha} \right). \end{aligned} \quad (11)$$

A local coordinate system for each grain pair can be defined. The grain-pair forces and moments, as well as displacement and rotation vectors can subsequently be decomposed in normal and tangential components. Considering a quadratic form for  $W^{\alpha}$  results in the macro-scale constitutive relationships in the macro-scale coordinate system as follows [33]

$$\begin{aligned} \tau_{ij} &= C_{ijkl}^{\text{M}} \epsilon_{kl}, \\ \sigma_{ij} &= C_{ijkl}^{\text{m}} \gamma_{kl}, \\ \mu_{ijk} &= \left( A_{ijklmn}^{\text{g}} + A_{ijklmn}^{\text{u}} \right) \phi_{l,mn}, \end{aligned} \quad (12)$$

where  $C_{ijkl}^{\text{M}}$  and  $C_{ijkl}^{\text{m}}$  are fourth rank tensors, and  $A_{ijklmn}^{\text{g}}$  and  $A_{ijklmn}^{\text{u}}$  are tensors of rank six, defined as (refer to Misra and Poorsolhjouy [33] for more details)

$$\begin{aligned} C_{ijkl}^{\text{M}} &= \frac{1}{V'} \sum_{\alpha} K_{ik}^{\text{M}} J_l^{\alpha} J_j^{\alpha}, \quad C_{ijkl}^{\text{m}} = \frac{1}{V'} \sum_{\alpha} K_{ik}^{\text{m}} J_l^{\alpha} J_j^{\alpha}, \\ A_{ijklmn}^{\text{g}} &= \frac{1}{V'} \sum_{\alpha} K_{il}^{\text{g}} J_m^{\alpha} J_{jk}^{\alpha}, \quad A_{ijklmn}^{\text{u}} = \frac{1}{V'} \sum_{\alpha} G_{pq}^{\text{u}} e_{mlq} e_{jlp} J_k^{\alpha} J_n^{\alpha}. \end{aligned} \quad (13)$$

In Eq. (13),  $\mathbf{K}^{\text{M}}$ ,  $\mathbf{K}^{\text{m}}$ ,  $\mathbf{K}^{\text{g}}$ , and  $\mathbf{G}^{\text{u}}$  denote average, fluctuation, second gradient, and rotational inter-granular stiffness matrices. We note that, in general, grain-pair interaction is nonlinear and includes dissipation. However, for small deformations (small amplitude of vibration) a quadratic form of grain-pair deformation energy based on the micro-scale kinematic measures is considered valid.

In what follows, we will derive the equations of motion for a moving granular medium observed from a stationary reference frame. The granular medium is assumed to move with a known constant velocity  $\mathbf{v}$ , a vector with components in directions of  $X_1$ ,  $X_2$ , and  $X_3$ , respectively, with  $\mathbf{X}$  being the stationary frame of reference. Although the axially moving continua are non-conservative with respect to the fact that the total energy is not generally constant, and the collection of material points establishing the material inside the control volume changes with time, the standard form of Hamilton's principle can still be applied to derive the equations of motion, provided that the end supports are fixed [12,39].

The variation of macro-scale deformation energy density, using Eqs. (4) and (8), can be written as

$$\begin{aligned} \delta W &= \tau_{ij} \delta \epsilon_{ij} + \sigma_{ij} \delta \gamma_{ij} + \mu_{ijk} \delta \phi_{i,j,k} \\ &= \tau_{ij} \delta \bar{\phi}_{(i,j)} + \sigma_{ij} (\delta \bar{\phi}_{(i,j)} - \delta \phi_{i,j}) + \mu_{ijk} \delta \phi_{i,j,k}. \end{aligned} \quad (14)$$

Leibniz differentiation rule can be applied to Eq. (14), resulting

$$\begin{aligned} \delta W &= [(\tau_{ij} + \sigma_{ij}) \delta \bar{\phi}_{i,j}]_j - (\tau_{ij} + \sigma_{ij})_j \delta \bar{\phi}_i - \sigma_{ij} \delta \psi_{ij} \\ &\quad + (\mu_{ijk} \delta \psi_{ij})_k - \mu_{ijk,k} \delta \psi_{ij}. \end{aligned} \quad (15)$$

Defining  $\bar{W} = \int_V W dV$  as the total macro-scale deformation energy, its variation is obtained utilizing Gauss's divergence theorem and Eq. (15) as

$$\begin{aligned} \delta \bar{W} &= - \int_V (\tau_{ij} + \sigma_{ij})_j \delta \bar{\phi}_i dV - \int_V (\mu_{ijk,k} + \sigma_{ij}) \delta \psi_{ij} dV \\ &\quad + \int_S (\tau_{ij} + \sigma_{ij}) n_j \delta \bar{\phi}_i dS + \int_S \mu_{ijk} n_k \delta \psi_{ij} dS. \end{aligned} \quad (16)$$

With regards to Eq. (16), the following form for the variation of total external work is considered

$$\delta \bar{W}_{\text{ext}} = \int_V f_i \delta \bar{\phi}_i dV + \int_V \Phi_{ij} \delta \psi_{ij} dV + \int_S t_i \delta \bar{\phi}_i dS + \int_S T_{ij} \delta \psi_{ij} dS, \quad (17)$$

where  $f_i$  is the non-contact volumic force per unit volume,  $t_i$  is the contact surface force per unit area,  $\Phi_{ij}$  is the non-contact volumic double force per unit volume, and  $T_{ij}$  is the contact double force per unit area.

Non-relativistic kinetic energy density  $T$  associated with the material's motion can be written, using the Stokes' (material) derivative

$$\frac{D}{Dt} = \frac{\partial}{\partial t} + v \frac{\partial}{\partial x}, \quad (18)$$

and the defined forms of kinetic energy in [24,32] as

$$T = \frac{1}{V'} \int_{V'} \frac{1}{2} \rho' \left( v_i + \dot{\phi}_i + \frac{\partial \phi_i}{\partial x_j} v_j \right) \left( v_i + \dot{\phi}_i + \frac{\partial \phi_i}{\partial x_k} v_k \right) dV'. \quad (19)$$

In Eq. (19),  $\rho'$  is defined as the micro-scale mass density per unit macro-volume. In general,  $\rho'$  can be non-uniform inside the RVE. Here we only consider a constant  $\rho'$  in the RVE and the continuum. The macro-scale mass density,  $\rho$ , is obtained as

$$\rho = \frac{1}{V'} \int_{V'} \rho' dV' = \frac{\rho'}{V'} \int_{V'} dV' = \rho'. \quad (20)$$

Eq. (19), after substituting for  $\Phi_i$  and using Eq. (20), can be written as

$$\begin{aligned} T &= \frac{1}{V'} \int_{V'} \frac{1}{2} \rho \left( v_i + \dot{\phi}_i + \psi_{ij} x'_j + \frac{\partial \bar{\phi}_i}{\partial x_j} v_j + \psi_{i,j,k} x'_j v_k \right) \\ &\quad \times \left( v_i + \dot{\phi}_i + \psi_{ik} x'_k + \frac{\partial \bar{\phi}_i}{\partial x_k} v_k + \psi_{i,m,n} x'_m v_n \right) dV'. \end{aligned} \quad (21)$$

Expanding Eq. (21), and noting that the integrals of linear integrands in  $x'_j$  vanish, the kinetic energy density takes the form

$$\begin{aligned} T &= \frac{1}{2} \rho \left( \dot{\phi}_i \dot{\phi}_i + v_i v_i + 2v_i \dot{\phi}_i + 2v_i v_j \bar{\phi}_{i,j} + 2\dot{\phi}_i \bar{\phi}_{i,j} v_j + \bar{\phi}_{i,m} \bar{\phi}_{i,j} v_m v_j \right) \\ &\quad + \frac{1}{2} \rho d_{jk} (\psi_{ij} \psi_{ik} + 2\psi_{ij} \psi_{ik,m} v_m + \psi_{ij,l} \psi_{ik,n} v_l v_n), \end{aligned} \quad (22)$$



where  $d_{jk}$  is

$$d_{jk} = \frac{1}{\sqrt{V}} \int_{V'} x'_j x'_k dV' \quad (23)$$

We remark here that the expression for the kinetic energy density in Eq. (21) is significantly different from that found in [31–33], which focuses upon non-moving granular media. In the derived expression Eq. (22), the effect of velocity of the axially moving granular medium is included by considering Eulerian description of grain and the grain-structure motion. It is notable that the Eq. (22) will simplify to the previously published work if one considers a vanishing axial velocity for non-moving media. In this case, Eulerian and Lagrangian descriptions of motion give identical results and the kinetic energy density will reduce to  $T = \frac{1}{2} \rho \dot{\phi}_i \dot{\phi}_i + \frac{1}{2} \rho d_{jk} \psi_{ij} \psi_{ik}$ . In the present derivation, the key aspect is the inclusion of the convective terms in the kinetic energy density expression. These inclusion are two-fold, one due to the classical convective term that will appear as a result of the bulk axial velocity  $v_i$ , and the second due to the effect of bulk axial velocity on the micro-motions.

Throughout the paper, we consider a cubic RVE with parallel edges to  $x'$  and length of  $2d$ . In this case, Eq. (23) is written as

$$d_{jk} = \frac{1}{3} d^2 \delta_{jk}, \quad (24)$$

where  $\delta_{jk}$  is the Kronecker delta. The total kinetic energy  $\bar{T}$  is written as

$$\bar{T} = \int_V T dV. \quad (25)$$

Using Eqs. (22) and (25), and integrating by parts with the assumption that the values of  $\dot{\phi}_j$  and  $\psi_{ij}$  are known at  $t = t_0, t_1$ , the variational of the kinetic energy functional is

$$\begin{aligned} \delta \int_{t_0}^{t_1} \bar{T} dt &= \int_{t_0}^{t_1} \int_V \rho v_i v_j \delta \dot{\phi}_{i,j} dV dt - \int_{t_0}^{t_1} \int_V \rho \dot{\phi}_i \delta \dot{\phi}_i dV dt \\ &+ \int_{t_0}^{t_1} \int_V \rho v_j \dot{\phi}_i \delta \dot{\phi}_{i,j} dV dt - \int_{t_0}^{t_1} \int_V \rho v_j \dot{\phi}_{i,j} \delta \dot{\phi}_i dV dt \\ &+ \int_{t_0}^{t_1} \int_V \rho v_m v_j \dot{\phi}_{i,m} \delta \dot{\phi}_{i,j} dV dt - \int_{t_0}^{t_1} \int_V \frac{1}{3} \rho d^2 \dot{\psi}_{ij} \delta \psi_{ij} dV dt \\ &+ \int_{t_0}^{t_1} \int_V \frac{1}{3} \rho d^2 v_m \dot{\psi}_{ij} \delta \psi_{ij,m} dV dt \\ &- \int_{t_0}^{t_1} \int_V \frac{1}{3} \rho d^2 v_m \dot{\psi}_{ij,m} \delta \psi_{ij} dV dt \\ &+ \int_{t_0}^{t_1} \int_V \frac{1}{3} \rho d^2 v_m v_n \dot{\psi}_{ij,m} \delta \psi_{ij,n} dV dt. \end{aligned} \quad (26)$$

Using Leibniz differentiation rule, we can write for the integrands of the first, third, fifth, seventh and the ninth terms on the right hand side of Eq. (26),

$$\begin{aligned} \rho v_i v_j \delta \dot{\phi}_{i,j} &= (\rho v_i v_j \delta \dot{\phi}_i)_{,j}, \\ \rho v_j \dot{\phi}_i \delta \dot{\phi}_{i,j} &= (\rho v_j \dot{\phi}_i \delta \dot{\phi}_i)_{,j} - (\rho v_j \dot{\phi}_i)_{,j} \delta \dot{\phi}_i \\ &= (\rho v_j \dot{\phi}_i \delta \dot{\phi}_i)_{,j} - \rho v_j \dot{\phi}_{i,j} \delta \dot{\phi}_i, \\ \rho v_m v_j \dot{\phi}_{i,m} \delta \dot{\phi}_{i,j} &= (\rho v_m v_j \dot{\phi}_{i,m} \delta \dot{\phi}_i)_{,j} - \rho v_m v_j \dot{\phi}_{i,m,j} \delta \dot{\phi}_i, \\ \frac{1}{3} \rho d^2 v_m \dot{\psi}_{ij} \delta \psi_{ij,m} &= \left( \frac{1}{3} \rho d^2 v_m \dot{\psi}_{ij} \delta \psi_{ij} \right)_{,m} - \frac{1}{3} \rho d^2 v_m \dot{\psi}_{ij,m} \delta \psi_{ij}, \\ \frac{1}{3} \rho d^2 v_m v_n \dot{\psi}_{ij,m} \delta \psi_{ij,n} &= \left( \frac{1}{3} \rho d^2 v_m v_n \dot{\psi}_{ij,m} \delta \psi_{ij} \right)_{,n} - \frac{1}{3} \rho d^2 v_m v_n \dot{\psi}_{ij,mn} \delta \psi_{ij}. \end{aligned} \quad (27)$$

Gauss's divergence theorem can now be applied to give, for the first, third, fifth, seventh and the ninth terms on the right hand side

of Eq. (26), using Eq. (27),

$$\begin{aligned} \int_{t_0}^{t_1} \int_V \rho v_i v_j \delta \dot{\phi}_{i,j} dV dt &= \int_{t_0}^{t_1} \int_S \rho v_i v_j n_j \delta \dot{\phi}_i dS dt, \\ \int_{t_0}^{t_1} \int_V \rho v_j \dot{\phi}_i \delta \dot{\phi}_{i,j} dV dt &= \int_{t_0}^{t_1} \int_S \rho v_j \dot{\phi}_i n_j \delta \dot{\phi}_i dS dt \\ &- \int_{t_0}^{t_1} \int_V \rho v_j \dot{\phi}_{i,j} \delta \dot{\phi}_i dV dt, \\ \int_{t_0}^{t_1} \int_V \rho v_m v_j \dot{\phi}_{i,m} \delta \dot{\phi}_{i,j} dV dt &= \int_{t_0}^{t_1} \int_S \rho v_m v_j \dot{\phi}_{i,m} n_j \delta \dot{\phi}_i dS dt \\ &- \int_{t_0}^{t_1} \int_V \rho v_m v_j \dot{\phi}_{i,m,j} \delta \dot{\phi}_i dV dt, \\ \int_{t_0}^{t_1} \int_V \frac{1}{3} \rho d^2 v_m \dot{\psi}_{ij} \delta \psi_{ij,m} dV dt &= \int_{t_0}^{t_1} \int_S \frac{1}{3} \rho d^2 v_m \dot{\psi}_{ij} n_m \delta \psi_{ij} dS dt \\ &- \int_{t_0}^{t_1} \int_V \frac{1}{3} \rho d^2 v_m \dot{\psi}_{ij,m} \delta \psi_{ij} dV dt, \\ \int_{t_0}^{t_1} \int_V \frac{1}{3} \rho d^2 v_m v_n \dot{\psi}_{ij,m} \delta \psi_{ij,n} dV dt &= \int_{t_0}^{t_1} \int_S \frac{1}{3} \rho d^2 v_m v_n \dot{\psi}_{ij,m} n_n \delta \psi_{ij} dS dt \\ &- \int_{t_0}^{t_1} \int_V \frac{1}{3} \rho d^2 v_m v_n \dot{\psi}_{ij,mn} \delta \psi_{ij} dV dt. \end{aligned} \quad (28)$$

Governing equations of motion are derived using Hamilton's principle, written as

$$\delta \int_{t_0}^{t_1} (\bar{T} - \bar{W} + \bar{W}_{ext}) dt = 0. \quad (29)$$

Substituting Eqs. (16), (17), and (26) in Eq. (29), and using Eq. (28), result in the balance equations

$$\begin{aligned} (\tau_{ij} + \sigma_{ij})_{,j} + f_i - 2\rho v_j \dot{\phi}_{i,j} - \rho v_m v_j \dot{\phi}_{i,mj} &= \rho \ddot{\phi}_i, \\ \mu_{ijk,k} + \sigma_{ij} + \Phi_{ij} - \frac{2}{3} \rho d^2 v_m \dot{\psi}_{ij,m} - \frac{1}{3} \rho d^2 v_m v_n \dot{\psi}_{ij,mn} &= \frac{1}{3} \rho d^2 \ddot{\psi}_{ij}, \end{aligned} \quad (30)$$

Moreover, the advantage of the variational approach is that we can clearly define the boundary conditions. The two natural boundary conditions given in terms of the stress measures are

$$\begin{aligned} (\tau_{ij} + \sigma_{ij} - \rho v_i v_j - \rho v_j \dot{\phi}_i - \rho v_m v_j \dot{\phi}_{i,m}) n_j &= t_i, \\ (\mu_{ijk} - \frac{1}{3} \rho d^2 v_k \dot{\psi}_{ij} - \frac{1}{3} \rho d^2 v_m v_k \dot{\psi}_{ij,m}) n_k &= T_{ij}. \end{aligned} \quad (31)$$

Finally, displacement equations of motion can be derived, using the constitutive equations of Eq. (12) in Eq. (30). Considering null volumic forces and volumic double forces, the displacement equations of motion are

$$\begin{aligned} (C_{ijkl}^m + C_{ijkl}^m) \dot{\phi}_{k,lj} - C_{ijkl}^m \psi_{kl,j} - 2\rho v_j \dot{\phi}_{i,j} - \rho v_m v_j \dot{\phi}_{i,mj} &= \rho \ddot{\phi}_i, \\ (A_{ijklmn}^g + A_{ijklmn}^u) \psi_{lm,nk} + C_{ijkl}^m \dot{\phi}_{k,l} - C_{ijkl}^m \psi_{kl} - \frac{2}{3} \rho d^2 v_m \dot{\psi}_{ij,m} \\ - \frac{1}{3} \rho d^2 v_m v_n \dot{\psi}_{ij,mn} &= \frac{1}{3} \rho d^2 \ddot{\psi}_{ij}. \end{aligned} \quad (32)$$

### 3. Dispersion analysis in axially moving 1D continuum

In what follows, we consider the longitudinal wave propagating along  $X_1$  axis in a one dimensional infinite continuum moving with velocity  $v_1$  in  $X_1$  direction between two fixed ends. A schematic of the general problem has been shown in Fig. 2. A 1D homogenous continuum can be non-homogenous in the RVE in terms of micro-scale mass density and grain-pair interactions. Fig. 2 depicts the former, while the latter is rather difficult to picturize. Our focus in this section is along the assumptions made to derive Eq. (32), and therefore we assume a constant micro-scale mass density. Therefore, the inhomogeneity only comes from grain-pair interactions within the RVE. For brevity, the subscript 1 will be dropped in the following equations. The displacement equations of motion in this case are

$$\begin{aligned} (P + Q) \dot{\phi}_{,xx} - Q \psi_{,x} - 2\rho v \dot{\phi}_{,x} - \rho v^2 \dot{\phi}_{,xx} &= \rho \ddot{\phi}, \\ R \psi_{,xx} + Q \dot{\phi}_{,x} - Q \psi - 2I v \dot{\psi}_{,x} - I v^2 \psi_{,xx} &= I \ddot{\psi}, \end{aligned} \quad (33)$$

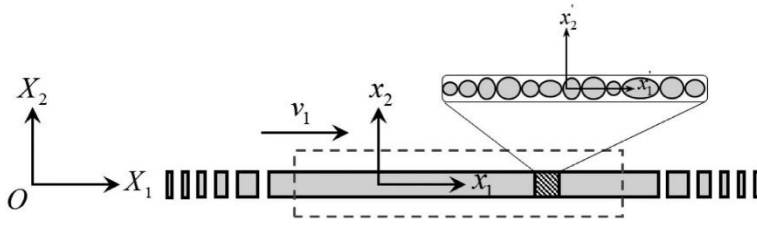


Fig. 2. Schematic of the 1D axially moving media with granular microstructure. A material point in the macro-scale coordinate system is itself a collection of grains that can differ in micro-density, micro-morphology and micro-mechanical properties.

where the symbols  $P$ ,  $Q$ ,  $R$ , and  $I$  have been used for conciseness, and have the values of  $C_{1111}^M$ ,  $C_{1111}^m$ ,  $A_{111111}^g + A_{111111}^u$  and  $\frac{1}{3}\rho d^2$ , respectively. Eq. (33) are coupled partial differential equations that describe axial deformations of the 1D continuum fragment confined within the shown dashed boundaries in Fig. 2. As discussed before, while the material is moving, the control volume is kept constant. The dashed boundary is assumed to be sufficiently large that the waves do not reach the boundaries, i.e., reflection of the waves is neglected [2]. This assumption has been taken to facilitate the comparison between the dispersive behavior of non-moving infinite 1D continuum [31,32] and the current problem. The convective acceleration terms in Eq. (33), i.e.  $2v\dot{\phi}_{,x}$  and  $2v\dot{\psi}_{,x}$ , (referred as skew-symmetric, gyroscopic, or with analogy to [12] Coriolis) may result in complex modes with non-constant phase in the free motion analysis [14]. The acceleration terms  $\dot{\phi}$  and  $\dot{\psi}$  are called local accelerations, while  $v^2\dot{\phi}_{,xx}$  and  $v^2\dot{\psi}_{,xx}$  are centripetal components.

For a sufficiently large span length of the control volume, the solution is represented as d'Alembert waves by assuming harmonic solutions for both position  $x$  and time  $t$  [12]. Considering the solutions in Eq. (33) to be plane harmonic waves [31,32,38] results in oscillatory motion in both time and spatial coordinate, written as

$$\tilde{\phi} = \text{Re}(Aie^{i(kx-\omega t)}), \quad \tilde{\psi} = \text{Re}(Be^{i(kx-\omega t)}), \quad (34)$$

where  $k$  is the wavenumber,  $\omega$  is the angular frequency,  $A$  and  $B$  are the complex amplitudes of the macro-displacement and micro-displacement-gradient, respectively, and  $i^2 = -1$ . Denoting wavelength by  $\lambda$ , the relation between the wavenumber and wavelength is expressed as

$$k = \frac{2\pi}{\lambda}, \quad (35)$$

and the frequency  $f$  is related to  $\omega$  with the expression

$$\omega = 2\pi f. \quad (36)$$

In what follows, for brevity, the term “frequency” is used for  $\omega$  instead of the term “angular frequency”. By substituting the solutions in Eq. (34) in Eq. (33), we have the system of linear equations in the matrix form

$$\begin{bmatrix} c_0^2 k^2 - v^2 k^2 + 2v\omega k & c_A^2 k \\ \frac{k}{p^2} & c_1^2 k^2 - v^2 k^2 + \frac{1}{p^2} + 2v\omega k \end{bmatrix} \begin{bmatrix} A \\ B \end{bmatrix} = \omega^2 \begin{bmatrix} A \\ B \end{bmatrix}, \quad (37)$$

where we have introduced the velocities  $c_0$ ,  $c_1$ ,  $c_A$ , and characteristic time  $p$  as [30–32]

$$c_0^2 = \frac{P+Q}{\rho}, \quad c_1^2 = \frac{R}{I}, \quad c_A^2 = \frac{Q}{\rho}, \quad p^2 = \frac{I}{Q}. \quad (38)$$

In order to obtain the dimensionless form of the equations, we define, the dimensionless wavenumber and frequency as

$$\xi = pc_0 k, \quad \eta = p\omega, \quad (39)$$

and dimensionless velocities as

$$\begin{aligned} \gamma_A &= \frac{c_A}{c_0} = \sqrt{\frac{Q}{P+Q}}, \\ \gamma_1 &= \frac{c_1}{c_0} = \sqrt{\frac{R}{P+Q}} \sqrt{\frac{\rho}{I}}, \\ \hat{v} &= \frac{v}{c_0}. \end{aligned} \quad (40)$$

Utilizing the dimensionless parameters defined in Eqs. (39) and (40), we obtain the following solutions for the dimensionless frequency

$$\begin{aligned} \eta &= \hat{v}\xi + \frac{1}{2} \sqrt{2\gamma_1^2 \xi^2 + 2\xi^2 + 2\sqrt{\gamma_1^4 \xi^4 - 2\gamma_1^2 \xi^2 + 2\gamma_1^2 \xi^2 + \xi^4 + 4\gamma_A^2 \xi^2 - 2\xi^2 + 1} + 2}, \\ \eta &= \hat{v}\xi - \frac{1}{2} \sqrt{2\gamma_1^2 \xi^2 + 2\xi^2 + 2\sqrt{\gamma_1^4 \xi^4 - 2\gamma_1^2 \xi^2 + 2\gamma_1^2 \xi^2 + \xi^4 + 4\gamma_A^2 \xi^2 - 2\xi^2 + 1} + 2}, \\ \eta &= \hat{v}\xi + \frac{1}{2} \sqrt{2\gamma_1^2 \xi^2 + 2\xi^2 - 2\sqrt{\gamma_1^4 \xi^4 - 2\gamma_1^2 \xi^2 + 2\gamma_1^2 \xi^2 + \xi^4 + 4\gamma_A^2 \xi^2 - 2\xi^2 + 1} + 2}, \\ \eta &= \hat{v}\xi - \frac{1}{2} \sqrt{2\gamma_1^2 \xi^2 + 2\xi^2 - 2\sqrt{\gamma_1^4 \xi^4 - 2\gamma_1^2 \xi^2 + 2\gamma_1^2 \xi^2 + \xi^4 + 4\gamma_A^2 \xi^2 - 2\xi^2 + 1} + 2}. \end{aligned} \quad (41)$$

Eq. (41) are the most general form of the frequency solutions for the problem at hand.

#### 4. Effects of axial velocity and granular microstructure

Before analyzing these general solutions, we briefly study the simplified forms of the problem. As a special simplified case where the microstructure, and correspondingly the material properties related to microstructure are absent, Eq. (33) can be simplified. Upon substituting plane wave solution form of the left equation in Eq. (34) and nondimensionalizing the axial velocity using the last of Eq. (40), the following dispersion relation is found

$$(1 - \hat{v}^2)k^2 + \frac{2\hat{v}\omega k}{c_0} - \frac{\omega^2}{c_0^2} = 0. \quad (42)$$

Eq. (42) is similar to what has been presented in [2], and after solving for  $\omega$  yields

$$\omega = c_0(\hat{v} \pm 1)k. \quad (43)$$

By multiplying both sides of Eq. (43) by a nonzero characteristic time constant  $p'$ , the dimensionless form of Eq. (43) is written as

$$\hat{\omega} = (\hat{v} \pm 1)\hat{k}, \quad (44)$$

where

$$\hat{\omega} = p'\omega, \quad \hat{k} = p'c_0 k, \quad (45)$$

are the dimensionless frequency and wavenumber, respectively. Eq. (44) shows a non-dispersive non-symmetric behavior in the propagating forward and backward wave branches for an axially moving long thin 1D continuum (also referred to as rod in [2]). Fig. 3 shows the two forward and backward branches for vanishing and non-zero values of  $\hat{v}$ . Clearly, for the non-moving (stationary) case where  $\hat{v} = 0$ , the dimensionless phase velocity ( $\hat{\omega}/\hat{k}$ ) and dimensionless group velocity ( $d\hat{\omega}/d\hat{k}$ ) of the forward and backward wave branches are equal in magnitude and different in sign, suggesting existence of symmetry in the propagating waves. In this case, the slopes of the wave branches are unity and Eq. (44) simplifies to the dispersion relation of the classical 1D wave and suggests elastic reciprocity in the forward and backward waves.

For the case where  $\hat{v} \neq 0$ , the effect of axial velocity on the dispersion curve can be analyzed using Eq. (44). In this case, the phase and group velocities (the slopes) for the forward and backward wave branches are



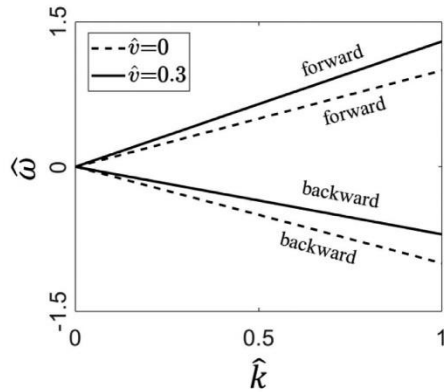


Fig. 3. Dispersion curves for an axially moving 1D continuum without microstructure for two cases of zero and non-zero dimensionless velocities.

$\hat{\omega} + 1$  and  $\hat{\omega} - 1$ , respectively. This suggests that the effect of axial velocity on the dimensionless phase and group velocity values is observed as a translation by the amount of the dimensionless axial velocity  $\hat{v}$ . This change in velocities is attributed to a linear momentum bias resulting from the axial velocity  $\hat{v}$  [2]. The dimensionless form of the dispersion relation for a non-moving 1D medium based upon classical analysis described as  $\hat{\omega} = \pm \hat{k}$  undergoes a shift in frequency by the amount of  $\hat{v}\hat{k}$ . When the dimensionless axial velocity is less than unity (which corresponds to axial velocity less than the wave velocity in non-moving medium), the phase and group velocities for the forward wave are positive in sign, while those for the backward wave are negative in sign. For the extreme cases, where the dimensionless axial velocity is 1 or greater than 1, the predictions of Eq. (44) are the following. For dimensionless axial velocity  $\hat{v} = 1$ , the backward wave disappears and only one forward wave propagates. The phase (and group) velocity for this forward propagating wave is twice that for the non-moving medium. In this case, the stationary observer on one of the end supports will not experience any vibration. For dimensionless axial velocities larger than unity (corresponding to axial velocities larger than the wave velocity of the non-moving medium), the backward wave flips over the forward side. The stationary observer on the support corresponding to the backward wave will not experience and vibration, while the observer on the support corresponding to the forward wave will see two wave arrivals. Based on Eq. (44), for any real wavenumber, the frequency is always real, therefore, there is no instability or attenuation for these propagating waves. It is also notable that in the case of classical analysis, the absence of microstructural effects lead to non-dispersive behavior as

both dimensionless phase and group velocities are equal and constant for each forward and backward wave.

For a material with granular microstructure, however, the wave propagation analysis exhibits dispersive behavior, i.e., the wave velocities are functions of wavenumber (or frequency). For vanishing values of axial velocity (stationary case), solutions presented in Eq. (41) take the form [31]

$$\eta = \pm \frac{1}{2} \sqrt{2\gamma_1^2 \xi^2 + 2\xi^2 + 2\sqrt{\gamma_1^4 \xi^4 - 2\gamma_1^2 \xi^4 + 2\gamma_1^2 \xi^2 + \xi^4 + 4\gamma_A^2 \xi^2 - 2\xi^2 + 1} + 2},$$

$$\eta = \pm \frac{1}{2} \sqrt{2\gamma_1^2 \xi^2 + 2\xi^2 - 2\sqrt{\gamma_1^4 \xi^4 - 2\gamma_1^2 \xi^4 + 2\gamma_1^2 \xi^2 + \xi^4 + 4\gamma_A^2 \xi^2 - 2\xi^2 + 1} + 2}. \tag{46}$$

Dispersion curves for two different granular structures for zero axial velocity using Eq. (46) have been plotted in Fig. 4. The material parameters chosen for Fig. 4(a) and (b) are  $\gamma_A = 0.7$ ,  $\gamma_1 = 0.05$ , and  $\gamma_A = 0.5$ ,  $\gamma_1 = 0.3$ , respectively. These values have been chosen to show two different cases of wave propagation in terms of the existence of stopbands. Note that for a specific granular structure, identification of material parameters can be done, for instance, as has been described in [40]. The frequency solutions in Eq. (46) lead to the emergence of four wave branches in two groups, two forward and two backward waves, with each group having one acoustic and one optical branch. While the acoustic branches start at zero frequency and zero wavenumber, for the optical branches zero wavenumber produces a dimensionless frequency of unity, meaning that for dimensionless frequencies smaller than unity there is no optical branch. In this case, the forward and backward waves are symmetrically propagating as their governing equations are different only by a sign. This symmetry in propagating waves can also be attributed to the lack of linear momentum bias in non-moving media. Different grain-pair interactions and/or micro-morphological aspects in the microstructure of the granular material result in different values in stiffness tensors, which consequently lead to different behaviors in the propagation of waves. Two cases wherein one shows frequency band gaps and the other does not, have been exemplified in Fig. 4(a) and (b), respectively. In both cases, corresponding phase and group velocities for each wave branch have the same direction. In other words, for the forward wave branches, phase and group velocities are positive in sign, and for the backward wave branches, phase and group velocities are all negative in sign. Note that in these cases the frequency solutions are all real, excluding instability or attenuation.

For a nonzero value of the dimensionless axial velocity,  $\hat{v}$ , however, there exists asymmetry in propagation of the forward and backward wave branches. The asymmetry coming from the axially moving velocity of the medium, along with the microstructural length and inertial effects, brings about interesting observations in wave propagation phenomenon. For the same value of geometrical and mechanical properties of the granular structure studied in Fig. 4(a) and (b), the dispersion

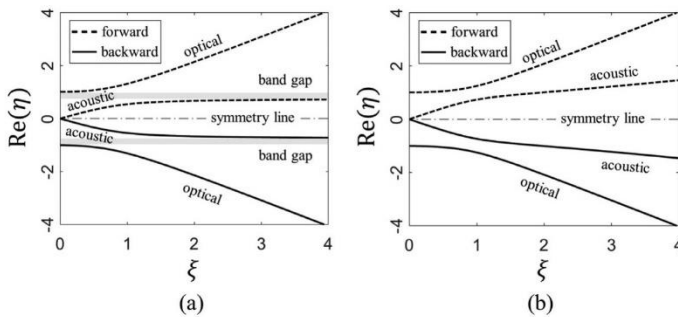


Fig. 4. Dispersion curves for non-moving 1D materials with granular microstructure. (a) The case of  $\gamma_A = 0.7$ ,  $\gamma_1 = 0.05$ . (b) The case of  $\gamma_A = 0.5$ ,  $\gamma_1 = 0.3$ .

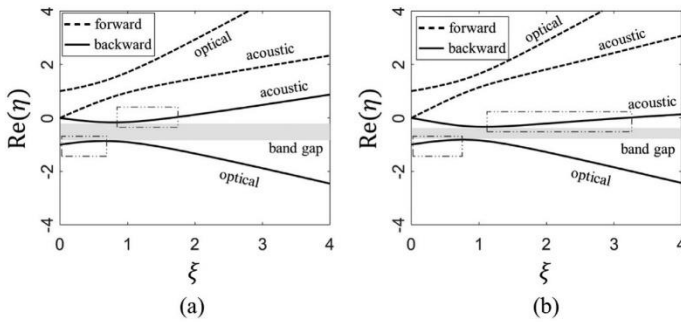


Fig. 5. Dispersion curves for axially moving 1D materials with granular microstructure with dimensionless axial velocity  $\hat{v} = 0.4$ . (a) The case of  $\gamma_A = 0.7$ ,  $\gamma_1 = 0.05$ . (b) The case of  $\gamma_A = 0.5$ ,  $\gamma_1 = 0.3$ .

curves for  $\hat{v} = 0.4$  have been plotted in Fig. 5(a) and (b), respectively, based upon Eq. (41). In this example the dimensionless axial velocity is taken to be 40% (which can be considered somewhat large) of the conventional wave velocity,  $c_0$ , such that the trends in the plots are clearly visible.

For the case of Fig. 5(a), a comparison with Fig. 4(a) reveals narrowing and widening in the frequency band gaps in the forward and backward waves, respectively. Of course, the axial velocity in this case is large enough that the stopband for the forward waves has disappeared. As is seen from Fig. 5(a), the symmetry between forward and backward waves is broken. This leads to difference in velocities in the forward and backward acoustic, as well as optical, wave branches. The same effects can also be seen by comparing Figs. 4(b) and 5(b). In this case, non-existing frequency band gaps in the backward waves in Fig. 4(b) appear for the case of the moving granular medium of Fig. 5(b). This created band gap is “induced” by the axial velocity of the granular medium, and is in contrast to the “inherent” band gap shown by the non-moving granular medium. One remarkable result is that in frequency ranges corresponding to the band gap in the backward waves, the stationary observer on one end support experiences the vibration, while the stationary observer on the other end support does not. Using Eq. (41), for axially moving 1D granular media, the effect of axial velocity on the dimensionless phase and group velocity values is seen to be a translation by the amount of the dimensionless axial velocity  $\hat{v}$ . This observation is similar to the findings for axially moving 1D continuum without microstructure. Interestingly, the effect of axial velocity on the dispersion curve also follows that of an axially moving 1D material without microstructure, where the frequency solutions undergo a shift by the amount of  $\hat{v}\hat{k}$ . When increasing the value of the dimensionless axial velocity,  $\hat{v}$ , the forward waves band gap (if exists) starts disappearing, and the backward waves band gap (if exist) starts growing (or appearing and growing if it did not exist). As the value of the axial velocity reaches  $\hat{v} = 1$ , Eq. (41) predicts a complete reversal of the backward acoustic branch (in contrast to partial reversal in only certain wavenumbers observed in both cases in Fig. 5 for  $\hat{v} = 0.4$ ), meaning that the acoustic branch is not propagated backward. The optical backward branch still starts at a dimensionless frequency of magnitude 1 with negative phase velocity and positive group velocity, but reaches the line  $\eta = 0$  as its asymptote in large wavenumbers, suggesting that the backward optical branch disappears for large wavenumbers. As the value of the dimensionless axial velocity  $\hat{v}$  becomes larger than unity, the backward optical branch starts propagating as a forward wave, and hence, there will be no waves propagating backwards and four wave branches propagating forward. In this case, the stationary receiver on the support corresponding to the backward direction will not experience any vibration.

One other interesting observation from Fig. 5 is the presence of regions (shown in the plots by dash-dotted blocks) in which the sign of the phase and group velocities are different for the particular wave branches. This phenomenon is generally known as negative group ve-

locity (NGV). In the case of NGV, “the peak of the transmitted pulse exits the material before the peak of the incident pulse enters the material” [41]. A consequence of NGV is that the peak of the pulse propagates in the opposite direction. However, energy maintains forward flow [42]. NGV has also been recognized for deformation waves in microstructured solids with multiple scales [43] and for granular media with negative grain-pair second gradient stiffnesses [31].

## 5. Summary and conclusions

In this paper, the governing equations of motion for an axially moving material with granular microstructure were derived using Hamilton’s Principle. Subsequently, the predicted dispersive behavior of axially moving 1D materials with granular microstructure was explored. The study presented can be summarized as follows: 1) The special simplified case where the micro-scale effect is absent results in asymmetry in the forward and backward propagating waves for non-zero axial velocities, but there is no dispersion as has been reported in the literature. This simplified case considers the medium as a classical Cauchy material resulting in no distinction between phase and group velocities for each forward and backward waves. 2) For a non-moving medium with granular microstructure, there is symmetry in propagating forward and backward waves, but the behavior is dispersive. There are two wave branches in forward and backward waves, one acoustic and one optical branch, where the optical branches start at dimensionless frequency of magnitude 1 corresponding to zero wavenumber, and the acoustic branches start at dimensionless frequency and wavenumber of zero. 3) For an axially moving medium with granular microstructure, asymmetry in propagation of wave branches for forward and backward waves is observed. Such an asymmetry results in different phase and group velocities for forward and backward waves (for both acoustic and optical branches), narrowing the frequency band gaps range for forward waves, and widening frequency range for which backward stopband exists. 4) In the cases where no band gap is observed for non-moving medium with granular microstructure, it is possible that the stopband is created in the backward propagating waves. This generally means that the backward waves in certain frequencies die exponentially in space, and therefore, there is no vibration sensed by the support receiving the backward waves if the excitation is in the bandgap range. 5) Finally, one notices regions where the phase and group velocities are different in sign, resulting in the phenomenon called negative group velocity.

In what was presented, the effects of material parameters on the dispersive behavior was shown using two examples of granular structures. The macro-mechanical parameters in the studied theory are functions of grain-pair stiffnesses introduced in [33]. For a granular material, one can obtain the macro-mechanical parameters using sufficient experiments with proper boundary conditions, or using numerical techniques such as one described in [40] for a 2D granular material. Such parameters can then be fed into the continuum models to investigate



the dispersive behavior of such media, using the approach introduced in this paper. Clearly, the stopbands created by the axial velocity and the non-symmetric dispersive behavior of axially moving granular materials should be considered in engineering design and application, especially when stop-band filtering is of interest. The model presented here can be used to analyze dynamic behavior of materials with granular microstructure when axially moved between two fixed ends. Solution of inverse problems is also possible using granular micromechanics approach. Several recent published works have studied stationary granular metamaterials' behavior where grains interactions can be customized to give preferred dynamic characteristics (see the review paper in [44]). The analysis provided here can be used to obtain parameters needed for the design of granular metamaterial for particular applications of axially moving medium in which vibration control or stopbands over certain frequency range is required. The approach is rich as it can treat granular metamaterials with periodic RVEs comprising more than one type of grain, and is especially fruitful in treating physics involving axially moving media in which non-local and higher gradient effects are important, e.g., biomedical nanorobotics devices (see for example [20,22]). Further, the axially moving systems comprising granular metamaterials with dielectric properties have the potential to be further tuned for their wave propagation characteristics to give band gaps in desired frequency ranges [32]. The granular micromechanics approach for design and analysis of the mentioned problem is as follows. Requiring a granular metamaterial for a particular application with a desired dispersive behavior, one can find the macro-mechanical parameters leading to the desired behavior, obtaining equalities and inequalities regarding the grain-pair stiffness values. This is possible since the explicit form of the functions are available in the theory of granular micromechanics, providing a complete domain to search for possible solutions. The obtained microstructural parameters can then be realized through additive manufacturing techniques, as for pantographic metamaterials [45–47], to develop a desired granular metamaterial. Such inverse approach to design granular metamaterials using granular micromechanics theory will be pursued in future publications.

#### Statement of competing interest

None.

#### Acknowledgements

This research is supported in part by the United States National Science Foundation grant CMMI –1727433.

#### References

- Marynowski K, Kapitaniak T. Dynamics of axially moving continua. *Int J Mech Sci* 2014;81:26–41. doi:10.1016/j.ijmechsci.2014.01.017.
- Attarzadeh MA, Nough M. Elastic wave propagation in moving phononic crystals and correlations with stationary spatiotemporally modulated systems. *AIP Adv* 2018;8:105302. doi:10.1063/1.5042252.
- Liu JJ, Li C, Fan XL, Tong LH. Transverse free vibration and stability of axially moving nanoplates based on nonlocal elasticity theory. *Appl Math Model* 2017;45:65–84. doi:10.1016/j.apm.2016.12.006.
- Lowe RL, Cooley CG. A Newtonian mechanics formulation for the vibration of translating and rotating elastic continua. *J Vib Control* 2019;25(10):1639–52. doi:10.1177/1077546319825675.
- Tang Y, Luo E, Yang X. Complex modes and traveling waves in axially moving Timoshenko beams. *Appl Math Mech* 2018;39:597–608. doi:10.1007/s10483-018-2312-8.
- Barakat R. Transverse vibrations of a moving thin rod. *J Acoust Soc Am* 1968;43:533–9. doi:10.1121/1.1910862.
- Steinboeck A, Baumgart M, Stadler G, Saxinger M, Kugi A. Dynamical models of axially moving rods with tensile and bending stiffness. *IFAC-PapersOnLine* 2015;48:598–603. doi:10.1016/j.ifacol.2015.05.041.
- Li Y, Aron D, Rahn CD. Adaptive vibration isolation for axially moving strings: theory and experiment. *Automatica* 2002;38:379–90. doi:10.1016/S0005-1098(01)00219-9.
- Tan CA, Ying S. Active wave control of the axially moving String: theory and experiment. *J Sound Vib* 2000;236:861–80. doi:10.1006/jsvl.2000.3040.
- Michon G, Manin I, Remond D, Dufour R, Parker RG. Parametric instability of an axially moving belt subjected to multifrequency excitations: experiments and analytical validation. *J Appl Mech* 2008;75:41004–8.
- Pellicano F, Fregolent A, Bertuzzi A, Vestroni F. Primary and parametric non-linear resonances of a power transmission belt: experimental and theoretical analysis. *J Sound Vib* 2001;244:669–84. doi:10.1006/jsvl.2000.3488.
- Wickert JA, Mote CD. Linear transverse vibration of an axially moving string-particle system. *J Acoust Soc Am* 1988;84:963–9. doi:10.1121/1.396611.
- Wickert JA, Mote CD. On the energetics of axially moving continua. *J Acoust Soc Am* 1989;85:1365–8. doi:10.1121/1.397418.
- Wickert JA, Mote CDJ. Classical vibration analysis of axially moving continua. *J Appl Mech* 1990;57:738–44.
- Vetyukov Y. Non-material finite element modelling of large vibrations of axially moving strings and beams. *J Sound Vib* 2018;414:299–317. doi:10.1016/j.jsv.2017.11.010.
- Chen L-Q. Analysis and control of transverse vibrations of axially moving strings. *Appl Mech Rev* 2005;58:91–116.
- Sorokin VS, Thomsen JJ. Wave propagation in axially moving periodic strings. *J Sound Vib* 2017;393:133–44. doi:10.1016/j.jsv.2017.01.014.
- Yuh J, Young T. Dynamic modeling of an axially moving beam in rotation: simulation and experiment. *J Dyn Syst Meas Control* 1991;113:34–40.
- Duan Y-C, Wang J-P, Wang J-Q, Liu Y-W, Shao F. Theoretical and experimental study on the transverse vibration properties of an axially moving nested cantilever beam. *J Sound Vib* 2014;333:2885–97. doi:10.1016/j.jsv.2014.02.021.
- Li C. Nonlocal thermo-electro-mechanical coupling vibrations of axially moving piezoelectric nanobeams. *Mech Based Des Struct Mach* 2017;45:463–78.
- Shin C, Kim W, Chung J. Free in-plane vibration of an axially moving membrane. *J Sound Vib* 2004;272:137–54. doi:10.1016/S0022-460X(03)00323-7.
- Li C, Liu JJ, Cheng M, Fan XL. Nonlocal vibrations and stabilities in parametric resonance of axially moving viscoelastic piezoelectric nanoplate subjected to thermo-electro-mechanical forces. *Compos Part B Eng* 2017;116:153–69.
- Gugliuzza A, Politano A, Drioli E. The advent of graphene and other two-dimensional materials in membrane science and technology. *Curr Opin Chem Eng* 2017;16:78–85. doi:10.1016/j.coche.2017.03.003.
- Politano A, Argurio P, Di Profio G, Sanna V, Cupolillo A, Chakraborty S, et al. Photothermal membrane distillation for seawater desalination. *Adv Mater* 2017;29:1603504. doi:10.1002/adma.201603504.
- Politano A, Cupolillo A, Di Profio G, Arafat HA, Chiarello G, Curcio E. When plasmonics meets membrane technology. *J Phys Condens Matter* 2016;28:363003. doi:10.1088/0953-8984/28/36/363003.
- Verre S, Ombres L, Politano A. Evaluation of the free-vibration frequency and the variation of the bending rigidity of graphene nanoplates: the role of the shape geometry and boundary conditions. *J Nanosci Nanotechnol* 2017;17:8827–34. doi:10.1166/jnn.2017.13906.
- Politano A, Marino AR, Campi D, Farías D, Miranda R, Chiarello G. Elastic properties of a macroscopic graphene sample from phonon dispersion measurements. *Carbon N Y* 2012;50:4903–10. doi:10.1016/j.carbon.2012.06.019.
- Arani AG, Haghparast E, BabaAkbar Zarei H. Nonlocal vibration of axially moving graphene sheet resting on orthotropic visco-Pasternak foundation under longitudinal magnetic field. *Phys B Condens Matter* 2016;495:35–49. doi:10.1016/j.physb.2016.04.039.
- Banichuk N, Jeronen J, Neittaanmäki P, Saksa T, Tuovinen T. Mechanics of moving materials, 207. Springer International Publishing; 2014. doi:10.1007/978-3-319-01745-7.
- Berezovski A, Engelbrecht J, Salupere A, Tamm K, Peets T, Berezovski M. Dispersive waves in microstructured solids. *Int J Solids Struct* 2013;50:1981–90. doi:10.1016/j.jlstr.2013.02.018.
- Misra A, NejadSadeghi N. Longitudinal and transverse elastic waves in 1D granular materials modeled as micromorphic continua. *Wave Motion* 2019;90:175–95. doi:10.1016/j.wavemoti.2019.05.005.
- NejadSadeghi N, Placidi L, Romeo M, Misra A. Frequency band gaps in dielectric granular metamaterials modulated by electric field. *Mech Res Commun* 2019;95. doi:10.1016/j.mechrescom.2019.01.006.
- Misra A, Poorsolhjouy P. Granular micromechanics based micromorphic model predicts frequency band gaps. *Contin Mech Thermodyn* 2016;28:215–34. doi:10.1007/s00161-015-0420-y.
- Mikhasev G, Avdeichik E, Prikazhnikov D. Free vibrations of nonlocally elastic rods. *Math Mech Solids* 2018;24:1279–93. doi:10.1177/1081286518785942.
- Xu X-J, Zheng M-L, Wang X-C. On vibrations of nonlocal rods: boundary conditions, exact solutions and their asymptotics. *Int J Eng Sci* 2017;119:217–31. doi:10.1016/j.ijengsci.2017.06.025.
- Misra A, Poorsolhjouy P. Grain- and macro-scale kinematics for granular micromechanics based small deformation micromorphic continuum model. *Mech Res Commun* 2017;81:1–6. doi:10.1016/j.mechrescom.2017.01.006.
- Misra A, Placidi L, Turco E. Variational methods for continuum models of granular materials, 2019, 1–11. doi:10.1007/978-3-662-53605-6\_343-1.
- Mindlin RD. Micro-structure in linear elasticity. *Arch Ration Mech Anal* 1964;16:51–78. doi:10.1007/BF00248490.
- Thurman AL, Mote CDJ. Free, periodic, nonlinear oscillation of an axially moving strip. *J Appl Mech* 1969;36:83–91.
- Misra A, Poorsolhjouy P. Identification of higher-order elastic constants for grain assemblies based upon granular micromechanics. *Math Mech Complex Syst* 2015;3:285–308. doi:10.2140/memocs.2015.3.285.
- Gehring GM, Schweinsberg A, Barsi C, Kostinski N, Boyd RW. Observation of backward pulse propagation through a medium with a negative group velocity. *Science* 2006;312:895 (80-).P-897. doi:10.1126/science.1124524.

- [42] Peets T, Kartofelev D, Tamm K, Engelbrecht J. Waves in microstructured solids and negative group velocity. *EPL (Europhysics Lett)* 2013;103:16001. doi:10.1209/0295-5075/103/16001.
- [43] Tamm K, Peets T, Engelbrecht J, Kartofelev D. Negative group velocity in solids. *Wave Motion* 2017;71:127–38. doi:10.1016/J.WAVEMOTI.2016.04.010.
- [44] Kim E, Yang J. Wave propagation in granular metamaterials. *Funct Compos Struct* 2019;1:12002.
- [45] Nejadi Sadeghi N., De Angelo M., Drobnicki R., Lekszycki T., dell'Isola F., Misra A. Parametric experimentation on pantographic unit cells reveals local extremum configuration. *Exp Mech* 2019;1–13. doi:10.1007/s11340-019-00515-1.
- [46] dell'Isola F., Seppecher P., Spagnuolo M., Barchiesi E., Hild F., Lekszycki T., et al. Advances in pantographic structures: design, manufacturing, models, experiments and image analyses. *Contin Mech Thermodyn* 2019;1–52. doi:10.1007/s00161-019-00806-x.
- [47] dell'Isola F, Turco E, Misra A, Vangelatos Z, Grigoropoulos C, Melissinaki V, et al. Force-displacement relationship in micro-metric pantographs: experiments and numerical simulations. *Comptes Rendus Mécanique* 2019;347:397–405. doi:10.1016/J.CRME.2019.03.015.



## Appendix E: Paper P5

### Title:

Role of higher-order inertia in modulating elastic wave dispersion in materials with granular microstructure

### Authors:


Nima NejadiSadeghi

Anil Misra

### Journal:

International Journal of Mechanical Sciences

### Permission from journal:



Role of higher-order inertia in modulating elastic wave dispersion in materials with granular microstructure

Author: Nima NejadiSadeghi, Anil Misra  
Publication: International Journal of Mechanical Sciences  
Publisher: Elsevier  
Date: 1 November 2020

© 2020 Elsevier Ltd. All rights reserved.

---

Journal Author Rights

Please note that, as the author of this Elsevier article, you retain the right to include it in a thesis or dissertation, provided it is not published commercially. Permission is not required, but please ensure that you reference the journal as the original source. For more information on this and on your other retained rights, please visit: <https://www.elsevier.com/about/our-business/policies/copyright#Author-rights>

[BACK](#) [CLOSE WINDOW](#)

### Credit authorship statement:

A.M. and N.N. conceived the idea. N.N. developed the model and performed calculations and analysis. All authors contributed to the discussion of all aspects of this work. N.N. wrote the manuscript. All authors edited the manuscript.



Contents lists available at ScienceDirect

## International Journal of Mechanical Sciences

journal homepage: [www.elsevier.com/locate/ijmecsci](http://www.elsevier.com/locate/ijmecsci)

## Role of higher-order inertia in modulating elastic wave dispersion in materials with granular microstructure

Nima Nejadi Sadeghi<sup>a</sup>, Anil Misra<sup>b,\*</sup><sup>a</sup> Mechanical Engineering Department, University of Kansas, 1530 W 15th Street, Learned Hall, Lawrence, KS 66047-7609, United States<sup>b</sup> Civil, Environmental and Architectural Engineering Department, University of Kansas, 1530 W 15th Street, Learned Hall, Lawrence, KS 66045-7609, United States

## ARTICLE INFO

## Keywords:

Granular microstructure  
 Granular micromechanics  
 Higher-order inertia  
 Dispersion relation  
 Frequency band gaps  
 Granular metamaterials

## ABSTRACT

(Meta-) materials with granular microstructures exhibit nonlinear dispersive wave propagation, which is typically attributed to the presence of a microstructure. However, this behavior can arise from two additional sources in a linear non-dissipative system – the grain-scale or micromechanical characteristics and the grain-scale or micro-inertial characteristics. The microstructure, the grain-scale mechanical and the grain-scale inertial properties in combination may be designated as micro-mechano-morphology. From a continuum modeling viewpoint, the observed dispersion behavior that accounts for micro-mechano-morphology of materials with granular microstructures can be described using a granular micromechanics based micromorphic model (Nejadi Sadeghi and Misra 2019b, Misra and Poursolhjouy 2016). Following the approach outlined in these works, we elaborate on the effect of micro-scale inertia upon the wave propagation behavior. The work is motivated by the observation of negative group velocity of optical waves seen in simulations using discrete models of granular media. We show that higher-order inertia is necessary for describing this phenomena using continuum models. We further show that this phenomena can be modulated by micro-scale mass density distributions, thus affecting the widths of potential frequency band-gaps, including the negative group velocity of the acoustic branch.

## 1. Introduction

## 1.1. Micro-mechano-morphological effects

Materials with granular microstructure are characterized as materials composed of many individual grains mediated by interfaces. Due to their prevalence in diverse areas of engineering and science, it is necessary to promote the understanding on how such materials behave when excited externally. In addition to the materials with granular microstructure found in nature, recently emerged *granular metamaterials* also share many features with granular solids and are worth studying, especially for vibration mitigation applications [1, 2]. The collective behavior of granular structures (granular solids and granular metamaterials) is mainly connected to their micro-mechano-morphology. In other words, grain-pair interactions, composition and morphological aspects of granular structures in micro-scale dictate their macro-scale mechanical behavior. While for problems consisting of hundreds to thousands of grains a discrete model may be utilized [3–5], as the size of the structure grows (e.g. for granular structures comprising millions of grains) continuum models remain the most efficient. Continuum description of a material with granular microstructure expresses the macroscopic behavior of the material in an averaged sense based on the microstructural

properties of the structure in a less computationally expensive manner. Indeed, continuum models do not predict the trajectory of each grain inside the granular structure. However, given the incomplete information about the granular structure in terms of the grain-pair interaction properties and the accurate positions and geometries for all the grains in contact, an approximate description based on insufficient data is adequate.

Classical continuum mechanics declares a material point with its size approaching zero. Such a description is enough to describe and characterize the local effects (immediate neighborhood). However, the complexity of the granular medium in both mechanical and morphological aspects necessitates a refined description of the behavior of granular materials that takes into account the non-local effect of grain-interactions [6] and grain rotations [7], to predict phenomena such as dispersion in propagating elastic waves [8–12]. Dispersion in waves propagating through granular structures is pertinent to the existence of an inherent characteristic length comparable to the wavelength of excitation at high frequencies [9, 13]. The characteristic length is often attributed to granular materials microstructural aspects (see for example [14]), however, it should also account for the micro- or grain-scale mechanical characteristics and the micro- or the grain-scale inertial characteristics. The microstructure, the grain-scale mechanical and the grain-scale in-

\* Corresponding author.

E-mail address: [amisra@ku.edu](mailto:amisra@ku.edu) (A. Misra).<https://doi.org/10.1016/j.ijmecsci.2020.105867>

Received 11 April 2020; Received in revised form 23 May 2020; Accepted 4 June 2020

Available online 13 June 2020

0020-7403/© 2020 Elsevier Ltd. All rights reserved.

ertial properties in combination can be designated as micro-mechano-morphology. It is, therefore, imperative to include the information about the granular material's micro-mechano-morphology in formulating the continuum wave equations. Granular micromechanics approach (GMA) results in a non-classical continuum mechanics model for describing the mechanical behavior of granular structures considering the micro-mechano-morphological effects using refined kinematics [6, 15]. As a generalization of the classical continuum mechanics viewpoint, a material point in GMA is considered a collection of grains interacting with each other via different inter-granular mechanisms. The GMA treats the problem in a statistical sense by considering the mean behavior of grain pairs.

### 1.2. Motivation

In its most general forms, the GMA leads to micromorphic models of degree  $n$  [6], and treats grain-spins using as independent kinematic quantities [7]. In its simplest form, the GMA devolves to the classical Cauchy-form of continuum models. In our earlier publications, we have studied the elastic wave propagation in a material with granular microstructure utilizing GMA based micromorphic theory of degree 1 described in [6, 15]. The results from our previous work [9] have shown interesting information about wave propagation in granular media. These include wave dispersion as well as the occurrence of a slow longitudinal wave that follows the primary longitudinal wave as seen in the discrete simulations reported by [5]. It is noteworthy, however, that in nonlinear-dissipative systems (as in [5]), wave dispersion may be affected by multiple dissipation mechanisms (including viscous, frictional dissipation at the grain scales), and therefore, can depend upon the loading history in addition to the micro-mechano-morphology. The relative influences of these factors need careful investigations. The GMA based continuum model provides a systematic way to explore the influences of the many confounding factors, such as grain-pair elastic and dissipative interactions and grain inertia, which influence the macro-scale behavior of granular systems [6, 7, 16]. For example, longitudinal and transverse elastic wave propagation in 1D granular materials studied using GMA based model revealed the existence of multiple wave branches in both forward and backward waves, dispersion in wave propagation, where waves with different frequencies propagate with different velocities, and the possibility of the existence of frequency band gaps [9]. This model, enhanced to account for the effect of the external electric field, showed the possibility of modulating and tuning wave dispersion in granular materials composed of dielectric grains [8]. Thus, the GMA based continuum model can serve as a basis for designing experiments as well as discrete simulations. To this end, we note that our previous model failed to capture completely certain aspects of phononic negative group velocity (NGV) that are predicted by discrete models and recent works on wave propagation characteristics in granular media, e.g., [17].

We remark that phononic waves with NGV are known for 1D composite materials described by Rytov model of layered system using wave equations of classical continuum mechanics and specification of the layer properties [18–20]. The phenomenon of NGV has also been observed in other systems. For example, the appearance of NGV has been recognized in layered materials in electromagnetics [21] and in metamaterials with negative permittivity and negative permeability [22]. In soft composites, NGV in transverse or shear waves is believed to cause elastic instabilities in fibrous composites [23]. In elastic composites with periodic microstructure, NGV was accomplished by utilizing the idea of local resonances to produce low-frequency negative passband [24], or by embedding stiff inclusions in soft matrix [25]. NGV was also observed in 2D metamaterials modeled as mass spring systems with nonlocal effect [26] and in 1D lattice chain incorporating nonlocal effects [27]. Moreover, in solids with multi-scale microstructure, NGV is predicted for particular material parameters [28]. The present paper focuses upon granular materials that are homogeneous at the scale of investigation but are microscopically inhomogeneous. The aim of the present work is

to develop non-classical wave equations that addresses different aspects of wave dispersion in macroscopically homogeneous granular systems.

To illustrate the issue of negative group velocity in granular media, we consider a discrete bead-spring model of 20 grains as shown in Fig. 1a. This set of grains are taken to comprise the representative volume element (RVE) of an infinitely extending 1D granular material. The grain-pair interactions are modeled as linear elastic springs (denoted as  $k_i$ ,  $i = 1, 2, \dots, n$ ) whose stiffnesses have no asymmetry under tension or compression (such that the grains maintain enduring interactions during the wave propagation). Further, the spring stiffnesses are randomly distributed in a prescribed range and the grains are treated as rigid masses (denoted as  $m_i$ ,  $i = 1, 2, \dots, n$ ) of radius of 0.5 mm with varying grain mass densities. The distributions of grain-pair stiffnesses and grain mass densities used in our discrete simulations are shown in Fig. 1b and c. The dispersion curve of the considered structure can be now calculated from the equations of motion for grains in the RVE, assuming a harmonic form of solution for their displacement, and applying periodic boundary conditions. The computed dispersion relation for this model in the irreducible Brillouin zone is illustrated in Fig. 2a. The dispersion curve shown here has as many wave branches as the degrees of freedom in the RVE. Here we focus upon the dispersion curves for the first two wave branches, one optical and the other acoustic, replotted in Fig. 2b, which are at the lowest frequency range for comparison with the lowest frequency modes that have been predicted by the GMA based micromorphic model of degree 1 [9]. The acoustic branch in both models (discrete model and the model in [9]) shows similar characteristics. However, the optical branch predicted by the discrete simulation shows negative group velocity, which is in contrast to the previous format of GMA [9] which predicts positive and increasing group velocity.

This apparent discrepancy in predictions by the GMA based continuum model can be resolved by recognizing the existence of higher order inertia terms that appear in GMA based micromorphic theory of degree 1 as shown in our recent work on extended granular micromechanics approach [6]. We note that NGV is also predicted using classical micromorphic continuum models, by considering the cross-linking terms between macro- and micro-scale kinematic variables [29, 30]. In contrast, the models that do not consider these cross-linking terms predict positive group velocity in the optical branch [9, 31, 32]. In the present paper, we show that models that do not consider the cross-linking of macro- and micro-scale kinematic variables terms but include higher order inertia terms also predict NGV. Notably, the higher-order inertia term is, typically, absent in the classical micromorphic theories of degree 1, although such inertial terms are often included in 2nd gradient elasticity (see for example [33–36]). The higher order inertia terms arise from the variations in the micro-inertial properties as a combined effect of grain-sizes, compositions and the grain scale morphology (granular arrangement). Vibration and wave propagation characteristics of granular systems have been shown to be affected by specific granular arrangements and varying grain sizes in the recent works of [37–39]. In particular, mass ratio of the grains within a diatomic granular structure has been shown to affect the width and location of the frequency band gap, which reveals the micro-inertial effects on the band structure [17]. However, to the knowledge of the authors, no study has yet been done to generalize the micro-inertial influence on the propagating waves in a granular structure. To this end, we introduce an extended form of kinetic energy that includes the rates of micro-scale kinematic measures and its conjugate higher order micro-inertia. Our aim in the present paper is to highlight the role of higher order micro-inertia terms in the dispersive behavior of granular materials through the example of wave propagation in an infinite 1D continuum with granular microstructure. In particular, we illustrate how the grain mass density distribution can lead to modulation of the dynamic behavior of materials with granular microstructure. A 1D system proves to be expedient in describing the physics involved in the problem while reducing the complexity of the system under study, compared to a general 3D case.



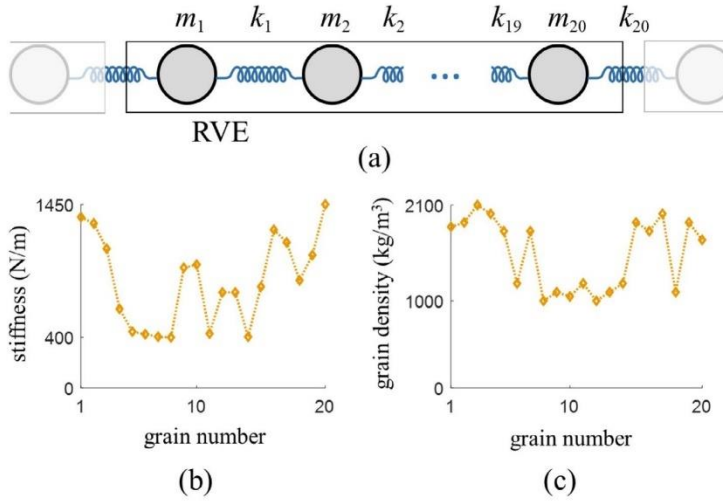


Fig. 1. (a) Schematic of the 1D RVE modeled as masses and springs, (b) the variation in the grain-pair stiffness in the RVE, and (c) the variation in the grain mass density in the RVE.

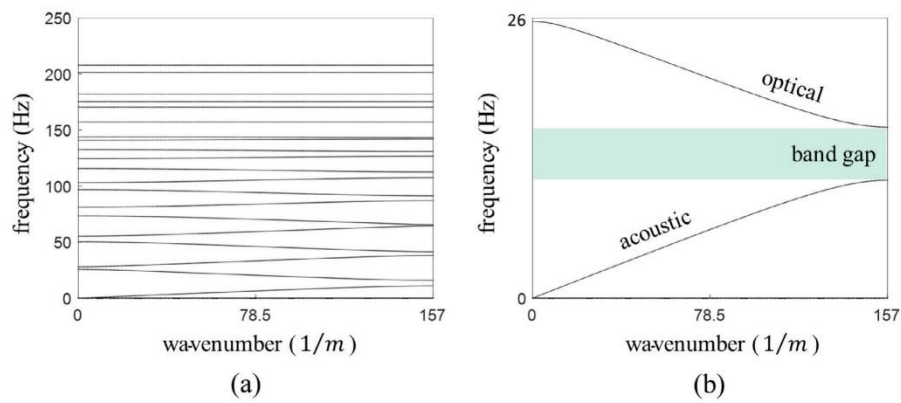


Fig. 2. (a) Dispersion curve from discrete simulation of the granular structure modeled as masses and springs, and (b) the first two wave branches in the dispersion curve from discrete simulation of the granular structure.

The organization of the paper is as follows. An overview of the granular micromechanics approach is provided in Section 2, where the kinematics of GMA based micromorphic theory of degree 1 and the variational approach to obtain the balance equations are described. Section 3 is devoted to study the longitudinal elastic wave propagation in a 1D material with granular microstructure taking into account the effect of higher order inertia terms. Finally, Section 4 presents the summary of the work and the concluding remarks.

## 2. GMA based micromorphic theory of degree 1

### 2.1. Kinematic variables

In this section, we briefly introduce the continuum framework for GMA. The reader is referred to the references [6, 15] for an extensive description of the approach. In GMA, a granular structure is considered as a continuum with the volume  $V$  bounded by the surface  $S$  where the material point  $P$  can be identified using a macro-scale Euclidean

coordinate system  $x_i$  (see Fig. 3). The material point  $P$  is assumed to have the macro-scale mass density  $\rho$ , volume  $dV = V'$ , and differential mass  $dm = \rho dV = \rho V'$ . Denoting by  $\mathbf{X}$  and  $\mathbf{x} = \chi(\mathbf{X}, t)$  the position vectors of the point  $P$  at initial and current configurations (at time  $t$ ), respectively, the macro-scale displacement vector  $\mathbf{u}$  ascribed to the point  $P$  is defined as  $\mathbf{u} = \mathbf{x} - \mathbf{X}$ . The material point  $P$ , microscopically, is an assemblage of grains and can be referred to as a statistical/representative volume element (RVE) with volume  $dV = V'$ . The positions of grains inside the RVE can be distinguished utilizing a micro-scale coordinate system  $x'_i$  attached to the center of mass (COM) of the material point  $P$ , parallel to the macro-scale coordinate system  $x_i$ , and moving with the macro-scale displacement  $\mathbf{u}$ . Denoting by  $\mathbf{X}'$  and  $\mathbf{x}' = \chi'(\mathbf{X}, \mathbf{X}', t)$  the position vectors of the grain  $p$  centroid at initial and current configurations, respectively, the micro-scale displacement vector  $\mathbf{u}'$  ascribed to the grain  $p$  is defined as  $\mathbf{u}' = \mathbf{x}' - \mathbf{X}'$ .

In the current format of GMA, we consider, in both micro- and macro-scales, infinitesimal deformation in granular media. We also assume that macro-scale and micro-scale displacements are both continuous and dif-

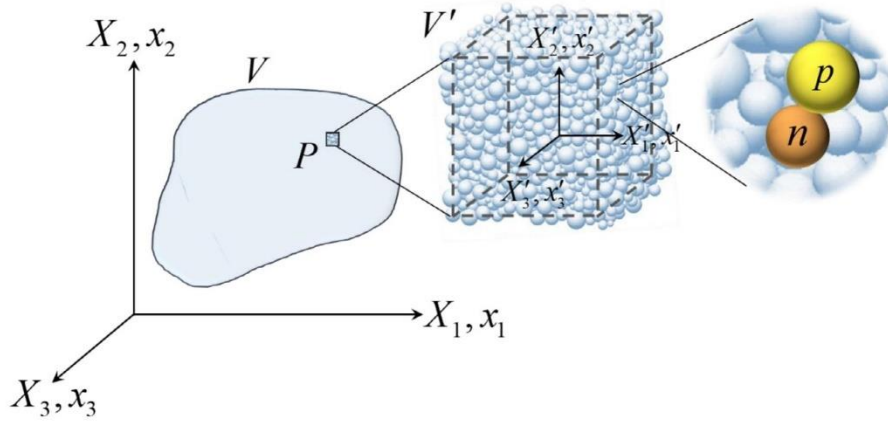


Fig. 3. Schematic of the continuum material point,  $P$ , and its granular microstructure magnified for better visualization, where the  $x'$  coordinate system is attached to its center of mass.

differentiable functions of  $x_i$  and  $x'_i$  up to the desired order. Therefore, we have the following form for the macro- and micro-scale displacements

$$u_i = u_i(x_j, t), \quad u'_i = u'_i(x_j, x'_j, t). \quad (1)$$

For a micromorphic theory of degree 1, the micro-scale displacement  $u'_i$  can be written using a polynomial expansion and keeping up to the second order terms with respect to  $x'$  about the COM of the RVE as [6]

$$u'_i = \psi_{ij}x'_j + \psi_{ijk}x'_jx'_k. \quad (2)$$

In Eq. (2),  $\psi_{ij}$  and  $\psi_{ijk}$  are, respectively, second and third rank micro-deformation tensors only functions of  $x$  and  $t$ . In Eq. (2) and henceforward, summation convention over repeated indices is implied unless noted otherwise. Without loss of generality, we further assume that the micro-deformation tensor  $\psi_{ijk}$  is symmetric with respect to indices  $j$  and  $k$  [6, 40]. With regards to Eq. (2), the total displacement vector for the grains inside the RVE can be written as

$$\phi_i = u_i + u'_i = \bar{\phi}_i + \psi_{ij}x'_j + \psi_{ijk}x'_jx'_k. \quad (3)$$

where  $\bar{\phi}_i = u_i$  is adopted to harmonize the variable names with previous publications [6, 8–10, 15]. We introduce the following relative deformation tensors [6, 30, 40]

$$\gamma_{ij} = \bar{\phi}_{i,j} - \psi_{ij}, \quad \gamma_{ijk} = \psi_{ijk} - \psi_{ijk}, \quad (4)$$

where, henceforth, comma in the subscript denotes differentiation with respect to the spatial coordinates. In Eq. (4), the differentiation is taken with respect to the macro-scale coordinate system basis vectors. For a micromorphic theory of degree 1, and as a constitutive choice, we assume that the relative deformation tensor  $\gamma_{ijk}$  is zero. Such an assumption reads  $\psi_{ijk} = \psi_{ijk}$ . As noted in [6], this assumption changes the independent nature of  $\psi_{ijk}$  to a dependent one. We further note that under additional assumptions of vanishing relative deformation tensor  $\gamma_{ij}$ , the theory will devolve to a 2nd gradient theory, which is known to have wide applications [41–43] and has been deduced through homogenization of certain lattice structures (see for example [44–46]).

For the neighboring grains  $n$  and  $p$ , utilizing Eq. (3) and (4), the relative displacement between grains can be decomposed as

$$\delta_i^{np} = \phi_i^p - \phi_i^n = \delta_i^M - \delta_i^m + \delta_i^g, \quad (5)$$

where the following micro-scale kinematic measures are recognized

$$\delta_i^M = \bar{\phi}_{i,j}J_j^{np}, \quad \delta_i^m = \gamma_{ij}J_j^{np}, \quad \delta_i^g = \psi_{ijk}J_j^{np}. \quad (6)$$

In Eq. (5) and (6), we have defined the geometry moment measures  $J_j^{np} = I_j^p - I_j^n$  and  $J_{jk}^{np} = I_{jk}^p - I_{jk}^n$ , where  $I_j^n$  represents the  $j^{\text{th}}$  component of the vector joining the COM of the RVE to the grain  $q$  centroid. Moreover,  $\delta^M$  indicates the part of the relative displacement due to the macro-scale displacement gradient,  $\delta^m$  denotes the portion of the relative displacement due to the fluctuation between the macro-scale gradient  $\bar{\phi}_{i,j}$  and the micro-scale kinematic measure  $\psi$ , and  $\delta^g$  represents the part of the relative displacement due to the second gradient.

The macro-scale rotation,  $\bar{\kappa}_i$ , in the macro-scale coordinate system is defined as

$$\bar{\kappa}_i = \frac{1}{2}e_{lki}u_{k,l} = \frac{1}{2}e_{lki}\bar{\phi}_{k,l}, \quad (7)$$

where the differentiation is with respect to the macro-scale coordinate system  $x_i$  and  $e_{lki}$  is the permutation symbol. Similarly, the micro-scale rotation,  $\hat{\kappa}_i$ , in the micro-scale coordinate system is defined as

$$\hat{\kappa}_i = \frac{1}{2}e_{lki}u'_{k,l} = \frac{1}{2}e_{lki}\phi_{k,l}, \quad (8)$$

where the differentiation is with respect to the micro-scale coordinate system  $x'_i$ . The relative rotation of two neighboring grains  $n$  and  $p$  inside the material point  $P$  only takes into account the effect of the micro-scale rotation,  $\hat{\kappa}_i$ . We note here that the grain spin effect is not considered in the current formulation of GMA. Utilizing Eq. (8), the relative rotation between two neighboring grains  $n$  and  $p$ ,  $\theta_i^{np}$ , can be written as

$$\theta_i^{np} = e_{lki}\psi_{kl,j}J_j^{np}. \quad (9)$$

The micro-scale kinematic measures introduced in Eq. (6) and (9) are considered deformation mechanisms in which the deformation energy is stored.

## 2.2. Constitutive equations

We assume the macro-scale deformation energy density to be a function of the macro-scale kinematic measures, i.e., of the form  $W = W(\bar{\phi}_{(i,j)}, \gamma_{ij}, \psi_{ijk})$ , where  $\bar{\phi}_{(i,j)}$  is the symmetric part of the macro-scale displacement gradient. Considering the assumed form of the macro-scale deformation energy density with its mentioned components ensures an objective expression for the energy density that is invariant to rigid rotation of the coordinate system. The macro-scale stress measures of Cauchy stress, relative stress, and double stress are defined as conjugates to the continuum kinematic measures, respectively as

$$\tau_{ij} = \frac{\partial W}{\partial \bar{\phi}_{(i,j)}}, \quad \sigma_{ij} = \frac{\partial W}{\partial \gamma_{ij}}, \quad \mu_{ijk} = \frac{\partial W}{\partial \psi_{ijk}}. \quad (10)$$



The macro-scale deformation energy density can be identified in terms of the micro-scale deformation energy density as

$$W = \frac{1}{V'} \sum_{\alpha} W^{\alpha}(\delta_i^{\alpha M}, \delta_i^{\alpha m}, \delta_i^{\alpha g}, \theta_i^{\alpha u}), \quad (11)$$

where  $W^{\alpha}$  represents the micro-scale deformation energy for the  $\alpha^{\text{th}}$  interacting pair of grains. Intergranular forces and moments can be defined as conjugates to the micro-scale kinematic measures as

$$\frac{\partial W}{\partial \delta_i^{\alpha \zeta}} = f_i^{\alpha \zeta}; \quad \zeta = M, m, g, \quad \frac{\partial W}{\partial \theta_i^{\alpha u}} = m_i^{\alpha u}. \quad (12)$$

Substituting Eq. (11) into Eq. (10), and using Eq. (6), (9), and (12), it follows that the macro-scale stress measures can be expressed in terms of the intergranular forces and moments and the geometry moment measures [15]. For a non-dissipative linear system a quadratic form of micro-scale deformation energy density  $W^{\alpha}$  can be considered. To this end, the micro-scale kinematic measures in Eq. (6) and (9) can be decomposed into their normal ( $n$ ) and two other tangential ( $s$  and  $t$ ) components, with the normal being along the direction of the line connecting the centroids of the two grains. As an example, the micro-scale deformation energy density used in this paper can be expressed in the quadratic form  $W^{\alpha} = \frac{1}{2} \sum_{\zeta} K_i^{\alpha \zeta} (\delta_i^{\alpha \zeta})^2 + \frac{1}{2} \sum_{i} G_i^{\alpha u} (\theta_i^{\alpha u})^2$  with  $i = n, s, t$ , and  $\zeta = M, m, g$ , and where different  $K$  and  $G$  parameters represent grain-pair stiffness parameters for the macro-scale,  $M$ , micro-scale,  $m$ , and second gradient,  $g$ , mechanisms involved in the deformation [15]. We note that the assumed form for the micro-scale deformation energy density  $W^{\alpha}$  does not consider the terms that cross-link different micro-scale kinematic measures in the current analysis. The assumed form of micro-scale deformation energy density,  $W^{\alpha}$ , leads to the macro-scale constitutive relationships presented below [15, 47]

$$\tau_{ij} = C_{ijkl}^M \epsilon_{kl}, \quad \sigma_{ij} = C_{ijkl}^m \gamma_{kl}, \quad \mu_{ijk} = (A_{ijklmn}^g + A_{ijklmn}^u) \psi_{lmn}. \quad (13)$$

In Eq. (13),  $C_{ijkl}^M$  and  $C_{ijkl}^m$  are fourth rank stiffness tensors, and  $A_{ijklmn}^g$  and  $A_{ijklmn}^u$  are sixth rank stiffness tensors, defined as functions of the grain-pair interaction stiffnesses  $K$  and  $G$  and geometry moment measures for all the grain pairs within the RVE. In Eq. (13), the superscript  $M$  denotes macro-stiffness,  $m$  denotes the micro-stiffness,  $g$  denotes the second gradient stiffness, and  $u$  represents the rotational stiffness.

### 2.3. Governing equations of motion

In this paper, we obtain the equations of motion based on the principle of stationary action. Hamilton's principle states that the action functional is minimum, and is expressed as

$$\delta \int_{t_0}^{t_1} (\tilde{T} - \tilde{W} + \tilde{W}_{ext}) dt = 0, \quad (14)$$

where the terms  $\tilde{T}$ ,  $\tilde{W}$ , and  $\tilde{W}_{ext}$  are defined in what follows.  $\tilde{T} = \int_V T dV$  is the total kinetic energy, where  $T$  is the kinetic energy density, utilizing König's theorem [48] defined as [6]

$$T = \frac{1}{V'} \int_{V'} \frac{1}{2} \rho' \phi_i \phi_i dV' = \frac{1}{2} \rho \dot{\phi}_i \dot{\phi}_i + \frac{1}{2} \rho_{jm} \dot{\psi}_{ij} \dot{\psi}_{im} + \rho_{jmn} \dot{\psi}_{ij} \dot{\psi}_{im,n} + \frac{1}{2} \rho_{jkmn} \dot{\psi}_{ij,k} \dot{\psi}_{im,n}. \quad (15)$$

In Eq. (15),  $\rho'$  is the micro-scale mass density per unit macro-volume, which can be non-uniform within the RVE (a function of the micro-scale coordinate system  $x'_i$ ), and each over-dot henceforward represents differentiation with respect to the temporal coordinate. Moreover, the following inertia measures have been defined [6]

$$\rho = \frac{1}{V'} \int_{V'} \rho' dV', \quad \rho_{jm} = \frac{1}{V'} \int_{V'} \rho' x'_j x'_m dV', \quad \rho_{jmn} = \frac{1}{V'} \int_{V'} \rho' x'_j x'_m x'_n dV', \quad \rho_{jkmn} = \frac{1}{V'} \int_{V'} \rho' x'_j x'_k x'_m x'_n dV', \quad (16)$$

where, clearly, the macro-scale mass density  $\rho$  and other measures of inertia depend on the micro-scale mass density  $\rho'$  and its distribution within the RVE. In what follows, we consider that the material is homogenous at the macro-scale, that is the macro-scale mass density  $\rho$  is independent of the macro-scale coordinate system,  $x_i$ . The kinetic energy density defined in Eq. (15) is an extension of the ones introduced in earlier publications for GMA based micromorphic theory of degree 1, e.g. in [8–10, 15]. The additional terms in the description of the kinetic energy affect the prediction of the dynamic behavior of granular media by introducing, or re-allocating, energies in the existing degrees of freedom of the problem. Moreover, the additional terms are accompanied by higher order inertia measures that were otherwise absent in [8–10, 15]. Clearly, the micro-scale mass density distribution in the RVE can alter the higher order inertia measures, while potentially keeping the macro-scale mass density  $\rho$  constant. This allows us to imagine two morphologically different systems with identical constituents and equal macro-scale mass density showing different wave propagation characteristics or two morphologically identical systems with different constituents and equal macro-scale mass density showing different wave propagation characteristics. This reveals (micro-) morphological and compositional effects on vibration characteristics of granular media. Now if the grain-pair interactions between all constituent grains are kept constant, the dynamic properties of the granular medium changes solely because of the change in inertia measures. This aspect is elaborated in the following sections.

In Eq. (14),  $\tilde{W} = \int_V W dV$  is the total macro-scale deformation energy, and  $\tilde{W}_{ext}$  is the total external energy where its form is inspired by the expression for the total macro-scale deformation energy  $\tilde{W}$ , with components described below. Thus from Eq. (14) we get [6]

$$\int_{t_0}^{t_1} \int_V \left[ (\tau_{ij} + \sigma_{ij})_{,j} + f_i - \rho \ddot{\phi}_i \right] \delta \phi_i dV dt + \int_{t_0}^{t_1} \int_V \left[ \sigma_{ij} + \mu_{ijk} + \Phi_{ij} - \rho_{jk} \ddot{\psi}_{in} + \rho_{jkmn} \ddot{\psi}_{il,mn} \right] \delta \psi_{ij} dV dt + \int_{t_0}^{t_1} \int_S \left[ t_i - (\tau_{ij} + \sigma_{ij}) n_j \right] \delta \phi_i dS dt + \int_{t_0}^{t_1} \int_S \left[ T_{ij} - (\rho_{jkl} \ddot{\psi}_{il} + \rho_{jklm} \ddot{\psi}_{il,m} + \mu_{ijk}) n_k \right] \delta \psi_{ij} dS dt = 0 \quad (17)$$

In Eq. (17),  $f_i$  is the non-contact body force per unit volume,  $t_i$  is the contact traction defined as a surface force per unit area,  $\Phi_{ij}$  is the non-contact body double force per unit volume, and  $T_{ij}$  is the contact double traction defined as double force per unit area. Moreover,  $n_j$  represents the  $j^{\text{th}}$  component of the normal to the surface  $S$ . In what follows, we assume zero non-contact body forces and double forces.

Equations of motion and natural boundary conditions are obtained, utilizing the fundamental lemma of calculus of variations and the constitutive relations in Eq. (13), as

$$(C_{ijkl}^M + C_{ijkl}^m) \ddot{\phi}_{k,lj} - C_{ijkl}^m \psi_{kl,j} = \rho \ddot{\phi}_{i,j}, \quad (18a)$$

$$(A_{ijklmn}^g + A_{ijklmn}^u) \psi_{lm,nk} + C_{ijkl}^m \ddot{\phi}_{k,l} - C_{ijkl}^m \psi_{kl} = \rho_{jk} \ddot{\psi}_{ilk} - \rho_{jklm} \ddot{\psi}_{il,mk}, \quad (18b)$$

$$(\tau_{ij} + \sigma_{ij}) n_j = t_i \quad (19a)$$

$$(\rho_{jkl} \ddot{\psi}_{il} + \rho_{jklm} \ddot{\psi}_{il,m} + \mu_{ijk}) n_k = T_{ij} \quad (19b)$$

It is noteworthy that the term  $\rho_{jklm} \ddot{\psi}_{il,mk}$  in Eq. (18b) is typically not considered in micromorphic models of degree 1, such as the previous models found in [8–10]. We further note that the 3rd rank inertial tensor appears in the boundary conditions and not in the governing equations. Note that in the 2nd gradient theory presented in [49], the 3rd rank inertial tensor appears in the governing equation, while there is no discussion of the boundary conditions.

### 3. Longitudinal elastic wave propagation in a 1D continuum with granular microstructure

We here focus on the longitudinal wave propagation in an infinite 1D continuum in macro- and micro-scales along the  $x_1$  axis. A represen-



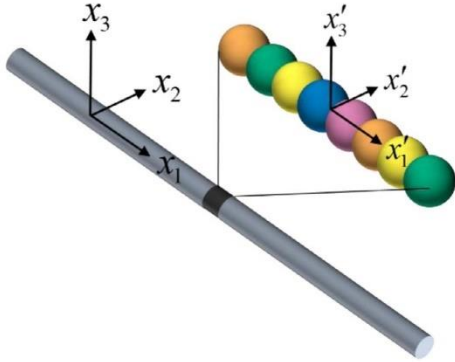


Fig. 4. Schematic of a 1D continuum in  $x_1$  direction with granular microstructure in  $x_1'$  direction. A material point in the macro-scale coordinate system is a collection of grains that can differ in micro-density, micro-morphology and micro-mechanical properties, represented here by grains with different colors.

tation of the general problem is shown in Fig. 4, where different grain colors represent different micro-scale mass density  $\rho'$  and elastic properties. For brevity, we drop the subscript 1 from the axis  $x_1$  and denote it by  $x$ . Similarly, we represent  $\bar{\phi}_1$  and  $\psi_{11}$  by  $\bar{\phi}$  and  $\psi$ , and  $C_{1111}^M$ ,  $C_{1111}^m$ , and  $A_{11111}^g$  by  $C^M$ ,  $C^m$ , and  $A^g$ , respectively. Note that in the 1D case under study,  $A_{11111}^g = 0$  [15]. The equations of motion, Eq. (18), for the current 1D case reduce to the following equations

$$(C^M + C^m)\bar{\phi}_{,xx} - C^m\psi_{,x} = \rho\bar{\phi}, \quad (20a)$$

$$A^g\psi_{,xx} + C^m\bar{\phi}_{,x} - C^m\psi = \rho_{11}\ddot{\psi} - \rho_{1111}\ddot{\psi}_{,xx}. \quad (20b)$$

Note that in Eq. (20),  $\rho_{11}$  and  $\rho_{1111}$  are the inertia measures defined in Eq. (16).

For the equations of motion in Eq. (20), we assume plane wave solutions, solutions harmonic in both position,  $x$ , and time,  $t$ , expressed as

$$\bar{\phi} = \text{Re}(Aie^{i(kx-\omega t)}), \quad \psi = \text{Re}(Be^{i(kx-\omega t)}) \quad (21)$$

where  $k$  is the angular wavenumber,  $\omega$  is the angular frequency, and  $i^2 = -1$ . Furthermore,  $A$  and  $B$  are the amplitudes and can assume complex values. Throughout this paper, “angular frequency” and “angular wavenumber” are referred to as “frequency” and “wavenumber” for brevity and have the units of radians per second and radians per meter, respectively. Upon substituting Eq. (21) in Eq. (20), the equations of motion can be recast in the following generalized eigenvalue problem

$$\begin{bmatrix} c_0^2 k^2 + c_A^2 k^2 & c_A^2 k \\ c_A^2 k & c_1^2 \varepsilon_1^2 k^2 + c_A^2 \end{bmatrix} \begin{bmatrix} A \\ B \end{bmatrix} = \omega^2 \begin{bmatrix} 1 & 0 \\ 0 & \varepsilon_1^2 + \varepsilon_2^4 k^2 \end{bmatrix} \begin{bmatrix} A \\ B \end{bmatrix}, \quad (22)$$

where we have defined the macro-scale, micro-scale relative deformation, and second gradient velocities  $c_0$ ,  $c_A$ , and  $c_1$ , respectively, and two characteristic lengths  $\varepsilon_1$  and  $\varepsilon_2$ , respectively, as

$$c_0^2 = \frac{C^M}{\rho}, \quad c_A^2 = \frac{C^m}{\rho}, \quad c_1^2 = \frac{A^g}{\rho_{11}}, \quad \varepsilon_1^2 = \frac{\rho_{11}}{\rho}, \quad \varepsilon_2^4 = \frac{\rho_{1111}}{\rho}. \quad (23)$$

Eq. (22) has nontrivial solution if

$$(c_0^2 k^2 + c_A^2 k^2 - \omega^2)(c_1^2 \varepsilon_1^2 k^2 + c_A^2 - \varepsilon_1^2 \omega^2 - \varepsilon_2^4 k^2 \omega^2) - c_A^4 k^2 = 0. \quad (24)$$

Eq. (24) is the dispersion relation for the problem under study and can be considered as the solution for an eigenvalue problem with matrix form of equations given in Eq. (22) (see Refs. [50, 51] for rigorous mathematical description regarding phononic eigenvalue problems). This equation relates the frequency and the wavenumber and can be utilized to obtain dispersion curves. However, it is useful to nondimensionalize Eq. (24). To this end, we define the characteristic time

$p$ , dimensionless velocities,  $\gamma_A$ , and  $\gamma_1$ , dimensionless term corresponding to inertial effect,  $\chi$ , dimensionless frequency,  $\eta$ , and dimensionless wavenumber,  $\xi$ , as

$$p = \frac{\varepsilon_1}{c_0}, \quad \gamma_A = \frac{c_A}{c_0}, \quad \gamma_1 = \frac{c_1}{c_0}, \quad \chi = \frac{\varepsilon_2}{\varepsilon_1}, \quad \eta = p\omega, \quad \xi = \varepsilon_1 k. \quad (25)$$

Using Eq. (25), the dimensionless form of the dispersion relation in Eq. (24) is

$$(\eta^2 - \xi^2 - \gamma_A^2 \xi^2)(\eta^2 - \gamma_1^2 \xi^2 - \gamma_A^2 + \chi^4 \xi^2 \eta^2) - \gamma_A^4 \xi^2 = 0 \quad (26)$$

The maximum order of the dimensionless frequency  $\eta$  in Eq. (26) is four, meaning that there will be four solutions in the form  $\eta = \eta(\xi)$ . Two of the solutions are forward and the other two are backward wave branches. The forward and backward wave branches are symmetric with respect to the line  $\eta = 0$  in the dispersion curve with horizontal and vertical axes as  $\xi$  and  $\eta$ , respectively. Therefore, we only consider the forward wave branches here. Furthermore, for each wave branch, the dimensionless phase velocity,  $v_p$ , and group velocity,  $v_g$ , are obtained as

$$v_p = \frac{\eta}{\xi}, \quad v_g = \frac{d\eta}{d\xi}. \quad (27)$$

Before analyzing the solutions of Eq. (26), it is fruitful to discuss the physical meaning of the parameters involved in Eq. (26). The dimensionless velocity  $\gamma_A$  is defined as the ratio of two velocities, whose definition can be simplified to  $\gamma_A = \sqrt{\frac{C^m}{C^M}}$ . As a result,  $\gamma_A$  is a function of the macro-stiffness and micro-stiffness and represents the relative magnitude of micro-stiffness with respect to the macro-stiffness. The dimensionless velocity  $\gamma_1$  can also be simplified to  $\gamma_1 = \frac{1}{\varepsilon_1} \sqrt{\frac{A^g}{C^M}}$ , where contrary to the dimensionless velocity  $\gamma_A$ , it is a function of both stiffnesses and inertia measures. The term  $\sqrt{\frac{A^g}{C^M}}$  represents the static length scale for the current problem, therefore, the value of  $\gamma_1$  is a ratio between the static and the dynamic length scale  $\varepsilon_1$ . Keeping the granular structure unchanged in terms of the distribution of masses, as the second gradient stiffness increases, so does the value for  $\gamma_1$ . On the other hand, keeping the stiffnesses of the granular material unchanged, as the second order inertia measure  $\rho_{11}$  increases (or equivalently as  $\varepsilon_1$  increases), the value for  $\gamma_1$  decreases. Finally, the expression for the dimensionless parameter  $\chi$  can be recast as  $\chi = \sqrt{\frac{\rho_{1111}}{\rho_{11}}}$ , which encompasses the effect of inertia. For a case where the micro-scale mass density  $\rho'$  is constant, using Eq. (16), the expression for the dimensionless parameter  $\chi$  is simplified to  $\chi = 1.1583$ . A different distribution for the micro-scale mass density  $\rho'$  will result in different values for  $\chi$ , as exemplified in Fig. 5 for a variety of micro-scale mass density distributions.

Returning to the dispersion relation in Eq. (26), we consider a granular medium with material constants  $\gamma_A = 0.7$ ,  $\gamma_1 = 10^{-6}$ , and  $\chi = 1.1583$  to explore the GMA predictions of wave propagation characteristics. The chosen values are taken to be representative of a case in which band gaps are present [9, 15]. The solutions of Eq. (26) when solved for dimensionless frequency are plotted in the dispersion curve presented in Fig. 6a. There exists one acoustic branch starting at the origin, and one optical branch starting at a nonzero dimensionless frequency. The starting dimensionless frequency point for the optical branch can be obtained using Eq. (26) and substituting  $\xi = 0$ . This results in dimensionless frequency  $\eta = \gamma_A$ , as shown in Fig. 6a, or a real frequency  $\omega = \sqrt{\frac{C^m}{\rho_{11}}}$ . The asymptotes of the two wave branches can be obtained, discarding second order terms from Eq. (26), and solving for the dimensionless frequency. As a result, the asymptotes are

$$\eta = \sqrt{\gamma_A^2 + 1}\xi, \quad \eta = \frac{\gamma_1 \xi}{\sqrt{\chi^4 \xi^2 + 1}}, \quad (28)$$

or in terms of real frequency and wavenumber,

$$\omega = \sqrt{\frac{C^M + C^m}{\rho}} k, \quad \omega = \sqrt{\frac{A^g}{\rho_{1111} k^2 + \rho_{11}}} k \quad (29)$$

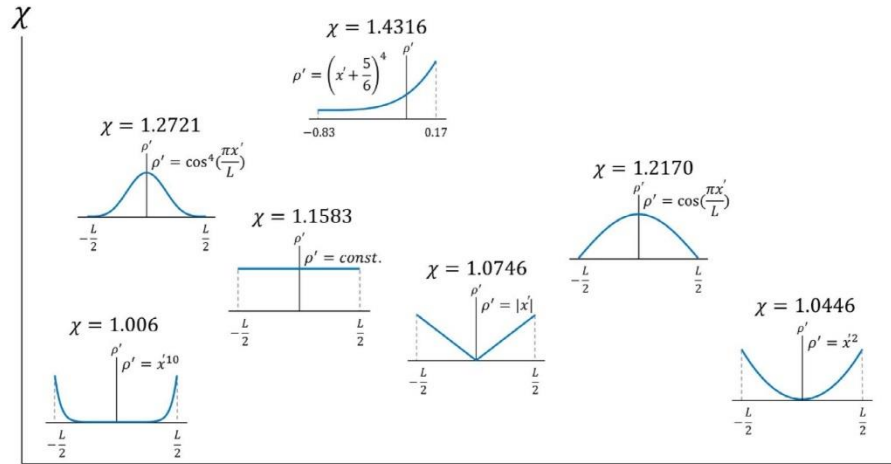


Fig. 5. Examples of possible micro-scale mass density  $\rho'$  distributions in a 1D RVE and their correspondent dimensionless value  $\chi$ .

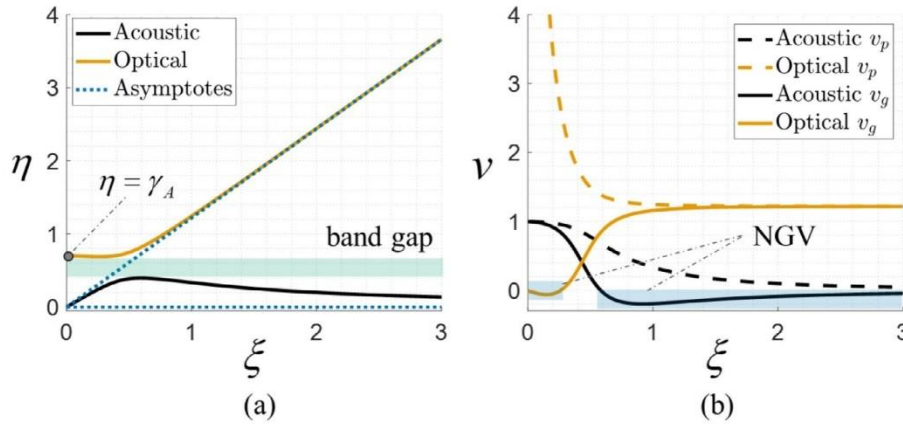


Fig. 6. (a) Dispersion curve for a 1D material with granular microstructure. (b) Phase and group velocities for acoustic and optical wave branches in a 1D material with granular microstructure.

These asymptotes are shown in Fig. 6a. The asymptote  $\eta = \sqrt{\gamma_A^2 + 1\xi}$  is a straight line and as seen in Fig. 6a, it fits the optical wave branch at large wavenumber and frequencies. On the other hand, the asymptote  $\eta = \frac{\gamma_1 \xi}{\sqrt{\gamma_1^4 \xi^2 + 1}}$  is not a straight line and shows the asymptotic value the acoustic branch takes. For the very small value of  $\gamma_1$  taken in this example, this asymptote can be approximated by  $\eta = 0$ . This means that the acoustic branch ceases to propagate in very large wavenumbers (small wavelengths). For some frequency range depicted by a green box in Fig. 6a, there is no real solution for the wavenumber. This frequency range is called frequency band gap (or stop band), and is associated with frequencies that do not propagate through the medium. Fig. 6b shows the phase and group velocities associated with the acoustic and optical branches. The difference between the phase and group velocities for each wave branch can cause a change in the shape of propagating pulse. The phase velocity values for both wave branches decrease as wavenumber becomes larger, therefore, the granular material with the assumed material parameters shows *normal dispersion*. One interesting observa-

tion in Fig. 6b is the existence of certain wavenumbers in which the signs of phase and group velocities corresponding to each wave branch are opposite. This phenomena is called negative group velocity (NGV) in the literature and is associated with backward propagation of the peak of the pulse [52]. From a physical viewpoint, NGV in a material with granular microstructure results from the resonance of sub-wavelength micro-structural elements (grain-scales) inherent in granular materials. From a mathematical viewpoint, the NGV results from the presence of the higher order inertia conjugate to rate of micro-deformation that appears in the presented continuum model, which leads to the term  $\psi_{,xx}$  with both time and space derivatives in the equations of motion. As is seen in Fig. 6b, the NGV in the granular material is predicted to be wavenumber (frequency) dependent. Since group velocity is an integral entity depending on the collective behavior of a number of harmonics in relation to each other, the occurrence of NGV suggests smaller effective dispersion in the granular material [28]. To evaluate the physical mechanisms for the phenomena, we have performed parametric studies to investigate how the material parameters contribute to the appearance

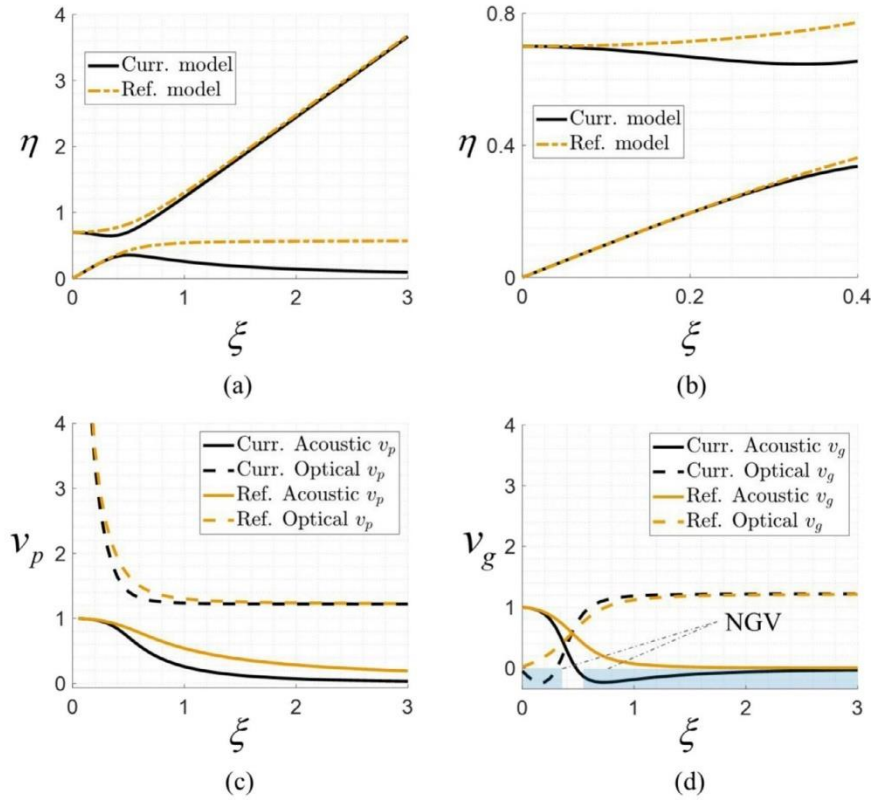


Fig. 7. Dispersion curve comparison between the reference (Ref.) model in [9] and the current (Curr.) model in (a) dimensionless wavenumbers ranging from 0 to 3, and (b) dimensionless wavenumbers ranging from 0 to 0.4. (c) Phase velocity comparison between the reference model and the current model. (d) Group velocity comparison between the reference model and the current model.

of NGV. Results (not shown here) revealed that for fixed values of  $\gamma_1$  and  $\chi$ , larger values of the parameter  $\gamma_A$  (or equivalently larger micro-scale stiffness  $C^m$  compared to a fixed value for the macro-scale stiffness  $C^M$ ) result in increasing NGV. For fixed values of  $\gamma_A$  and  $\chi$ , larger values of  $\gamma_1$  (which represents the ratio of static and dynamic length scales) result in positive group velocity, while NGV is observed for small values of  $\gamma_1$ . For fixed values of  $\gamma_A$  and  $\gamma_1$ , larger values of  $\chi$  predict higher NGV. To summarize, granular media with larger values of  $\gamma_A$  and  $\chi$ , and smaller value for the parameter  $\gamma_1$  are expected to show NGV in their optical branch. The parametric studies show that the NGV phenomena is controlled by the micro-deformation and its rate whose energy content can be modulated by parameters,  $\gamma_1$ ,  $\gamma_A$  and  $\chi$ . Importantly, these parameters represent the effect of micro-mechano-morphology of granular material. For example, emergent micro-deformation phenomena for static case can be observed in defective granular structures as discussed in [47] or in granular structures with particular grain-pair interactions as in [16], as well as in discrete mass-spring models that include interactions with non-nearest neighbor [26, 27]. It is also worthwhile to mention that NGV in longitudinal wave propagation has been observed in the context of axially moving materials with granular microstructure [10]. NGV phenomenon has also been predicted for transverse waves in granular systems with particular grain-pair interactions [9].

As mentioned earlier in the paper, the current format of equations of motion for the problem under study includes an additional term corre-

sponding to the effect of higher order inertia. It is worthwhile to study how this additional term contributes to the wave propagation characteristics of granular medium. Therefore, we consider two cases, where in one case the higher order inertia  $\rho_{1111}$  is taken to be zero, reducing the equations of motion in Eq. (20) to the one adopted in [9], and in the other case the higher order inertia assumes a nonzero value and Eq. (20) holds fully. The dispersion curve of these cases are illustrated in Fig. 7a and are referred to as the current model and the reference model, respectively. In both cases we have used the same parameter constants used to produce the dispersion curve for Fig. 6, except for the dimensionless value  $\chi$ , which in the reference model is zero and in the current model has been assumed 1.4 to enhance the contrast between the findings of the two models. Results in Fig. 7a reveal the fact that the additional term corresponding to higher order inertia affects the acoustic wave branch in large wavenumbers, while altering the behavior of the optical wave branch at small wavenumbers. In other words, the acoustic wave branches for the two models agree in small wavenumbers, and the optical wave branches for the two models agree in large wavenumbers. To investigate such observations, we consider two regions of wavenumbers. In small wavenumbers, Eq. (26) can be approximated by

$$(\chi^4 \xi^2 + 1)\eta^4 - ((\gamma_1^2 + \gamma_A^2 + 1)\xi^2 + \gamma_A^2)\eta^2 + \gamma_A^2 \xi^2 = 0. \quad (30)$$

Eq. (30) is a quadratic equation in  $\eta^2$  and can be easily solved to give the equations for the acoustic and optical wave branches at small



wavenumbers. For the optical branch, the first term on the left side in Eq. (30) is not small and contributes to the solution. This term contains the information about the micro-scale mass density distribution, and therefore, the optical branch behavior is affected by the higher order inertia in small wavenumbers. For the acoustic branch, however, further simplifications can be made. Since the acoustic branch starts at zero frequency, the first term on the left side can be neglected. As a result, the frequency solution for the acoustic wave branch at small wavenumbers can be simplified to

$$\eta = \frac{\gamma_A \xi^2}{\sqrt{(\gamma_1^2 + \gamma_A^2 + 1)\xi^2 + \gamma_A^2}}. \quad (31)$$

As is clear from Eq. (31), the acoustic wave branch frequency solution is independent of higher order inertia effect in small wavenumbers. The same argument can be stated for the large wavenumber (small wavelength) behavior of the two wave branches using the asymptotes in Eq. (29). Clearly, the optical branch is independent of the higher order inertia in large wavenumbers, while the acoustic branch is affected by the higher order inertia.

We further note the change in stop band frequency range predicted by the two models, where the current model predicts stop band of frequencies lower than the one predicted by the reference model. Based on Fig. 7c and d, we note that, for the acoustic branch, the reference model predicts a diminishing positive group velocity and decreasing phase velocity for large wavenumbers, while the current model predicts a diminishing negative group velocity and vanishing phase velocity. For the optical wave branch, large wavenumber behavior of both models is the same, while in small wavenumbers, we observe that the current model predicts negative group velocity, which gradually reaches zero, and becomes positive as wavenumber increases. We further observe the change of location for the frequency stop bands in the two models, where the current model predicts lower frequency ranges for the band gaps, compared to the prediction of the reference model. While the model predictions can be extended to very large wavenumbers and frequencies, it is understood that the model predictions below wavelengths of the size of the RVE are not generally reliable as the homogenization is done in the scale of RVE. For example, for grains with diameters in the order of millimeters, and an RVE size in the order of 1000 grains, the dimensionless wavenumber limit of reliability on the theory predictions is less than 0.4. The reference model and current model predictions in the corresponding limiting wavenumber range are depicted in Fig. 7b. Finally, assuming negligible values for the dimensionless parameters  $\gamma_1$  and  $\gamma_A$ , the dispersion curve in Eq. (26) simplifies to the nondispersive relation  $\eta = \xi$  which in terms of real frequency and wavenumber reads  $\omega = c_0 k$ . Therefore, the model developed here simplifies to a classical model.

#### 4. Conclusions

In this paper, we have theoretically investigated the elastic wave dispersion characteristics in an infinite 1D continua with granular microstructure. We have focused on the effect of higher order inertia terms that appear in the enhanced micromorphic model based upon GMA [6]. The additional term, which is absent in the previous formats of micromorphic models of degree 1 (including those presented by the authors [8–10, 15]), has a profound effect on the dynamic behavior of granular media. The results presented in the current paper, when compared to the previous model results, show, not only better agreement with the wave propagation characteristics observed experimentally and numerically in the literature, e.g., in [17, 53, 54], but predict additional effects. In particular, the higher order inertia terms most-noticeably affect the prediction of the optical wave branch behavior. It is remarkable that the higher-order inertia terms are controlled by the micro-scale mass density distribution in the RVE. Thus, it is possible to conceive of homogeneous materials with the same macro-scale mass density and different higher-order inertia. In these materials, the re-allocation of kinetic energies in

the micro- and macro-scale degrees of freedom can introduce interesting modulation of wave propagation. The theoretical results reported in this paper can be a precursor and motivation for an experimental effort, which can otherwise be difficult to conceive, plan and execute given the multitude factors that can affect wave propagation and their measurements. Moreover, these theoretical results can promote the development of dynamic identification procedure that can be applied for simulating wave propagation in random granular assemblies across a wide range of frequencies. We note that the existing dynamic discrete models typically include dissipation, such that the intermixing of microstructural, micro-inertial and imposed dissipation effects confounds the results of wave propagation simulations.

The micromorphic based continuum model presented in this paper assumes non-dissipative linear behavior in micro- and macro-scales. While many granular systems feature nonlinear grain-pair interactions, understanding linear elastic behavior has practical significance for small amplitude vibrations, where assuming a quadratic potential is valid. Furthermore, the considered model is specialized for infinitesimal deformations, and therefore, it is applicable to small amplitude vibrations.

For an accurate description of a material with granular microstructure, one needs complete information about the micro-mechanomorphic aspect of the granular material, e.g., the position, size, and shape of the grains, their inertial properties, and the interaction mechanisms between all grains in contact. GMA treats the problem in an averaged sense by reducing the number of parameters from thousands (if not millions) to a few continuum material constants. The analysis presented in the current paper can be potentially used to identify the continuum material parameters of granular media from experiments or numerical simulations. To describe a one-dimensional material with granular microstructure using GMA introduced in the paper and the assumed form of deformation energy densities, one needs to identify 6 material constants. These constant are the macro-scale mass density,  $\rho$ , micro-scale mass density,  $\rho'$ , and the knowledge on its distribution (which results in the dependent inertia measures  $\rho_{11}$  and  $\rho_{1111}$ ), the RVE size,  $L$ , the macro-scale stiffness,  $C^M$ , the micro-scale stiffness,  $C^m$ , and the second gradient stiffness,  $A^\xi$ . These 6 material parameters can be identified by performing a constrained optimization problem with the cost function being the difference between the results of the predictions of the theory and the experimental or discrete simulation results. A similar approach can be found in [29, 55, 56] where the material constants of a micromorphic model were determined based on experimental, atomistic, or finite element simulation results through phonon dispersion relations. We also note the identification methods discussed for static elastic properties in [47, 57].

Furthermore, it is noteworthy that while atomistic and discrete simulations can describe the dispersive behavior of materials in very short wavelengths (large wavenumbers), when compared to such simulations, a micromorphic-based continuum model is able to describe the behavior of materials with good accuracy up to wavelengths suitably larger than the corresponding characteristic length of the system [29, 56]. For smaller wavelengths, the accuracy of the results decreases and the predictions of the theory needs further investigation by comparison with experimental or discrete simulation results. It is encouraging to note that, the predicted zero group velocity in the optical branch suggesting non-propagating wave mode, has been observed for granular crystals with nonlinear grain-pair interactions in hybridized modes [58]. The use of the GMA based micromorphic model expands the applicability of continuum models to regions beyond what classical continuum mechanics is able to predict, while revealing the relevant micro-mechanisms.

It is evident that the current approach is useful for not only describing the dynamic behavior of natural granular materials, but the methodology can be applied to design granular metamaterials for vibration mitigation purposes. Notably, such design can utilize granular-structure, grain-pair interaction properties as well as the micro-scale mass density effects in the macro-scale behavior of such media. We further note that since the GMA links the grain-scale behavior to the macro-scale consist-



ing of millions of particles, the resultant continuum model provides a systematic approach to explore the influences of both micro- and macro-scale parameters, which often have confounding and contradicting effects on the wave propagation behavior. We also note that a large number of published literature is focused upon problems that are restricted to study the systems with unit cells of one or very few grains, with limited variation in grain composition [17, 53, 54, 59–61]. The advancements in additive manufacturing technology, however, allows us to envision and realize granular metamaterials with specified micro-scale mass density distributions resulting in tailored vibration characteristics predicted in the present paper. Further verification of the continuum predictions presented here will be performed using discrete simulations with grains in future publications.

#### Author statement

Both the authors participated equally in the conception of the project and preparation of the final manuscript.

#### Declaration of Competing Interests

Authors have no competing interests to declare.

The authors declare that they have no known competing financial interests or personal relationships that could have appeared to influence the work reported in this paper.

#### Acknowledgements

This research is supported in part by the United States National Science Foundation grant CMMI –1727433.

#### References

- [1] Kim E, Review Yang J. Wave propagation in granular metamaterials. *Funct Compos Struct* 2019;1:012002. doi:10.1088/2631-6331/ab0c7e.
- [2] Gantounis G, Serra-Garcia M, Homma K, Mendoza JM, Daraio C. Granular metamaterials for vibration mitigation. *J Appl Phys* 2013;114. doi:10.1063/1.4820521.
- [3] Turco E, dell'Isola F, Misra A. A nonlinear Lagrangian particle model for grains assemblies including grain relative rotations. *Int J Numer Anal Methods Geomech* 2019;43:1051–79. doi:10.1002/nag.2915.
- [4] Cundall PA, Strack ODL. A discrete numerical model for granular assemblies. *Geotechnique* 1979;29:47–65.
- [5] Cheng H, Ludwig S, Saitoh K, Magnanimo V. Elastic wave propagation in dry granular media: effects of probing characteristics and stress history. *Int J Solids Struct* 2020;187:85–99. doi:10.1016/j.jisolsstr.2019.03.030.
- [6] Nejadi Sadeghi N, Misra A. Extended granular micromechanics approach: a micromorphic theory of degree  $n$ . *Math Mech Solids* 2019;25(2):407–29. doi:10.1177/1081286519879479.
- [7] Poorsolhjoui P, Misra A. Granular micromechanics based continuum model for grain rotations and grain rotation waves. *J Mech Phys Solids* 2019;129:244–60. doi:10.1016/j.jmps.2019.05.012.
- [8] Nejadi Sadeghi N, Placidi L, Romeo M, Misra A. Frequency band gaps in dielectric granular metamaterials modulated by electric field. *Mech Res Commun* 2019;95. doi:10.1016/j.mechrescom.2019.01.006.
- [9] Misra A, Nejadi Sadeghi N. Longitudinal and transverse elastic waves in 1D granular materials modeled as micromorphic continua. *Wave Motion* 2019;90:175–95. doi:10.1016/j.wavemoti.2019.05.005.
- [10] Nejadi Sadeghi N, Misra A. Axially moving materials with granular microstructure. *Int J Mech Sci* 2019;161–162:105042. doi:10.1016/j.ijmecsci.2019.105042.
- [11] Sadd MH, Tai Q, Shukla A. Contact law effects on wave propagation in particulate materials using distinct element modeling. *Int J Non Linear Mech* 1993;28:251–65. doi:10.1016/0020-7462(93)90061-0.
- [12] Papargyri-Beskou S, Mylonakis G. Wave dispersion studies in granular media by analytical and analytical-numerical methods. *Soil Dyn Earthq Eng* 2009;29:883–7. doi:10.1016/j.soildyn.2008.10.003.
- [13] Berezovski A, Engelbrecht J, Salupere A, Tamm K, Peets T, Berezovski M. Dispersive waves in microstructured solids. *Int J Solids Struct* 2013;50:1981–90. doi:10.1016/j.jisolsstr.2013.02.018.
- [14] Pal RK, Waymel RF, Geubelle PH, Lambros J. Tunable Wave Propagation in Granular Crystals by Altering Lattice Network Topology. *J Eng Mater Technol Trans ASME* 2017;139. doi:10.1115/1.4034820.
- [15] Misra A, Poorsolhjoui P. Granular micromechanics based micromorphic model predicts frequency band gaps. *Contin Mech Thermodyn* 2016;28:215–34. doi:10.1007/s00161-015-0420-y.
- [16] Misra A, Nejadi Sadeghi N, De Angelo M, Placidi L. Chiral metamaterial predicted by granular micromechanics: verified with 1D example synthesized using additive manufacturing. *Contin Mech Thermodyn* 2020. doi:10.1007/s00161-020-00862-8.
- [17] Wei LS, Wang YZ, Wang YS. Nonreciprocal transmission of nonlinear elastic wave metamaterials by incremental harmonic balance method. *Int J Mech Sci* 2020;173:105433. doi:10.1016/j.ijmecsci.2020.105433.
- [18] Kosevich AM. On a simple model of the photonic or phononic crystal. *JETP Lett* 2001;74:559–63. doi:10.1134/1.1450291.
- [19] Rytov S M. Acoustical Properties of a Thinly Laminated Medium. *Sov. Phys.-Acoust.* 1956;2:68–80.
- [20] Hussein MI, Leamy MJ, Ruzzene M. Dynamics of phononic materials and structures: historical origins, recent progress, and future outlook. *Appl Mech Rev* 2014;66. doi:10.1115/1.4026911.
- [21] Fredkin DR, Ron A. Effectively left-handed (negative index) composite material. *Appl Phys Lett* 2002;81:1753–5. doi:10.1063/1.1505119.
- [22] Lee SH, Park CM, Seo YM, Wang ZG, Kim CK. Composite acoustic medium with simultaneously negative density and modulus. *Phys Rev Lett* 2010;104:054301. doi:10.1103/PhysRevLett.104.054301.
- [23] Slesarenko V, Galich PI, Li J, Fang NX, Rudykh S. Foreshadowing elastic instabilities by negative group velocity in soft composites. *Appl Phys Lett* 2018;113:031901. doi:10.1063/1.5042077.
- [24] Nemat-Nasser S, Willis JR, Srivastava A, Amirikhizi AV. Homogenization of periodic elastic composites and locally resonant sonic materials. *Phys Rev B - Condens Matter Mater Phys* 2011;83:104103. doi:10.1103/PhysRevB.83.104103.
- [25] Minagawa S, Nemat-Nasser S. Harmonic waves in three-dimensional elastic composites. *Int J Solids Struct* 1976;12:769–77. doi:10.1016/0020-7683(76)90041-X.
- [26] Wang J, Huang Y, Chen W, Zhu W. Abnormal wave propagation behaviors in two-dimensional mass-spring structures with nonlocal effect. *Math Mech Solids* 2019;24:3632–43. doi:10.1177/1081286519853606.
- [27] Wang J, Zhou W, Huang Y, Lyu C, Chen W, Zhu W. Controllable wave propagation in a weakly nonlinear monoatomic lattice chain with nonlocal interaction and active control. *Appl Math Mech (English Ed)* 2018;39:1059–70. doi:10.1007/s10483-018-2360-6.
- [28] Tamm K, Peets T, Engelbrecht J, Kartofelev D. Negative group velocity in solids. *Wave Motion* 2017;71:127–38. doi:10.1016/j.wavemoti.2016.04.010.
- [29] Chen Y, Lee JD. Determining material constants in micromorphic theory through phonon dispersion relations. *Int J Eng Sci* 2003;41:871–86. doi:10.1016/S0020-7225(02)00321-X.
- [30] Mindlin RD. Micro-structure in linear elasticity. *Arch Ration Mech Anal* 1964;16:51–78. doi:10.1007/BF00248490.
- [31] Madeo A, Neff P, Ghiba I-D, Placidi L, Rosi G. Band gaps in the relaxed linear micromorphic continuum. *ZAMM - J Appl Math Mech / Zeitschrift Für Angew Math Und Mech* 2015;95:880–7. doi:10.1002/zamm.201400036.
- [32] Madeo A, Neff P, Ghiba ID, Placidi L, Rosi G. Wave propagation in relaxed micromorphic continua: modeling metamaterials with frequency band-gaps. *Contin Mech Thermodyn* 2015;27:551–70. doi:10.1007/s00161-013-0329-2.
- [33] Rosi G, Placidi L, Auffray N. On the validity range of strain-gradient elasticity: a mixed static-dynamic identification procedure. *Eur J Mech A/Solids* 2018;69:179–91. doi:10.1016/j.euromechsol.2017.12.005.
- [34] Eremeyev VA, Rosi G, Nalli S. Comparison of anti-plane surface waves in strain-gradient materials and materials with surface stresses. *Math Mech Solids* 2019;24:2526–35. doi:10.1177/1081286518769960.
- [35] Rosi G, Auffray N. Anisotropic and dispersive wave propagation within strain-gradient framework. *Wave Motion* 2016;63:120–34. doi:10.1016/j.wavemoti.2016.01.009.
- [36] Ben-Amoz M. A dynamic theory for composite materials. *Zeitschrift Für Angew Math Und Phys ZAMP* 1976;27:83–99. doi:10.1007/BF01595244.
- [37] Doney RL, Agui JH, Sen S. Energy partitioning and impulse dispersion in the decorated, tapered, strongly nonlinear granular alignment: a system with many potential applications. *J Appl Phys* 2009;106. doi:10.1063/1.3190485.
- [38] Doney RL, Sen S. Impulse absorption by tapered horizontal alignments of elastic spheres. *Phys Rev E - Stat Nonlinear. Soft Matter Phys* 2005;72. doi:10.1103/PhysRevE.72.041304.
- [39] Wang J, Chu X, Zhang J, Liu H. The effects of microstructure on wave velocity and wavefront in granular assemblies with binary-sized particles. *Int J Solids Struct* 2019;159:156–62. doi:10.1016/j.jisolsstr.2018.09.026.
- [40] Germain P. The Method of Virtual Power in Continuum Mechanics. Part 2: microstructure. *SIAM J Appl Math* 1973;25:556–75. doi:10.1137/0125053.
- [41] dell'Isola F, Seppecher P, Alibert JJ, Lekszycki T, Grygoruk R, Pawlikowski M, et al. Pantographic metamaterials: an example of mathematically driven design and of its technological challenges. *Contin Mech Thermodyn* 2019;31:851–84. doi:10.1007/s00161-018-0689-8.
- [42] Giorgio I, Grygoruk R, dell'Isola F, Steigmann DJ. Pattern formation in the three-dimensional deformations of fibered sheets. *Mech Res Commun* 2015;69:164–71. doi:10.1016/j.mechrescom.2015.08.005.
- [43] Giorgio I, Rizzi NL, Turco E. Continuum modelling of pantographic sheets for out-of-plane bifurcation and vibrational analysis. *Proc R Soc A Math Phys Eng Sci* 2017;473. doi:10.1098/rspa.2017.0636.
- [44] Abdoul-Anziz H, Seppecher P. Strain gradient and generalized continua obtained by homogenizing frame lattices. *Math Mech Complex Syst* 2018;6:213–50. doi:10.2140/memocs.2018.6.213.
- [45] Alibert J-J, Seppecher P, dell'Isola F. Truss Modular Beams with Deformation Energy Depending on Higher Displacement Gradients. *Math Mech Solids* 2003;8:51–73. doi:10.1177/1081286503008001658.

- [46] Seppecher P, Alibert JJ, dell'Isola F. Linear elastic trusses leading to continua with exotic mechanical interactions. *J Phys Conf Ser* 2011;319 Institute of Physics Publishing. doi:10.1088/1742-6596/319/1/012018.
- [47] Misra A, Poorsolhjoui P. Identification of higher-order elastic constants for grain assemblies based upon granular micromechanics. *Math Mech Complex Syst* 2015;3:285–308. doi:10.2140/memocs.2015.3.285.
- [48] Essén H. Average angular velocity. *Eur J Phys* 1993;14:201–5. doi:10.1088/0143-0807/14/5/002.
- [49] Bacigalupo A, Gambarotta L. Second-gradient homogenized model for wave propagation in heterogeneous periodic media. *Int J Solids Struct* 2014;51:1052–65. doi:10.1016/j.ijsolstr.2013.12.001.
- [50] Mokhtari AA, Lu Y, Srivastava A. On the properties of phononic eigenvalue problems. *J Mech Phys Solids* 2019;131:167–79. doi:10.1016/j.jmps.2019.07.005.
- [51] Mokhtari AA, Lu Y, Srivastava A. On the emergence of negative effective density and modulus in 2-phase phononic crystals. *J Mech Phys Solids* 2019;126:256–71. doi:10.1016/j.jmps.2019.02.016.
- [52] Gehring GM, Schweinsberg A, Barsi C, Kostinski N, Boyd RW. Observation of backward pulse propagation through a medium with a negative group velocity. *Science* (80-) 2006;312:895 LP – 897. doi:10.1126/science.1124524.
- [53] Boechler N, Yang J, Theocharis G, Kevrekidis PG, Daraio C. Tunable vibrational band gaps in one-dimensional diatomic granular crystals with three-particle unit cells. *J Appl Phys*. 2011;109. doi:10.1063/1.3556455.
- [54] Jensen JS. Phononic band gaps and vibrations in one- and two-dimensional mass-spring structures. *J Sound Vib* 2003;266:1053–78. doi:10.1016/S0022-460X(02)01629-2.
- [55] Madeo A, Collet M, Miniaci M, Billon K, Ouisse M, Neff P. Modeling phononic crystals via the weighted relaxed micromorphic model with free and gradient micro-inertia. *J Elast* 2018;130:59–83. doi:10.1007/s10659-017-9633-6.
- [56] Zeng X, Chen Y, Lee JD. Determining material constants in nonlocal micromorphic theory through phonon dispersion relations. *Int J Eng Sci* 2006;44:1334–45. doi:10.1016/j.ijengsci.2006.08.002.
- [57] Placidi L, Andreaus U, Della Corte A, Lekszycki T. Gedanken experiments for the determination of two-dimensional linear second gradient elasticity coefficients. *Zeitschrift Fur Angew Math Und Phys* 2015;66:3699–725. doi:10.1007/s00033-015-0588-9.
- [58] Zhang Q, Venegas R, Umnova O, Lan Y. Tuning coupled wave dispersion in a granular chain on a V-shaped rail. *Wave Motion* 2019;90:51–65. doi:10.1016/j.wavemoti.2019.04.009.
- [59] Chong C, Porter MA, Kevrekidis PG, Daraio C. Nonlinear coherent structures in granular crystals. *J Phys Condens Matter* 2017;29. doi:10.1088/1361-648X/aa7672.
- [60] Ghavanloo E, Fazelzadeh SA, Rafii-Tabar H. Formulation of an efficient continuum mechanics-based model to study wave propagation in one-dimensional diatomic lattices. *Mech Res Commun* 2020;103. doi:10.1016/j.mechrescom.2019.103467.
- [61] Fraternali F, Porter MA, Daraio C. Optimal design of composite granular protectors. *Mech Adv Mater Struct* 2010;17:1–19. doi:10.1080/15376490802710779.



**Appendix F: Paper P6****Title:**

On the statics and dynamics of granular-microstructured rods with higher order effects

**Authors:**

Nima Nejadi Sadeghi

Anil Misra

**Journal:**

Mathematics and Mechanics of Solids (accepted for publication)

**Credit authorship statement:**

A.M. and N.N. conceived the idea. N.N. developed the model and performed calculations and analysis. All authors contributed to the discussion of all aspects of this work. N.N. wrote the manuscript. All authors edited the manuscript.

**On the statics and dynamics of granular-microstructured rods with higher order effects**

Nima NejadSadeghi<sup>1</sup> and Anil Misra<sup>2\*</sup>

<sup>1</sup>Mechanical Engineering Department,  
University of Kansas, 1530 W 15<sup>th</sup> Street, Learned Hall, Lawrence, KS 66047-7609

<sup>2</sup>Civil, Environmental and Architectural Engineering Department,  
University of Kansas, 1530 W 15<sup>th</sup> Street, Learned Hall, Lawrence, KS 66045-7609.

\*corresponding author: Ph: (785) 864-1750, Fax: (785) 864-5631, Email: amisra@ku.edu

*Mathematics and Mechanics of Solids*

**Abstract**

Granular-microstructured rods show strong dependence of grain-scale interactions in their mechanical behavior, and therefore, their proper description requires theories beyond the classical theory of continuum mechanics. Recently, the authors have derived a micromorphic continuum theory of degree  $n$  based upon the granular micromechanics approach (GMA). Here, the GMA is further specialized for a one-dimensional material with granular microstructure that can be described as a micromorphic medium of degree 1. To this end, the constitutive relationships, governing equations of motion and variationally consistent boundary conditions are derived. Furthermore, the static and dynamic length scales are linked to the second gradient stiffness and micro-scale mass density distribution, respectively. The behavior of a one-dimensional granular structure for different boundary conditions is studied in both static and dynamic problems. The effect of material constants and the size effects on the response of the material is also investigated through parametric studies. In the static problem, the size-dependency of the system is observed in the width of the emergent boundary layers for certain imposed boundary conditions. In the dynamic problem, microstructural effects are always present and are manifested as deviations in the natural frequencies of the system from their classical counterparts.

Keywords: free vibration; micromorphic theory; size effect; granular micromechanics; microstructured solids.

## 1. Introduction

Small-sized structures are being increasingly utilized in applications such as nano- and micro-electro-mechanical systems (NEMS/MEMS) and Atomic Force Microscopes (AFMs). In these structures, the effect of the microstructure on the behavior of the material is significant. Such a microstructure can be the constituent grains in a granular medium or a collection of beam elements in pantographic materials [1]. In addition, microstructured materials have also been widely used in the context of mechanical metamaterials to obtain desired unusual behavior that natural materials do not exhibit [2, 3]. For such materials (or structures depending on the scale of observation), there exists inconsistencies between the experimental findings and the classical continuum mechanics predictions [4–7]. Such variations in the observed behavior and classical continuum theory predictions pertain to the existence of the micro-mechano-morphological effects. These effects on the mechanical behavior of the materials become noticeable, especially in dynamic problems where the wavelengths of excitation are comparable to the characteristic lengths of such systems [8]. To account for the discrepancies between the theoretical predictions and experimental observations, and to overcome the inherent limitations of the classical continuum theory, non-classical continuum theories were developed, among which we refer to the works in [9–14].

To investigate the predictions of such non-classical theories, one-dimensional models are often utilized. A particular widely-studied example of such one-dimensional structures is rods. There have been several recently published articles on the analysis of one-dimensional rods utilizing non-classical continuum theories such as stress gradient (also called nonlocal), strain gradient (also called gradient elasticity), and nonlocal strain gradient models to capture the microstructural effects in static and dynamic problems [15–32]. We note that these effects have also been reported in the studies concerned with the vibration and buckling phenomena in beams, e.g. in [33–36], small-scaled truss and frame models, e.g., in [37], two-dimensional problems, e.g., in [38, 39], and metamaterials [40].

In the present paper, we expound upon a particular form of a microstructured solid, namely a one-dimensional material with granular microstructure, which is modeled as a micromorphic media of degree one using the granular micromechanics approach (GMA). GMA is a micromorphic theory equipped with an enriched kinematics to describe grain motion, in which the derived governing



equations of motion constituents are related to the granular mechano-structure of the material [41, 42]. The mathematical model derived through GMA has shown interesting results in the prediction of acoustic (material deformation) and optical (internal deformation) wave branches in granular media undergoing excitation [43–45]. The dispersive behavior predicted by GMA reflects many aspects of granular structures dynamic behavior (e.g., existence of frequency band gaps and negative group velocity), and can potentially be employed to obtain the continuum material constants of granular media [46–48].

It is notable that the dispersion analysis of infinite media does not fully reveal the effects of the length scale parameters and the applied boundary conditions on the behavior of the granular media. Therefore, it is our purpose here to further elucidate the contribution of different length scale parameters, stiffness and inertial measures (micro-mechano-morphology) to the behavior of finite length one-dimensional granular media in both static and dynamic uniaxial loading under different boundary conditions. Such analyses are essential for understanding the complex behavior of such media and to help designing suitable experimental setup to extract and identify the material parameters defining granular materials, which currently proves challenging, if not impossible. Moreover, the findings of the present paper help analyzing a myriad of granular materials found in nature, as well as serve as a design tool to conceive granular metamaterials that can be realized through additive manufacturing technologies for particular applications [49, 50].

The structure of the paper is as follows. Section 2 describes the granular micromechanics approach to model one-dimensional continua with granular microstructure. Section 3 is devoted to the static behavior analysis of one-dimensional continua with granular microstructure subjected to different boundary conditions. In section 4, the dynamic behavior of one-dimensional continua with granular microstructure is investigated through free vibration analysis. Finally, section 5 presents the summary of the work and the concluding remarks.

## **2. GMA based micromorphic theory of degree 1 for a 1D rod**

This section introduces the continuum framework for GMA based micromorphic theory of degree 1 to model a one-dimensional granular structure. The model adopted in the current paper assumes linear elastic mechanisms of deformation with no damping. The references [41, 42, 45] describe

the framework for a three-dimensional granular structure. The reader is referred to the mentioned articles for more detailed description.

## 2.1. Kinematic variables

Let us consider a one-dimensional object of length  $L$  with an underlying granular microstructure composed of many grains with random mechanical and inertial properties (hereafter referred as 1D granular rod), as shown in Fig. 1. At the spatial scale, in which the object may be treated as a continuum, the material point P can be identified using the macro-scale coordinate system  $X$ . Material point P is considered to have the macro-scale linear mass density  $\rho$  (given as mass per unit length), differential length  $dX$ , and differential mass of  $dm = \rho dX$  in the initial configuration. We denote by  $X$  and  $x = \Xi(X, t)$  the position of the point P at initial and current configurations, respectively, where  $\Xi$  is the macro-scale placement function and  $t$  denotes time. The macro-scale displacement is defined as  $u = x - X$ . At a finer spatial scale, material point P is a collection of grains and is referred to as a volume element (VE) with length  $L' = dX$ . For a periodic granular structure, such as a granular composite made of several grains repeating periodically, the VE is identical to the notion of a unit cell, and for non-periodic granular structures, it is the volume of the granular material over which the local (micro-scale) deformation is homogenized. In the latter case, the VE is chosen as per the requirement of the mechanical problem and such that it contains sufficiently large number of grains to justify the continuity assumption. The position of each grain within the VE is identified using the micro-scale coordinate system  $X'$  of the finer spatial scale. This coordinate system is attached to the center of mass (COM) of the material point P, is taken to be parallel to the macro-scale coordinate system  $X$ , and displaces in consonance with the macro-scale displacement  $u$ . The micro-scale displacement  $u'$  is expressed as  $u' = x' - X'$  where  $X'$  and  $x' = \Xi'(X, X', t)$  denote the position vectors of a grain centroid at initial and current configurations, respectively, and  $\Xi'$  is the micro-scale placement function. We assume that both the micro- and macro-scale deformations are infinitesimal, and are continuous and differentiable functions of the micro- and macro-scale coordinates up to the desired order, such that we can write

$$u = u(x, t), \quad u' = u'(x, x', t). \quad (1)$$

For a micromorphic theory of degree 1, the micro-scale displacement  $u'$  can be written in the form below using a polynomial expansion with respect to  $x'$  about the COM of the VE [41].

$$u' = \psi_{11}x' + \psi_{111}(x')^2. \quad (2)$$

In Eq. (2),  $\psi_{11}$  and  $\psi_{111}$  are functions of  $x$  and  $t$  only, and account for the local deformation within the VE. We note that although for systems with small number of particles (or layers in composites modeled as one dimensional) a more accurate approximation of displacement can be made by subdividing the VE into different regions with different strain regimes (e.g., see [51, 52]), for large number of particles (or layers), such approaches become increasingly complicated and a linear or quadratic approximation within the whole domain of VE remains the most feasible (e.g., see [53]). We note here that efforts at formal homogenization (continualization) of mass-spring systems, such as in [54, 55], also propose multiscale decomposition of displacement field among the possible approaches for developing continuum models. Using Eq. (2), the total displacement vector for the grains within the VE are written as

$$\phi = u + u' = \bar{\phi} + \psi_{11}x' + \psi_{111}(x')^2. \quad (3)$$

where  $\bar{\phi} = u$  is adopted such that the variable names are in harmony with previous publications [41, 42]. For a micromorphic theory of degree one, we utilize the following relative deformation measures [12, 13, 41]

$$\gamma_{11} = \bar{\phi}_{,x} - \psi_{11}, \quad \gamma_{111} = \psi_{11,x} - \psi_{111}, \quad (4)$$

where, hereafter, differentiation with respect to the spatial coordinates is denoted by a comma in the subscript. In Eq. (4), the differentiation is performed with respect to the macro-scale coordinate system. For a micromorphic theory of degree 1, and as a constitutive choice, we assume here that the relative deformation measure  $\gamma_{111}$  vanishes, therefore we have  $\psi_{111} = \psi_{11,x}$ . Note that if we further assume that the relative deformation measure  $\gamma_{11}$  vanishes, a second gradient model is obtained [41].

The relative displacement between two neighboring grains  $n$  and  $p$ ,  $\delta^{np}$ , can be written, using Eq. (3) and Eq. (4), as

$$\delta^{np} = \phi^p - \phi^n = \delta^M - \delta^m + \delta^g, \quad (5)$$

where the following micro-scale kinematic measures are introduced

$$\delta^M = \bar{\phi}_{,x} J_1^{np}, \quad \delta^m = \gamma_{11} J_1^{np}, \quad \delta^g = \psi_{11,x} J_2^{np}. \quad (6)$$

In Eq. (6),  $\delta^M$  signifies the portion of the relative displacement due to the macro-scale displacement gradient  $\bar{\phi}_{,x}$ ,  $\delta^m$  represents the portion of the relative displacement due to the fluctuation between the macro-scale displacement gradient  $\bar{\phi}_{,x}$  and the micro-scale kinematic measure  $\psi_{11}$ , and  $\delta^g$  denotes the portion of the relative displacement due to the second gradient term. Furthermore, we have defined the geometry moment measures  $J_1^{np} = l^p - l^n$  and  $J_2^{np} = l^p l^p - l^n l^n$ , where  $l^q$  represents the vector joining the COM of the VE to the grain  $q$  centroid. Note that  $J_2^{np} = (l^p - l^n)(l^p + l^n) = J_1^{np}(l^p + l^n)$  which implies that for grains  $n$  and  $p$ , the farther they are from the COM of the VE, the higher the second gradient contribution to the relative displacement,  $\delta^g$ .

## 2.2. Constitutive equations

We assume the macro-scale deformation energy density to be a function of the continuum kinematic measures  $\bar{\phi}_{,x}$ ,  $\gamma_{11}$ , and  $\psi_{11,x}$ , i.e., of the form  $W = W(\bar{\phi}_{,x}, \gamma_{11}, \psi_{11,x})$ . Macro-scale stress measures, namely, Cauchy stress,  $\tau_{11}$ , relative stress,  $\sigma_{11}$ , and double stress,  $\mu_{111}$ , are defined as conjugates to the continuum kinematic measures, and expressed as

$$\tau_{11} = \frac{\partial W}{\partial \bar{\phi}_{,x}}, \quad \sigma_{11} = \frac{\partial W}{\partial \gamma_{11}}, \quad \mu_{111} = \frac{\partial W}{\partial \psi_{11,x}}. \quad (7)$$

The macro-scale deformation energy density can also be expressed in terms of the micro-scale deformation energy density as

$$W = \frac{1}{L'} \sum_{\alpha} W^{\alpha}(\delta^{\alpha M}, \delta^{\alpha m}, \delta^{\alpha g}), \quad (8)$$



where  $W^\alpha$  represents the micro-scale deformation energy for the  $\alpha^{\text{th}}$  interacting pair of grains within the VE. Intergranular forces can be defined as conjugates to the micro-scale kinematic measures as

$$\frac{\partial W^\alpha}{\partial \delta^{\alpha\text{M}}} = f^{\alpha\text{M}}, \quad \frac{\partial W^\alpha}{\partial \delta^{\alpha\text{m}}} = f^{\alpha\text{m}}, \quad \frac{\partial W^\alpha}{\partial \delta^{\alpha\text{g}}} = f^{\alpha\text{g}}. \quad (9)$$

Substituting Eq. (8) in Eq. (7) and employing Eq. (6) and Eq. (9), the macro-scale stress measures are expressed as

$$\tau_{11} = \frac{1}{L'} \sum_{\alpha} f^{\alpha\text{M}} J_1^{\alpha}, \quad \sigma_{11} = \frac{1}{L'} \sum_{\alpha} f^{\alpha\text{m}} J_1^{\alpha}, \quad \mu_{111} = \frac{1}{L'} \sum_{\alpha} f^{\alpha\text{g}} J_2^{\alpha}. \quad (10)$$

Eq. (10) defines the macro-scale stress measures in terms of micro-scale force measures and geometry moment measures, where  $J_1^{\alpha}$  and  $J_2^{\alpha}$  for the  $\alpha^{\text{th}}$  grain pair for interacting grains n and p are evaluated as  $J_1^{\text{np}}$  and  $J_2^{\text{np}}$ , respectively.

For formulating micro-scale constitutive equations relating micro-scale kinematic measures to their conjugate intergranular force measures, the following form for the micro-scale deformation energy for the  $\alpha^{\text{th}}$  grain pair is considered

$$W^\alpha = \frac{1}{2} K^{\alpha\text{M}} (\delta^{\alpha\text{M}})^2 + \frac{1}{2} K^{\alpha\text{m}} (\delta^{\alpha\text{m}})^2 + K^{\alpha\text{Mm}} \delta^{\alpha\text{M}} \delta^{\alpha\text{m}} + \frac{1}{2} K^{\alpha\text{g}} (\delta^{\alpha\text{g}})^2. \quad (11)$$

Based on Eq. (11), there are four linear mechanisms involved in the deformation of a grain pair in contact, each quadratic in form.  $K^{ai}$ ,  $i = \text{M, m, Mm, g}$  are the stiffnesses associated with their corresponding mechanisms.

Intergranular forces introduced in Eq. (9) are obtained, using Eq. (11), as

$$\begin{aligned} f^{\alpha\text{M}} &= \frac{\partial W^\alpha}{\partial \delta^{\alpha\text{M}}} = K^{\alpha\text{M}} \delta^{\alpha\text{M}} + K^{\alpha\text{Mm}} \delta^{\alpha\text{m}}, \\ f^{\alpha\text{m}} &= \frac{\partial W^\alpha}{\partial \delta^{\alpha\text{m}}} = K^{\alpha\text{m}} \delta^{\alpha\text{m}} + K^{\alpha\text{Mm}} \delta^{\alpha\text{M}}, \\ f^{\alpha\text{g}} &= \frac{\partial W^\alpha}{\partial \delta^{\alpha\text{g}}} = K^{\alpha\text{g}} \delta^{\alpha\text{g}}. \end{aligned} \quad (12)$$

Finally, using Eq. (12), the macro-scale constitutive relationships in Eq. (10) are described as

$$\begin{aligned}
\tau_{11} &= (C^M + C^{Mm}) \bar{\phi}_{,x} - C^{Mm} \psi_{11}, \\
\sigma_{11} &= (C^{Mm} + C^m) \bar{\phi}_{,x} - C^m \psi_{11}, \\
\mu_{111} &= C^g \psi_{11,x},
\end{aligned} \tag{13}$$

where the macro-scale stiffnesses  $C^M$ ,  $C^m$ ,  $C^{Mm}$ , and  $C^g$  are expressed as

$$\begin{aligned}
C^M &= \frac{1}{L'} \sum_{\alpha} K^{\alpha M} J_1^{\alpha} J_1^{\alpha}, & C^m &= \frac{1}{L'} \sum_{\alpha} K^{\alpha m} J_1^{\alpha} J_1^{\alpha}, \\
C^{Mm} &= \frac{1}{L'} \sum_{\alpha} K^{\alpha Mm} J_1^{\alpha} J_1^{\alpha}, & C^g &= \frac{1}{L'} \sum_{\alpha} K^{\alpha g} J_2^{\alpha} J_2^{\alpha}.
\end{aligned} \tag{14}$$

For the stiffnesses introduced in Eq. (14), the superscript M denotes the stiffness due to macro-scale deformation, the superscript m denotes the micro-scale (relative deformation) stiffness that acts analogous to the shear rigidity in Timoshenko beam model, the superscript Mm denotes the coupling (cross-linking) stiffness between the macro- and micro-scale deformations, and the superscript g denotes the second gradient stiffness. We note here that the stiffness measures in Eq. (14) possess inherent length scales within their definitions that are natural consequences of the assumed kinematic field of motion for the grains. Accordingly,  $\sqrt{\frac{C^g}{C^M}}$  is considered as the static length scale for the current problem.

### 2.3. Governing equations of motion

Hamilton's principle is used to obtain equations of motion for the 1D granular rod. Hamilton's principle requires the action functional to be minimum, and is expressed as

$$\int_{t_0}^{t_1} (\delta \tilde{T} - \delta \tilde{W} + \delta \tilde{W}_{ext}) dt = 0, \tag{15}$$

where  $\delta$  is the variation symbol and the terms  $\tilde{T}$ ,  $\tilde{W}$ , and  $\tilde{W}_{ext}$  are defined in the following. The term  $\tilde{T} = \int_L T dx$  is the total kinetic energy of the granular structure, in which  $T$  is the kinetic energy density, utilizing König's theorem [56] defined and expanded as [41]

$$T = \frac{1}{L} \int_L \frac{1}{2} \rho' \dot{\phi} \dot{\phi} dx' = \frac{1}{2} \rho \dot{\phi} \dot{\phi} + \frac{1}{2} \rho_{11} \dot{\psi}_{11} \dot{\psi}_{11} + \rho_{111} \dot{\psi}_{11} \dot{\psi}_{11,x} + \frac{1}{2} \rho_{1111} \dot{\psi}_{11,x} \dot{\psi}_{11,x}. \tag{16}$$

In Eq. (16),  $\rho'$  is the micro-scale mass density per unit macro-volume, and over-dots here and henceforward represent differentiation with respect to time. The following inertia measures have been defined [41]

$$\rho = \frac{1}{L'} \int_{L'} \rho' dx', \quad \rho_{11} = \frac{1}{L'} \int_{L'} \rho'(x')^2 dx', \quad \rho_{111} = \frac{1}{L'} \int_{L'} \rho'(x')^3 dx', \quad \rho_{1111} = \frac{1}{L'} \int_{L'} \rho'(x')^4 dx'. \quad (17)$$

The term  $\rho$  represents the macro-scale mass density and is an average of the micro-scale mass density  $\rho'$  within the VE. On the other hand, the other inertia measures introduced in Eq. (17) are functions of the micro-scale mass density and its spatial distribution and inherently include the length scales existing in the dynamic problem. In particular, the inertia measure  $\rho_{111}$  is due to non-symmetric micro-scale mass density distribution in the VE, e.g., for a graded granular material in micro-scale, and vanishes for symmetric micro-scale mass density distributions [45]. Interestingly, and as a consequence of Eq. (17), these length scales are not independent, but are related to each other through the micro-scale mass density  $\rho'$  distribution. In other words, for a known micro-scale mass density  $\rho'$  distribution within the VE, these length scales are fixed [45]. The kinetic energy introduced in Eq. (16) results from the assumed kinematic field in Eq. (3). We note that the additional velocity gradient terms appearing in Eq. (16) are not postulated *a priori* as often done in higher order continuum modeling (which are typically introduced to improve the dispersion predictions). This form of kinetic energy includes terms that are absent in classical continuum mechanics formulation to account for the non-uniform distribution of velocity in the VE, and expands upon the terms currently postulated in nonlocal strain gradient elasticity (e.g. in [31]). The existence of velocity gradient terms in the description of the kinetic energy has also been observed in gradient elasticity models to describe lattices with distributed mass properties [15] and in works concerning modeling the effect of micro-inertia in heterogeneous materials, e.g., in [57]. Moreover, velocity gradient terms have been also adopted to model wave dispersion in nonlinear pantographic beams and related to the distributed masses along the rigid links [58]. For the kinetic energy in Eq. (16) to be positive definite, the inequality  $\rho_{11}\rho_{1111} - \rho_{111}^2 > 0$  must hold. This inequality is obtained by rewriting Eq. (16) in the form  $T = \frac{1}{2} \check{\mathbf{x}}^T \check{\mathbf{A}} \check{\mathbf{x}}$ , where  $\check{\mathbf{x}} = \left[ \dot{\phi} \ \dot{\psi}_{11} \ \dot{\psi}_{11,x} \right]^T$ , and requiring that the matrix  $\check{\mathbf{A}}$  be positive definite.

In Eq. (15),  $\delta\tilde{W} = \int_L \delta W dx$  represents the variation of total macro-scale deformation energy, expressed as

$$\delta\tilde{W} = -\int_L (\tau_{11} + \sigma_{11})_{,x} \delta\bar{\phi} dx - \int_L (\mu_{111,x} + \sigma_{11}) \delta\psi_{11} dx + (\tau_{11} + \sigma_{11}) \delta\bar{\phi} \Big|_{x=0}^{x=L} + \mu_{111} \delta\psi_{11} \Big|_{x=0}^{x=L}. \quad (18)$$

Finally, the term  $\delta\tilde{W}_{ext}$  in Eq. (15) corresponds to the variation of total external energy defined as

$$\delta\tilde{W}_{ext} = \int_L \underline{f} \delta\bar{\phi} dx + \int_L \underline{\Phi} \delta\psi_{11} dx + \underline{t} \delta\bar{\phi} \Big|_{x=0}^{x=L} + \underline{T} \delta\psi_{11} \Big|_{x=0}^{x=L}. \quad (19)$$

In Eq. (19),  $\underline{f}$  is the non-contact body force per unit length,  $\underline{t}$  is the contact traction,  $\underline{\Phi}$  is the non-contact body double force per unit length, and  $\underline{T}$  is the contact double traction. Substituting Eq. (16), Eq. (18), and Eq. (19) in the expression for Hamilton's principle in Eq. (15) results in

$$\begin{aligned} & \int_{t_0}^{t_1} \int_L \left[ (\tau_{11} + \sigma_{11})_{,x} + \underline{f} - \rho \ddot{\phi} \right] \delta\bar{\phi} dx dt \\ & + \int_{t_0}^{t_1} \int_L \left[ \sigma_{11} + \mu_{111,x} + \underline{\Phi} - \rho_{11} \dot{\psi}_{11} + \rho_{1111} \dot{\psi}_{11,xx} + (\rho_{111})_{,x} \dot{\psi}_{11} + (\rho_{1111})_{,x} \dot{\psi}_{11,x} \right] \delta\psi_{11} dx dt \\ & + \int_{t_0}^{t_1} \left[ (\underline{t} - \tau_{11} - \sigma_{11}) \delta\bar{\phi} \Big|_{x=0}^{x=L} dt + \int_{t_0}^{t_1} \left[ (\underline{T} - \rho_{11} \dot{\psi}_{11} - \rho_{1111} \dot{\psi}_{11,xx} - \mu_{111}) \delta\psi_{11} \Big|_{x=0}^{x=L} dt \right] = 0 \end{aligned} \quad (20)$$

From Eq. (20) it follows that, after assuming zero non-contact body forces and double forces, using the constitutive equations in Eq. (13), and assuming spatial independence of the macro-scale stiffnesses, the equations of motion for the problem domain  $0 \leq x \leq L$  are expressed as

$$\left( C^M + C^m + 2C^{Mm} \right) \bar{\phi}_{,xx} - \left( C^m + C^{Mm} \right) \psi_{11,x} = \rho \ddot{\phi}, \quad (21a)$$

$$C^g \psi_{11,xx} + \left( C^{Mm} + C^m \right) \bar{\phi}_{,x} - C^m \psi_{11} = \rho_{11} \dot{\psi}_{11} - \rho_{1111} \dot{\psi}_{11,xx} - (\rho_{111})_{,x} \dot{\psi}_{11} - (\rho_{1111})_{,x} \dot{\psi}_{11,x}. \quad (21b)$$

From Eq. (20), the boundary conditions are stated as

$$\left( \underline{t} - \left( C^M + C^m + 2C^{Mm} \right) \bar{\phi}_{,x} + \left( C^m + C^{Mm} \right) \psi_{11} \right) \delta\bar{\phi} = 0 \quad \text{at } x = 0 \text{ and } L, \quad (22a)$$

$$\left( \underline{T} - \rho_{11} \dot{\psi}_{11} - \rho_{1111} \dot{\psi}_{11,x} - C^g \psi_{11,x} \right) \delta\psi_{11} = 0 \quad \text{at } x = 0 \text{ and } L. \quad (22b)$$

We remark the presence of terms with time derivative in the boundary conditions in Eq. (22b). The existence of time derivative terms in the boundary conditions are also discussed in the analysis of nonlocal strain gradient rods [31].

In this paper, we assume that the micro-scale mass density,  $\rho'$ , is constant in both micro- and macro-scale coordinate systems. Consequently, the equations of motion reduce to

$$\left(C^M + C^m + 2C^{Mm}\right)\bar{\phi}_{,xx} - \left(C^m + C^{Mm}\right)\psi_{11,x} = \rho\ddot{\bar{\phi}}, \quad (23a)$$

$$C^g\psi_{11,xx} + \left(C^{Mm} + C^m\right)\bar{\phi}_{,x} - C^m\psi_{11} = \rho_{11}\ddot{\psi}_{11} - \rho_{1111}\ddot{\psi}_{11,xx}. \quad (23b)$$

Moreover, the boundary conditions in Eq. (22) reduce to

$$\left(\underline{t} - \left(C^M + C^m + 2C^{Mm}\right)\bar{\phi}_{,x} + \left(C^m + C^{Mm}\right)\psi_{11}\right)\delta\bar{\phi} = 0 \quad \text{at } x = 0 \text{ and } L, \quad (24a)$$

$$\left(\underline{T} - \rho_{1111}\ddot{\psi}_{11,x} - C^g\psi_{11,x}\right)\delta\psi_{11} = 0 \quad \text{at } x = 0 \text{ and } L. \quad (24b)$$

#### 2.4. Dimensionless form of the governing equations

For further discussion, it is useful to reduce the number of parameters by nondimensionalizing the equations of motion in Eq. (23) to exclude the explicit physical parameters of the system. To this end, we first define three dynamic length scales  $l_1$ ,  $l_2$ , and  $l_3$  as

$$l_1^2 = \frac{\rho_{11}}{\rho}, \quad l_2^3 = \frac{\rho_{111}}{\rho}, \quad l_3^4 = \frac{\rho_{1111}}{\rho}, \quad (25)$$

which, for the constant micro-scale mass density,  $\rho'$ , lead to  $l_1^2 = \frac{(L')^2}{12}$ ,  $l_2^3 = 0$ ,  $l_3^4 = \frac{(L')^4}{80}$ ,

where  $L'$  is the VE size [45]. Additionally, we introduce the following dimensionless variables and parameters

$$\tilde{\bar{\phi}} = \frac{\bar{\phi}}{L}, \quad \tilde{\psi}_{11} = \psi_{11}, \quad \tilde{x} = \frac{x}{L}, \quad \tilde{t} = \frac{t}{\sqrt{\frac{\rho L^2}{C^M}}}, \quad \alpha_m = \frac{C^m}{C^M}, \quad \alpha_{Mm} = \frac{C^{Mm}}{C^M}, \quad l_s = \frac{1}{L}\sqrt{\frac{C^g}{C^M}}, \quad n = \frac{L}{L'}. \quad (26)$$



It is understood that the parameter  $\alpha_m$  gives the ratio of the micro-scale (relative deformation) stiffness to the macro-scale stiffness,  $\alpha_{Mm}$  represents the ratio of the cross-linking stiffness to the macro-scale stiffness, and  $l_s$  is the dimensionless static length scale, where it is clear that larger values for  $l_s$  signify more noticeable second gradient effects. Moreover,  $n$  shows how large the macro-scale structure length is compared to the VE length. Now, using Eq. (25) and Eq. (26), the dimensionless form of the equations of motion in Eq. (23) is stated as

$$(1 + \alpha_m + 2\alpha_{Mm}) \tilde{\phi}_{,\tilde{x}\tilde{x}} - (\alpha_m + \alpha_{Mm}) \tilde{\psi}_{11,\tilde{x}} = \ddot{\phi}, \quad (27a)$$

$$l_s^2 \tilde{\psi}_{11,\tilde{x}\tilde{x}} + (\alpha_m + \alpha_{Mm}) \tilde{\phi}_{,\tilde{x}} - \alpha_m \tilde{\psi}_{11} = \frac{1}{12n^2} \ddot{\psi}_{11} - \frac{1}{80n^4} \ddot{\psi}_{11,\tilde{x}\tilde{x}}. \quad (27b)$$

The dimensionless spatial domain of the problem is  $0 \leq \tilde{x} \leq 1$ . We emphasize that the coefficients on the right hand side of Eq. (27b) are not arbitrary, but are natural consequences of the assumed micro-scale mass density,  $\rho'$ , distribution. Indeed, these coefficients differ if one considers a different distribution for the micro-scale mass density,  $\rho'$ , within the VE [45]. We note that the dimensionless material constants  $\alpha_m$  and  $\alpha_{Mm}$  must satisfy the positive definiteness of the macro-scale deformation energy density. This necessitates the inequality  $\alpha_m - \alpha_{Mm}^2 > 0$  to hold.

The dimensionless form of the boundary conditions in Eq. (24) is expressed as

$$\left( \tilde{t} - (1 + \alpha_m + 2\alpha_{Mm}) \tilde{\phi}_{,\tilde{x}} + (\alpha_m + \alpha_{Mm}) \tilde{\psi}_{11} \right) \delta \tilde{\phi} = 0 \quad \text{at } \tilde{x} = 0 \text{ and } 1, \quad (28a)$$

$$\left( \tilde{T} - \frac{1}{80n^4} \ddot{\psi}_{11,\tilde{x}\tilde{x}} - l_s^2 \tilde{\psi}_{11,\tilde{x}\tilde{x}} \right) \delta \tilde{\psi}_{11} = 0 \quad \text{at } \tilde{x} = 0 \text{ and } 1. \quad (28b)$$

where  $\tilde{t} = \frac{t}{C^M}$  and  $\tilde{T} = \frac{T}{C^M L}$  are dimensionless contact traction and contact double traction, respectively.

The governing equations of motion in Eq. (27) result from the assumption of the existence of the relative deformation field  $\gamma_{11}$ , i.e., the macro-scale displacement gradient  $\bar{\phi}_{,x}$  is different from the micro-scale kinematic measure  $\psi_{11}$ . They are also predicated on the assumption of the existence

of a VE with a finite size, yet very small, compared to the macroscopic length of the structure. For the case of vanishing coupling stiffness  $\alpha_{Mm}$ , if we also assume that  $\alpha_m \rightarrow \infty$ , or equivalently, if the relative deformation measure  $\gamma_{11}$  is zero, i.e.,  $\tilde{\psi}_{11} = \tilde{\phi}_{,x}$ , we obtain the governing equation of motion of the form  $\left(1 - \frac{1}{12n^2} \frac{\partial^2}{\partial \tilde{x}^2} + \frac{1}{80n^4} \frac{\partial^4}{\partial \tilde{x}^4}\right) \ddot{\tilde{\phi}} = \left(1 - l_s^2 \frac{\partial^2}{\partial \tilde{x}^2}\right) \tilde{\phi}_{,\tilde{x}\tilde{x}}$ . The derived equation has a more general form although it has similarities with the nonlocal strain gradient models presented in [27, 31] and the model presented in [59], where the term  $\frac{1}{\sqrt{12}n}$  can be considered to be the dimensionless typical nonlocal parameter, and the term  $\frac{1}{\sqrt{80}n^2}$  is considered as an additional higher gradient nonlocal parameter. Note that the model presented in [31] can be deemed as a special case of the present model with only one term as the nonlocal parameter, and the model in [59] treats the dynamic length scales as independent constants without an explicit relation to the micro-scale mass density distribution. If we further assume  $\frac{L'}{L} \rightarrow 0$  (equivalently, if  $n \rightarrow \infty$ ), we recover the equation of motion of a rod based on strain-gradient elasticity of the dimensionless form  $\ddot{\tilde{\phi}} = \left(1 - l_s^2 \frac{\partial^2}{\partial \tilde{x}^2}\right) \tilde{\phi}_{,\tilde{x}\tilde{x}}$ , similar to the form reported in [30]. This approximation, in the limit as  $n \rightarrow \infty$ , shows that for practical cases, with finite  $n$ , the small scale effects described by the vanishing terms cannot be assumed to be insignificant although they may not be easily detectable in large-scale structures. Finally, in the absence of the static length scale  $l_s$ , the classical form of the governing equation is retrieved.

### 3. Static behavior

#### 3.1. General solution

Here we focus on the static deformation of the 1D granular rod. The governing equations in Eq. (27) for the static case reduce to the following balance equations

$$(1 + \alpha_m + 2\alpha_{Mm}) \tilde{\phi}_{,\tilde{x}\tilde{x}} - (\alpha_m + \alpha_{Mm}) \tilde{\psi}_{11,\tilde{x}} = 0, \quad (29a)$$

$$l_s^2 \tilde{\psi}_{11,\tilde{x}\tilde{x}} + (\alpha_m + \alpha_{Mm}) \tilde{\phi}_{,\tilde{x}} - \alpha_m \tilde{\psi}_{11} = 0, \quad (29b)$$

where the spatial domain for the problem is  $0 \leq \tilde{x} \leq 1$ . Using Eq. (28), the boundary conditions for the static case are written as

$$\left( \tilde{T} - (1 + \alpha_m + 2\alpha_{Mm}) \tilde{\phi}_{,\tilde{x}} + (\alpha_m + \alpha_{Mm}) \tilde{\psi}_{11} \right) \delta \tilde{\phi} = 0 \quad \text{at } \tilde{x} = 0 \text{ and } 1, \quad (30a)$$

$$\left( \tilde{T} - l_s^2 \tilde{\psi}_{11,\tilde{x}} \right) \delta \tilde{\psi}_{11} = 0 \quad \text{at } \tilde{x} = 0 \text{ and } 1. \quad (30b)$$

Here, an analytical solution for Eq. (29) is sought. To this end, Eq. (29b) is differentiated with respect to the spatial variable to obtain

$$l_s^2 \tilde{\psi}_{11,\tilde{x}\tilde{x}\tilde{x}} + (\alpha_m + \alpha_{Mm}) \tilde{\phi}_{,\tilde{x}\tilde{x}} - \alpha_m \tilde{\psi}_{11,\tilde{x}} = 0. \quad (31)$$

Substituting for  $\tilde{\phi}_{,\tilde{x}\tilde{x}}$  from Eq. (29a) into Eq. (31) gives

$$\tilde{\psi}_{11,\tilde{x}\tilde{x}\tilde{x}} - \kappa^2 \tilde{\psi}_{11,\tilde{x}} = 0, \quad \kappa^2 = \frac{\alpha_m - \alpha_{Mm}^2}{l_s^2 (1 + \alpha_m + 2\alpha_{Mm})}. \quad (32)$$

Eq. (32) can be readily solved to obtain a solution for the micro-scale kinematic measure,  $\tilde{\psi}_{11}$ , expressed as

$$\tilde{\psi}_{11} = \hat{C}_1 \cosh(\kappa \tilde{x}) + \hat{C}_2 \sinh(\kappa \tilde{x}) + \hat{C}_3, \quad (33)$$

where  $\hat{C}_1$ ,  $\hat{C}_2$ , and  $\hat{C}_3$  are constants of integration. From substituting Eq. (33) in Eq. (29a) it follows that

$$\tilde{\phi} = \frac{\alpha_m + \alpha_{Mm}}{\kappa(1 + \alpha_m + 2\alpha_{Mm})} \hat{C}_1 \sinh(\kappa \tilde{x}) + \frac{\alpha_m + \alpha_{Mm}}{\kappa(1 + \alpha_m + 2\alpha_{Mm})} \hat{C}_2 \cosh(\kappa \tilde{x}) + \hat{C}_5 \tilde{x} + \hat{C}_4, \quad (34)$$

where  $\hat{C}_4$  and  $\hat{C}_5$  are additional constants of integration to be determined. The solution for the macro-scale displacement  $\tilde{\phi}$  expressed in Eq. (34) bears similarities with the solution obtained

following the strain gradient theory for a microbar in [30], and for the gradient-elastic bar in [25]. Substituting Eq. (33) and Eq. (34) in Eq. (29b) results in  $\widehat{C}_5 = \widehat{C}_3$ , thereby reducing the number of unknown constants from five to four.

We here consider three possible scenarios for the applied boundary conditions in order to explore the static behavior of the 1D granular rod. These boundary conditions are all following the conventional macro-scale displacement-control experimental setup where the macro-scale displacement is fixed at one end and prescribed at the other end. The three considered experiments are different in terms of the boundary conditions imposed on the micro-scale kinematic measure  $\tilde{\psi}_{11}$  where either the value for  $\tilde{\psi}_{11}$  (geometrical boundary condition) or the value for  $\tilde{\psi}_{11,x}$  (natural boundary condition, i.e., the double traction) is prescribed at the ends (boundaries) of the structure. Such experiments, although performed computationally here, may help devise experiments to observe and extract micro-scale phenomena for materials with granular microstructure by demonstrating the level of the effect of the non-classical boundary conditions on the response of the system in a static case. For illustration of the predicted behavior, we consider a material with constants  $\alpha_m = 0.5$ ,  $\alpha_{Mm} = -0.4$ , and  $l_s = 0.05$ , for all three scenarios. This choice of parameters is known to yield interesting dynamic behavior of granular structures, namely the emergence of frequency band gaps and negative group velocity, while the deformation energy remains positive definite [43, 45]. In addition, certain micro-morphologies (e.g., see structure C in [60]) yield elastic constants of similar type.

### 3.2.Scenario 1

In the first scenario, demonstrated in Fig. 2(a), we consider the geometric boundary conditions of the form

$$\tilde{\phi}(0) = 0, \quad \tilde{\psi}_{11}(0) = 0, \quad \tilde{\phi}(1) = \bar{\phi}_r, \quad \tilde{\psi}_{11}(1) = \psi_r. \quad (35)$$

Eq. (35) implies that on the left end of the domain, both kinematic measures are fixed, and on the right end, both kinematic measures have prescribed values. Imposing the boundary conditions in Eq. (35) results in the following system of linear equations from which the constants  $\widehat{C}_1$ ,  $\widehat{C}_2$ ,  $\widehat{C}_3$ , and  $\widehat{C}_4$  are readily calculated

$$\begin{bmatrix} 0 & \frac{\alpha_m + \alpha_{Mm}}{\kappa(1 + \alpha_m + 2\alpha_{Mm})} & 0 & 1 \\ 1 & 0 & 1 & 0 \\ \frac{\alpha_m + \alpha_{Mm}}{\kappa(1 + \alpha_m + 2\alpha_{Mm})} \sinh(\kappa) & \frac{\alpha_m + \alpha_{Mm}}{\kappa(1 + \alpha_m + 2\alpha_{Mm})} \cosh(\kappa) & 1 & 1 \\ \cosh(\kappa) & \sinh(\kappa) & 1 & 0 \end{bmatrix} \begin{Bmatrix} \widehat{C}_1 \\ \widehat{C}_2 \\ \widehat{C}_3 \\ \widehat{C}_4 \end{Bmatrix} = \begin{Bmatrix} 0 \\ 0 \\ \bar{\phi}_r \\ \psi_r \end{Bmatrix}. \quad (36)$$

Moreover, the dimensionless macro-scale deformation energy density  $\tilde{W} = \frac{W}{C^M}$  is calculated as

$$\tilde{W} = \frac{1}{2} \tilde{\phi}_{,\tilde{x}}^2 + \frac{1}{2} \alpha_m (\tilde{\phi}_{,\tilde{x}} - \tilde{\psi}_{11})^2 + \alpha_{Mm} \tilde{\phi}_{,\tilde{x}} (\tilde{\phi}_{,\tilde{x}} - \tilde{\psi}_{11}) + \frac{1}{2} l_s^2 \tilde{\psi}_{11,\tilde{x}}^2. \quad (37)$$

Fig. 3(a) corresponds to the case where  $\bar{\phi}_r = 0.01$  and  $\psi_r = 0$ , Fig. 3(b) corresponds to the case where  $\bar{\phi}_r = 0$  and  $\psi_r = 0.01$ , and Fig. 3(c) shows the results for the case where  $\bar{\phi}_r = 0.01$  and  $\psi_r = 0.01$ . According to the results in Fig. 3(a), having the kinematic measure  $\tilde{\psi}_{11}$  fixed has negligible observable contribution on the behavior of the macro-scale displacement  $\tilde{\phi}$ , however, results in larger energy stored in the boundary layers. From the results shown in Fig. 3(b) for the case of zero macro-scale displacement  $\tilde{\phi}$  and imposed nonzero micro-scale kinematic measure  $\tilde{\psi}_{11}$  at the right end, we observe that while macroscopically the length of the structure has not changed, regions  $(\kappa)$  undergoing compression and tension exist within the material. Also, due to the difference in values between the macro-scale displacement gradient  $\tilde{\phi}_{,\tilde{x}}$  and micro-scale kinematic measure  $\tilde{\psi}_{11}$ , high deformation energy concentration is observed in the right boundary layer, while the rest of the material experiences negligible stored deformation energy. Fig. 3(c) results are the superposition of the two results in Fig. 3(a) and Fig. 3(b), which in terms of the macro-scale displacement  $\tilde{\phi}$  shows near linear trend, and in terms of the deformation energy density reveals localization in the left end and uniform deformation energy density in the rest of the domain.

### 3.3.Scenario 2

In the second scenario with results given in Fig. 4, we consider the following boundary conditions



$$\tilde{\phi}(0) = 0, \quad \tilde{\psi}_{11,\tilde{x}}(0) = 0, \quad \tilde{\phi}(1) = \bar{\phi}_r, \quad \tilde{\psi}_{11,\tilde{x}}(1) = \psi'_r, \quad (38)$$

which, in addition to the macro-scale displacement boundary conditions, imposes zero double traction on the left end, and a prescribed double traction on the right end. Such boundary conditions lead to the following system of linear equations for the constants  $\hat{C}_1, \hat{C}_2, \hat{C}_3,$  and  $\hat{C}_4,$

$$\begin{bmatrix} 0 & \frac{\alpha_m + \alpha_{Mm}}{\kappa(1 + \alpha_m + 2\alpha_{Mm})} & 0 & 1 \\ 0 & \kappa & 0 & 0 \\ \frac{\alpha_m + \alpha_{Mm}}{\kappa(1 + \alpha_m + 2\alpha_{Mm})} \sinh(\kappa) & \frac{\alpha_m + \alpha_{Mm}}{\kappa(1 + \alpha_m + 2\alpha_{Mm})} \cosh(\kappa) & 1 & 1 \\ \kappa \sinh(\kappa) & \kappa \cosh(\kappa) & 0 & 0 \end{bmatrix} \begin{Bmatrix} \hat{C}_1 \\ \hat{C}_2 \\ \hat{C}_3 \\ \hat{C}_4 \end{Bmatrix} = \begin{Bmatrix} 0 \\ 0 \\ \bar{\phi}_r \\ \psi'_r \end{Bmatrix}. \quad (39)$$

Fig. 4(a) corresponds to the case where  $\bar{\phi}_r = 0.01$  and  $\psi'_r = 0$ , Fig. 4(b) corresponds to the case where  $\bar{\phi}_r = 0$  and  $\psi'_r = 0.01$ , and Fig. 4(c) shows the results for the case where  $\bar{\phi}_r = 0.01$  and  $\psi'_r = 0.01$ . According to the results in Fig. 4(a), having the double traction zero at both ends results in a solution equal to a classical continuum. The macro-scale displacement  $\tilde{\phi}$  is perfectly linear and there is no contribution of energy due to the relative motion and second gradient deformation. Specifying a nonzero double traction on the right end, for which case the results are shown in Fig. 4(b), follows the same behavior as of the one in Fig. 3(b). For the superposition of the cases in Fig. 4(a) and Fig. 4(b), shown in Fig. 4(c), except for the right boundary layer, the energy content within the structure is equal to the classical case and the macro-scale displacement  $\tilde{\phi}$  follows an almost linear regime.

### 3.4.Scenario 3

In the third scenario with results presented in Fig. 5, we consider the mixed boundary conditions expressed as

$$\tilde{\phi}(0) = 0, \quad \tilde{\psi}_{11,\tilde{x}}(0) = 0, \quad \tilde{\phi}(1) = \bar{\phi}_r, \quad \tilde{\psi}_{11}(1) = \psi_r. \quad (40)$$

Similar to the approach taken in previous scenarios, the constants  $\widehat{C}_1$ ,  $\widehat{C}_2$ ,  $\widehat{C}_3$ , and  $\widehat{C}_4$  are obtained by solving the following system of linear equations

$$\begin{bmatrix} 0 & \frac{\alpha_m + \alpha_{Mm}}{\kappa(1 + \alpha_m + 2\alpha_{Mm})} & 0 & 1 \\ 0 & \kappa & 0 & 0 \\ \frac{\alpha_m + \alpha_{Mm}}{\kappa(1 + \alpha_m + 2\alpha_{Mm})} \sinh(\kappa) & \frac{\alpha_m + \alpha_{Mm}}{\kappa(1 + \alpha_m + 2\alpha_{Mm})} \cosh(\kappa) & 1 & 1 \\ \cosh(\kappa) & \sinh(\kappa) & 1 & 0 \end{bmatrix} \begin{Bmatrix} \widehat{C}_1 \\ \widehat{C}_2 \\ \widehat{C}_3 \\ \widehat{C}_4 \end{Bmatrix} = \begin{Bmatrix} 0 \\ 0 \\ \bar{\phi}_r \\ \psi_r \end{Bmatrix}. \quad (41)$$

Fig. 5(a) corresponds to the case where  $\bar{\phi}_r = 0.01$  and  $\psi_r = 0$ , Fig. 5(b) corresponds to the case where  $\bar{\phi}_r = 0$  and  $\psi_r = 0.01$ , and Fig. 5(c) shows the results for the case where  $\bar{\phi}_r = 0.01$  and  $\psi_r = 0.01$ . A fixed micro-scale kinematic measure at the right end in Fig. 5(a) results in large deformation energy stored in the right boundary layer and uniform energy density distribution in the rest of the domain. This stored energy can be attributed to the difference in value between the imposed macro-scale displacement gradient  $\tilde{\phi}_{,\bar{x}}$  and the micro-scale kinematic measure  $\tilde{\psi}_{11}$  at the right end. The results in Fig. (5b) are qualitatively similar to those in Fig. 3(b) and Fig. 4(b) and follow the same discussion. Interestingly, the results in Fig. 5(c) are similar to the ones in Fig. 4(a). This case corresponds to a zero double traction at the left end and a prescribed value for the micro-scale kinematic measure  $\tilde{\psi}_{11}$  equal to the macro-scale strain at the right end. In this case, similar to the one in Fig. 4(a), the macro-scale displacement  $\tilde{\phi}$  is linear and the deformation energy density due to the macro-scale displacement gradient is the sole contributor to the total deformation energy density.

Based on the observations from the results in Figs. 3-5, the following conclusions can be drawn. First, imposing fixed and prescribed macro-scale displacements  $\tilde{\phi}$  at left and right ends of the structure, respectively, one observes a classical-like behavior only if at each end, the contact double traction is held to be zero, or the micro-scale kinematic measure  $\tilde{\psi}_{11}$  is assigned a value equal to the macro-scale displacement gradient  $\tilde{\phi}_{,\bar{x}}$  (macro-scale strain). For the cases where the macro-scale displacement gradient  $\tilde{\phi}_{,\bar{x}}$  and micro-scale kinematic measure  $\tilde{\psi}_{11}$  have non-equal

values on the boundary, localized deformation energy density of finite thickness near that boundary is observed, while the deformation energy density in the rest of the domain of the problem is rather uniform. Second, for fixed macro-scale displacement  $\tilde{\phi}$  applied at both boundaries and imposed double traction or micro-scale kinematic measure  $\tilde{\psi}_{11}$  at one end, we notice both compression and tension (negative and positive macro-scale displacement gradient  $\tilde{\phi}_{,\bar{x}}$ ) induced within the granular structure. Third, the gradients appearing because of the imposed field variables  $\tilde{\phi}$  and  $\tilde{\psi}_{11}$  at both ends only exist close to the outer boundaries of the structure, thereby signifying the existence of boundary layers. Finally, one notices the small change in the macro-scale displacement  $\tilde{\phi}$  in response to the alterations in the imposed non-classical boundary conditions. Nevertheless, such small changes have large influence on the energy localization near the boundaries, and such energy localization becomes even more noticeable as the size of the rod shrinks.

### 3.5. Parametric study

To further explore the effect of the material constants  $\alpha_m$ ,  $\alpha_{Mm}$ , and  $l_s$  on the behavior of the field variables  $\tilde{\phi}$  and  $\tilde{\psi}_{11}$ , a parametric study is performed. We consider two cases of boundary conditions for this investigation. Fig. 6 shows the results for the following applied boundary conditions

$$\tilde{\phi}(0) = 0, \quad \tilde{\psi}_{11}(0) = 0, \quad \tilde{\phi}(1) = 0.01, \quad \tilde{\psi}_{11}(1) = 0, \quad (42)$$

and Fig. 7 shows the results for the following boundary conditions

$$\tilde{\phi}(0) = 0, \quad \tilde{\psi}_{11}(0) = 0, \quad \tilde{\phi}(1) = 0, \quad \tilde{\psi}_{11}(1) = 0.01. \quad (43)$$

In both studies, the baseline material constants are taken as  $\alpha_m = 0.5$ ,  $\alpha_{Mm} = -0.4$  and  $l_s = 0.05$ . In Fig. 6(a) and Fig. 7(a) the material constant  $\alpha_m$  is varied, in Fig. 6(b) and Fig. 7(b) the material constant  $\alpha_{Mm}$  is varied, and in Fig. 6(c) and Fig. 7(c) the material constant  $l_s$  is varied. We here

recognize that a growth in the material constant  $l_s$  can be interpreted as either an increase in the second gradient stiffness of the material, or as a decrease in the size of the rod under study.

For the case of boundary conditions in Eq. (42) with the results shown in Fig. 6, a change in the values of the parameters  $\alpha_m$ ,  $\alpha_{Mm}$ , and  $l_s$  has small effect on the solution for the macro-scale displacement  $\tilde{\phi}$ . However, it is evident that increasing  $\alpha_m$  or  $\alpha_{Mm}$  alters the solution for  $\tilde{\psi}_{11}$  significantly. Moreover, increasing  $\alpha_m$  and  $\alpha_{Mm}$ , decreases and increases the size of the boundary layer, respectively. An increase in the value of  $l_s$  reduces the maximum for  $\tilde{\psi}_{11}$  and increases the size of the boundary layer. The change of the size of the boundary layer due the value of the parameter  $l_s$  may be explained using the definition of the parameter  $\kappa$ . A larger value for the parameter  $l_s$  results in smaller value for  $\kappa$  which consequently leads to larger boundary layer.

For the case of the boundary conditions in Eq. (43) with the results shown in Fig. 7, increasing  $\alpha_m$  results in a change from positive to negative sign for the macro-scale displacement  $\tilde{\phi}$ , which switches the regions of compression and tension (see Fig. 7(a)). According to Fig. 7(a), the micro-scale kinematic measure  $\tilde{\psi}_{11}$  follows the same trend, although the sign of the solution for  $\tilde{\psi}_{11}$  becomes negative as  $\alpha_m$  increases while the boundary layer thickness decreases somewhat. Fig. 7(b) shows the results for the change in the value of  $\alpha_{Mm}$ . Increasing  $\alpha_{Mm}$  also changes the sign of the macro-scale displacement  $\tilde{\phi}$ . Furthermore, as the value of  $\alpha_{Mm}$  increases, the boundary layer size increases by a small amount. Fig. 7(c) shows that increasing  $l_s$  results in an increase in the magnitude of the macro-scale displacement  $\tilde{\phi}$  as well as an increase in the size of the boundary layer.

The size effect of the rod can be observed in Fig. 6(c) and Fig. 7(c), where a decrease in the size of the sample (increase in the value of  $l_s$ ) results in a larger boundary layer which implies that the localization zone of the strain energy has grown and spread towards the center of the rod. In this case, the average deformation energy density absorbed by the material has increased compared to the same material with larger size, thus suggesting a stiffening effect.

## 4. Free vibration behavior

### 4.1. General solution

In this section, we analyze the free vibration characteristics of the 1D granular rod. The dimensionless form of the governing equations of motion are stated in Eq. (27) with the boundary conditions expressed in Eq. (28). For small harmonic vibration, the following form of solution (plane wave solution) is assumed

$$\tilde{\phi}(\tilde{x}, \tilde{t}) = \bar{\Phi}(\tilde{x})e^{i\omega\tilde{t}}, \quad \tilde{\psi}_{11}(\tilde{x}, \tilde{t}) = \Psi(\tilde{x})e^{i\omega\tilde{t}}, \quad (44)$$

where  $\bar{\Phi}$  and  $\Psi$  are the dimensionless space parts of the solutions and  $\omega$  is the dimensionless angular natural frequency. Substitution of Eq. (44) into the governing equations of motion in Eq. (27) results in the following equations

$$(1 + \alpha_m + 2\alpha_{Mm})\bar{\Phi}_{,\tilde{x}\tilde{x}} - (\alpha_m + \alpha_{Mm})\Psi_{,\tilde{x}} = -\omega^2\bar{\Phi}, \quad (45a)$$

$$l_s^2\Psi_{,\tilde{x}\tilde{x}} + (\alpha_m + \alpha_{Mm})\bar{\Phi}_{,\tilde{x}} - \alpha_m\Psi = -\frac{\omega^2}{12n^2}\Psi + \frac{\omega^2}{80n^4}\Psi_{,\tilde{x}\tilde{x}}. \quad (45b)$$

The above equations can be uncoupled to obtain two fourth order homogenous linear ordinary differential equations with constant coefficients as follows

$$z_1\bar{\Phi}_{,\tilde{x}\tilde{x}\tilde{x}\tilde{x}} + z_2\bar{\Phi}_{,\tilde{x}\tilde{x}} + z_3\bar{\Phi} = 0, \quad (46a)$$

$$z_1\Psi_{,\tilde{x}\tilde{x}\tilde{x}\tilde{x}} + z_2\Psi_{,\tilde{x}\tilde{x}} + z_3\Psi = 0, \quad (46b)$$

where

$$\begin{aligned} z_1 &= 3(\omega^2 - 80l_s^2n^4)(1 + \alpha_m + 2\alpha_{Mm}), \\ z_2 &= 240n^4(\alpha_m - \alpha_{Mm}^2 - l_s^2\omega^2) - 20n^2\omega^2(1 + \alpha_m + 2\alpha_{Mm}) + 3\omega^4, \\ z_3 &= 20n^2\omega^2(12\alpha_m n^2 - \omega^2). \end{aligned} \quad (47)$$

The general solutions for the differential equations in Eq. (46) can be presented as



$$\bar{\Phi} = \hat{\Phi}_1 \cos(k_1 \tilde{x}) + \hat{\Phi}_2 \sin(k_1 \tilde{x}) + \hat{\Phi}_3 \cosh(k_2 \tilde{x}) + \hat{\Phi}_4 \sinh(k_2 \tilde{x}), \quad (48a)$$

$$\bar{\Psi} = \hat{\Psi}_1 \cos(k_1 \tilde{x}) + \hat{\Psi}_2 \sin(k_1 \tilde{x}) + \hat{\Psi}_3 \cosh(k_2 \tilde{x}) + \hat{\Psi}_4 \sinh(k_2 \tilde{x}), \quad (48b)$$

where

$$k_1 = \left( \frac{z_2 - \sqrt{z_2^2 - 4z_1 z_3}}{2z_1} \right)^{\frac{1}{2}}, \quad k_2 = \left( \frac{-z_2 - \sqrt{z_2^2 - 4z_1 z_3}}{2z_1} \right)^{\frac{1}{2}}. \quad (49)$$

In Eq. (48),  $k_1$  and  $k_2$  are the dimensionless angular wavenumbers, and are functions of the material parameters and the angular frequency  $\omega$ . Also,  $\hat{\Phi}_i, \hat{\Psi}_i, i=1, \dots, 4$  are constant to be determined by the appropriate boundary conditions, which, using Eq. (45a), are related as

$$\begin{aligned} \hat{\Psi}_1 = \alpha \hat{\Phi}_2, \quad \hat{\Psi}_2 = -\alpha \hat{\Phi}_1, \quad \text{where} \quad \alpha = \frac{(1 + \alpha_m + 2\alpha_{Mm})k_1^2 - \omega^2}{(\alpha_m + \alpha_{Mm})k_1}, \\ \hat{\Psi}_3 = \beta \hat{\Phi}_4, \quad \hat{\Psi}_4 = \beta \hat{\Phi}_3 \quad \text{where} \quad \beta = \frac{(1 + \alpha_m + 2\alpha_{Mm})k_2^2 + \omega^2}{(\alpha_m + \alpha_{Mm})k_2}. \end{aligned} \quad (50)$$

In what follows, we study the free vibration characteristics of the 1D granular rod subjected to four types of boundary conditions. The first three types of boundary conditions are examined following the same motivation discussed in the static case: for identical classical boundary conditions, how does a change in the non-classical boundary conditions affect the response of the system. The fourth type of boundary conditions is investigated to have a more complete comparison with the results of the models found in the literature. For the analyses to follow, we consider the same material constants as for the static case, namely,  $\alpha_m = 0.5$ ,  $\alpha_{Mm} = -0.4$ ,  $l_s = 0.05$ , and  $n = 100$ , and compare the resulting natural frequencies and mode shapes with the solutions of a classical rod problem. We note that, in the following results, the mode shapes of the classical rod have been scaled such that they have the same amplitude as the macro-scale displacement  $\tilde{\phi}$  amplitude for the mode shapes of the present model.

#### 4.2. Clamped strained-clamped strained (CS-CS)

The boundary conditions associated with the CS-CS case are defined as

$$\bar{\Phi}(0)=0, \quad \Psi(0)=0, \quad \bar{\Phi}(1)=0, \quad \Psi(1)=0. \quad (51)$$

Eq. (51) enforces that the macro-scale displacement  $\tilde{\phi}$  and the micro-scale kinematic measure  $\tilde{\psi}_{11}$  are identically fixed at both ends. Enforcing Eq. (51), and by using Eq. (50), the following set of algebraic equations result from Eq. (48)

$$\begin{bmatrix} 1 & 0 & 1 & 0 \\ 0 & \alpha & 0 & \beta \\ \cos(k_1) & \sin(k_1) & \cosh(k_2) & \sinh(k_2) \\ -\alpha \sin(k_1) & \alpha \cos(k_1) & \beta \sinh(k_2) & \beta \cosh(k_2) \end{bmatrix} \begin{Bmatrix} \hat{\Phi}_1 \\ \hat{\Phi}_2 \\ \hat{\Phi}_3 \\ \hat{\Phi}_4 \end{Bmatrix} = \begin{Bmatrix} 0 \\ 0 \\ 0 \\ 0 \end{Bmatrix}. \quad (52)$$

The necessary condition to have non-zero solutions for Eq. (52) is that the determinant of the coefficient matrix is zero, i.e.

$$(\alpha^2 - \beta^2) \sin(k_1) \sinh(k_2) + 2\alpha\beta (\cos(k_1) \cosh(k_2) - 1) = 0. \quad (53)$$

Eq. (53) is a transcendental equation denoting the general characteristic equation for the CS-CS boundary conditions and is equivalent to the characteristic equation for the clamped-clamped case of the nonlocal strain gradient rod in [31] for  $\alpha = k_1$  and  $\beta = k_2$ .

Fig. 8(a-c) show the first three mode shapes and natural frequencies. The mode shapes corresponding to the macro-scale displacement  $\tilde{\phi}$  are similar to that's for the classical one-dimensional continua for the material parameters considered here. Denoting by  $\omega_i$  and  $\omega_i^c$ , respectively, the  $i^{\text{th}}$  natural frequency of the current model and the classical continuum model, the first three natural frequencies in the CS-CS boundary condition case for the chosen material parameters are smaller than their classical continuum counterparts and are evaluated as  $\omega_1 = 0.8283\omega_1^c$ ,  $\omega_2 = 0.8290\omega_2^c$ , and  $\omega_3 = 0.8300\omega_3^c$ .

#### 4.3. Clamped strained-clamped forcing (CS-CF)

The boundary conditions associated with the CS-CF case are obtained by having the macro-scale displacement  $\tilde{\phi}$  at both ends fixed, the micro-scale kinematic measure  $\tilde{\psi}_{11}$  fixed at the left end, and the double traction zero (free) at the right end. Explicitly, the boundary conditions are stated as

$$\bar{\Phi}(0) = 0, \quad \Psi(0) = 0, \quad \bar{\Phi}(1) = 0, \quad \Psi_{,x}(1) = 0, \quad (54)$$

where the last condition is obtained by introducing the solution in Eq. (44) into the boundary condition in Eq. (28b). Enforcing Eq. (54), and by using Eq. (50), the following set of algebraic equations result from Eq. (48)

$$\begin{bmatrix} 1 & 0 & 1 & 0 \\ 0 & \alpha & 0 & \beta \\ \cos(k_1) & \sin(k_1) & \cosh(k_2) & \sinh(k_2) \\ -\alpha k_1 \cos(k_1) & -\alpha k_1 \sin(k_1) & \beta k_2 \cosh(k_2) & \beta k_2 \sinh(k_2) \end{bmatrix} \begin{Bmatrix} \hat{\Phi}_1 \\ \hat{\Phi}_2 \\ \hat{\Phi}_3 \\ \hat{\Phi}_4 \end{Bmatrix} = \begin{Bmatrix} 0 \\ 0 \\ 0 \\ 0 \end{Bmatrix}. \quad (55)$$

The characteristic equation corresponding to Eq. (55) is

$$(\alpha k_1 + \beta k_2) [\alpha \cos(k_1) \sinh(k_2) - \beta \sin(k_1) \cosh(k_2)] = 0. \quad (56)$$

Eq. (56) is the general characteristic equation for the CS-CF boundary conditions and for  $\alpha = k_1$  and  $\beta = k_2$  it becomes equivalent to the characteristic equation for the clamped-simply supported case of the nonlocal strain gradient rod described in [31].

Fig. 8(d-f) show the first three mode shapes and natural frequencies. Similar to the results for the CS-CS case, the mode shapes corresponding to the macro-scale displacement  $\tilde{\phi}$  for the CS-CF case are approximately same as the mode shapes of classical 1D bar. The first three natural frequencies in the CS-CF boundary condition case are smaller than their classical continuum counterparts for the material parameters considered here, and have values of  $\omega_1 = 0.8267\omega_1^c$ ,  $\omega_2 = 0.8278\omega_2^c$ , and  $\omega_3 = 0.8292\omega_3^c$ , respectively.

#### 4.4. Clamped forcing-clamped forcing (CF-CF)

The boundary conditions associated with the CF-CF case are expressed as

$$\bar{\Phi}(0)=0, \quad \Psi_{,\bar{x}}(0)=0, \quad \bar{\Phi}(1)=0, \quad \Psi_{,\bar{x}}(1)=0. \quad (57)$$

Enforcing the boundary conditions in Eq. (57), the following set of algebraic equations result from Eq. (48)

$$\begin{bmatrix} 1 & 0 & 1 & 0 \\ -\alpha k_1 & 0 & \beta k_2 & 0 \\ \cos(k_1) & \sin(k_1) & \cosh(k_2) & \sinh(k_2) \\ -\alpha k_1 \cos(k_1) & -\alpha k_1 \sin(k_1) & \beta k_2 \cosh(k_2) & \beta k_2 \sinh(k_2) \end{bmatrix} \begin{Bmatrix} \hat{\bar{\Phi}}_1 \\ \hat{\bar{\Phi}}_2 \\ \hat{\bar{\Phi}}_3 \\ \hat{\bar{\Phi}}_4 \end{Bmatrix} = \begin{Bmatrix} 0 \\ 0 \\ 0 \\ 0 \end{Bmatrix}. \quad (58)$$

The characteristic equation corresponding to Eq. (58) is

$$(\alpha k_1 + \beta k_2)^2 \sin(k_1) \sinh(k_2) = 0. \quad (59)$$

Eq. (59) is the general characteristic equation for the CF-CF boundary conditions, and for  $\alpha = k_1$  and  $\beta = k_2$ , it becomes of similar form to the characteristic equation for the simply supported-simply supported case of the nonlocal strain gradient rod in [31], the nonlocal strain gradient rod in [27], and the strain gradient rod in [30].

Fig. 8(g-i) show the first three mode shapes and natural frequencies. Similar to previous cases, the mode shapes corresponding to the macro-scale displacement  $\tilde{\phi}$  for the CF-CF case are similar to that of the classical 1D continua. The first three natural frequencies in the CF-CF boundary condition case are smaller than their classical continuum counterparts for the material parameters chosen in this study, and have values of  $\omega_1 = 0.8252\omega_1^c$ ,  $\omega_2 = 0.8266\omega_2^c$ , and  $\omega_3 = 0.8283\omega_3^c$ , respectively.

#### 4.5. Clamped forcing-free strained (CF-FS)

The boundary conditions associated with the CF-FS case are expressed as

$$\bar{\Phi}(0)=0, \quad \Psi_{,\bar{x}}(0)=0, \quad \bar{\Phi}_{,\bar{x}}(1)=0, \quad \Psi(1)=0. \quad (60)$$

With regards to Eq. (60), Eq. (48) results in the following set of algebraic equations

$$\begin{bmatrix} 1 & 0 & 1 & 0 \\ -\alpha k_1 & 0 & \beta k_2 & 0 \\ -k_1 \sin(k_1) & k_1 \cos(k_1) & k_2 \sinh(k_2) & k_2 \cosh(k_2) \\ -\alpha \sin(k_1) & \alpha \cos(k_1) & \beta \sinh(k_2) & \beta \cosh(k_2) \end{bmatrix} \begin{Bmatrix} \hat{\Phi}_1 \\ \hat{\Phi}_2 \\ \hat{\Phi}_3 \\ \hat{\Phi}_4 \end{Bmatrix} = \begin{Bmatrix} 0 \\ 0 \\ 0 \\ 0 \end{Bmatrix}. \quad (61)$$

The characteristic equation corresponding to Eq. (61) is

$$(\alpha k_1 + \beta k_2)(\alpha k_2 - \beta k_1) \cos(k_1) \cosh(k_2) = 0. \quad (62)$$

Eq. (62) is the general characteristic equation for the CF-FS boundary conditions and for  $\alpha = k_1$  and  $\beta = k_2$  it becomes of similar form to the characteristic equation for the CF-FS case of the nonlocal strain gradient rod in [27]. The first three natural frequencies for the CF-FS case are  $\omega_1 = 0.8247\omega_1^c$ ,  $\omega_2 = 0.8258\omega_2^c$ , and  $\omega_3 = 0.8275\omega_3^c$ , respectively, which are lower than classical continuum predictions for the material parameters considered. In addition, the macro-scale displacement  $\tilde{\phi}$  mode shapes are close to the classical continuum predictions.

Based on the results of the four different examples studied above, several observations and conclusions can be made. Firstly, the mode shapes of the macro-scale displacement  $\tilde{\phi}$  are similar to that of a classical continuum, although for a different choice of material parameters (for example if we had  $\alpha_{Mm} = 0$ ), small deviations from the mode shapes of classical rod are observed (results not shown). Such a deviation is the result of the presence of terms containing the second wavenumber  $k_2$  in Eq. (48), which, for the problems studied here, had negligible amplitude compared to the leading term containing  $k_1$ . Moreover, one concludes from the first three visited examples that even when the double traction is prescribed as zero on the boundaries, the microstructural effects alter the natural frequency of the system. This is in contradistinction to the results from the static problem where a classical form of solution is obtained if the non-classical terms are not excited. This distinction in the behavior of the system in static and dynamic problems



are due to the presence of the terms containing dynamic length scales in the governing equations of motion.

#### 4.6. Parametric study

In order to study the effect of different material constants on the dynamic behavior of one-dimensional materials with granular microstructure, we have plotted the ratio of the first three natural frequencies for the three CS-CS, CS-CF, and CF-CF cases to their classical counterparts for different material parameters with the base material constants at  $\alpha_m = 0.5$ ,  $\alpha_{Mm} = 0$ ,  $l_s = 0.05$ , and  $n = 100$  in Fig. 9. Based on the results in Fig. 9, the following conclusions can be drawn. First, an increase in the micro-scale (relative deformation) stiffness,  $\alpha_m$ , leads to larger natural frequencies (Fig. 9(a)). This result is expected as additional stiffness increases the natural frequency of the system. Second, contrary to the trend observed for the effect of the parameter  $\alpha_m$ , an increase in the cross-linking stiffness  $\alpha_{Mm}$  is accompanied by an initial increase in the value of the natural frequencies, followed by a decrease (Fig. 9(b)). Therefore, the effect of the parameter  $\alpha_{Mm}$  can be either softening or stiffening. Third, increasing the length scale parameter  $l_s$  results in an increase in the value of the natural frequencies (Fig. 9(f)), hence implying stiffening of the material when either the second gradient stiffness becomes larger or when the rod size becomes smaller. For  $l_s$  values large enough, an asymptotic value for the natural frequencies are obtained. Similar observation has been made for the rod modeled using nonlocal strain gradient theory [31]. Fourth, the natural frequencies can be smaller or larger than their classical counterparts, depending on the material constants. Fifth, one observes that the effect of different boundary conditions on the natural frequencies is rather small for a wide range of material parameters. For higher modes, however, the effect of different boundary conditions on the results becomes increasingly significant. Finally, it is interesting to note that the higher mode frequencies are not integer multiples of the fundamental mode, which is a departure from the results for classical 1D elastic rod under the considered boundary conditions, and seems to suggest an apparent internal damping.

### 5. Conclusion and Summary (prognosis towards experimental design)

Mechanical response of materials with granular microstructures are known to be influenced by the grain-scale mechano-morphology. Here we have utilized the granular micromechanics approach (GMA) based continuum theory to reveal certain peculiar aspects of the mechanical behavior of a material with granular microstructure. To keep the development tractable and understandable, we have focused upon a 1D rod composed of granular materials. To this end, the governing equations of motion and the variationally consistent boundary conditions for a one-dimensional material with granular microstructure were obtained using the principle of least action. Closed-form solutions for both the static and dynamic problems were obtained and the effect of different boundary conditions and material parameters on the response of the material were investigated. The key findings of the presented work are:

1. That micromorphicity due to micro-mechano-morphological properties has a significant influence on the static and free vibration response of rods with granular microstructure.
2. In the static case, we observe that the dependency of the structural response on the imposed boundary conditions is most obvious near the boundaries of the structure where gradients of strain are large. In addition, the size-dependency effects are manifested in the width of the emergent boundary layers.
3. In the dynamic case, the length scale parameter has stiffening effect, i.e., as the size of the structure shrinks, the behavior is predicted to be stiffer, a finding which classical theory does not predict.
4. The mode shapes corresponding to the micro-scale kinematic measure  $\tilde{\psi}_{11}$  are not identical to that of the macro-scale displacement gradient  $\tilde{\phi}_{,x}$ , as distinct from that for a second gradient model and account for the energy due to the relative deformation in macro- and micro-scales.
5. Additional kinematic constraints and simplifications imposed on the presented model leads to several (nonlocal) strain gradient models introduced in the literature, and therefore, the current model, encompasses such models as special cases.

6. While the cases studied in the static problem show microstructural effects of the system under certain boundary conditions, the effect of the microstructure is always present in the dynamic problem for any form of applied boundary conditions.
7. The dynamic length scale parameters (referred to as nonlocal parameters in the literature) in the current model are directly linked to the micro-scale mass density distribution of the system under study and do not take arbitrary values.
8. The model predicts measurable effects such that experimental approaches/protocols can be designed to detect these effects.
9. While a 1D system is helpful in understanding the underlying physics behind the observed phenomena, many engineering applications are concerned with higher dimensional systems. GMA based micromorphic model of degree one presented here can be systematically expanded to include 2D and 3D systems [41], or to model deflection in beams [61].

To conclude, appreciating the complexity of the materials with granular microstructure and the limitations on the current experimental prescriptions to observe and extract microstructural effects, the results of the current paper can promote the understanding of such complex systems and what to expect if experiments are to be devised. Furthermore, the results of the current paper will serve as a prelude to our future work on static deformation, vibration and elastic wave propagation simulations of initial/boundary value problems for structures made of granular media.

### **Statement of Competing Interest**

Authors have no competing interests to declare.

### **Acknowledgements**

This research is supported in part by the United States National Science Foundation grant CMMI-1727433.

## References

- [1] Barchiesi E, dell'Isola F, Laudato M, Placidi L, Seppecher P. A 1D continuum model for beams with pantographic microstructure: asymptotic micro-macro identification and numerical results. In: *Advanced Structured Materials*. Springer Verlag, pp. 43–74.
- [2] Del Vescovo D, Giorgio I. Dynamic problems for metamaterials: Review of existing models and ideas for further research. *Int J Eng Sci* 2014; 80: 153–172.
- [3] Barchiesi E. Multi-scale and multi-physics: towards next-generation engineering materials. *Continuum Mechanics and Thermodynamics* 2020; 32: 541–554.
- [4] Gonella S, Steven Greene M, Liu WK. Characterization of heterogeneous solids via wave methods in computational microelasticity. *J Mech Phys Solids* 2011; 59: 959–974.
- [5] Lam DCC, Yang F, Chong ACM, Wang J, Tong P. Experiments and theory in strain gradient elasticity. *J Mech Phys Solids* 2003; 51: 1477–1508.
- [6] Rosi G, Auffray N, Combescure C. On the failure of classic elasticity in predicting elastic wave propagation in gyroid lattices for very long wavelengths. *Symmetry* 2020; 12(8): 1243.
- [7] Sun L, Han RPS, Wang J, Lim CT. Modeling the size-dependent elastic properties of polymeric nanofibers. *Nanotechnology* 2008; 19: 455706.
- [8] Berezovski A, Engelbrecht J, Salupere A, Tamm K, Peets T, Berezovski M. Dispersive waves in microstructured solids. *Int J Solids Struct* 2013; 50: 1981–1990.
- [9] Eringen AC. *Microcontinuum Field Theories*. Springer New York, 1999.
- [10] Eringen AC, Edelen DGB. On nonlocal elasticity. *Int J Eng Sci* 1972; 10: 233–248.
- [11] Eringen AC. Plane waves in nonlocal micropolar elasticity. *Int J Eng Sci* 1984; 22: 1113–1121.
- [12] Mindlin RD. Micro-structure in linear elasticity. *Arch Ration Mech Anal* 1964; 16: 51–78.
- [13] Germain P. The Method of Virtual Power in Continuum Mechanics. Part 2: Microstructure. *SIAM J Appl Math* 1973; 25: 556–575.
- [14] Toupin RA. Theories of elasticity with couple-stress. *Arch Ration Mech Anal* 1964; 17: 85–112.
- [15] Challamel N, Wang CM, Elishakoff I. Nonlocal or gradient elasticity macroscopic models: A question of concentrated or distributed microstructure. *Mech Res Commun* 2016; 71: 25–31.
- [16] Seppecher P, Alibert JJ, Isola FD. Linear elastic trusses leading to continua with exotic mechanical interactions. In: *Journal of Physics: Conference Series* 2011 Sep 15 (Vol. 319, No. 1, p. 012018). IOP Publishing.
- [17] Barretta R, Faghidian SA, Luciano R. Longitudinal vibrations of nano-rods by stress-driven integral elasticity. *Mech Adv Mater Struct* 2019; 26: 1307–1315.
- [18] Chang CS, Gao J. Wave Propagation in Granular Rod Using High-Gradient Theory. *J Eng Mech* 1997; 123: 52–59.
- [19] Zhu X, Li L. Closed form solution for a nonlocal strain gradient rod in tension. *Int J Eng Sci* 2017; 119: 16–28.
- [20] Ayad M, Karathanasopoulos N, Ganghoffer JF, Lakiss H. Higher-gradient and micro-inertia contributions on the mechanical response of composite beam structures. *Int J Eng Sci* 2020; 154: 103318.

- [21] Dontsov E V., Tokmashev RD, Guzina BB. A physical perspective of the length scales in gradient elasticity through the prism of wave dispersion. *Int J Solids Struct* 2013; 50: 3674–3684.
- [22] Güven U. A generalized nonlocal elasticity solution for the propagation of longitudinal stress waves in bars. *Eur J Mech A/Solids* 2014; 45: 75–79.
- [23] Papargyri-Beskou S, Beskos D. Static analysis of gradient elastic bars, beams, plates and shells. *Open Mech J* 2010; 4: 65–73.
- [24] De Domenico D, Askes H, Aifantis EC. Discussion of “Derivation of Mindlin’s first and second strain gradient elastic theory via simple lattice and continuum models” by Polyzos and Fotiadis. *International Journal of Solids and Structures* 2020; 191–192: 646–651.
- [25] Tsepoura KG, Papargyri-Beskou S, Polyzos D, Beskos DE. Static and dynamic analysis of a gradient-elastic bar in tension. *Arch Appl Mech* 2002; 72: 483–497.
- [26] Adhikari S, Murmu T, McCarthy MA. Dynamic finite element analysis of axially vibrating nonlocal rods. *Finite Elem Anal Des* 2013; 63: 42–50.
- [27] Li L, Hu Y, Li X. Longitudinal vibration of size-dependent rods via nonlocal strain gradient theory. *Int J Mech Sci* 2016; 115–116: 135–144.
- [28] Aydogdu M. Axial vibration of the nanorods with the nonlocal continuum rod model. *Phys E Low-Dimensional Syst Nanostructures* 2009; 41: 861–864.
- [29] Numanoglu HM, Akgöz B, Civalek Ö. On dynamic analysis of nanorods. *Int J Eng Sci* 2018; 130: 33–50.
- [30] Kahrobaiyan MH, Asghari M, Ahmadian MT. Longitudinal behavior of strain gradient bars. *Int J Eng Sci* 2013; 66–67: 44–59.
- [31] Xu XJ, Zheng ML, Wang XC. On vibrations of nonlocal rods: Boundary conditions, exact solutions and their asymptotics. *Int J Eng Sci* 2017; 119: 217–231.
- [32] Benvenuti E, Simone A. One-dimensional nonlocal and gradient elasticity: Closed-form solution and size effect. *Mech Res Commun* 2013; 48: 46–51.
- [33] Challamel N, Zhang Z, Wang CM. Nonlocal equivalent continua for buckling and vibration analyses of microstructured beams. *J Nanomechanics Micromechanics* 2015; 5: A4014004.
- [34] Rahmani O, Pedram O. Analysis and modeling the size effect on vibration of functionally graded nanobeams based on nonlocal Timoshenko beam theory. *Int J Eng Sci* 2014; 77: 55–70.
- [35] Fafalis DA, Filopoulos SP, Tsamasphyros GJ. On the capability of generalized continuum theories to capture dispersion characteristics at the atomic scale. *Eur J Mech A/Solids* 2012; 36: 25–37.
- [36] Darban H, Luciano R, Caporale A, Fabbrocino F. Higher modes of buckling in shear deformable nanobeams. *Int J Eng Sci* 2020; 154: 103338.
- [37] Numanoglu HM, Civalek Ö. On the dynamics of small-sized structures. *Int J Eng Sci* 2019; 145: 103164.
- [38] Andraeus U, dell’Isola F, Giorgio I, Placidi L, Lekszycki T, Rizzi NL. Numerical simulations of classical problems in two-dimensional (non) linear second gradient elasticity. *Int J Eng Sci* 2016; 108: 34–50.
- [39] Farajpour A, Howard CQ, Robertson WSP. On size-dependent mechanics of nanoplates. *Int J*



*Eng Sci* 2020; 156: 103368.

- [40] Yang H, Müller WH. Size effects of mechanical metamaterials: a computational study based on a second-order asymptotic homogenization method. *Arch Appl Mech* 2020; 1–17.
- [41] NejadSadeghi N, Misra A. Extended granular micromechanics approach: a micromorphic theory of degree  $n$ . *Math Mech Solids* 2020; 25: 407–429.
- [42] Misra A, Poorsolhjoui P. Granular micromechanics based micromorphic model predicts frequency band gaps. *Contin Mech Thermodyn* 2016; 28: 215–234.
- [43] Misra A, NejadSadeghi N. Longitudinal and transverse elastic waves in 1D granular materials modeled as micromorphic continua. *Wave Motion* 2019; 90: 175–195.
- [44] NejadSadeghi N, Placidi L, Romeo M, Misra A. Frequency band gaps in dielectric granular metamaterials modulated by electric field. *Mech Res Commun* 2019 ;95:96-103.
- [45] NejadSadeghi N, Misra A. Role of higher-order inertia in modulating elastic wave dispersion in materials with granular microstructure. *Int J Mech Sci* 2020; 185: 105867.
- [46] Zeng X, Chen Y, Lee JD. Determining material constants in nonlocal micromorphic theory through phonon dispersion relations. *Int J Eng Sci* 2006; 44: 1334–1345.
- [47] Chen Y, Lee JD. Connecting molecular dynamics to micromorphic theory.(I). Instantaneous and averaged mechanical variables. *Phys A Stat Mech its Appl* 2003; 322: 359–376.
- [48] Madeo A, Collet M, Miniaci M, Billon K, Ouisse M, Neff P. Modeling phononic crystals via the weighted relaxed micromorphic model with free and gradient micro-inertia. *J Elast* 2018; 130: 59–83.
- [49] Misra A, NejadSadeghi N, De Angelo M, Placidi L. Chiral metamaterial predicted by granular micromechanics: verified with 1D example synthesized using additive manufacturing. *Contin Mech Thermodyn* 2020; 32: 1497-1513.
- [50] Giorgio I, dell’Isola F, Misra A. Chirality in 2D Cosserat media related to stretch-micro-rotation coupling with links to granular micromechanics. *Int J Solids Struct* 2020; 202: 28–38.
- [51] Tan SH, Poh LH. Enriched homogenized model for viscoelastic plane wave propagation in periodic layered composites. *Adv Model Simul Eng Sci* 2020; 7: 4.
- [52] Tan SH, Poh LH. Homogenized Gradient Elasticity Model for Plane Wave Propagation in Bilaminate Composites. *J Eng Mech* 2018; 144: 04018075.
- [53] Misra A, Ouyang L, Chen J, Ching WY. Ab initio calculations of strain fields and failure patterns in silicon nitride intergranular glassy films. *Philosophical Magazine* 2007; 87(25): 3839-52.
- [54] Charlotte M, Truskinovsky L. Towards multi-scale continuum elasticity theory. *Contin Mech Thermodyn* 2008; 20: 133–161.
- [55] Charlotte M, Truskinovsky L. Lattice dynamics from a continuum viewpoint. *J Mech Phys Solids* 2012; 60: 1508–1544.
- [56] Essén H. Average angular velocity. *Eur J Phys* 1993; 14: 201–205.
- [57] Wang ZP, Sun CT. Modeling micro-inertia in heterogeneous materials under dynamic loading. *Wave Motion* 2002; 36: 473–485.
- [58] Barchiesi E, Laudato M, Di Cosmo F. Wave dispersion in non-linear pantographic beams. *Mech Res Commun* 2018; 94: 128–132.

- [59] De Domenico D, Askes H. A new multi-scale dispersive gradient elasticity model with micro-inertia: Formulation and C0-finite element implementation. *Int J Numer Methods Eng* 2016; 108: 485–512.
- [60] Misra A, Poorsolhjouy P. Identification of higher-order elastic constants for grain assemblies based upon granular micromechanics. *Math Mech Complex Syst* 2015; 3: 285–308.
- [61] Angelo M De, Placidi L, Nejadi Sadeghi N, Misra A. Non-standard Timoshenko beam model for chiral metamaterial: identification of stiffness parameters. *Mech Res Commun* 2019; 103462.

## List of Figures

**Fig 1.** Schematic of a one-dimensional granular structure modeled as a one-dimensional continuum, and the material point P and its granular microstructure magnified for better visualization.

**Fig 2.** Schematic of the applied boundary conditions for the static problem describing the behavior of a 1D granular rod in (a) the first scenario, (b) the second scenario, and (c) the third scenario.

**Fig 3.** Results for the static behavior of a 1D granular rod with material constants  $\alpha_m = 0.5$ ,  $\alpha_{Mm} = -0.4$ , and  $l_s = 0.05$  with imposed boundary conditions (a)  $\bar{\phi}_r = 0.01$  and  $\psi_r = 0$ , (b)  $\bar{\phi}_r = 0$  and  $\psi_r = 0.01$ , and (c)  $\bar{\phi}_r = 0.01$  and  $\psi_r = 0.01$  in the first scenario.

**Fig 4.** Results for the static behavior of a 1D granular rod with material constants  $\alpha_m = 0.5$ ,  $\alpha_{Mm} = -0.4$ , and  $l_s = 0.05$  with imposed boundary conditions (a)  $\bar{\phi}_r = 0.01$  and  $\psi_r' = 0$ , (b)  $\bar{\phi}_r = 0$  and  $\psi_r' = 0.01$ , and (c)  $\bar{\phi}_r = 0.01$  and  $\psi_r' = 0.01$  in the second scenario.

**Fig 5.** Results for the static behavior of a 1D granular rod with material constants  $\alpha_m = 0.5$ ,  $\alpha_{Mm} = -0.4$ , and  $l_s = 0.05$  with imposed boundary conditions (a)  $\bar{\phi}_r = 0.01$  and  $\psi_r = 0$ , (b)  $\bar{\phi}_r = 0$  and  $\psi_r = 0.01$ , and (c)  $\bar{\phi}_r = 0.01$  and  $\psi_r = 0.01$  in the third scenario.

**Fig 6.** Results comparing the effect of the material constants (a)  $\alpha_m$ , (b)  $\alpha_{Mm}$ , and (c)  $l_s$  on the behavior of a 1D granular rod with material constants based at  $\alpha_m = 0.5$ ,  $\alpha_{Mm} = -0.4$ , and  $l_s = 0.05$ , for the imposed boundary conditions  $\tilde{\phi}(0) = \tilde{\psi}_{11}(0) = \tilde{\psi}_{11}(1) = 0$ ,  $\tilde{\phi}(1) = 0.01$ .

**Fig 7.** Results comparing the effect of the material constants (a)  $\alpha_m$ , (b)  $\alpha_{Mm}$ , and (c)  $l_s$  on the behavior of a 1D granular rod with material constants based at  $\alpha_m = 0.5$ ,  $\alpha_{Mm} = -0.4$ , and  $l_s = 0.05$ , for the imposed boundary conditions  $\tilde{\phi}(0) = \tilde{\psi}_{11}(0) = \tilde{\phi}(1) = 0$ ,  $\tilde{\psi}_{11}(1) = 0.01$ .

**Fig 8.** First, second, and third natural frequencies and their corresponding mode shapes for the (a-c) CS-CS case, (d-f) CS-CF case, (g-i) CF-CF case, and (j-l) CF-FS case of boundary conditions for a 1D granular rod with material constants  $\alpha_m = 0.5$ ,  $\alpha_{Mm} = -0.4$ ,  $l_s = 0.05$ , and  $n = 100$ .

**Fig 9.** Effect of the material constants (a)  $\alpha_m$ , (b)  $\alpha_{Mm}$ , and (c)  $l_s$  on the first three natural frequencies for a 1D granular rod with material constants based at  $\alpha_m = 0.5$ ,  $\alpha_{Mm} = 0$ ,  $l_s = 0.05$ , and  $n = 100$ .





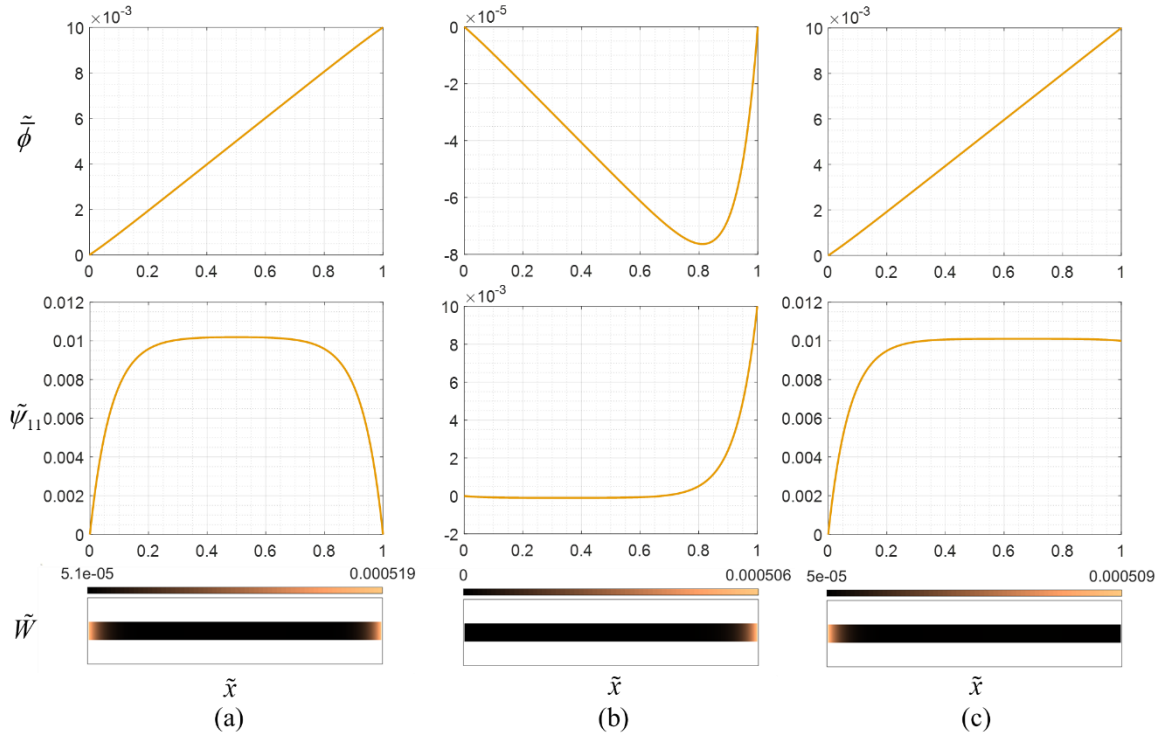


**Fig 3.** Results for the static behavior of a 1D granular rod with material constants  $\alpha_m = 0.5$ ,  $\alpha_{Mm} = -0.4$ , and  $l_s = 0.05$  with imposed boundary conditions (a)  $\bar{\phi}_r = 0.01$  and  $\psi_r = 0$ , (b)  $\bar{\phi}_r = 0$  and  $\psi_r = 0.01$ , and (c)  $\bar{\phi}_r = 0.01$  and  $\psi_r = 0.01$  in the first scenario.

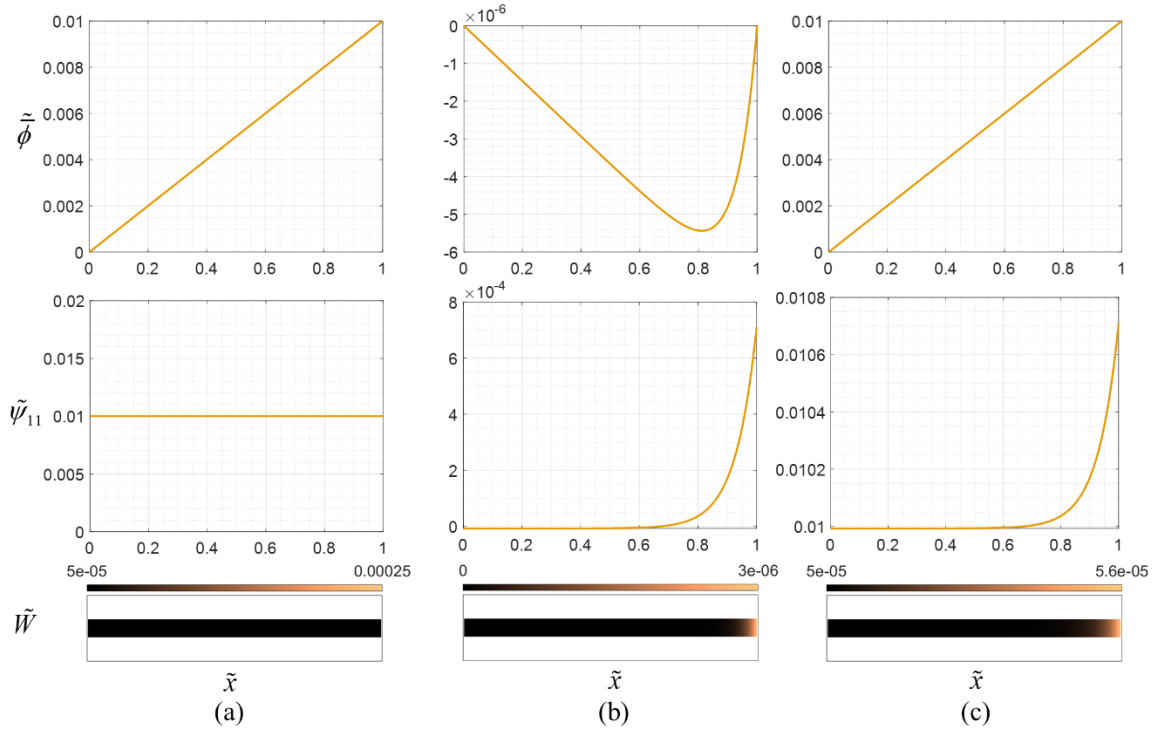


**Fig 4.** Results for the static behavior of a 1D granular rod with material constants  $\alpha_m = 0.5$ ,  $\alpha_{Mm} = -0.4$ , and  $l_s = 0.05$  with imposed boundary conditions (a)  $\bar{\phi}_r = 0.01$  and  $\psi'_r = 0$ , (b)  $\bar{\phi}_r = 0$  and  $\psi'_r = 0.01$ , and (c)  $\bar{\phi}_r = 0.01$  and  $\psi'_r = 0.01$  in the second scenario.

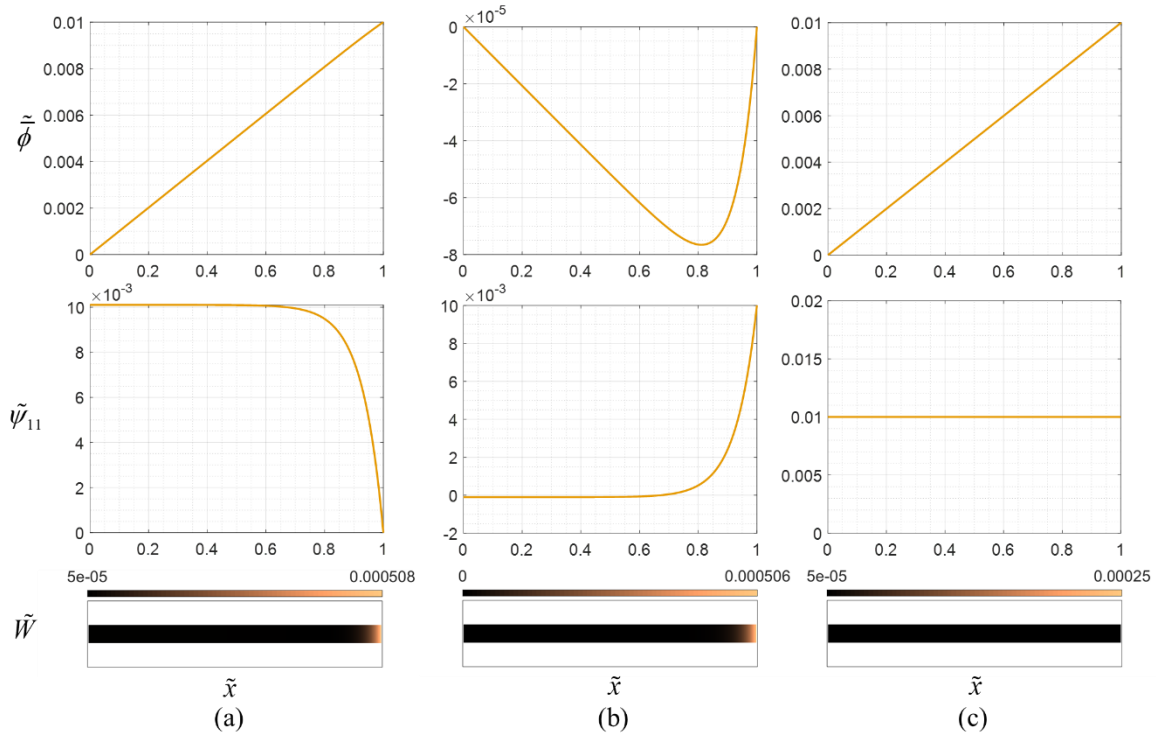


**Fig 5.** Results for the static behavior of a 1D granular rod with material constants  $\alpha_m = 0.5$ ,  $\alpha_{Mm} = -0.4$ , and  $l_s = 0.05$  with imposed boundary conditions (a)  $\bar{\phi}_r = 0.01$  and  $\psi_r = 0$ , (b)  $\bar{\phi}_r = 0$  and  $\psi_r = 0.01$ , and (c)  $\bar{\phi}_r = 0.01$  and  $\psi_r = 0.01$  in the third scenario.

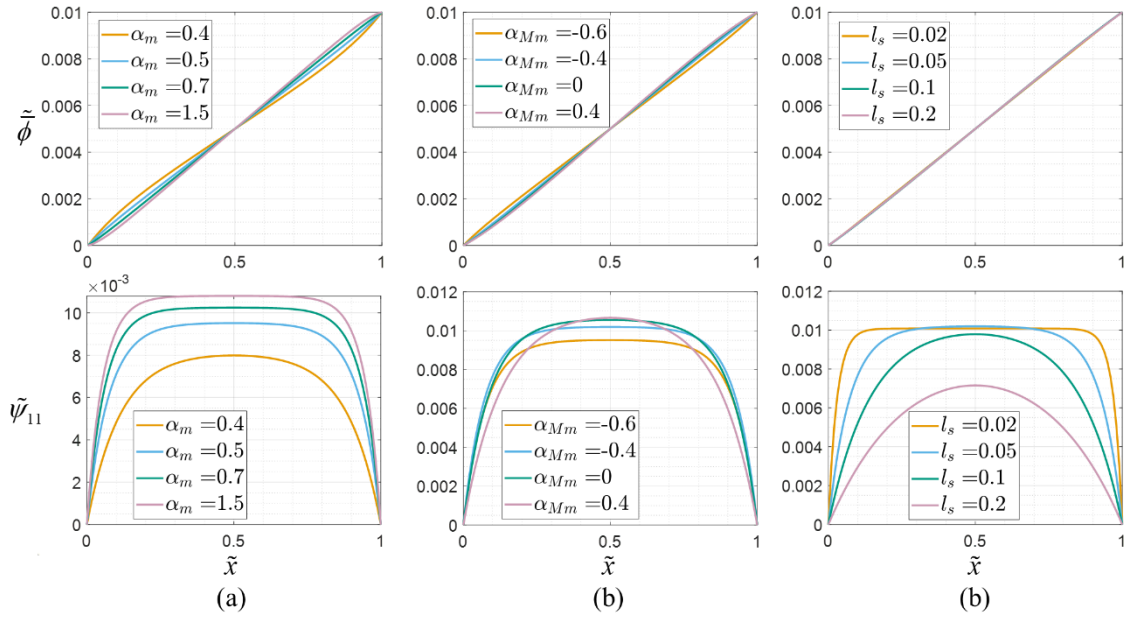


**Fig 6.** Results comparing the effect of the material constants (a)  $\alpha_m$ , (b)  $\alpha_{Mm}$ , and (c)  $l_s$  on the behavior of a 1D granular rod with material constants based at  $\alpha_m = 0.5$ ,  $\alpha_{Mm} = -0.4$ , and  $l_s = 0.05$ , for the imposed boundary conditions  $\tilde{\phi}(0) = \tilde{\psi}_{11}(0) = \tilde{\psi}_{11}(1) = 0$ ,  $\tilde{\phi}(1) = 0.01$ .

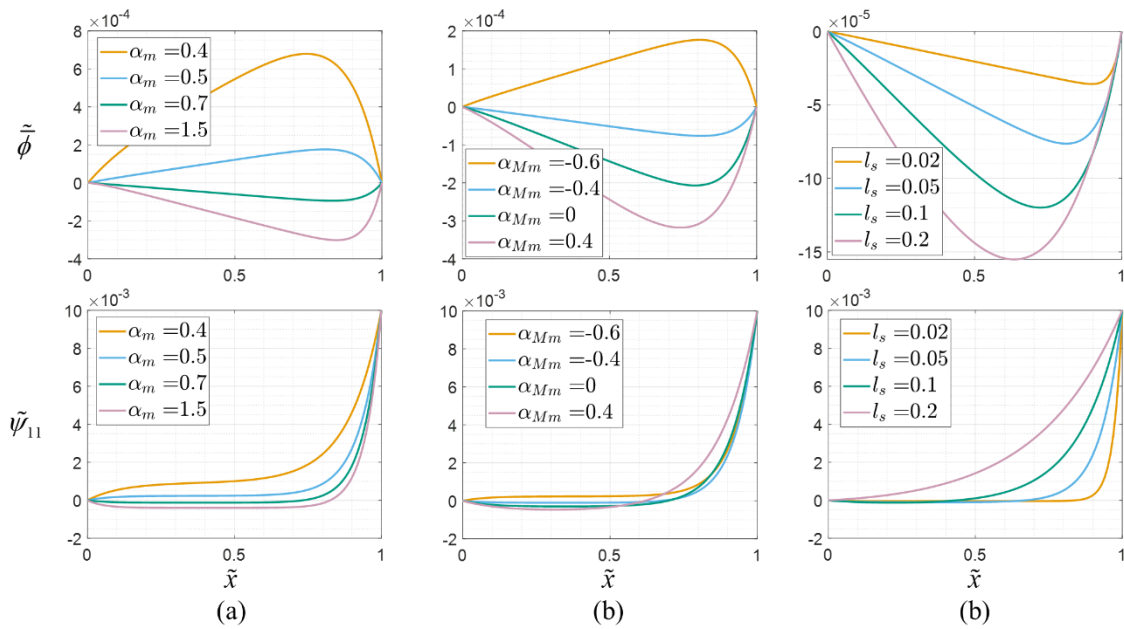


**Fig 7.** Results comparing the effect of the material constants (a)  $\alpha_m$ , (b)  $\alpha_{Mm}$ , and (c)  $l_s$  on the behavior of a 1D granular rod with material constants based at  $\alpha_m = 0.5$ ,  $\alpha_{Mm} = -0.4$ , and  $l_s = 0.05$ , for the imposed boundary conditions  $\tilde{\phi}(0) = \tilde{\psi}_{11}(0) = \tilde{\phi}(1) = 0$ ,  $\tilde{\psi}_{11}(1) = 0.01$ .

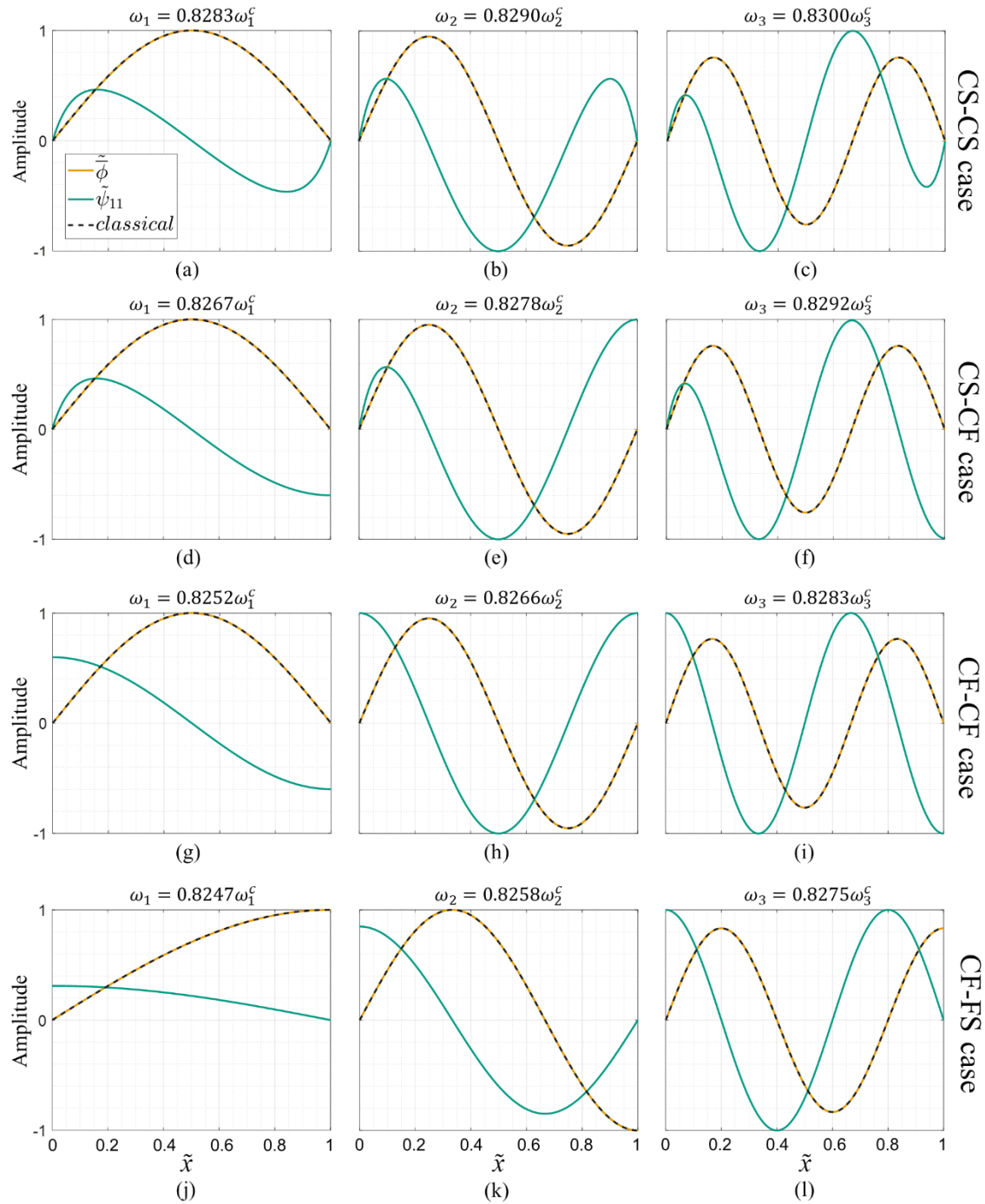


**Fig 8.** First, second, and third natural frequencies and their corresponding mode shapes for the (a-c) CS-CS case, (d-f) CS-CF case, (g-i) CF-CF case, and (j-l) CF-FS case of boundary conditions for a 1D granular rod with material constants  $\alpha_m = 0.5$ ,  $\alpha_{Mm} = -0.4$ ,  $l_s = 0.05$ , and

$$n = 100.$$



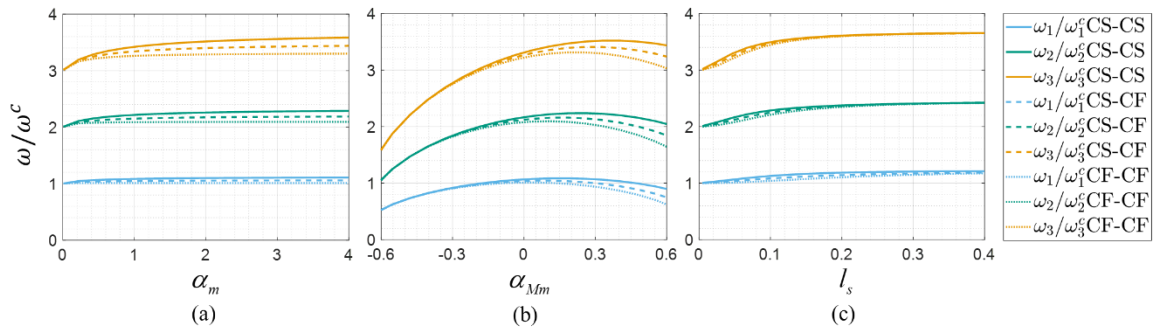


**Fig 9.** Effect of the material constants (a)  $\alpha_m$ , (b)  $\alpha_{Mm}$ , and (c)  $l_s$  on the first three natural frequencies for a 1D granular rod with material constants based at  $\alpha_m = 0.5$ ,  $\alpha_{Mm} = 0$ ,  $l_s = 0.05$ , and  $n = 100$ .

**Appendix G: Paper P7****Title:**

Investigating the domain of validity of one-dimensional micropolar chiral granular model through parametric experimentation

**Authors:**

Nima NejadiSadeghi

Francois Hild

Anil Misra

**Journal:**

Submitted to Mechanics and Physics of Solids

**Credit authorship statement:**

A.M. conceived the idea. N.N. developed the model and performed analysis. F.H. and N.N. developed image processing methodology. All authors contributed to the discussion of all aspects of this work. N.N. wrote the manuscript. All authors edited the manuscript.

**Investigating the domain of validity of one-dimensional micropolar chiral granular model through parametric experimentation**

Nima NejadSadeghi<sup>1</sup>, Francois Hild<sup>2</sup>, and Anil Misra<sup>3\*</sup>

<sup>1</sup>Mechanical Engineering Department,  
University of Kansas, 1530 W 15<sup>th</sup> Street, Learned Hall, Lawrence, KS 66047-7609  
<sup>2</sup>Université Paris-Saclay, ENS Paris-Saclay, CNRS, LMT - Laboratoire de Mécanique et  
Technologie, France  
<sup>3</sup>Civil, Environmental and Architectural Engineering Department,  
University of Kansas, 1530 W 15<sup>th</sup> Street, Learned Hall, Lawrence, KS 66045-7609.  
\*corresponding author: Ph: (785) 864-1750, Fax: (785) 864-5631, Email: amisra@ku.edu

For possible publication in:

*Journal of the Mechanics and Physics of Solids*

**Abstract**

The significance of chirality lies in its wide range of applications in diverse branches of science, and hence, understanding the mechanisms leading to chirality deems necessary. This paper focuses upon chiral granular (meta-) materials and investigates the role of different micro-level deformation mechanisms on the macroscopic chiral behavior of the system incorporating the coupling between the deformation mechanisms in different axes and rotations. To this end, a granular micromechanics based micropolar model is obtained through Hamilton's principle to describe chirality in a one-dimensional chiral granular string in a two-dimensional deformation plane. The domain of validity of the proposed model is thereafter investigated through parametric experimentation by considering a particular chiral granular string composed of 11 grains with each grain interacting with its neighboring grains through some form of mechanism that induces chirality. The granular string is varied in two geometrical parameters that describe the interaction between the two grains, hence providing parametric spaces with respect to the considered geometrical parameters. Digital image correlation is used to analyze the results of tensile experimentation on the granular strings and to investigate the range of applicability of the model to predict the behavior of granular strings by comparing the predicted displacements and rotation fields by the model and the experimental results.

Keywords: Granular metamaterial, Chirality, Generalized continua, tensile experiment, Digital image correlation.

## 1. Introduction

Materials with chiral behavior are not invariant to coordinate inversion. Explicitly, Chirality is an example of non-centrosymmetry where the plane-mirrored image of a geometry cannot be mapped into itself by rotations and translations alone. Its significance lies in its applications in diverse branches of science, including physics, biology, and optics (Nguyen et al., 2006; Ni et al., 2019; Nieves et al., 2018; Takane et al., 2019). In chiral metamaterials, exemplars of applications include vibration attenuation and negative coefficient of thermal expansion. For a comprehensive list of applications of chiral metamaterials, we refer to the review paper (Wu et al., 2019).

Chiral lattices have extensively been studied in terms of their phononic properties (Chen et al., 2020; Liu et al., 2011; Rosi and Auffray, 2016; Spadoni et al., 2009). In particular, the Reference (Spadoni et al., 2009) investigated the effect of different geometrical parameters on the band structure of such lattices, and the Reference (Rosi and Auffray, 2016) studied the wave propagation characteristics of hexagonal chiral lattices modeled as second gradient media. In Addition, the acoustical activity in mechanical metamaterials with chirality was recently experimentally studied (Frenzel et al., 2019). The concept of chirality in lattices has been extended to chiral metacomposites by including inclusions in order to obtain low-frequency stop bands in their band structure (Liu et al., 2011).

Chiral effects are also present in static mechanical systems. Several recent researches have attempted to address the static deformation characteristics of chiral media. For instance, the work in (Alderson et al., 2010) relates the classical elastic constants to the in-plane deformation of different chiral honeycombs through finite element modeling and experiment. Moreover, the work in (Dirrenberger et al., 2011) utilizes a homogenization scheme implemented in finite element method to obtain the effective mechanical properties over a unit-cell. However, as it was experimentally shown recently by analyzing the deformation of a 2D non-centro-symmetric lattice under static load, classical Cauchy elasticity is not enough to fully predict chirality (Poncelet et al., 2018). In recent years, generalized continuum mechanics theories such as micropolar elasticity, micromorphic elasticity, and Willis equations have been adopted to address the shortcomings of classical continuum mechanics in describing chirality (Biswas et al., 2020; Chen and Huang, 2019; Chen et al., 2020, 2014; Duan et al., 2018; Frenzel et al., 2017; Giorgio et al., 2020; Ha et al.,

2016; Kadic et al., 2019; Lakes, 2001; Liu and Hu, 2016; Liu et al., 2012; Misra et al., 2020; Reasa and Lakes, 2019).

The literature on lattice chirality offers comprehensive studies on the chiral properties of particular pre-designed microstructural units using novel experimental and numerical schemes (see for example (Chen et al., 2014; Duan et al., 2018; Fernandez-Corbaton et al., 2019; Jiang and Li, 2018; Spadoni and Ruzzene, 2012)). Indeed, to further enhance the understanding on mechanical chirality, a general analysis in determining the effect of different factors contributing to chirality proves essential. Such an analysis seeks the role of different micro-level deformation mechanisms on the macroscopic chiral behavior of the system by incorporating the coupling between the deformation mechanisms in different axes and rotations.

To this end, in section 2 of the paper, we specialize the granular micromechanics approach (GMA) introduced earlier in (Nejadsadeghi and Misra, 2020a) to a micropolar model with the lowest dimension capable of showing chirality, namely, a 1D granular string in a 2D deformation plane. This consideration enables a tractable model, yet opens an avenue for rigorous analysis of the role different deformation mechanisms on chirality. In section 3, an example of a chiral granular string with a particular grain-pair interaction is proposed. The proposed granular string is studied through parametric experimentation by altering the geometrical parameters describing the grain-pair interaction mechanism. Thereafter, the digital image correlation (DIC) technique is overviewed and adopted to obtain full-field deformation measurement from the experiments. In section 4, the model parameters are fitted to the experimental results, where the effect of the alteration in grain-pair interactions and the range of validity of the micropolar model are discussed. Finally, section 5 summarizes the work and provides concluding remarks.

## 2. GMA based micropolar chiral model

### 2.1. Kinematic variables

For a micromorphic model of degree 1 describing a 3D material with granular microstructure, the displacement of grains within a volume element, adopting summation convention over repeated indices, is described as (Nejadsadeghi and Misra, 2020a, 2020b)

$$\phi_i = \bar{\phi}_i + \psi_{ij} x'_j + \psi_{ijk} x'_j x'_k, \quad (1)$$



where  $\bar{\phi}_i$  is the displacement of the center of mass of the volume element in the macro-scale coordinate system  $x_i$ , and  $\psi_{ij}$  and  $\psi_{ijk}$  are second and third rank micro-deformation tensors, respectively. In Eq. (1),  $\bar{\phi}_i$ ,  $\psi_{ij}$ , and  $\psi_{ijk}$  are all functions of  $x_i$  only, and  $x'_i$  is a micro-scale coordinate system parallel to the macro-scale coordinate system  $x_i$  and attached to the center of mass of the volume element. Note that the construction of Eq. (1) is predicated upon the assumption of infinitesimal deformation and continuity in both macro- and micro-scale (Nejadsadeghi and Misra, 2020a).

The kinematic description in Eq. (1) is rich and can model randomly-packed granular materials and (tailored) metamaterials with granular microstructure. Certain assumptions on the nature of the micro-deformation tensors  $\psi_{ij}$  and  $\psi_{ijk}$  has been shown to result in micropolar and second gradient theories (Nejadsadeghi and Misra, 2020a). In the current paper, we specialize the kinematic description in Eq. (1) to describe a 1D granular-microstructured solid (called a granular string) in the 2D  $x_1x_2$  deformation plane. Therefore, terms accompanying only  $x'_1$  remain. As a result, Eq. (1) is written in components as

$$\phi_1 = \bar{\phi}_1 + \psi_{11}x'_1 + \psi_{111}x'_1x'_1, \quad \phi_2 = \bar{\phi}_2 + \psi_{21}x'_1 + \psi_{211}x'_1x'_1. \quad (2)$$

We proceed by defining the relative measures (Giorgio et al., 2020; Nejadsadeghi and Misra, 2020a)

$$\gamma_{11} = \bar{\phi}_{1,1} - \psi_{11}, \quad \gamma_{111} = \psi_{11,1} - \psi_{111}, \quad \gamma_{21} = \bar{\phi}_{2,1} - \psi_{21}, \quad \gamma_{211} = \psi_{21,1} - \psi_{211}, \quad (3)$$

where, hereafter, differentiation with respect to the spatial coordinates is denoted by a comma in the subscript. For the kinematic description of  $\phi_1$ , assuming  $\gamma_{111} = 0$  results in a micromorphic rod model (Nejadsadeghi and Misra, 2020a). This form can account for micro-macro transfer of energy (coupling) and length scale effects in axial deformation of rods. A further assumption of  $\gamma_{11} = 0$  results in a second gradient model of a rod incorporating length scale effects. Within the scope of the current paper, however, we consider the case where the kinematic measure  $\psi_{111}$  vanishes in the description of  $\phi_1$  (as if the polynomial expansion of  $\phi_1$  is up to linear term instead of quadratic),

and assume  $\gamma_{11} = 0$ , which leads to  $\psi_{11} = \bar{\phi}_{1,1}$ . This consideration yields the simplest model in  $x_1$  direction (the classical model) that is needed for modeling chirality in a micropolar medium. For the kinematic description of the system in  $x_2$  direction ( $\phi_2$ ), we impose that  $\gamma_{211} = 0 \rightarrow \psi_{211} = \psi_{21,1}$ . As a result, there remains only one independent micro-scale kinematic measure,  $\psi_{21}$ . Considering Eq. (3) and the mentioned simplifications on the kinematic description of the system, Eq. (2) takes the form

$$\phi_1 = \bar{\phi}_1 + \bar{\phi}_{1,1}x'_1, \quad \phi_2 = \bar{\phi}_2 + \psi_{21}x'_1 + \psi_{21,1}x'_1x'_1. \quad (3)$$

We note that the considered kinematics of motion in Eq. (3) is general from which recognized models kinematics can be derived. In particular, neglecting any macro-scale motion in  $x_1$  direction results in the Timoshenko beam kinematics, while further constraining the system to have  $\gamma_{21} = 0 \rightarrow \psi_{21} = \bar{\phi}_{2,1}$  yields to the Euler-Bernoulli beam kinematics.

The relative displacement of the two neighboring grains n and p using Eq. (3) is written as

$$\begin{aligned} \delta_1^{np} &= \phi_1^p - \phi_1^n = \bar{\phi}_{1,1}J_1^{np}, \\ \delta_2^{np} &= \phi_2^p - \phi_2^n = \psi_{21}J_1^{np} + \psi_{21,1}J_2^{np} = \bar{\phi}_{2,1}J_1^{np} - \gamma_{21}J_1^{np} + \psi_{21,1}J_2^{np}, \end{aligned} \quad (4)$$

where  $J_1^{np} = l_1^p - l_1^n$  and  $J_2^{np} = l_1^p l_1^p - l_1^n l_1^n$  are geometry moment measures, and  $l_1^q$  represents the vector joining the center of mass of the volume element to the grain q centroid in  $x_1$  direction. In Eq. (4), one identifies three different micro-scale kinematic measures as

$$\delta_n = \bar{\phi}_{1,1}J_1^{np}, \quad \delta_s = \gamma_{21}J_1^{np}, \quad \delta_\theta = \psi_{21,1}J_2^{np}, \quad (5)$$

where  $\delta_n$  resembles the classical continuum relative displacement in  $x_1$  direction,  $\delta_s$  represents a portion of the relative displacement in  $x_2$  direction due to the fluctuations between the macro-scale displacement gradient  $\bar{\phi}_{2,1}$  and the micro-scale kinematic measure  $\psi_{21}$ , and  $\delta_\theta$  shows a portion of the relative displacement in  $x_2$  direction due to the second gradient effect.

## 2.2. Constitutive equations

We consider the macro-scale deformation energy density  $W$  to be a function of the continuum kinematic measures, i.e.,  $W = W(\bar{\phi}_{1,1}, \gamma_{21}, \psi_{21,1})$ . Note that the macro-scale deformation energy density  $W$  needs to be invariant to rigid body motion, and hence, the term  $\bar{\phi}_{2,1}$  alone cannot be a part of its description.

Conjugates to the continuum kinematic measures, macro-scale stress measures are introduced

$$\tau_{11} = \frac{\partial W}{\partial \bar{\phi}_{1,1}}, \quad \sigma_{21} = \frac{\partial W}{\partial \gamma_{21}}, \quad \mu_{211} = \frac{\partial W}{\partial \psi_{21,1}}, \quad (6)$$

where we recognize  $\tau_{11}$  as Cauchy stress,  $\sigma_{21}$  as relative stress, and  $\mu_{211}$  as double stress. The macro-scale deformation energy density  $W$  can also be expressed in terms of the micro-scale deformation energy density as

$$W = \frac{1}{L'} \sum_{\alpha} W^{\alpha}(\delta_n, \delta_s, \delta_{\theta}), \quad (7)$$

where  $W^{\alpha}$  is the micro-scale deformation energy for the  $\alpha^{\text{th}}$  interacting grain pair in the volume element. Conjugates to the micro-scale kinematic measures, intergranular forces (and moments)  $f_n$ ,  $f_s$ , and  $f_{\theta}$  are defined as

$$f_n = \frac{\partial W^{\alpha}}{\partial \delta_n}, \quad f_s = \frac{\partial W^{\alpha}}{\partial \delta_s}, \quad f_{\theta} = \frac{\partial W^{\alpha}}{\partial \delta_{\theta}}. \quad (8)$$

Substituting Eq. (7) in Eq. (6) and employing Eq. (5) and Eq. (8), the macro-scale stress measures are linked to the force measures in micro-scale through

$$\tau_{11} = \frac{1}{L'} \sum_{\alpha} f_n^{\alpha} J_1^{\alpha}, \quad \sigma_{21} = \frac{1}{L'} \sum_{\alpha} f_s^{\alpha} J_1^{\alpha}, \quad \mu_{211} = \frac{1}{L'} \sum_{\alpha} f_{\theta}^{\alpha} J_2^{\alpha}. \quad (10)$$

In Eq. (10) we note that  $J_1^{\alpha}$  and  $J_2^{\alpha}$  for the  $\alpha^{\text{th}}$  grain pair for interacting grains  $n$  and  $p$  are evaluated as  $J_1^{np}$  and  $J_2^{np}$ , respectively.

To obtain constitutive equations in both micro- and macro-scales, one needs to postulate an expression for the micro-scale deformation energy  $W^{\alpha}$ . As a first approximation towards linking

the micro-mechano-morphology of a granular-microstructured solid to its manifesting macroscopic chiral behavior, we limit ourselves to linear elastic mechanisms of deformation. Therefore, the below quadratic expression of the micro-scale deformation energy  $W^\alpha$  for the  $\alpha^{\text{th}}$  grain pair is considered.

$$W^\alpha = \frac{1}{2} K_n^\alpha (\delta_n^\alpha)^2 + \frac{1}{2} K_s^\alpha (\delta_s^\alpha)^2 + \frac{1}{2} K_\theta^\alpha (\delta_\theta^\alpha)^2 + K_{ns}^\alpha \delta_n^\alpha \delta_s^\alpha + K_{n\theta}^\alpha \delta_n^\alpha \delta_\theta^\alpha + K_{s\theta}^\alpha \delta_s^\alpha \delta_\theta^\alpha. \quad (11)$$

In Eq. (11),  $K_i^\alpha, i = n, s, \theta, ns, n\theta, s\theta$  are the stiffnesses associated with their corresponding mechanisms for the  $\alpha^{\text{th}}$  grain pair, all having the dimension of force per length. In particular,  $K_n^\alpha$  is the axial (normal) stiffness,  $K_s^\alpha$  is the shear stiffness, and  $K_\theta^\alpha$  is the rotational stiffness between two grains in contact. The term  $K_{ns}^\alpha$  couples normal and shear deformations, while  $K_{n\theta}^\alpha$  and  $K_{s\theta}^\alpha$  couple the normal and rotational, and shear and rotational deformations, respectively, and are included inspired by the experimental and discrete simulation observations in Ref. (Misra et al., 2020) and for completeness. We note that keeping only the first term in the micro-scale deformation energy description results in a classical rod model, keeping only the third term results in Euler Bernoulli beam model, keeping only second and third terms yields Timoshenko beam model, and keeping the first four terms leads to a model equivalent to the non-standard Timoshenko beam model in (Angelo et al., 2019) to describe chirality.

Intergranular forces introduced in Eq. (8) are obtained, using Eq. (11) as

$$\begin{aligned} f_n &= K_n^\alpha \delta_n^\alpha + K_{ns}^\alpha \delta_s^\alpha + K_{n\theta}^\alpha \delta_\theta^\alpha, \\ f_s &= K_s^\alpha \delta_s^\alpha + K_{ns}^\alpha \delta_n^\alpha + K_{s\theta}^\alpha \delta_\theta^\alpha, \\ f_\theta &= K_\theta^\alpha \delta_\theta^\alpha + K_{n\theta}^\alpha \delta_n^\alpha + K_{s\theta}^\alpha \delta_s^\alpha. \end{aligned} \quad (12)$$

Using Eq. (12), the macro-scale constitutive relations in Eq. (10) are written as

$$\begin{aligned} \tau_{11} &= C^n \bar{\phi}_{1,1} + C^{ns} \gamma_{21} + C^{n\theta} \psi_{21,1}, \\ \sigma_{21} &= C^s \gamma_{21} + C^{ns} \bar{\phi}_{1,1} + C^{s\theta} \psi_{21,1}, \\ \mu_{211} &= C^\theta \psi_{21,1} + C^{n\theta} \bar{\phi}_{1,1} + C^{s\theta} \gamma_{21}, \end{aligned} \quad (13)$$

where the macro-scale stiffnesses  $C^n, C^s, C^{ns}, C^{n\theta}$ , and  $C^{s\theta}$  are defined as

$$\begin{aligned}
C^n &= \frac{1}{L'} \sum_{\alpha} K_n^{\alpha} J_1^{\alpha} J_1^{\alpha}, \quad C^s = \frac{1}{L'} \sum_{\alpha} K_s^{\alpha} J_1^{\alpha} J_1^{\alpha}, \quad C^{\theta} = \frac{1}{L'} \sum_{\alpha} K_{\theta}^{\alpha} J_2^{\alpha} J_2^{\alpha}, \\
C^{ns} &= \frac{1}{L'} \sum_{\alpha} K_{ns}^{\alpha} J_1^{\alpha} J_1^{\alpha}, \quad C^{n\theta} = \frac{1}{L'} \sum_{\alpha} K_{n\theta}^{\alpha} J_1^{\alpha} J_2^{\alpha}, \quad C^{s\theta} = \frac{1}{L'} \sum_{\alpha} K_{s\theta}^{\alpha} J_1^{\alpha} J_2^{\alpha}.
\end{aligned} \tag{14}$$

Lastly, the corresponding macro-scale deformation energy density, following Eq. (11) and using Eq. (6) and Eq. (13) can be written as

$$W = \frac{1}{2} C^n (\bar{\phi}_{1,1})^2 + \frac{1}{2} C^s (\gamma_{21})^2 + \frac{1}{2} C^{\theta} (\psi_{21,1})^2 + C^{ns} \bar{\phi}_{1,1} \gamma_{21} + C^{n\theta} \bar{\phi}_{1,1} \psi_{21,1} + C^{s\theta} \gamma_{21} \psi_{21,1}, \tag{15}$$

with positive definiteness of energy requiring that

$$C^n > 0, \quad C^n C^s > (C^{ns})^2, \quad C^n C^s C^{\theta} + 2C^{ns} C^{n\theta} C^{s\theta} > C^n (C^{s\theta})^2 + C^s (C^{n\theta})^2 + C^{\theta} (C^{ns})^2. \tag{16}$$

### 2.3 Governing equations

The principle of virtual work, neglecting inertia terms, states that

$$-\delta\check{W} + \delta\check{W}_{ext} = 0, \tag{17}$$

where  $\delta$  is the variation symbol, and the terms  $\delta\check{W}$ , and  $\delta\check{W}_{ext}$  are defined in the following. In Eq.

(17),  $\delta\check{W} = \int_L \delta W dx$  represents the variation of total macro-scale deformation energy, expressed

as

$$\begin{aligned}
\delta\check{W} &= -\int_L \tau_{11,1} \delta\bar{\phi}_1 dx - \int_L \sigma_{21,1} \delta\bar{\phi}_2 dx - \int_L (\mu_{211,1} + \sigma_{21}) \delta\psi_{21} dx + \tau_{11} \delta\bar{\phi}_1 \Big|_{x=0}^{x=L} + \sigma_{21} \delta\bar{\phi}_2 \Big|_{x=0}^{x=L} + \mu_{211} \delta\psi_{21} \Big|_{x=0}^{x=L} \\
&.\tag{18}
\end{aligned}$$

The term  $\delta\check{W}_{ext}$  in Eq. (17) corresponds to the variation of total external energy. Considering non-contact volumic terms, it is defined as

$$\delta\check{W}_{ext} = t_1 \delta\bar{\phi}_1 \Big|_{x=0}^{x=L} + t_2 \delta\bar{\phi}_2 \Big|_{x=0}^{x=L} + T_{21} \delta\psi_{21} \Big|_{x=0}^{x=L}. \tag{19}$$

In Eq. (19),  $t_1$  and  $t_2$  are the contact tractions in  $x_1$  and  $x_2$  directions, respectively, and  $T_{21}$  is the contact double traction. Substituting Eq. (18) and Eq. (19) in Eq. (17) results in the balance equations

$$\tau_{11,1} = 0, \quad \sigma_{21,1} = 0, \quad \mu_{211,1} + \sigma_{21} = 0. \quad (20)$$

Finally, for the constitutive relations in Eq. (13), and assuming the macro-scale stiffnesses to have spatial independence, the balance equations in Eq. (20) are recast as

$$\begin{aligned} C^n \bar{\phi}_{1,11} + C^{ns} \bar{\phi}_{2,11} - C^{ns} \psi_{21,1} + C^{n0} \psi_{21,11} &= 0, \\ C^{ns} \bar{\phi}_{1,11} + C^s \bar{\phi}_{2,11} - C^s \psi_{21,1} + C^{s0} \psi_{21,11} &= 0, \\ C^{n0} \bar{\phi}_{1,11} + C^{ns} \bar{\phi}_{1,1} + C^{s0} \bar{\phi}_{2,11} + C^s \bar{\phi}_{2,1} - C^s \psi_{21} + C^0 \psi_{21,11} &= 0. \end{aligned} \quad (21)$$

Moreover, the boundary conditions are evaluated as

$$\begin{aligned} (t_1 - C^n \bar{\phi}_{1,1} - C^{ns} \bar{\phi}_{2,1} + C^{ns} \psi_{21} - C^{n0} \psi_{21,1}) \delta \bar{\phi}_1 &= 0, \quad \text{at } x=0, x=L, \\ (t_2 - C^s \bar{\phi}_{2,1} + C^s \psi_{21} - C^{ns} \bar{\phi}_{1,1} - C^{s0} \psi_{21,1}) \delta \bar{\phi}_2 &= 0, \quad \text{at } x=0, x=L, \\ (T_{21} - C^0 \psi_{21,1} - C^{n0} \bar{\phi}_{1,1} - C^{s0} \bar{\phi}_{2,1} + C^{s0} \psi_{21}) \delta \psi_{21} &= 0, \quad \text{at } x=0, x=L. \end{aligned} \quad (22)$$

Before examining the current model, let us compare it with the classical Timoshenko beam model with constant parameters. In the classical Timoshenko beam model, there is no axial effect of the beam, and therefore, the first equation in Eq. (21) vanishes. Moreover, there does not exist any coupling between different deformation modes, hence  $C^{ns} = C^{n0} = C^{s0} = 0$ . In this case, Eq. (21) takes the simplified form

$$\bar{\phi}_{2,11} - \psi_{21,1} = 0, \quad \bar{\phi}_{2,1} - \psi_{21} + \frac{C^0}{C^s} \psi_{21,11} = 0, \quad (23)$$

and the natural boundary conditions in Eq. (22) simplify to

$$t_2 = C^s \gamma_{21}, \quad T_{21} = C^0 \psi_{21,1}. \quad (24)$$

One recognizes that the ratio  $\frac{C^0}{C^s}$  is equivalent to the term  $\frac{EI}{\kappa AG}$  in formulation of classical

Timoshenko beam, where  $A$  is the cross section area (in the current paper we have assumed unity for cross section area),  $E$  is the elastic modulus,  $G$  is the shear modulus,  $I$  is the second moment of area, and  $\kappa$  is called the Timoshenko shear coefficient. Moreover,  $\psi_{21}$  represents the angle of rotation of the normal to the mid-surface of the beam,  $t_2$  is the shear force, and  $T_{21}$  is the bending moment.



#### 2.4. Dimensionless form of the governing equations

It is convenient to reduce the number of parameters involved in the problem by nondimensionalizing the governing equations in Eq. (21). To this end, we introduce the following dimensionless variables and parameters

$$\begin{aligned} \tilde{\phi}_1 &= \frac{\bar{\phi}_1}{L}, \quad \tilde{\phi}_2 = \frac{\bar{\phi}_2}{L}, \quad \tilde{\psi}_{21} = \psi_{21}, \quad \tilde{x} = \frac{x}{L}, \\ \alpha_s &= \frac{C^s}{C^n}, \quad \alpha_{ns} = \frac{C^{ns}}{C^n}, \quad l_{n\theta} = \frac{1}{L} \frac{C^{n\theta}}{C^n}, \quad l_{s\theta} = \frac{1}{L} \frac{C^{s\theta}}{C^n}, \quad l_\theta = \frac{1}{L} \sqrt{\frac{C^\theta}{C^n}} \end{aligned} \quad (25).$$

It is understood that the parameter  $\alpha_s$  is the ratio of the shear stiffness to the normal (axial) stiffness, and  $\alpha_{ns}$  represents the ratio of the normal-shear coupling stiffness to the normal stiffness. Moreover,  $l_{n\theta}$ ,  $l_{s\theta}$ , and  $l_\theta$  are dimensionless lengths related to the effective magnitude of normal-rotation coupling stiffness, shear-rotation coupling, and rotational stiffnesses, respectively. With regards to Eq. (25), the dimensionless form of the governing equations in Eq. (21) is

$$\begin{aligned} \tilde{\phi}_{1,11} + \alpha_{ns} \tilde{\phi}_{2,11} - \alpha_{ns} \tilde{\psi}_{21,1} + l_{n\theta} \tilde{\psi}_{21,11} &= 0, \\ \alpha_{ns} \tilde{\phi}_{1,11} + \alpha_s \tilde{\phi}_{2,11} - \alpha_s \tilde{\psi}_{21,1} + l_{s\theta} \tilde{\psi}_{21,11} &= 0, \\ l_{n\theta} \tilde{\phi}_{1,11} + \alpha_{ns} \tilde{\phi}_{1,1} + l_{s\theta} \tilde{\phi}_{2,11} + \alpha_s \tilde{\phi}_{2,1} - \alpha_s \tilde{\psi}_{21} + l_\theta^2 \tilde{\psi}_{21,11} &= 0. \end{aligned} \quad (26)$$

The dimensionless spatial domain of the problem is  $0 \leq \tilde{x} \leq 1$ , with dimensionless boundary conditions expressed as

$$\begin{aligned} \left( \tilde{t}_1 - \tilde{\phi}_{1,1} - \alpha_{ns} \tilde{\phi}_{2,1} + \alpha_{ns} \tilde{\psi}_{21} - l_{n\theta} \tilde{\psi}_{21,1} \right) \delta \tilde{\phi}_1 &= 0, \quad \text{at } \tilde{x} = 0, \tilde{x} = 1, \\ \left( \tilde{t}_2 - \alpha_s \tilde{\phi}_{2,1} + \alpha_s \tilde{\psi}_{21} - \alpha_{ns} \tilde{\phi}_{1,1} - l_{s\theta} \tilde{\psi}_{21,1} \right) \delta \tilde{\phi}_2 &= 0, \quad \text{at } \tilde{x} = 0, \tilde{x} = 1, \\ \left( \tilde{T}_{21} - l_\theta^2 \tilde{\psi}_{21,1} - l_{n\theta} \tilde{\phi}_{1,1} - l_{s\theta} \tilde{\phi}_{2,1} + l_{s\theta} \tilde{\psi}_{21} \right) \delta \tilde{\psi}_{21} &= 0, \quad \text{at } \tilde{x} = 0, \tilde{x} = 1, \end{aligned} \quad (27)$$

where  $\tilde{t}_1 = \frac{t_1}{C^n}$ ,  $\tilde{t}_2 = \frac{t_2}{C^n}$ , and  $\tilde{T}_{21} = \frac{T_{21}}{C^n L}$  are dimensionless normal traction (axial force), shear traction (shear force), and contact double traction (bending moment), respectively.

## 2.5. Analytical solution for tensile testing

We here focus on the general solution of Eq. (26). After some straightforward mathematical manipulation, one obtains the following form of solution

$$\begin{aligned}\tilde{\phi}_1 &= a_0 + a_1\tilde{x} + a_2\tilde{x}^2, \\ \tilde{\phi}_2 &= b_0 + b_1\tilde{x} + b_2\tilde{x}^2 + b_3\tilde{x}^3, \\ \tilde{\psi}_{21} &= e_0 + e_1\tilde{x} + e_2\tilde{x}^2,\end{aligned}\tag{28}$$

where  $b_i, i=0,1,2,3, a_i, e_i, i=0,1,2$  are 10 unknown coefficients to be determined. Substituting the solutions in Eq. (28) into the governing equations in Eq. (26) results in

$$\begin{aligned}a_2 &= \frac{\alpha_{ns}l_{s0} - \alpha_s l_{n0}}{\alpha_s - \alpha_{ns}^2} e_2, \quad b_2 = \frac{1}{2}e_1 + \frac{\alpha_{ns}l_{n0} - l_{s0}}{\alpha_s - \alpha_{ns}^2} e_2, \quad b_3 = \frac{e_2}{3}, \\ \alpha_{ns}a_1 + \alpha_s b_1 - \alpha_s e_0 + l_{s0}e_1 + \frac{2\alpha_s l_0^2 - 2l_{s0}^2 - 2\alpha_{ns}^2 l_0^2 + 4\alpha_{ns}l_{n0}l_{s0} - 2l_{n0}^2 \alpha_s}{\alpha_s - \alpha_{ns}^2} e_2 &= 0.\end{aligned}\tag{29}$$

Eq. (29) reduces the number of unknowns from 10 to 6. The remaining 6 unknowns are determined from the imposed boundary conditions. In the current paper, we focus on the uniaxial tensile test with boundary conditions

$$\tilde{\phi}_1(\tilde{x}=0) = 0, \quad \tilde{\phi}_1(\tilde{x}=1) = \bar{\phi}_r, \quad \tilde{\phi}_2(\tilde{x}=0) = \tilde{\phi}_2(\tilde{x}=1) = 0, \quad \tilde{\psi}_{21}(\tilde{x}=0) = \tilde{\psi}_{21}(\tilde{x}=1) = 0.\tag{30}$$

Based on Eq. (30), rotation, transverse displacement, and axial displacement are fixed at the left end, while rotation and transverse displacement are fixed at the right end and the axial displacement  $\bar{\phi}_r$  is imposed. Imposing Eq. (30) on Eq. (28) results

$$\begin{aligned}a_0 &= 0, \quad a_0 + a_1 + a_2 = \bar{\phi}_r, \\ b_0 &= 0, \quad b_0 + b_1 + b_2 + b_3 = 0, \\ e_0 &= 0, \quad e_0 + e_1 + e_2 = 0.\end{aligned}\tag{31}$$

Eq. (31), together with Eq. (29) is solved for the unknown coefficients in Eq. (28), resulting in

$$\begin{aligned}
a_1 &= \frac{(-\alpha_s - 12l_\theta^2)(\alpha_s - \alpha_{ns}^2) + 6\alpha_s \alpha_{ns} l_{n\theta} + 12\alpha_s l_{n\theta}^2 - 6\alpha_{ns}^2 l_{s\theta} - 24\alpha_{ns} l_{n\theta} l_{s\theta} + 12l_{s\theta}^2}{\kappa} \bar{\phi}_r, \\
a_2 &= \frac{-6\alpha_{ns} (\alpha_s l_{n\theta} - \alpha_{ns} l_{s\theta})}{\kappa} \bar{\phi}_r = \bar{\phi}_r - a_1, \\
b_1 &= \frac{\alpha_{ns} (\alpha_s - \alpha_{ns}^2 - 6\alpha_{ns} l_{n\theta} + 6l_{s\theta})}{\kappa} \bar{\phi}_r, \\
b_2 &= \frac{-\alpha_{ns} (3\alpha_s - 3\alpha_{ns}^2 - 6\alpha_{ns} l_{n\theta} + 6l_{s\theta})}{\kappa} \bar{\phi}_r, \\
b_3 &= \frac{2\alpha_{ns} (\alpha_s - \alpha_{ns}^2)}{\kappa} \bar{\phi}_r = -b_1 - b_2, \\
e_1 &= -3b_3, \quad e_2 = 3b_3, \quad a_0 = b_0 = e_0 = 0, \\
\text{where } \kappa &= -\alpha_s^2 + \alpha_s \alpha_{ns}^2 + 12\alpha_s l_{n\theta}^2 - 12\alpha_s l_\theta^2 + 12\alpha_{ns}^2 l_\theta^2 - 24\alpha_{ns} l_{n\theta} l_{s\theta} + 12l_{s\theta}^2.
\end{aligned} \tag{32}$$

To illustrate the model predictions, we consider three granular strings with stiffness constants  $\alpha_s = 0.5$ ,  $\alpha_{ns} = 0.5$ , and  $l_\theta = 0.1$ , with different  $l_{n\theta}$  and  $l_{s\theta}$  values as stated in the legend of Fig. 1. The axial displacement  $\tilde{\phi}_1$  is in general quadratic with respect to  $\tilde{x}$ , and for the case of  $l_{n\theta} = l_{s\theta} = 0$ , the axial displacement behavior reduces to linear. The transverse displacement  $\tilde{\phi}_2$  is a cubic function of  $\tilde{x}$ , and in the particular case of  $l_{n\theta} = l_{s\theta} = 0$ , the midpoint of the granular string overlaps with the inflection point of the transverse displacement function. This symmetry-like behavior is broken for non-vanishing  $l_{n\theta}$  or  $l_{s\theta}$ , where the inflection point is moved to some other point within or outside of the problem domain depending on the values the parameters  $l_{n\theta}$  and  $l_{s\theta}$  take. The rotation of particles,  $\tilde{\psi}_{21}$ , within the granular string follows a quadratic behavior, with its maximum value occurring at the midpoint of the granular string. The magnitude of rotation is affected by the magnitude of the parameters  $l_{n\theta}$  and  $l_{s\theta}$ .

### 3. Parametric Experimentation

It was discussed in section 2 that the proposed micropolar model based upon GMA predicts chirality in granular media tied to the deformation mechanisms between the interacting grains. In this section, we present the parametric experimentation on 3D printed chiral granular strings.

### 3.1. Prototypical model realization

Motivated by the predictions of the mathematical model presented in section 2, a chiral granular string is conceptualized. A schematic of the model is shown in Fig. 2(a) where the set of solid beams connecting two grains is considered as the mechanical (rheological) analog of the grain-pair interaction. To investigate the effect of deformation mechanisms, the geometrical parameters  $t$  and  $b$  associated with the mechanical analog of grain-pair interactions were varied, thus enabling a parametric study. This is shown in Fig. 2(a) where each sample with its unique set of parameters  $t$  and  $b$  is shown with a marker within the domain of geometrical parameters. With regards to the considered granular strings, the sample with the largest weight has almost 16% more weight than the samples with the least weight.

The CAD software SolidWorks (Dassault Systems SolidWorks Corporation, Waltham, MA, USA) was used to generate the granular string geometries based on Fig. 2(a). Each granular string is composed of 11 grains with out of plane thickness of 4 mm (Fig. 2(b)). The out of plane thickness value was chosen to admit 2D planar deformation analysis, while preventing warpage in the fabrication process. The granular strings were terminated at both ends with flat extensions designed to facilitate gripping in tensile experiments. The conceived granular strings were realized via the Low Force Stereolithography 3D printer Form 3 (FormLabs, USA), using the monomer “Durable Resin”, with XY resolution and layer thickness of  $\approx 50 \mu\text{m}$ . The Young’s modulus of the cured Durable resin is 1.0 GPa. The printed samples had a maximum of 0.1 mm variation in  $b$  and  $t$  parameters with respect to the nominal values. We note that for each granular string geometry, two samples were 3D printed and tested.

### 3.2. Experimental prescription

An ElectroForce 3200 (TA Instruments) testing machine was utilized to conduct tensile testing on the 3D printed granular strings. The testing machine is equipped with a load cell of capacity  $\pm 450$  N, a measurement uncertainty of 0.1%, and precision of 0.001 N, and a displacement transducer with a range of  $\pm 6.5$  mm, a measurement uncertainty of 0.1%, and precision of 0.001 mm. Fig. 2(b) shows a snapshot of a granular string being attached to the testing machine via the grips and being tested. The boundary conditions imposed by the grips on the sample resemble that of Eq. (30), and therefore, a comparison can be made between the theory’s predictions and experimental

results. A total extension of 10 mm (axial strain of  $\sim 0.095$ ) was imposed on the granular string specimens at a rate of 0.05 mm/s.

To extract grain kinematics data from the experiments, speckle pattern was applied on the surface of the granular string samples using black and white paint sprays (see Fig. 2(b)). Using a camera, ten images were taken in the reference configuration for the purpose of uncertainty quantifications, and consecutive images were taken from the samples during the experiment. The image acquisition setup is shown in Fig. 2(c) with the specifications listed in Table 1. To facilitate the image acquisition, a red background was adopted, and soft boxes were used to generate diffusive lighting. The captured images were transformed into black and white for performing DIC.

**Table 1.** DIC hardware parameters.

Camera	NIKON D300
Definition	4288×2848 pixels (RGB image)
Gray levels amplitude	8 bits
Lens	AF-S VR Micro-Nikkor 105mm f/2.8G ED
Aperture	$f/4.5$
Field of view	111×74 mm <sup>2</sup>
Image scale	60 $\mu\text{m}/\text{px}$ (B&W image)
Stand-off distance	$\approx 90\text{cm}$
Image acquisition rate	1/5 fps
Exposure time	20 ms
Patterning technique	Sprayed black paint
Pattern feature size	2.6 px

### 3.3. Digital Image Correlation (DIC)

The captured images of the experiments were post-processed using DIC to obtain full-field deformation information in different scales of observation. Correli 3.0 DIC framework was used in which Hencky-elastic regularization was implemented (Leclerc et al., n.d.). The DIC technique is based on the registration of the image  $I_0$  in the reference configuration and the image  $I_t$  in the

deformed configuration. The framework is constructed upon the conservation of gray level between the two images, and is stated as

$$I_0(\mathbf{x}) \cong I_t(\mathbf{x} + \mathbf{u}(\mathbf{x})), \quad (33)$$

where  $\mathbf{x}$  is the position vector of each pixel within the domain of study, and  $\mathbf{u}$  is the unknown displacement field. The problem is to find a displacement vector  $\mathbf{u}$  such that the squared differences between the reference image  $I_0(\mathbf{x})$  and the corrected deformed image  $I_t(\mathbf{x} + \mathbf{u}(\mathbf{x}))$  is minimized.

Let us consider a displacement field  $\mathbf{u}$  with the following form

$$\mathbf{u}(\mathbf{x}, \mathbf{a}) = \sum_i \mathbf{N}_i(\mathbf{x}, \underline{a}_i), \quad (34)$$

where summation convention is not exercised, and  $\underline{a}_i$  is the associated degree of freedom with the  $i$ -th trial displacement field vector  $\mathbf{N}_i(\mathbf{x}, \underline{a}_i)$ . We note that the expression for  $\mathbf{u}$  in Eq. (34) can be linear or nonlinear function of the degrees of freedoms  $\underline{a}_i$  depending on the assumed kinematics. The registration minimizes the mean square of the pixel-wise gray level residual  $\rho$  over a region of interest (ROI),  $\eta^2(\underline{\mathbf{a}})$ , defined as

$$\eta^2(\underline{\mathbf{a}}) = \sum_{\text{ROI}} \rho^2(\mathbf{x}, \underline{\mathbf{a}}), \quad (35)$$

where

$$\rho(\mathbf{x}, \underline{\mathbf{a}}) = I_t(\mathbf{x} + \mathbf{u}(\mathbf{x}, \underline{\mathbf{a}})) - I_0(\mathbf{x}). \quad (36)$$

We note that the minimization scheme in Eq. (35) is nonlinear and the degrees of freedom vector  $\underline{\mathbf{a}}$  is obtained by iteration using Gauss-Newton method. To this end, let us assume that the degrees of freedom (nodal displacements) vector  $\underline{\mathbf{a}}$  is close to the solution. Using Taylor expansion we write



$$\begin{aligned}\eta^2(\underline{\mathbf{a}} + \delta\underline{\mathbf{a}}) &= \sum_{\mathbf{x}} \left( I_t(\mathbf{x} + \mathbf{u}(\mathbf{x}, \underline{\mathbf{a}} + \delta\underline{\mathbf{a}})) - I_0(\mathbf{x}) \right)^2 \\ &\approx \sum_{\mathbf{x}} \left( I_t(\mathbf{x} + \mathbf{u}(\mathbf{x}, \underline{\mathbf{a}})) + \delta\underline{\mathbf{a}} \mathbf{N}(\mathbf{x}) \cdot \nabla I_t(\mathbf{x} + \mathbf{u}(\mathbf{x}, \underline{\mathbf{a}})) - I_0(\mathbf{x}) \right)^2,\end{aligned}\quad (37)$$

where  $\delta\underline{\mathbf{a}}$  is a small change to be added to the values in the degrees of freedom  $\underline{\mathbf{a}}^{(n)}$  in the  $n^{\text{th}}$  iteration as follows

$$\underline{\mathbf{a}}^{(n+1)} = \underline{\mathbf{a}}^{(n)} + \delta\underline{\mathbf{a}}. \quad (38)$$

The minimization is therefore stated as

$$\frac{\partial \eta^2}{\partial (\delta\underline{\mathbf{a}})} (\delta\underline{\mathbf{a}}) = \mathbf{0}, \quad (39)$$

which can be reshaped to take the form

$$M_{ij} \delta a_j = b_i, \quad (40)$$

with

$$\begin{aligned}M_{ij} &= \sum_{\mathbf{x}} (\mathbf{N}_i(\mathbf{x}) \cdot \nabla I_t(\mathbf{x}, \underline{\mathbf{a}})) (\mathbf{N}_j(\mathbf{x}) \cdot \nabla I_t(\mathbf{x}, \underline{\mathbf{a}})), \\ b_i &= \sum_{\mathbf{x}} (\mathbf{N}_i(\mathbf{x}) \cdot \nabla I_t(\mathbf{x}, \underline{\mathbf{a}})) (I_0(\mathbf{x}) - I_t(\mathbf{x}, \underline{\mathbf{a}})).\end{aligned}\quad (41)$$

To quantify the uncertainty levels of the DIC, all possible combinations of the reference images taken before the execution of each experiment were analyzed using DIC. For a value of 10 as the number of reference images, the total number of DIC analyses is 45. To account for the small fluctuations of displacement caused by the actuator of the machine, the linear macro-scale axial displacement of each analysis is subtracted from the displacements in axial direction, and the mean displacement/rotation values of the analyses in other directions were subtracted from their corresponding displacement/rotation components in those directions. Standard deviation values were then calculated for each degree of freedom with respect to the 45 DIC analyses. Table 2 gives the uncertainties for the DIC analyses performed at different levels (introduced in the following).

**Table 2.** Standard uncertainties for the DIC analyses at different levels.

	Axial direction	Transverse direction	Rotation
Macro-scale	0.024 px ( $1.5 \times 10^{-3}$ mm)	0.024 px ( $1.5 \times 10^{-3}$ mm)	-
Micro-scale	0.024 px ( $1.5 \times 10^{-3}$ mm)	0.024 px ( $1.5 \times 10^{-3}$ mm)	-
Meso-scale	0.021 px ( $1.3 \times 10^{-3}$ mm)	0.021 px ( $1.3 \times 10^{-3}$ mm)	$1.5 \times 10^{-4}$

Fig. 3(a) shows the first, three intermediate, and the last images of a sample granular string with  $t=1.2$  mm and  $b=1$  mm under tensile experiment. Different levels of DIC were performed on the images and are discussed here. The first level of DIC, here referred to as the macro-scale DIC, is when the granular string is deemed as a continuous bar of homogenous cross-section. The macro-scale DIC assumes that the granular string is a small finite volume of a larger body with indistinguishable grains, and as a result, is useful when macro-scale continuum models are to be developed. It serves a second purpose as well, as its results provide a good initialization for the solution of other levels of DIC (and hence lowering the number of iterations significantly). Fig. 3(b) shows the finite element-wise spatial discretization of the domain for the macro-scale DIC analysis using T3 elements with element size of 33 px (about 2 mm). It was observed that no significant gain is obtained by using a finer mesh, and the discretization shown in Fig. 3(b) is good enough to represent some aspects of the system behavior. Fig. 3(d) and Fig. 3(f), show, respectively, the transverse and axial displacement for the macro-scale analysis considering the full range of applied deformation. One observes the chiral behavior of the granular string with resemblance to the theoretical predictions in Fig. 1. With regards to Fig. 3(h), an observed increase in the root mean square (RMS) value of the gray level residuals suggests that the macro-scale analysis becomes less accurate as the deformation progresses. The increase in the RMS value can be partly attributed to the kinematic assumption not being accurate enough when deformation in the grain-pair interaction mechanisms (beams and bars) becomes large. This issue is amplified by the fact that the macro-scale DIC discretization does not differentiate the granular string from the background. Therefore, one requires to define a domain encompassing the structure of interest with the minimum inclusion of the background to better capture the deformation kinematics. Accordingly, the nominal geometry of the granular string, called the mask, was created, and using DIC a registration was performed to backtrack the mask to the image of the granular string in its initial configuration (Hild et al., 2021). This process results in obtaining the domain wherein the

structure of interest resides, with significantly lower amount of background, if any (see Fig. 3(c)). Similar to the macro-scale DIC, the domain was spatially discretized using T3 elements with element size of 10 px (about 0.63 mm). The mesh is shown in Fig. 3(c). We call the DIC analysis corresponding to this mesh a micro-scale DIC. The micro-scale DIC solution was initialized using the macro-scale DIC solution. Fig. 3(e) and Fig. 3(g) show the transverse and axial displacements in the granular string, respectively, using the micro-scale DIC. One observes a noticeable similarity between the displacement fields obtained from the macro- and micro-scale DIC analyses. However, the RMS of gray level residuals for the micro-scale DIC shown in Fig. 3(i) suggests more accuracy compared to the macro-scale DIC as the deformation progresses, since the relative increase in the RMS value is lower.

The results from the macro- and micro-scale analyses provide interesting evidence of the presence of chirality. While the realized granular string in the current research can be viewed as a chiral lattice structure (similar to chiral lattices proposed in the literature where deformable/rigid nodes are connected via different beam/rod elements), it can also be deemed as a granular (meta-) material with a series of rigid grains interacting with each other through some specific grain-pair interaction mechanisms. To authenticate this hypothesis, one can assess the strain distribution (which is proportional to stress distribution for assumed linear constituent material as a first order approximation) within the granular string. Figs. 3(j-l) show, respectively, the normal strain field in transverse direction, normal strain field in axial direction, and shear strain field for the full range of applied deformation. It is understood from the figures that grains experience negligible deformation compared to the interactions. Moreover, Fig. 3(m) shows the results for the dimensionless form of the strain energy measure (strain energy divided by half of the Young's modulus of the constituent material). This plot also confirms that the energy expenditure is mainly localized in the grain-pair interaction mechanism, and not in the grains. Therefore, in what follows, we mainly focus on the kinematics of grains induced by their interaction mechanisms.

To this end, a called meso-scale DIC analysis with three degrees of freedom for each grain can be performed to extract the motion of grains, namely the axial displacement,  $t_1$ , the transverse displacement,  $t_2$ , and the rotation,  $\theta$ , of each grain about their center of masses. In this case, Eq. (34) is written as

$$\mathbf{u}(\mathbf{x}, \mathbf{t}, \theta) = \mathbf{t} + (\mathbf{R}(\theta) - \mathbf{I})\mathbf{x}, \quad (42)$$

where

$$\mathbf{t} = \begin{bmatrix} t_1 \\ t_2 \end{bmatrix}, \quad \mathbf{R}(\theta) = \begin{bmatrix} \cos(\theta) - 1 & -\sin(\theta) \\ \sin(\theta) & \cos(\theta) - 1 \end{bmatrix}. \quad (43)$$

It is noteworthy to mention that for the meso-scale analysis, each grain is considered a separate region of interest, and therefore, DIC with initialized solutions from micro-scale analysis was performed on each grain independently. For the purpose of illustration, consider the granular string with  $t=1.2$  mm and  $b=1$  mm, with results shown in Fig. 4. Fig. 4(a) shows the RMS of the gray level residuals corresponding to the 11 grains under study for all DIC calculations (images). Grain 1 corresponds to the grain attached to the fixed grip, and grain 11 is attached to the moving grip. Fig. 4(b) shows the axial displacement of grains. The transverse displacement of grains can be seen in Fig. 4(c), and the rigid rotation of grains is plotted in Fig. 4(d). We note the qualitative agreement between the results shown in Fig. 4 and the theoretical predictions in Fig. 1.

#### 4. Results and discussion

A quantitative evaluation of the granular strings behavior based on the proposed micropolar model can be made by comparing the displacements and rotation fields of the model and those of the experiments. This approach enables us to evaluate the effect of geometric parameters  $b$  and  $t$  on the behavior of the system, without needing to identify the stiffnesses associated with each granular string. Moreover, it serves as a tool to assess the domain of validity of the model predictions in terms of the resultant deformation fields. To this end, the grain positions, and axial and transverse displacements were nondimensionalized with respect to the length of the granular string to harmonize the experimental results with the expressions in Eq. (28).

To obtain the model parameters  $a_i, e_i, i=0,1,2, b_i, i=0,1,2,3$ , a least squares optimization with equality constraints is adopted. Explicitly, we intend to minimize the function  $f(\tilde{\mathbf{x}}) = \|\tilde{\mathbf{A}}\tilde{\mathbf{x}} - \tilde{\mathbf{b}}\|^2$  subject to linear constraints  $\tilde{\mathbf{C}}\tilde{\mathbf{x}} = \tilde{\mathbf{d}}$ . In this problem,  $\tilde{\mathbf{x}}$  is a column vector of length 10 and is composed of the model parameters  $a_i, e_i, i=0,1,2, b_i, i=0,1,2,3$  (to be solved for).  $\tilde{\mathbf{A}}$  is a 33-by-

10 matrix with its nonzero components functions of the location of grains according to Eq. (28), and  $\check{\mathbf{b}}$  is a column vector of length 33 with its components being the experimentally obtained displacements and rotations of grains. The matrix  $\check{\mathbf{C}}$  is 7-by-10 and together with the 7-vector  $\check{\mathbf{d}}$  provide the linear constraints below

$$\begin{aligned}
 a_0 &= \text{measured axial displacement of grain adjacent to fixed grip,} \\
 a_0 + a_1 + a_2 &= \text{measured axial displacement of grain adjacent to moving grip,} \\
 b_0 &= \text{measured transverse displacement of grain adjacent to fixed grip,} \\
 b_0 + b_1 + b_2 + b_3 &= \text{measured transverse displacement of grain adjacent to moving grip,} \\
 e_0 &= \text{measured rotation of grain adjacent to fixed grip,} \\
 e_0 + e_1 + e_2 &= \text{measured rotation of grain adjacent to moving grip,}
 \end{aligned} \tag{44}$$

and the relation  $e_1 + 3b_3 = 0$ . Introducing the Lagrange multiplier vector  $\check{\mathbf{z}}$ , setting up the Lagrangian function, and requiring it to be minimized, one needs to solve the following matrix to obtain the parameters

$$\begin{bmatrix} \check{\mathbf{A}}^T \check{\mathbf{A}} & \check{\mathbf{C}}^T \\ \check{\mathbf{C}} & \mathbf{0} \end{bmatrix} \begin{bmatrix} \check{\mathbf{x}} \\ \check{\mathbf{z}} \end{bmatrix} = \begin{bmatrix} \check{\mathbf{A}}^T \check{\mathbf{b}} \\ \check{\mathbf{d}} \end{bmatrix}. \tag{44}$$

Moreover, each row of  $\check{\mathbf{A}}$  and  $\check{\mathbf{b}}$  corresponding to displacements was divided by the length-nondimensionalized value of the uncertainties associated with that displacement, and each row of  $\check{\mathbf{A}}$  and  $\check{\mathbf{b}}$  corresponding rotations was divided by the value of the rotational uncertainty. Finally, to improve the conditioning of the system of equations in Eq. (44),  $\check{\mathbf{C}}$  and  $\check{\mathbf{d}}$  were multiplied by  $\frac{\text{norm}(\check{\mathbf{A}})}{\text{norm}(\check{\mathbf{C}})}$ .

Due to the linear constraints, the model parameters  $a_0$ ,  $b_0$ , and  $e_0$  assume very negligible values, and the other model parameters follow the relations in Eq. (32). Therefore, after introducing normalized form of model parameters  $\check{\square} = \frac{\square}{\phi_r}$ , where  $\square$  represents a model parameter, it is enough to report only the normalized model parameters  $\check{a}_1$ ,  $\check{b}_1$ , and  $\check{b}_2$ . Moreover, the axial displacement,

$\tilde{\phi}_1$ , transverse displacement,  $\tilde{\phi}_2$ , and rotation,  $\tilde{\psi}_{21}$ , are related to the noted normalized model parameters through the following relations

$$\begin{aligned}\frac{\tilde{\phi}_1}{\phi_r} &= \tilde{a}_1 \tilde{x} + (1 - \tilde{a}_1) \tilde{x}^2, \\ \frac{\tilde{\phi}_2}{\phi_r} &= \tilde{b}_1 \tilde{x} + \tilde{b}_2 \tilde{x}^2 - (\tilde{b}_1 + \tilde{b}_2) \tilde{x}^3, \\ \frac{\tilde{\psi}_{21}}{\phi_r} &= 3(\tilde{b}_1 + \tilde{b}_2) \left( \frac{1}{4} - \left( \tilde{x} - \frac{1}{2} \right)^2 \right).\end{aligned}\tag{45}$$

We here consider two cases to study, where in one case we focus on the deformation of the granular string with an imposed axial strain of  $\sim 0.035$  and in the other case the full deformation (axial strain of  $0.095$ ) is considered. Fig. 5 shows the fitted normalized model parameters  $\tilde{a}_1$ ,  $\tilde{b}_1$ , and  $\tilde{b}_2$  for the considered granular strings for axial strains of  $0.035$  (two left columns) and  $0.095$  (two right columns), respectively. Moreover, Fig. 6 shows the goodness of the fits for the considered granular strings for axial strains of  $0.035$  (two top rows) and  $0.095$  (two bottom rows), respectively. The goodness of the fits are shown with the symbol  $\chi$  and are plotted for the axial and transverse displacement fields, rotation field, and for the global behavior of the model. The goodness of the fits for different fields are calculated as RMS of the residuals for each grain within the granular structure, divided by the dimensionless uncertainty, where the residuals are defined as the dimensionless difference between the model prediction and the experimental observations. Moreover, the global goodness of the fit,  $\chi_{\text{global}}$ , is computed as the RMS of the goodness of the fits in axial, transverse, and rotation components and is a representative of the global quality of the model. From the results in Fig. 5 and Fig. 6, the following comments can be made.

It is observed that  $\tilde{a}_1$  does not assume the value of unity, although close to it, for all the configurations of the grain-pair interaction and for the both considered axial strains. Moreover, the value of  $\tilde{a}_1$  for each configuration is almost constant in both axial strains and therefore, is independent of the imposed axial strain. Given the scatter observed in the plots corresponding to  $\tilde{a}_1$  for all  $b$  and  $t$  values, an average value of  $\tilde{a}_1 = 0.982$  can be reported to describe all the samples



at all axial strains. Since based on the model the quadratic term with coefficient  $\tilde{a}_2 = 1 - \tilde{a}_1$  in the axial displacement emerges only if normal-rotational and shear-rotational stiffnesses are present, it is deduced that such mechanisms exist in the studied chiral granular string. However, their corresponding stiffness values are rather small. Moreover, having similar  $\tilde{a}_1$  values for all the samples allows us to conclude that the change in the geometrical parameters  $t$  and  $b$  has minimal effect on the axial behavior of the sample under tension predicted by the model. This statement is supported by considering the goodness of the fits for the axial displacement where all  $\chi_{\text{axial}}$  values are within a narrow range, and therefore suggest that all fits are of the same quality for each considered axial strain. Nevertheless, the average value of  $\chi_{\text{axial}}$  at axial strain of 0.095 is almost two times larger than its counterpart at axial strain of 0.035, which suggests some degradation in the quality of the model at larger strains to predict the axial behavior of the system.

Regarding the parameters  $\tilde{b}_1$  and  $\tilde{b}_2$ , we note that a large scatter is observed for the samples with  $t = 0.3$  mm and  $t = 0.6$  mm due to having soft grain-pair interaction mechanisms with very thin beams. Based on Fig. 5, and observing close values with small fluctuations for  $\tilde{b}_1$  and  $\tilde{b}_2$  with respect to the geometrical parameters  $t$  and  $b$  at axial strain of 0.035 (except for the two mentioned samples), the average values of  $\tilde{b}_1 = -0.902$  and  $\tilde{b}_2 = 2.338$  can be reported for all the samples at this axial strain. This statement is also supported by the values of  $\chi_{\text{transverse}}$  and  $\chi_{\text{rotational}}$  at axial strain of 0.035 where except for the two samples with  $t = 0.3$  mm and  $t = 0.6$  mm, close values with small scatters are observed for each group of varying  $b$  and  $t$  samples. We also note, comparing  $\chi_{\text{transverse}}$  and  $\chi_{\text{rotational}}$  values of the two groups of varying  $b$  and  $t$  at axial strain of 0.035, that the samples in the group of varying  $b$  are better described using the proposed model. Furthermore, comparing different axial strains results, we observe a decrease in the magnitude of both  $\tilde{b}_1$  and  $\tilde{b}_2$ , with the average values of  $\tilde{b}_1 = -0.647$  and  $\tilde{b}_2 = 1.813$  for the axial strain of 0.095. However, we must note that  $\chi_{\text{transverse}}$  and  $\chi_{\text{rotational}}$  values at axial strain of 0.095 has increased compared to the axial strain of 0.035, which is suggestive of degradation in the quality of the model in predicting the transverse displacement and rotation of grains at larger strains. Moreover, the

change observed in the values of  $\tilde{b}_1$  and  $\tilde{b}_2$  with respect to the imposed axial strain suggests a change in the intergranular stiffnesses as the deformation progresses, which is mainly due to the significance of nonlinearities in the grain-pair interaction mechanisms. It is also observed that at both axial strains and almost all samples, the quality of the model to predict transverse displacement is slightly better than its quality to model the rotation of grains.

In general, and for both the axial strains considered,  $\chi_{\text{transverse}}$  and  $\chi_{\text{rotational}}$  assume larger values than  $\chi_{\text{axial}}$ . This is partly due to the fact that the model fitting schemes for the transverse displacement and rotation are coupled (and hence more constrained) than the uncoupled axial displacement model fitting. It is also observed that all  $\chi$  values increase as the deformation progresses, and therefore, the model is less able to correctly predict the behavior of the system at larger strains. This is mainly due to the fact that the nonlinearities in the grain-pair interaction become significant, while the model is predicated upon linear interaction mechanisms between the grains. Moreover, an increase in  $\chi_{\text{transverse}}$  and  $\chi_{\text{rotational}}$  values is observed as the geometrical parameter  $t$  increases in axial strain of 0.095. This increase suggests that the model is less predictive in granular systems with larger geometrical parameter  $t$  in large strains.

To seek more insight on the emergence of nonlinearities in grain-pair interactions, we remark the transition between different deformation mechanisms within the range of the geometrical parameters  $b$  and  $t$  considered. Fig. 7 and Fig. 8 show the dimensionless strain energy density distribution for the samples at axial strains of 0.035 and 0.095, respectively. While the strain energy density magnitude is different in granular strings between the two axial strains (as is expected), a similar deformation mechanism is observed for each granular string in both axial strains. Moreover, as the geometrical parameter  $b$  increases, the main deformation mechanism shifts from the two beams identified with  $b$  to the middle beam identified with  $t$ . Conversely, for small values of the geometrical parameter  $t$ , the middle beam identified with  $t$  undergoes the maximum deformation, and as  $t$  increases, the deformation of the two beams identified with their thickness  $b$  becomes dominant. We here note that the observed trends of  $\chi_{\text{transverse}}$  and  $\chi_{\text{rotational}}$  at axial strain of 0.095 can be explained using Fig. 8 results. In particular, for samples with very small  $b$ , it is the geometric nonlinearity, and for samples with very large  $b$ , the material nonlinearity

is the main cause for lower model quality (larger  $\chi_{\text{transverse}}$  and  $\chi_{\text{rotational}}$  values). This contributes to having large  $\chi_{\text{transverse}}$  and  $\chi_{\text{rotational}}$  values in both ends of the spectrum and lower values for the samples in the middle of the range. On the other hand, for samples with very small  $t$ , it is the material nonlinearity, and for samples with very large  $t$ , the geometrical nonlinearity is the primary reason for lower model quality (larger  $\chi_{\text{transverse}}$  and  $\chi_{\text{rotational}}$  values). In particular, we note that since the model quality decreases considerably as the geometrical parameter  $t$  increases, the geometrical nonlinearity has a more pronounced effect on the capability of the model.

## 5. Summary and conclusions

In the present paper, a theoretical micropolar model based on GMA was developed to describe the chiral behavior of a 1D granular string in a 2D deformation plane. The introduced model incorporated normal, shear, and rotational stiffnesses, along with normal-shear, normal-rotational, and shear-rotational coupling stiffnesses, all modeled as linear deformation mechanisms. The model was studied to predict the behavior of chiral granular strings in uniaxial tension and the effects of normal-rotational and shear-rotational coupling stiffnesses were explored. Inspired by the theoretical model, chiral granular strings with particular interaction mechanisms were realized through 3D printing and were tested in a uniaxial testing machine, providing a parametric experimental study by varying two geometrical parameters defining the interaction between grains. To access the full-field deformation in the samples, DIC at different scales was applied, where it was shown that the 3D printed granular strings can be representatives of granular media composed of rigid grains interacting with each other through some grain-pair interaction mechanisms. To evaluate the model predictions, the model parameters were obtained through fitting to the experimentally obtained displacements and rotation fields of the granular strings. The results showed independence of the axial displacement to the values of the geometrical parameters. Moreover, the analysis showed that material and geometrical nonlinearities in the grain-pair interaction mechanisms become significant in larger axial strains, thus giving the limit of applicability of the model with respect to the applied strain.

Within the scope of the presented work, several uncertainties were present that are worth noting. These uncertainties can, in a broad sense, be categorized into two different groups of aleatoric and

epistemic uncertainties. Examples of aleatoric uncertainty in the present work are the measurement uncertainties in DIC and the experimental uncertainties due to the application of the boundary conditions on the granular strings, which may have added/suppressed other forms of deformation to/from experimental observations, and may differ from one sample to the other. Another aleatoric uncertainty in this work is the parametric variability of the 3D printed specimens. In particular, the 3D printed granular strings had small deviations in their printed values of  $t$  and  $b$  from their nominal ones. This variation is present in different grain-pair mechanisms for each granular string, and in the two identically printed samples. An example of epistemic uncertainty involved in the present work are the limited number of samples for each granular string with particular geometrical parameter values. Moreover, structural uncertainties in both the theoretical micropolar model and the interpolation functions assumptions in DIC are acknowledged. Additionally, numerical uncertainties due to the implementation of the DIC and other optimization algorithms were present.

The micropolar model presented here incorporates coupling between all deformation mechanisms, and therefore, accounts for the complex phenomena that occur in the interacting grain pairs. This was shown by comparing the model prediction results and the experimental results. However, similar to what is typified in Fig. (4), the experimental results of the displacements and rotations of grains in large applied strains have peculiarities that cannot be addressed fully by the proposed micropolar model predictions. While the transverse displacement of grains follow a field similar to the model's predictions, large transverse displacements are observed in the grains nearest to the boundaries of the granular strings. The same argument holds for the rotation of grains, where large values of rotations are observed near the ends of the structure as opposed to a quadratic field predicted by the model. These responses are not predicted in the linear micropolar model presented here, and may be due to the effect of boundary layer and nonlinear interaction between the grains. Therefore, for a rather simple 1D granular string, the presented micropolar model with linear interaction mechanisms can adequately describe the overall behavior of the system far from the boundaries and in small axial strains.

### **Statement of Competing Interest**

Authors have no competing interests to declare.

### **Acknowledgements**

This research is supported in part by the United States National Science Foundation grant CMMI-1727433.

## References

- Alderson, A., Alderson, K.L., Attard, D., Evans, K.E., Gatt, R., Grima, J.N., Miller, W., Ravirala, N., Smith, C.W., Zied, K., 2010. Elastic constants of 3-, 4- and 6-connected chiral and anti-chiral honeycombs subject to uniaxial in-plane loading. *Compos. Sci. Technol.* 70, 1042–1048. <https://doi.org/10.1016/j.compscitech.2009.07.009>
- Angelo, M. De, Placidi, L., NejadSadeghi, N., Misra, A., 2019. Non-standard Timoshenko beam model for chiral metamaterial: identification of stiffness parameters. *Mech. Res. Commun.* 103462. <https://doi.org/10.1016/j.mechrescom.2019.103462>
- Biswas, R., Poh, L.H., Shedbale, A.S., 2020. A micromorphic computational homogenization framework for auxetic tetra-chiral structures. *J. Mech. Phys. Solids* 135, 103801. <https://doi.org/10.1016/j.jmps.2019.103801>
- Chen, W., Huang, X., 2019. Topological design of 3D chiral metamaterials based on couple-stress homogenization. *J. Mech. Phys. Solids* 131, 372–386. <https://doi.org/10.1016/j.jmps.2019.07.014>
- Chen, Y., Frenzel, T., Guenneau, S., Kadic, M., Wegener, M., 2020. Mapping acoustical activity in 3D chiral mechanical metamaterials onto micropolar continuum elasticity. *J. Mech. Phys. Solids* 137, 103877. <https://doi.org/10.1016/j.jmps.2020.103877>
- Chen, Y., Liu, X.N., Hu, G.K., Sun, Q.P., Zheng, Q.S., 2014. Micropolar continuum modelling of bi-dimensional tetrachiral lattices. *Proc. R. Soc. A Math. Phys. Eng. Sci.* 470, 20130734. <https://doi.org/10.1098/rspa.2013.0734>
- Dirrenberger, J., Forest, S., Jeulin, D., Colin, C., 2011. Homogenization of periodic auxetic materials, in: *Procedia Engineering*. Elsevier Ltd, pp. 1847–1852. <https://doi.org/10.1016/j.proeng.2011.04.307>
- Duan, S., Wen, W., Fang, D., 2018. A predictive micropolar continuum model for a novel three-dimensional chiral lattice with size effect and tension-twist coupling behavior. *J. Mech. Phys. Solids* 121, 23–46. <https://doi.org/10.1016/j.jmps.2018.07.016>
- Fernandez-Corbaton, I., Rockstuhl, C., Ziemke, P., Gumbsch, P., Albiez, A., Schwaiger, R., Frenzel, T., Kadic, M., Wegener, M., 2019. New Twists of 3D Chiral Metamaterials. *Adv. Mater.* 31, 1807742. <https://doi.org/10.1002/adma.201807742>
- Frenzel, T., Kadic, M., Wegener, M., 2017. Three-dimensional mechanical metamaterials with a twist. *Science* (80-. ). 358, 1072–1074. <https://doi.org/10.1126/science.aao4640>
- Frenzel, T., Köpfler, J., Jung, E., Kadic, M., Wegener, M., 2019. Ultrasound experiments on acoustical activity in chiral mechanical metamaterials. *Nat. Commun.* 10, 1–6. <https://doi.org/10.1038/s41467-019-11366-8>
- Giorgio, I., dell’Isola, F., Misra, A., 2020. Chirality in 2D Cosserat media related to stretch-micro-rotation coupling with links to granular micromechanics. *Int. J. Solids Struct.* 202, 28–38. <https://doi.org/10.1016/j.ijsolstr.2020.06.005>
- Ha, C.S., Plesha, M.E., Lakes, R.S., 2016. Chiral three-dimensional isotropic lattices with negative Poisson’s ratio. *Phys. status solidi* 253, 1243–1251. <https://doi.org/10.1002/pssb.201600055>
- Hild, F., Misra, A., dell’Isola, F., 2021. Multiscale DIC Applied to Pantographic Structures. *Exp. Mech.* 61, 431–443. <https://doi.org/10.1007/s11340-020-00636-y>
- Jiang, Y., Li, Y., 2018. Novel 3D-Printed Hybrid Auxetic Mechanical Metamaterial with Chirality-Induced Sequential Cell Opening Mechanisms. *Adv. Eng. Mater.* 20, 1700744.



<https://doi.org/10.1002/adem.201700744>

Kadic, M., Diatta, A., Frenzel, T., Guenneau, S., Wegener, M., 2019. Static chiral Willis continuum mechanics for three-dimensional chiral mechanical metamaterials. *Phys. Rev. B* 99, 214101. <https://doi.org/10.1103/PhysRevB.99.214101>

Lakes, R., 2001. Elastic and viscoelastic behavior of chiral materials. *Int. J. Mech. Sci.* 43, 1579–1589. [https://doi.org/10.1016/S0020-7403\(00\)00100-4](https://doi.org/10.1016/S0020-7403(00)00100-4)

Leclerc, H., Neggers, J., Mathieu, F., Roux, S., Hild, F., n.d. *Correli 3.0*. Agence pour la Protection des Programmes, Paris, 2015. IDDN. FR 1.

Liu, X., Hu, G., 2016. Elastic metamaterials making use of chirality: A review. *Stroj. Vestnik/Journal Mech. Eng.* <https://doi.org/10.5545/sv-jme.2016.3799>

Liu, X.N., Hu, G.K., Sun, C.T., Huang, G.L., 2011. Wave propagation characterization and design of two-dimensional elastic chiral metacomposite. *J. Sound Vib.* 330, 2536–2553. <https://doi.org/10.1016/j.jsv.2010.12.014>

Liu, X.N., Huang, G.L., Hu, G.K., 2012. Chiral effect in plane isotropic micropolar elasticity and its application to chiral lattices. *J. Mech. Phys. Solids* 60, 1907–1921. <https://doi.org/10.1016/j.jmps.2012.06.008>

Misra, A., NejadSadeghi, N., De Angelo, M., Placidi, L., 2020. Chiral metamaterial predicted by granular micromechanics: verified with 1D example synthesized using additive manufacturing. *Contin. Mech. Thermodyn.* <https://doi.org/10.1007/s00161-020-00862-8>

NejadSadeghi, N., Misra, A., 2020a. Extended granular micromechanics approach: a micromorphic theory of degree  $n$ . *Math. Mech. Solids* 25, 407–429. <https://doi.org/10.1177/1081286519879479>

NejadSadeghi, N., Misra, A., 2020b. Role of higher-order inertia in modulating elastic wave dispersion in materials with granular microstructure. *Int. J. Mech. Sci.* 185, 105867. <https://doi.org/10.1016/j.ijmecsci.2020.105867>

Nguyen, L.A., He, H., Pham-Huy, C., 2006. Chiral drugs: an overview. *Int. J. Biomed. Sci.* 2, 85–100.

Ni, X., Weiner, M., Alù, A., Khanikaev, A.B., 2019. Observation of higher-order topological acoustic states protected by generalized chiral symmetry. *Nat. Mater.* 18, 113–120. <https://doi.org/10.1038/s41563-018-0252-9>

Nieves, M.J., Carta, G., Jones, I.S., Movchan, A.B., Movchan, N. V., 2018. Vibrations and elastic waves in chiral multi-structures. *J. Mech. Phys. Solids* 121, 387–408. <https://doi.org/10.1016/j.jmps.2018.07.020>

Poncelet, M., Somera, A., Morel, C., Jailin, C., Auffray, N., 2018. An experimental evidence of the failure of Cauchy elasticity for the overall modeling of a non-centro-symmetric lattice under static loading. *Int. J. Solids Struct.* 147, 223–237. <https://doi.org/10.1016/j.ijsolstr.2018.05.028>

Reasa, D.R., Lakes, R.S., 2019. Cosserat Effects in Achiral and Chiral Cubic Lattices. *J. Appl. Mech.* 86. <https://doi.org/10.1115/1.4044047>

Rosi, G., Auffray, N., 2016. Anisotropic and dispersive wave propagation within strain-gradient framework. *Wave Motion* 63, 120–134. <https://doi.org/10.1016/j.wavemoti.2016.01.009>

Spadoni, A., Ruzzene, M., 2012. Elasto-static micropolar behavior of a chiral auxetic lattice. *J. Mech. Phys. Solids* 60, 156–171. <https://doi.org/10.1016/j.jmps.2011.09.012>

Spadoni, A., Ruzzene, M., Gonella, S., Scarpa, F., 2009. Phononic properties of hexagonal chiral lattices.

Wave Motion 46, 435–450. <https://doi.org/10.1016/j.wavemoti.2009.04.002>

Takane, D., Wang, Z., Souma, S., Nakayama, K., Nakamura, T., Oinuma, H., Nakata, Y., Iwasawa, H., Cacho, C., Kim, T., Horiba, K., Kumigashira, H., Takahashi, T., Ando, Y., Sato, T., 2019. Observation of Chiral Fermions with a Large Topological Charge and Associated Fermi-Arc Surface States in CoSi. *Phys. Rev. Lett.* 122. <https://doi.org/10.1103/PhysRevLett.122.076402>

Wu, W., Hu, W., Qian, G., Liao, H., Xu, X., Berto, F., 2019. Mechanical design and multifunctional applications of chiral mechanical metamaterials: A review. *Mater. Des.* <https://doi.org/10.1016/j.matdes.2019.107950>

## List of Figures

**Fig 1.** Micropolar model prediction of displacement and rotation fields of a one-dimensional chiral granular material under uniaxial tension.

**Fig 2.** The proposed granular string with (a) its geometrical structure and the space of specimens with different geometrical parameters, (b) the speckle pattern on the surface of the specimens, and (c) the experimental and picture acquisition setup.

**Fig 3.** The macro- and micro-scale DIC analyses results for a granular string with  $t=1.2$  mm and  $b=1$  mm.

**Fig 4.** The meso-scale DIC analysis results for a granular string with  $t=1.2$  mm and  $b=1$  mm.

**Fig 5.** Fitted model parameters for applied axial strain of 0.035 (two left columns) and applied axial strain of 0.095 (two right columns).

**Fig 6.** Goodness of fits for applied axial strain of 0.035 (two top rows) and applied axial strain of 0.095 (two bottom rows).

**Fig 7.** Strain energy density distribution in granular strings with different geometrical parameters for applied axial strain of 0.035.

**Fig 8.** Strain energy density distribution in granular strings with different geometrical parameters for applied axial strain of 0.095.

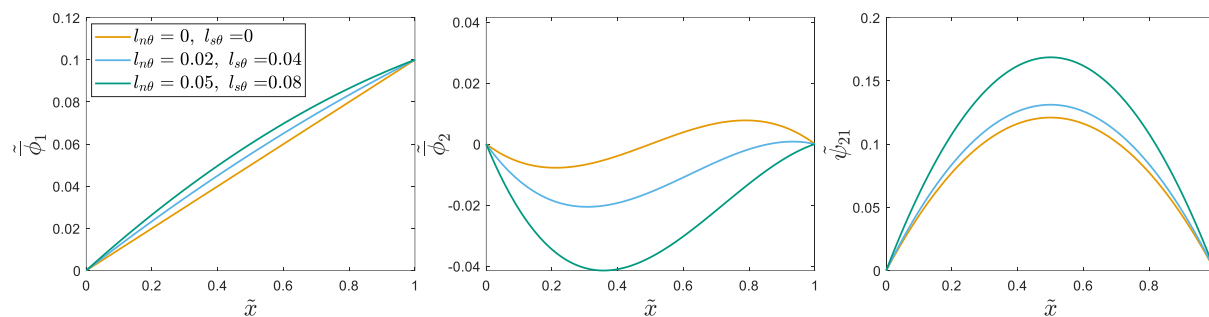


**Fig 1.** Micropolar model prediction of displacement and rotation fields of a one-dimensional chiral granular material under uniaxial tension.

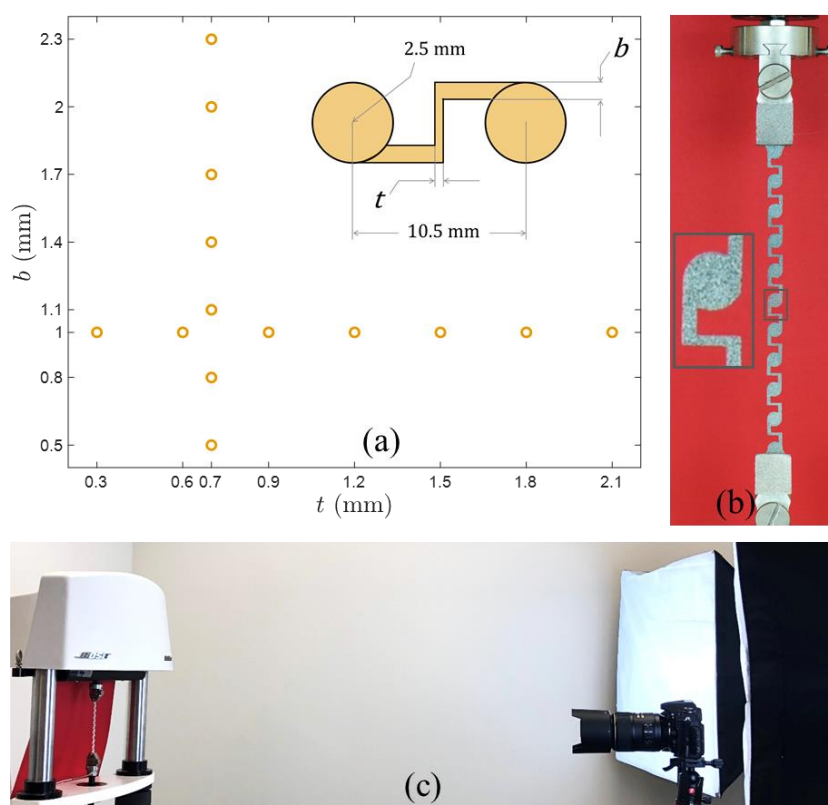


**Fig 2.** The proposed granular string with (a) its geometrical structure and the space of specimens with different geometrical parameters, (b) the speckle pattern on the surface of the specimens, and (c) the experimental and picture acquisition setup.

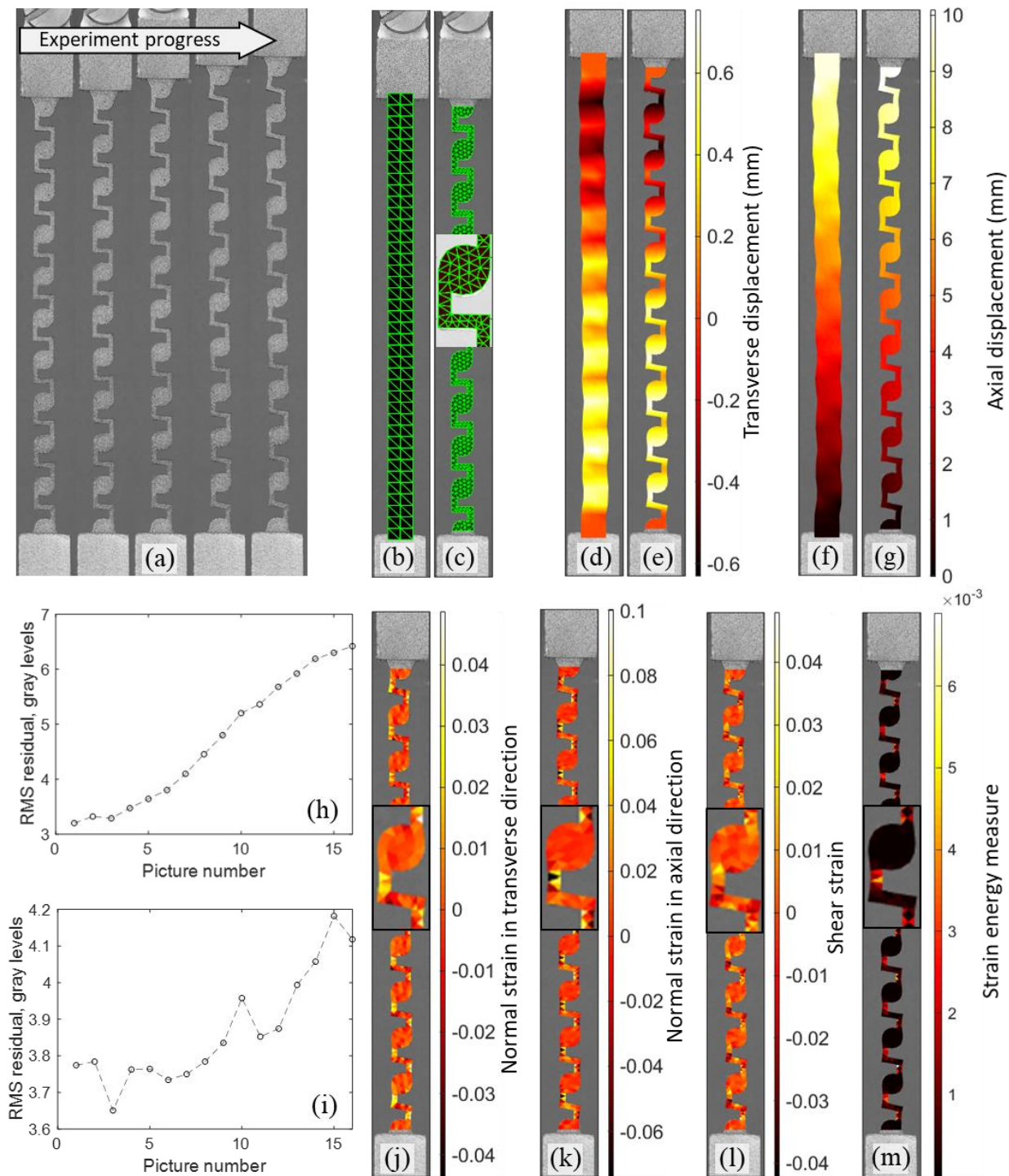


**Fig 3.** The macro- and micro-scale DIC analyses results for a granular string with  $t=1.2$  mm and  $b=1$  mm.

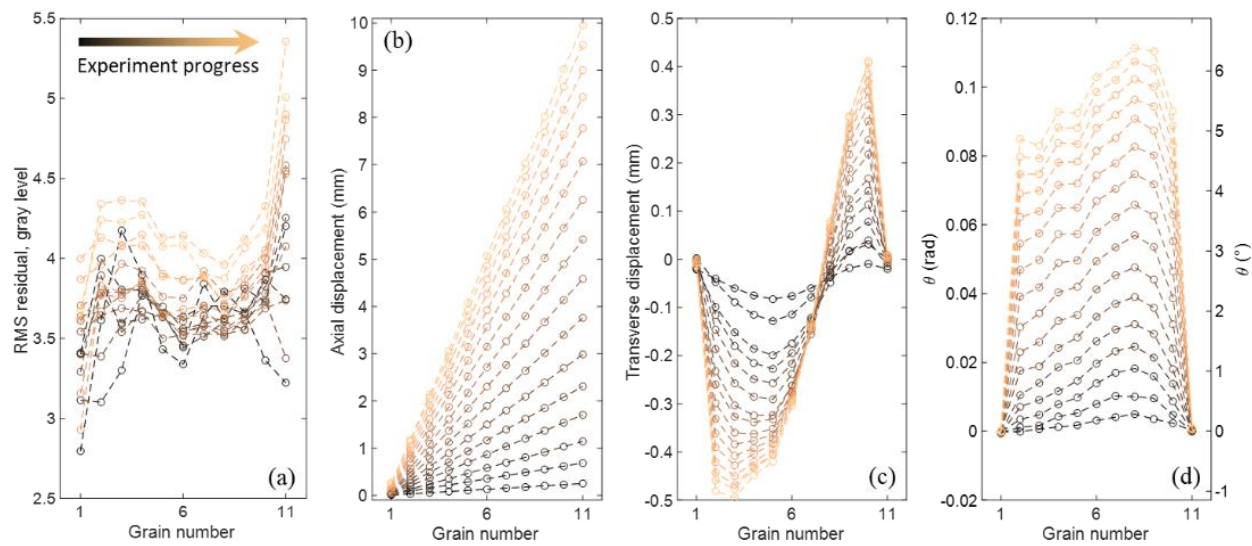


**Fig 4.** The meso-scale DIC analysis results for a granular string with  $t=1.2$  mm and  $b=1$  mm.

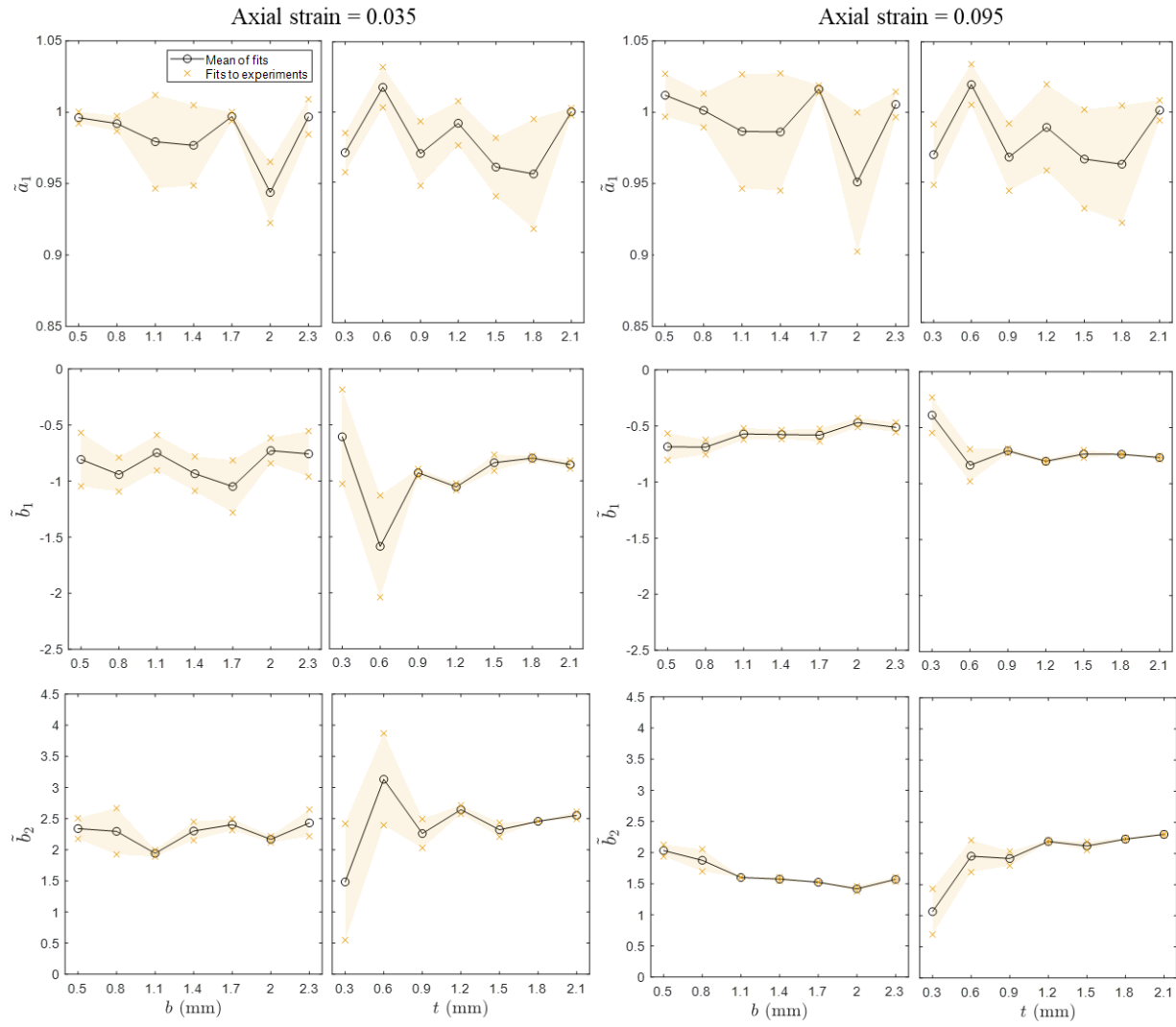


**Fig 5.** Fitted model parameters for applied axial strain of 0.035 (two left columns) and applied axial strain of 0.095 (two right columns).



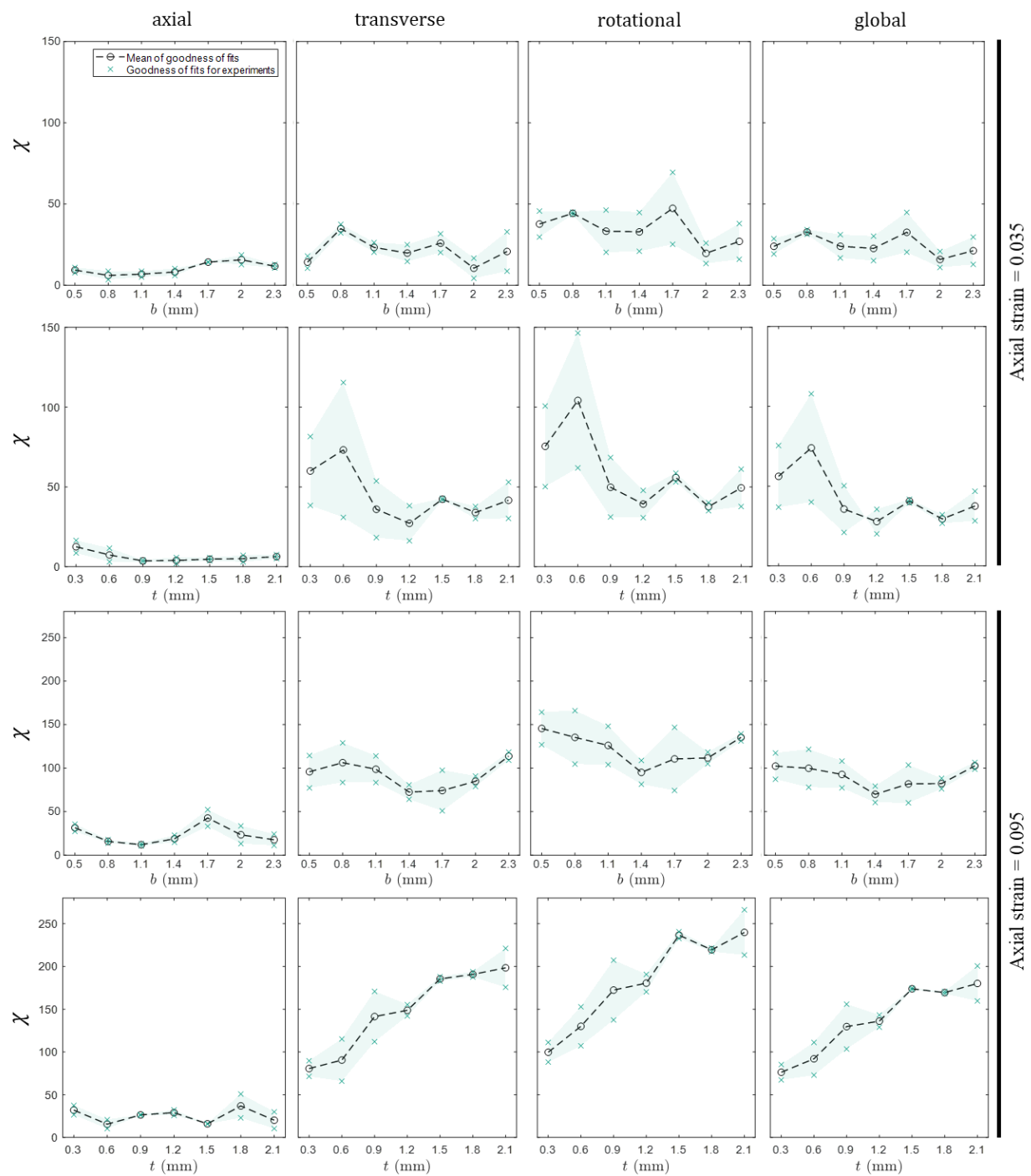


**Fig 6.** Goodness of fits for applied axial strain of 0.035 (two top rows) and applied axial strain of 0.095 (two bottom rows).

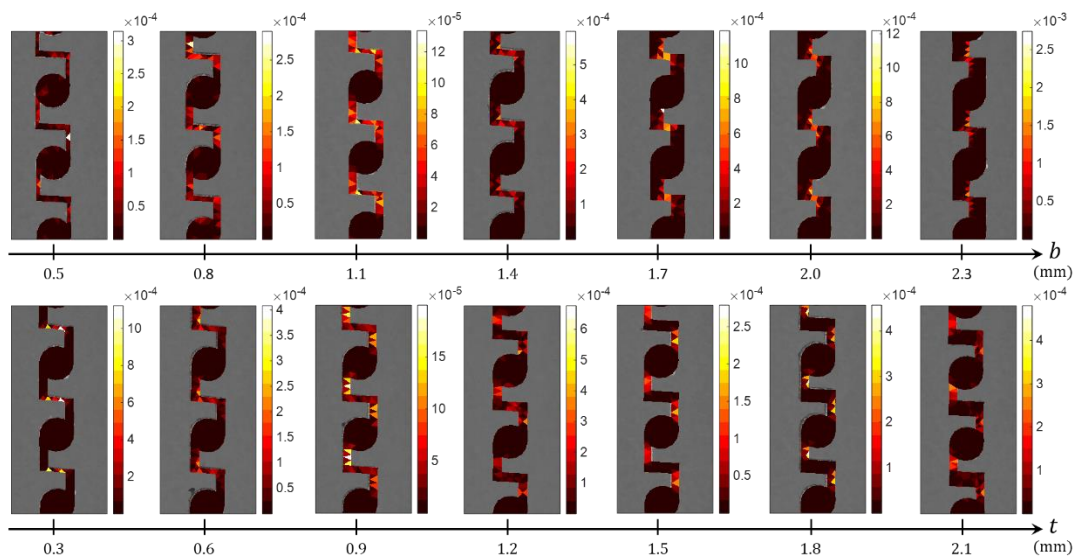


**Fig 7.** Strain energy density distribution in granular strings with different geometrical parameters for applied axial strain of 0.035.

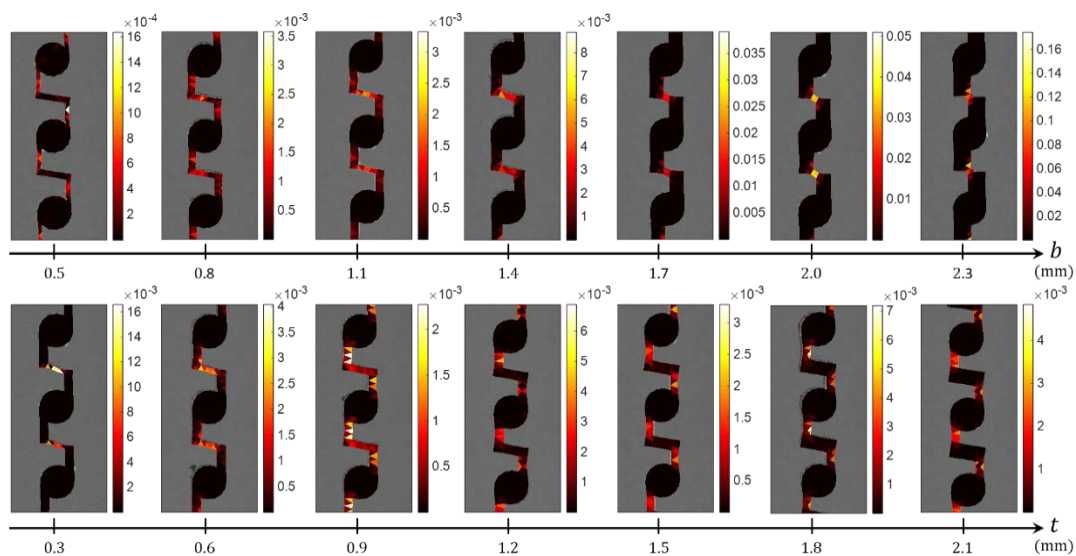


**Fig 8.** Strain energy density distribution in granular strings with different geometrical parameters for applied axial strain of 0.095.